

**Experimental Study of Wave Overtopping Performance
of Steep Low-Crested Structures**

**Experimentele studie van de golfoverslagperformantie
van constructies met steil talud en lage kruin**

David Gallach Sánchez

**Promotoren: prof. dr. ir. P. Troch, prof. dr. ir. A. Kortenhaus
Proefschrift ingediend tot het behalen van de graad van
Doctor in de ingenieurswetenschappen: bouwkunde**



**UNIVERSITEIT
GENT**

**Vakgroep Civiele Techniek
Voorzitter: prof. dr. ir. P. Troch
Faculteit Ingenieurswetenschappen en Architectuur
Academiejaar 2017 - 2018**

ISBN 978-94-6355-136-6

NUR 956

Wettelijk depot: D/2018/10.500/54

Examination Board

Supervisors:

prof. Peter Troch
prof. Andreas Kortenhaus

Coastal Engineering Research Group
Department of Civil Engineering
Faculty of Engineering and Architecture
Ghent University
Technologiepark 904
9052 Zwijnaarde, Belgium

Voting members:

prof. Filip De Turck (chairman)	Ghent University
prof. Adam Bezuijen (secretary)	Ghent University
prof. Tom De Mulder	Ghent University
prof. Alain De Wulf	Ghent University
prof. Thomas Lykke Andersen	Aalborg University (Denmark)
prof. Josep R. Medina Folgado	Universitat Politècnica de València (Spain)
dr. ir. Corrado Altomare	Ghent University
dr. ir. Tomohiro Suzuki	Waterbouwkundig Laboratorium (Belgium)

We choose to go to the Moon in this decade and do the other things, not because they are easy, but because they are hard, because that goal will serve to organize and measure the best of our energies and skills, because that challenge is one that we are willing to accept, one we are unwilling to postpone, and one which we intend to win.

— John F. Kennedy,
12th September 1962.

Acknowledgements

After more than four years of PhD, the time has come to thank all the people that helped me, supported me and encouraged me, making it easier to walk this path. During this period I not only learned about coastal engineering, research and how to be an engineer, I also grew as a person thanks to the people here mentioned.

Thank you to prof. Peter Troch, for the opportunity that he gave me to start the PhD. With his constant support and guidance I was able to successfully finish the research while learning the insights of coastal engineering. He also trusted me with many projects that improved my engineering skills. Thank you to prof. Andreas Kortenhuis for his valuable advice. His spot-on comments and remarks helped me to improve the quality of the research and of the publications.

Thank you to all the students that helped in the research by performing experiments and analysing the data. Without you it would have been an impossible task to perform more than 1200 tests. Thank you to all the fellow researchers that contributed to the research with interesting discussions and comments.

Thank you to the members of my examination board for their very valuable feedback and discussion over the research, and for their critical review of the dissertation which allowed me to improve it and to make it easier to read.

Thank you to the technical team of AWW: Sam, Dave, Tom and my office-mate Herman. Without their help during the experiments in the wave flume, this research would have been impossible to succeed. They were always willing to give me any support that I needed, also providing crucial ideas to improve the experiments. Special thanks for fixing (several times) my bike.

Thank you to Lien and Ellen for their help in any major or minor problem that I encountered, always with a smile on their face. Without them I probably would have been stranded in a sea of paperwork on many occasions.

Thank you to my fellow researchers at AWW: Ine, Minghao, Vicky, Peter, Gael, Panagiotis, Philip, Carlos, Brecht, Tim, Max and Vincent (and the ones who left AWW). It was a pleasure to share this ride with you. Thank you for many good moments and for your support on the tough times. Special thanks to Tom, Max, Panagiotis and Brecht for proofreading parts of the thesis, and to Tim for translating the summary into Dutch.

Gracias a Pablo, Rosa, Iñaki, Fede, Juan, Antonio, Julián y Txus por su apoyo desde la distancia y por los buenos momentos en cada viaje a Valencia. Era un alivio saber que siempre podía contar con ellos cuando lo necesitaba. Gracias a mis carnales Luis y Gael por compartir conmigo este tiempo en Gante, por los viajes, por las risas y por las fiestas.

Gracias a mis padres, a mis abuelos y al resto de mi familia por su continuo apoyo en todas las decisiones que he tomado, por ayudarme siempre cuando ha hecho falta. Siempre he sentido vuestro cariño desde Gante.

Y gracias a Almudena, por creer en mí cuando yo había dejado de hacerlo, por empujarme y arrastrarme hasta la línea de meta cuando ya no me quedaban fuerzas. Imposible contar con más apoyo del que tú me has dado.

David
Ghent, July 2018

Contents

List of Symbols	xiii
List of Acronyms	xix
Samenvatting	xxi
Summary	xxv
1 Introduction	1
1.1 Wave Overtopping	1
1.2 Application of Steep Low-Crested Structures	2
1.2.1 Coastal Structures	5
1.2.2 Overtopping Wave Energy Converters	8
1.3 Research Objectives	11
1.4 Outline	13
2 Literature Review on Wave Overtopping	15
2.1 Wave Overtopping Prediction in Perspective	15
2.2 Wave Overtopping Manuals	18
2.3 Average Overtopping Rate Prediction Formulae	20
2.3.1 Sloping Structures	20
2.3.2 Influence of Shallow Foreshores on Wave Overtopping	21
2.3.3 Steep Low-Crested Structures	23
2.3.4 Vertical Structures	29
2.3.5 Zero Freeboard	31

2.3.6	Effect of Roughness on Wave Overtopping	35
2.4	Individual Overtopping Volumes	38
2.4.1	Probability Distribution of Individual Overtopping Volumes	38
2.4.2	Estimation of Shape Factor B	40
2.4.3	Probability of Overtopping P_{ow}	45
2.4.4	Maximum Volume V_{max}	50
2.5	Summary	50
3	Research Methodology	53
3.1	Methodology Outline	53
3.2	Design of Hydraulic Model Tests	54
3.2.1	Relative Crest Freeboard R_c/H_{m0}	55
3.2.2	Slope Angle α	55
3.2.3	Relative Water Depth H_{m0}/h	56
3.2.4	Roughness of the Slope	56
3.3	Wave Overtopping Datasets	57
3.4	Assessment of the Accuracy of a Prediction	59
4	Experimental Setup and Test Programme	61
4.1	Experimental Setup	61
4.1.1	Wave Flume at Ghent University	61
4.1.2	Measurement Systems	64
4.1.3	Experimental Setup of Datasets	70
4.2	Test Programme	78
4.2.1	UG13 Dataset	78
4.2.2	UG14 and UG15 Datasets	79
4.2.3	UG16 Dataset	81
4.3	Processing of Data	83
4.3.1	Incident Wave Parameters Processing	83
4.3.2	Wave Overtopping Processing	84
4.4	Repeatability of the Overtopping Parameters	88
4.5	Summary	91

5	Data Analysis of Average Overtopping Rates	93
5.1	Average Overtopping Results	93
5.2	Comparison with Average Overtopping Prediction Formulae	96
5.2.1	Sloping Structures	96
5.2.2	Steep Low-Crested Structures	97
5.2.3	Vertical Structures	102
5.2.4	Zero Freeboard	103
5.2.5	Discussion	104
5.3	Influence of Shallow Water Conditions on Non-Breaking Overtopping	106
5.4	Update of the Overtopping Prediction for Steep Low-Crested Structures	109
5.4.1	Selection of Overtopping Data to Update the Prediction	110
5.4.2	Update of the Coefficients	111
5.4.3	Uncertainty of the Prediction Update	116
5.4.4	Comparison of Predictions and Discussion	117
5.5	Average Wave Overtopping Results for Tests with Roughness Elements	122
5.5.1	Blocks and Ribs	122
5.5.2	Stepped Revetments	124
5.6	Summary	128
6	Data Analysis of Individual Overtopping	131
6.1	Probability Distribution of Individual Overtopping Volumes	131
6.2	Shape Factor B	134
6.2.1	Results	134
6.2.2	Comparison with Prediction Formulae	138
6.2.3	New Prediction Formula	143
6.3	Probability of Overtopping P_{ow}	149
6.3.1	Results	149
6.3.2	Comparison with Prediction Formulae	154
6.3.3	New Prediction Formula	157

6.4	Scale Factor A	161
6.5	Individual Overtopping for Tests with Roughness Elements . .	163
6.5.1	Blocks and Ribs	163
6.5.2	Stepped Revetments	165
6.6	Summary	167
7	Conclusions	169
7.1	Overview of the Research	169
7.2	Conclusions on Average Overtopping	171
7.3	Conclusions on Individual Overtopping	173
7.4	Publications	175
7.5	Recommendations for Further Research	175
	References	177

List of Symbols

a	(-)	Coefficient in the three-parameter Weibull prediction of average overtopping rates $q/\sqrt{gH_{m0}^3} = a \exp[-(b R_c/H_{m0})^c]$
a_{update}	(-)	Coefficient a in the updated overtopping prediction formula for steep low-crested structures
a_{Victor}	(-)	Coefficient a in the overtopping prediction formula by Victor and Troch (2012b)
$a_{V\&B}$	(-)	Coefficient a in the overtopping prediction formula by Van der Meer and Bruce (2014)
A	(m ³ /m)	Scale factor in a two-parameter Weibull distribution of individual overtopping volumes
A_{calc}	(m ³ /m)	Calculated scale factor
A_{pred}	(m ³ /m)	Predicted scale factor
A'	(-)	Factor relating A to B : $A' = 1/\Gamma(1 + 1/B)$
b	(-)	Coefficient in the three-parameter Weibull prediction of average overtopping rates $q/\sqrt{gH_{m0}^3} = a \exp[-(b R_c/H_{m0})^c]$
b_{update}	(-)	Coefficient b in the updated overtopping prediction formula for steep low-crested structures
b_{Victor}	(-)	Coefficient b in the overtopping prediction formula by Victor and Troch (2012b)
$b_{V\&B}$	(-)	Coefficient b in the overtopping prediction formula by Van der Meer and Bruce (2014)
B	(-)	Shape factor in a two-parameter Weibull distribution of individual overtopping volumes
B_{measured}	(-)	Measured shape factor B

$B_{\text{predicted}}$	(-)	Predicted shape factor B
B_q	(m)	Width of the overtopping tray
c	(-)	Coefficient in the three-parameter Weibull prediction of average overtopping rates $q/\sqrt{gH_{m0}^3} = a \exp[-(b R_c/H_{m0})^c]$
c_{update}	(-)	Coefficient c in the updated overtopping prediction formula for steep low-crested structures
$c_{V\&B}$	(-)	Coefficient c in the overtopping prediction formula by Van der Meer and Bruce (2014)
C_r	(-)	Reflection coefficient
d_{st}	(m)	Position of the SWL relative to the nearest lower step edge
f_b	(m)	Block width
f_h	(m)	Block height
f_{HC}	(Hz)	High cut-off frequency
f_L	(m)	Block distance
f_{LC}	(Hz)	Low cut-off frequency
f_p	(Hz)	Peak wave frequency
g	(m/s ²)	Acceleration due to gravity
h	(m)	Water depth at the toe of the structure
h_*	(-)	Impulsiveness parameter
H_{m0}	(m)	Incident spectral wave height at the toe of the structure. $H_{m0} = 4\sqrt{m_0}$
$H_{m0,\text{deep}}$	(m)	Incident spectral wave height on deep water conditions
$H_{m0,\text{target}}$	(m)	Target incident spectral wave height
H_{m0}/S_h	(-)	Relative step height
H_s	(m)	Incident significant wave height at the toe of the structure
k_h	(m)	Characteristic step diameter
$L_{m-1,0}$	(m)	Linear wavelength associated to $T_{m-1,0}$
L_p	(m)	Peak wavelength
m	(-)	Foreshore slope at the toe of the structure

m_{-1}	(-)	First negative moment of the energy spectrum
m_0	(-)	Zeroth moment of the energy spectrum
M_{abs}	(kg)	Absolute mass added to the reservoir
M_{cul}	(kg)	Cumulative absolute mass of water
M_i	(kg)	Individual overtopping mass
$M_{\text{rel,cell}}$	(kg)	Relative mass measured in the weigh cell
n	(-)	Ratio between step width and step height $n = S_w/S_h = \cot \alpha$
N_{test}	(-)	Number of tests
N_{ow}	(-)	Number of overtopping waves
N_w	(-)	Number of incident waves
p	(-)	Coefficient in the new P_{ow} prediction
P_{ow}	(-)	Probability of overtopping
$P_{ow,\text{measured}}$	(-)	Measured probability of overtopping P_{ow}
$P_{ow,\text{predicted}}$	(-)	Predicted probability of overtopping P_{ow}
P_v	(-)	Theoretical exceedance probability
\hat{P}_v	(-)	Empirical exceedance probability
q	(m ³ /s/m)	Average overtopping rate
q_{meas_n}	(m ³ /s/m)	Average overtopping measured for the test n
q_{pred_n}	(m ³ /s/m)	Average overtopping predicted for the test n
r^2	(-)	Coefficient of determination
R_c	(m)	Crest freeboard
R_c/H_{m0}	(-)	Relative crest freeboard
$R_{u2\%}$	(m)	2% wave run-up
$R_{u2\%,\text{smooth}}$	(m)	2% wave run-up on a smooth slope
$s_{m-1,0}$	(-)	Wave steepness associated to $T_{m-1,0}$
s_{0p}	(-)	Peak wave steepness on deep water
S_h	(m)	Step height of a stepped revetment
S_w	(m)	Step width of a stepped revetment
t	(s)	Time
T_m	(s)	Mean wave period

$T_{m-1,0}$	(s)	Spectral incident wave period at the toe of the structure defined by m_{-1}/m_0
T_p	(s)	Peak incident wave period at the toe of the structure
T_0	(s)	Duration of the analysis window of a test
V	(m ³)	Individual overtopping volume for a given exceedance probability
V_i	(m ³ /m)	Individual overtopping volume
V_{\max}	(m ³ /m)	Maximum individual overtopping volume
\bar{V}_{meas}	(m ³ /m)	Measured mean overtopping volume
\bar{V}_{theor}	(m ³ /m)	Theoretical mean overtopping volume
w	(-)	Coefficient in the new prediction of B
w_{smooth}	(-)	Coefficient w for the smooth slope reference case in the new prediction of B
x	(-)	Coefficient in the new prediction of B
x_{smooth}	(-)	Coefficient x for the smooth slope reference case in the new prediction of B
y	(-)	Coefficient in the new prediction of B
y_{smooth}	(-)	Coefficient y for the smooth slope reference case in the new prediction of B
α	(°)	Slope angle
γ_b	(-)	Influence factor for a berm
γ_f	(-)	Influence factor for roughness elements on a slope and permeability of the structure
$\gamma_{f,min}$	(-)	Minimum influence factor for roughness elements on a slope
$\gamma_{f,0.58}$	(-)	Influence factor for roughness elements on a $\cot \alpha = 0.58$ slope
$\gamma_{f,1}$	(-)	Influence factor for roughness elements on a $\cot \alpha = 1$ slope
γ_h	(-)	Influence factor for the effect of a shallow foreshore
γ_v	(-)	Influence factor for a wall at the end of a slope
γ_β	(-)	Influence factor for oblique wave attack
$\Delta x_{AWA1,AWA2}$	(m)	Distance between AWA1 and AWA2

$\Delta x_{WG1,WG2}$	(m)	Distance between WG1 and WG2
$\Delta x_{WG1,WG3}$	(m)	Distance between WG1 and WG3
$\Delta x_{WG4,WG5}$	(m)	Distance between WG4 and WG5
$\Delta x_{WG4,WG6}$	(m)	Distance between WG4 and WG6
$\Delta x_{WG6,toe}$	(m)	Distance between WG6 and the toe of the structure
λ	(-)	Intersect of the Weibull fit of the exceedance probability of the individual overtopping volumes
μ	(Var.)	Average of a normally distributed parameter
$\xi_{m-1,0}$	(-)	Surf similarity parameter associated to $T_{m-1,0}$
ξ_p	(-)	Surf similarity parameter associated to T_p
ρ	(kg/m ³)	Density of the water
σ	(Var.)	Standard deviation of a normally distributed parameter
σ_{est}	(Var.)	Standard error of the estimate
σ'	(-)	Coefficient of variation $\sigma' = \sigma/\mu$ of a normally distributed parameter
χ	(-)	Coefficient relating P_{ow} to $R_{u2\%/H_{m0}}$
ψ	(-)	Slope of the Weibull fit of the exceedance probability of the individual overtopping volumes

List of Acronyms

AWA	Active wave absorption system
CEM	Coastal Engineering Manual
DAQ	Data acquisition system
FFT	Fast Fourier transform
OBREC	Overtopping Breakwater for Energy Conversion
OWEC	Overtopping wave energy converter
RF	Reliability factor in the CLASH database
RMSE	Root mean square error
RMSLE	Root mean square logarithmic error
RPM	Random Phase Method
RSS	Residual sum of squares
SPM	Shore Protection Manual
SSG	Seawave Slot-cone Generator
SWL	Still water level
Tapchan	Tapered Channel Wave Power Device
TAW	Technical Advisory Committee on Flood Defence, The Netherlands
Var	Variable
WEC	Wave energy converter
WG	Wave gauge
2D	Two dimensional
3D	Three dimensional

Samenvatting

Golfoverslag is een belangrijk fysisch proces binnen de kustbescherming. Het bepalen van golfoverslagdebieten is een belangrijk aspect in het ontwerp van kustwaterbouwkundige structuren. Golfoverslag events kunnen levensbedreigend zijn, leiden tot schade aan eigendommen en infrastructuur, en leiden tot significante economische verliezen. Traditioneel werd het gemiddeld golfoverslagdebiet als enige ontwerpparameter gehanteerd, hoewel recente inzichten bewijzen dat ook individuele golfoverslag moet overwogen worden als een belangrijke parameter in het ontwerp van kustbeschermingsstructuren. Een goede kennis van de fysische processen, gekoppeld aan golfoverslag, is dus van primordiaal belang om de veiligheid van kustwaterbouwkundige structuren te garanderen en potentiële risico's te minimaliseren. De wetenschappelijke literatuur levert verscheidene voorspellingsformules voor golfoverslag, toegepast op verschillende structuren en golfcondities, samengevat in de EurOtop handleiding.

In de huidige literatuur ontbreekt er echter een belangrijk type structuur, namelijk structuren met een hellingshoek $2 > \cot \alpha \geq 0$ en een relatieve kruin vrijboord $0.8 > R_c/H_{m0} \geq 0$. Dit type structuur kent belangrijke toepassingen in kustbescherming en overtopping-golfenergieconvertoren. Een deel van de reeks experimentele hydraulische modelproeven met steile laagkruinige structuren werd uitgevoerd aan de Universiteit Gent, resulterend in de UG10 dataset. De testreeks was echter onvolledig, aangezien niet alle hellingshoeken en relatieve kruin vrijboorden werden behandeld in UG10. Een literatuurstudie over de beschikbare golfoverslag kennis voor steile, laagkruinige structuren werd uitgevoerd. Voorspellingsformules voor golfoverslag toegepast op dit type structuren zijn zeldzaam. Kennisleemtes werden geïdentificeerd voor de steile hellingen, inclusief het limietgeval van een verticale structuur, alsook voor kleine relatieve vrijboorden, inclusief het limietgeval met een relatieve vrijboord gelijk aan nul. De relatie tussen de bepalende factoren van het overtoppingsproces is niet volledig gedefinieerd voor dit bereik van relatieve kruin vrijboorden en hellingshoeken. Een extra kenmerk werd geïdentificeerd in het effect van de structuurruwheid op de

golfoverslagdebieten van steile, laagkruinige structuren.

De algemene doelstellingen van dit onderzoek zijn (i) het versterken van de kennis over golfoverslag voor steile, laagkruinige structuren, (ii) waarbij zowel de gemiddelde golfoverslagdebieten als de (iii) individuele golfoverslagdebieten worden geanalyseerd, (iv) om de nauwkeurigheid van voorspellingsformules voor golfoverslag te bevorderen.

Om deze doelstellingen te bereiken, worden 2D hydraulische modelproeven uitgevoerd in de golfgoot van de Universiteit Gent, waar de golfcondities en golfoverslag worden opgemeten. Het experimentele testprogramma is ontworpen op basis van de eerder geformuleerde algemene doelstellingen. Het volledige bereik van de steile laagkruinige structuren wordt behandeld, waarbij de hellingshoek α varieert van gemiddeld tot verticaal, en de relatieve kruin vrijboord R_c/H_{m0} varieert van groot tot nul. Daarenboven wordt ook het effect van condities in ondiep water op het golfoverslagdebiet voor niet-brekende golven op steile laagkruinige structuren bestudeerd, door de relatieve golfhoogte H_{m0}/h te variëren, gaande van condities in relatief diep water, over het overgangsgebied, tot condities in relatief ondiep water. De reductie in golfoverslag, geïnduceerd door de ruwheid van de structuurhelling, wordt tevens bestudeerd, aangezien deze ruwheid een belangrijke factor is in het golfoverslagproces.

In totaal werden 1211 golfoverslag experimenten uitgevoerd, waarbij de metingen werden verdeeld over 4 datasets: UG13, UG14, UG15 and UG16. De UG13 dataset focust op laagkruinige structuren voor structuren in relatief diep water, waar de UG14 dataset zich focust op het overgangsgebied en UG15 op relatief ondiep water. De UG16 dataset bevat structuurhellingen met daarop artificeel ruwe elementen (blokken, langwerpige blokken en trapvormige bekleding) om het effect van de ruwheid op golfoverslagdebieten over steile laagkruinige structuren te analyseren.

De gemiddelde golfoverslagdebieten van alle tests werden verwerkt en geanalyseerd in functie van de bepalende parameters van het golfoverslag proces. De resultaten werden vergeleken met de bestaande voorspellingformules voor steile laagkruinige structuren, om hun nauwkeurigheid te bepalen. Deze nauwkeurigheid werd bepaald door het berekenen van RMSE (Root Mean Square Error) waarden en de bias voor elke voorspelling. De resultaten tonen aan dat de bestaande voorspellingsformules over het algemeen nauwkeurig zijn in het voorspellen van golfoverslag voor steile, laagkruinige structuren. In het geval van zeer kleine relatieve vrijboorden en in het geval zonder vrijboord, leiden de formules echter tot een onderschatting van de golfoverslag. Wanneer zeer steile structuren worden behandeld, leiden de bestaande formules tot een onderschatting van de golfoverslag voor grote

relatieve vrijboorden. Ook is er een toename van de gemiddelde golfoverslag voor grote relatieve vrijboorden wanneer er sprake is van condities in relatief ondiep water. Deze toename ligt echter wel binnen de betrouwbaarheidsinterval van de bestaande voorspellingsformules. Om de onnauwkeurigheden van de bestaande formules aan te pakken, wordt een nieuwe voorspellingsformule voorgesteld. Deze formule werd gefit doorheen de eerder beschikbare golfoverslag data, evenals doorheen de data, verkregen binnen dit onderzoek. De nieuwe formule verhoogt de nauwkeurigheid voor zeer steile hellingen en voor structuren zonder vrijboord, en behoudt tevens zijn nauwkeurigheid voor de klassieke gevallen. De reductie in golfoverslag door de ruwheid van de structuur is minder uitgesproken voor steilere hellingen. De reductie is echter hoger voor langwerpige blokken dan voor vierkante blokken aangezien de bedekte structuuroppervlakte hoger is. Bij trapvormige bekleding, neemt de reductie af voor toenemende waarden van de zogenaamde golfsbrekingparameter $\xi_{m-1,0}$. Wanneer het vrij wateroppervlak dicht tegen de hoogste rand van een trap staat, is deze reductie hoger door de interactie tussen de invallende en gereflecteerde golven op het trapfront.

De kansverdeling van de individuele golfoverslag volumes volgt een Weibull distributie, beschreven door twee parameters: de schaalfactor A en de vormfactor B . De waarschijnlijkheid van golfoverslag P_{ow} is het percentage van de invallende golven die over de structuur slaan. Deze drie parameters werden geanalyseerd voor alle uitgevoerde tests en gelinkt aan de bepalende parameters voor golfoverslag. De schaalfactor A kan beschreven worden aan de hand van B en P_{ow} , aangezien de overslagvolumes een Weibull distributie volgen. Een relatie tussen B en de hellingshoek α werd gevonden voor zeer kleine en onbestaande relatieve vrijboorden. Voor grote relatieve vrijboorden, wordt B constant, onafhankelijk van de gebruikte hellingshoeken. De bestaande voorspellingsformules voor B onderschatten de waarde van B voor zeer kleine en onbestaande relatieve vrijboorden. De waarschijnlijkheid van golfoverslag P_{ow} , in het geval van een onbestaande relatieve vrijboord, is theoretisch gezien gelijk aan 1 (iedere invallende golf slaat over de structuur). Uit de data-analyse blijkt echter dat P_{ow} varieert van 0.8 tot 1.0, door de interactie tussen invallende en gereflecteerde golven. De waarde van P_{ow} zakt voor grotere relatieve vrijboorden en voor steilere hellingen. Nieuwe voorspellingsformules voor B en P_{ow} werden voorgesteld en werden getoetst aan zowel de UG10 dataset als de nieuw verworven datasets. De nieuwe formule zorgt voor een significant hogere nauwkeurigheid dan de bestaande formule. De artificiele dekelementen, zorgend voor een hogere ruwheid, hebben geen invloed op de waardes van A , B en P_{ow} , in vergelijking met gladde hellingen.

Summary

Wave overtopping is a key process in coastal protection. The assessment of the wave overtopping rates is an important aspect in the design of coastal structures. Overtopping events can result in threat to human lives, damage of property and infrastructure and economic losses. Traditionally the average wave overtopping rate was the only overtopping parameter considered in the design, although recent insight reveals that individual wave overtopping should be considered also as a key design parameter of sea defence structures. A good knowledge of the physics behind wave overtopping is therefore necessary to improve the safety of coastal structures and to minimize the potential risks. Wave overtopping prediction formulae are widely available in scientific literature for various structural and wave conditions, summarized in the EurOtop manual.

One of the structure types not yet covered by the literature is for steep low-crested structures, with slope angles $2 > \cot \alpha \geq 0$ and relative crest freeboards $0.8 > R_c/H_{m0} \geq 0$. This type of structures is regularly applied for coastal protection and overtopping wave energy converters (OWECs). Part of the range of steep low-crested structures was covered in the past by hydraulic model tests carried out at Ghent University that resulted in the UG10 dataset. However, not the whole range of slope angles and relative crest freeboards was covered by the UG10 dataset. A literature review of the overtopping knowledge available for steep low-crested structures is carried out. The wave overtopping prediction formulae available for this type of structures are scarce. Knowledge gaps are identified for steep slopes up to the limit case with vertical structures, with small relative freeboards up to the limit case with zero freeboards. The relation between the driving parameters of the overtopping process is not fully defined for this range of relative crest freeboard and slope angles. Moreover, another knowledge gap for the effect of roughness on the overtopping rates of the steep low-crested structures is also existing.

The main objectives of this research are (i) to increase the knowledge of wave overtopping for steep low-crested structures, (ii) with an analysis of

the average overtopping rates and (iii) the individual overtopping volumes in order to (iv) improve the accuracy of the overtopping prediction formulae.

To meet these objectives, 2D hydraulic model tests are performed in the wave flume at Ghent University, measuring wave conditions and the overtopping. The test programme of the model tests is designed according to the main objectives defined for the research. The range of steep low-crested structures is fully covered, with slope angles α from mild to vertical structures and relative crest freeboards R_c/H_{m0} from large to zero. Moreover, the effect of the relatively shallow water conditions on the overtopping rates for non-breaking conditions on steep low-crested structures is also studied by varying the relative wave height H_{m0}/h for relatively deep water conditions, transitional conditions and relatively shallow water conditions. The overtopping reduction caused by the roughness of the structure slope is included in the research as it is one of the main parameters that drive the overtopping process.

In total, 1211 overtopping tests are performed, with the data divided in four different datasets: UG13, UG14, UG15 and UG16. The UG13 dataset focuses on steep low-crested structures for relatively deep water conditions, while UG14 focuses on the transitional zone of relative depths and UG15 on relatively shallow water conditions. The UG16 dataset covers artificial roughness elements (blocks, ribs and stepped revetments) on the structure slope to analyse the effect of roughness on the overtopping rates of steep low-crested structures.

The average overtopping rates of all the tests are processed and analysed with respect to the governing parameters of the overtopping process. The results are compared to the existing overtopping prediction formulae to assess their accuracy for steep low-crested structures. The accuracy is measured by calculating the root mean square error (RMSE) and the bias of each prediction. The results indicate that the existing prediction are in general accurate in predicting the overtopping for steep low-crested structures, although underpredicting the results for very small relative freeboards and the zero freeboard case, while for very steep slopes there is an underprediction for large relative freeboards. There is an increase of the average overtopping for large relative crest freeboards due to relatively shallow water conditions. However, this increase is within the prediction band of the existing prediction formulae. To solve the inaccuracies of the existing predictions, a new average overtopping prediction formula is suggested. This formula is fitted through existing overtopping data and the new data obtained in this research. The new prediction improves the accuracy for very steep slopes and the zero freeboard case while maintaining the accuracy for the rest of ranges. The overtopping reduction due to artificial roughness elements decrease for steeper slopes.

The reduction is larger for ribs than for blocks as the surface coverage is larger. For stepped revetments, this reduction is decreasing for increasing values of the surf similarity parameter $\xi_{m-1,0}$. If the still water level is close to the highest edge of a step, this reduction is larger due to the interaction between the incident and reflected waves on the step front.

The probability distribution of the individual overtopping volumes follow a two-parameter Weibull distribution described by the scale factor A and the shape factor B . The probability of overtopping P_{ow} is the percentage of the incident waves that overtop the structure. These three parameters are analysed for all the tests with respect to the governing parameters of the overtopping. The A factor is described by B and P_{ow} due to the volumes being Weibull distributed. A relation of B with the slope angle α is found for very small and zero relative freeboards, while for large relative freeboards the B values are constant for all the slope angles considered. The existing B prediction formulae are underpredicting the values for very small and zero relative freeboards. The probability of overtopping P_{ow} for the zero freeboard case is theoretically 1 (all the incident waves are overtopping). However, the data show that these values are ranging from 0.8 to 1 due to the interaction between the incident and reflected waves. The P_{ow} values decrease for larger relative freeboards and for steeper slopes. New prediction formulae for B and P_{ow} are presented, fitted through the datasets obtained in this research and the UG10 dataset. The new prediction formulae for B and P_{ow} solve the inaccuracies of the existing formulae. The roughness elements on the slope do not influence the values of A , B and P_{ow} compared to smooth slopes.

The knowledge gap of wave overtopping for steep low-crested structures has been filled in this research by acquiring new overtopping data, analysing its results and deriving conclusions that improve the knowledge about the wave overtopping process.

Chapter 1

Introduction

Wave overtopping is a key process in coastal protection. The assessment of the wave overtopping rates is an important aspect in the design of coastal structures. Overtopping events can result in threat to human lives, damage of property and infrastructure and economic losses if the sea defence structure is not correctly designed or is damaged. Traditionally the average wave overtopping rate was the only overtopping parameter considered in the design, although recent insight reveals that individual wave overtopping should be considered also as a key design parameter of sea defence structures. A good knowledge of the physics behind wave overtopping is therefore necessary to improve the safety of coastal structures and to minimize the potential risks.

1.1 Wave Overtopping

During wave attack, waves run up the slope of coastal structures (seawall, dikes, breakwaters, etc.) When the wave run-up is high enough, the waves will reach and pass the crest of the structure, which is defined as wave overtopping. A different form of overtopping can occur when waves break on the seaward slope of the coastal structure and part of the splash goes over the crest of the structure. The former type is called green overtopping, while the latter is called white overtopping. Another possibility is that the water is carried over the crest of the structure as a spray by action of the wind, although is less relevant in volume.

The wave overtopping process is ruled by various parameters, which can be divided in structural and wave parameters. Figure 1.1 shows a sketch of the most important of these parameters used in this research. The structural parameters are the crest freeboard of the structure R_c from the still water

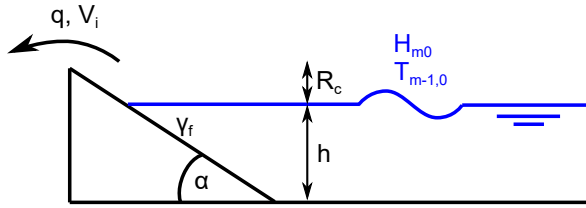


Figure 1.1: Sketch of the main wave and structural parameters governing the overtopping process.

level (SWL), the slope angle of the structure α , the water depth at the toe of the structure h and the roughness of the slope (represented by the influence factor for roughness elements on the slope, γ_f). The wave parameters are the spectral incident wave height at the toe of the structure H_{m0} and the spectral incident wave period at the toe of the structure defined by $T_{m-1,0} = m_{-1}/m_0$ (where m_{-1} is the first negative moment of the spectrum, and m_0 is the zeroth moment of the spectrum). The overtopping can be analysed with respect to the average overtopping rates q (with units of volumetric flow rate m^3/s) and the individual overtopping volumes V_i (with units of volume m^3).

Other parameters of use when studying the overtopping process are the linear wavelength $L_{m-1,0}$, the wave steepness $s_{m-1,0}$ and the surf similarity parameter $\xi_{m-1,0}$. The linear wavelength is defined in Eq. 1.1:

$$L_{m-1,0} = \frac{gT_{m-1,0}^2}{2\pi} \tanh\left(\frac{2\pi h}{L_{m-1,0}}\right) \quad (1.1)$$

The wave steepness is defined in Eq. 1.2:

$$s_{m-1,0} = \frac{H_{m0}}{L_{m-1,0}} \quad (1.2)$$

The surf similarity parameter is defined in Eq. 1.3 and it is used to determine the type of wave breaking occurring:

$$\xi_{m-1,0} = \frac{\tan \alpha}{\sqrt{s_{m-1,0}}} \quad (1.3)$$

1.2 Application of Steep Low-Crested Structures

Wave overtopping prediction formulae are widely available in scientific literature for various structural and wave conditions. Recent physical model research was focused on improving wave overtopping prediction by enlarging

the range of the application of the existing prediction formulae. Extensive research was done in the CLASH project (De Rouck et al., 2009) which consisted of physical model tests and field measurements of wave overtopping for rubble mound breakwaters and smooth slopes with various foreshore geometries, for both regular and irregular sea states. The CLASH project resulted in a very detailed database of wave overtopping results for the aforementioned conditions, and the development of neural networks on wave overtopping (e.g., Verhaeghe et al., 2008). The EurOtop (2007) manual proposed different wave overtopping prediction formulae based on the improved knowledge provided by the CLASH database.

Despite the huge amount of overtopping data collected with the CLASH project, there were still various data ranges that were not covered by the project. One of those ranges was for steep and very steep slopes with small, very small and zero relative freeboards: the so called steep low-crested structures, formed by structures with slope angles $2 > \cot \alpha \geq 0$ and relative crest freeboards $0.8 > R_c/H_{m0} \geq 0$.

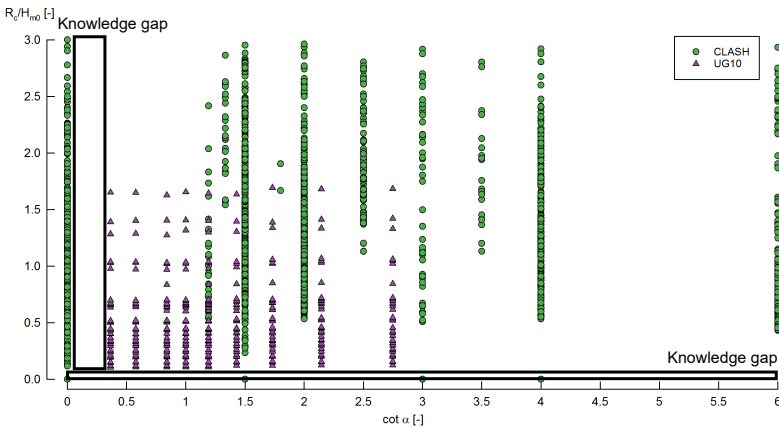


Figure 1.2: Range of slope angles $\cot \alpha$ and relative crest freeboards R_c/H_{m0} of the CLASH database and the UG10 dataset, identifying the knowledge gaps for steep low-crested structures.

Experiments carried out in Ghent University (Belgium) within the PhD research of Victor (2012) covered partially the steep low-crested structures knowledge gap of the CLASH database, forming the so called ‘UG10’ dataset. This dataset covers the range of slope angles $2.75 \geq \cot \alpha \geq 0.36$ and $1.69 \geq R_c/H_{m0} \geq 0.11$. However, not the whole range of slope angles and relative crest freeboards was covered by the UG10 dataset, as the initial focus of that PhD research was on floating wave energy converters with an overtoppable slope. As a result, there are still knowledge gaps in the scientific

literature on wave overtopping for very steep slopes and vertical walls, with very small and zero freeboards, which cover useful geometries for coastal structures. These knowledge gaps are seen in Figure 1.2, for slope angles $0 \leq \cot \alpha \leq 0.27$ and relative freeboards $0 \leq R_c/H_{m0} \leq 0.11$. Moreover, another knowledge gap for the effect of roughness on the overtopping rates of the steep low-crested structures is also existing.

The range of steep low-crested structures is interesting both for coastal structures and wave energy devices. The low-crested coastal structures are becoming of increasing importance due to the sea level rise associated with climate change, and vertical structures are widely used as sea defence structures. Wave energy converters (WECs) of the overtopping type benefit from the increased overtopping rates that the steep low-crested structures provide. These two applications of steep low-crested structures are explained in Section 1.2.1 and Section 1.2.2 respectively, together with the use of roughness elements on coastal structures to reduce the overtopping.

The definition ranges of relative crest freeboard R_c/H_{m0} and slope angle α that are used in this dissertation are shown in Table 1.1 and Table 1.2, respectively. These ranges and their nomenclature are based on the UG10 dataset. They should not be taken into consideration for design purposes as they may not correspond to the common definitions found in typical coastal structures.

Table 1.1: Range definition of slope angle α .

Slope Angle	$\cot \alpha$
Mild slopes	$\cot \alpha \geq 2$
Steep slopes	$2 > \cot \alpha > 0.27$
Very steep slopes	$0.27 \geq \cot \alpha > 0$
Vertical structures	$\cot \alpha = 0$

Table 1.2: Range definition of relative crest freeboards R_c/H_{m0} .

Relative Crest Freeboard	R_c/H_{m0}
Large relative freeboards	$R_c/H_{m0} \geq 0.8$
Small relative freeboards	$0.8 > R_c/H_{m0} \geq 0.11$
Very small relative freeboards	$0.11 > R_c/H_{m0} > 0$
Zero freeboard	$R_c/H_{m0} = 0$

1.2.1 Coastal Structures

Climate change is causing a sea level rise and an increase in storminess. For this reason, the crest freeboard of existing coastal structures is expected to be reduced during severe storms, increasing the risk of catastrophic overtopping and threatening the infrastructure and the lives of the people in the proximities of the worldwide coasts.

Overtopping knowledge on low-crested structures is needed to assess the safety of the existing coastal structures affected by the sea level rise. Also the knowledge should be applied to the design of new coastal structures as the sea level rise should be accounted for into the design phase to build safe coastal protections.

From an economic point of view, the design of low-crested structure leads to more economical structures as the overdesign is prevented while keeping the same level of coastal protection, as long as the overtopping rates are below the limits. The costs decrease comes from a reduction in the materials to build the coastal protection, which amounts to a large percentage of the total costs of the structure.



Figure 1.3: Vertical breakwater during a storm event in 2012 (Mount Batten, UK).
Photo: Declutter

The limit case of the (very) steep slopes are the vertical structures with $\cot \alpha = 0$, which are widely used as sea defence structures (Figure 1.3).

Vertical structures are usually used in harbour protection as they facilitate the berth of vessels on one of the sides. A vertical wall protection can also be designed in combination with a sloping dike with a shallow foreshore, a cross section seen on the Belgian coast. Although this type of structures has been thoroughly researched in the past, they can be included in the low-crested structures knowledge gap as the overtopping knowledge available for very small and zero freeboards is very limited.

Wave overtopping simulators simulate overtopping discharges for all kinds of wave conditions. The main goal of such devices is to test the strength of various types of seaward slopes covers for different storm conditions, and also to demonstrate how wave overtopping looks like. Various wave overtopping simulators have been developed and are functioning (Van der Meer et al., 2010, 2011; Thornton et al., 2011). To simulate real overtopping events, knowledge about individual wave overtopping volumes is necessary. The probability distribution of the individual volumes that determines the maximum volumes during a storm event depends on the type of structure. The determination of the tolerable overtopping discharges for structural design also depends on the maximum individual volume during a storm. The safety of pedestrians, vehicles and infrastructure is taken into account to determine the tolerable discharges. A good knowledge of the probability distributions depending of the type of structure will improve the simulation of the extreme overtopping events by the overtopping simulators and the design guidelines on the tolerable discharges. Therefore, analysing the individual overtopping is also necessary to fill the knowledge gap on wave overtopping for steep low-crested structures.

The roughness of the slope is another important factor that rules the overtopping process. An increased slope roughness generates more energy dissipation. With less energy available, less waves run up the slope of the structure and there is less overtopping. This roughness can be added artificially to a smooth slope to induce energy dissipation and the reduction of overtopping, or this roughness can be part of the working mechanism of the structure, as it is the case of rubble mound breakwaters. The armour layer of the rubble mound breakwater —formed either by rocks or concrete units— creates the roughness that, together with the breakwater permeability, reduces the overtopping rates.

The simplest roughness element that can be added to a smooth slope to create an artificial roughness is a block. Adding a number of blocks with a regular pattern on the slope of the structure dissipates the energy of the incoming waves. The total overtopping reduction depends on the surface area covered by the blocks and their dimensions. To increase the effectiveness of the overtopping reduction, the blocks can be transformed into ribs, which are

longer than blocks. Ribs increase the surface coverage of the slope increasing the overtopping reduction. The practical application of blocks and ribs is for dike revetments, normally with a mild slope.

Another solution to reduce the overtopping rates is to build stepped revetments. A stepped revetment consists of implementing steps of specific dimensions in a staircase-like pattern to reach the required crest height of the revetment. A stepped revetment can be more accessible and visually attractive than revetments with blocks or ribs, increasing the social acceptance of such kind of structures as they extend their use as sea defence structures to become city or coastal landmarks (Kerpen, 2017). Moreover, these structures are very effective in reducing the overtopping, requiring a smaller crest freeboard to reach a similar coastal protection against overtopping than other structures that induce less wave energy dissipation. Also, low-crested structures are more economical to build.

Numerous examples of stepped revetments can be found all over the world, such as the coastal protection shown in Figure 1.4 in Cleveleys (UK), the Sea Organ in Zadar (Croatia), the inner harbour protection in Baiona (Spain), or the outer breakwater in Varna (Bulgaria).



Figure 1.4: Stepped revetment as coastal protection in Cleveleys (UK). Photo: Philip Platt.

The overtopping reduction due to the roughness of the slope has been thoroughly investigated in the literature. For rubble mound breakwaters there are several investigations detailing the overtopping reduction coefficients to be applied for each type of armour unit. However, the slopes of the typical rubble mound breakwaters used as sea defence structures are between 1:3 and 1:1.5, which are in general milder than the considered range of steep low-crested structures. For artificial roughness elements, the investigation has been focused on blocks and ribs (EurOtop, 2016). Research of stepped revetments is also present in the scientific literature (Van Steeg et al., 2012; Kerpen, 2017, among others).

However, for blocks and ribs, and stepped revetments there is a knowledge gap for steep low-crested structures. The relations of the parameters that influence the overtopping process are not known for (very) steep slopes. Also for low-crested structures the research is scarce, even though it is an area of interest as aforementioned. Increasing the knowledge about the effect of roughness on overtopping for steep low-crested structures is of interest to expand the design possibilities of stepped revetments towards the steep slopes and to reduce the crest freeboard of the structures which are then more economical to build.

A permeable structure reduces the overtopping rate, as energy dissipation occurs if waves penetrate in the structure, reducing the amount of energy available for the run-up and overtopping process. This includes all type of structures (rubble mound breakwaters, dikes, stepped revetments, etc.) However, this effect of the permeability on overtopping is outside the scope of this research, which focuses only on smooth slopes in order to analyse the effect of other wave and structural parameters in the overtopping.

1.2.2 Overtopping Wave Energy Converters

Climate change and the associated sea level rise has caused a change in the policies of governments around the globe, impulsing the move from fossil fuels to renewable energies. The European Union has been one of the leaders in this process by presenting in 2010 an ambitious plan within the framework of the Europe 2020 strategy to limit the effects of climate change. By 2020, the greenhouse gas emissions should be a 20% lower than 1990 levels, 20% of energy should come from renewable sources, and there should be an increase in the energy efficiency of 20%. To achieve these targets the blue energy field and the research on wave energy has been developing in recent years, covering different types of wave energy converters (WECs).

One type of WEC is the overtopping wave energy converter (OWEC), based on the working principle of waves running-up a slope and overtopping

(i.e., kinetic and potential energy of the waves) into a reservoir (potential energy), which is emptied into the ocean through a set of low-head turbines, generating electricity (Falcão, 2010). Various OWEC prototypes were developed in the past for offshore and onshore application. The Wave Dragon (Kofoed et al., 2006) and the WaveCat (Fernandez et al., 2012) are offshore OWECs, with a working principle based on a floating structure with reflectors to guide the incoming waves towards a ramp in front of a reservoir where the water is collected. An onshore OWEC integrates a reservoir within a sea defence structure such as breakwaters at a lower level than the crest of the sea defence structure in order to capture the overtopped water of the incident waves. Examples of onshore OWECs developed are the Tapchan (Tapered Channel Wave Power Device, Mehlum (1986)), the SSG (Seawave Slot-cone Generator, Margheritini et al. (2009), see Figure 1.5), a multi-level OWEC with three reservoirs on top of each other and, more recently, the OBREC (Overtopping BReakwater for Energy Conversion, Vicinanza et al. (2014)).

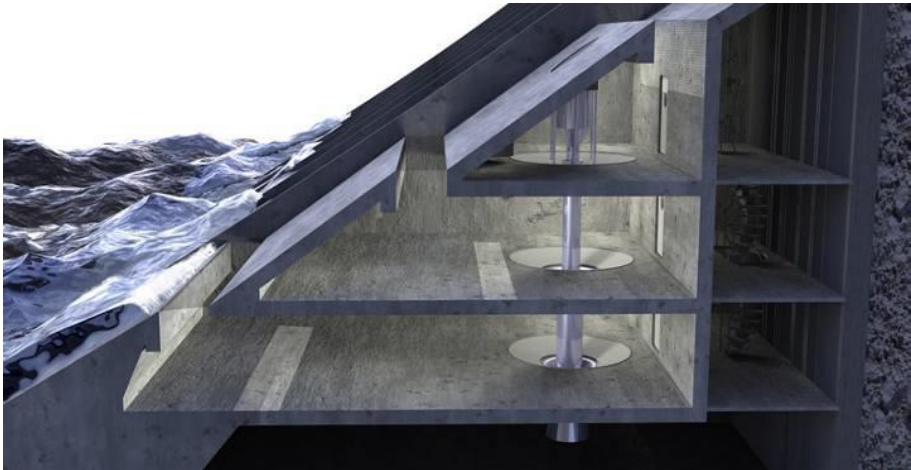


Figure 1.5: Artistic representation of a 3-level SSG (Vicinanza et al., 2012)

The geometry is a major consideration when designing an OWEC, as its design will determine the run-up and overtopping at the crest of the device. For OWEC design, the prediction of wave overtopping is crucial to correctly assess the capacity and production of the OWEC, and to design a structurally safe device.

Research progress on sea defence structures can be of use when predicting overtopping as the wave overtopping research of this type of structures is very extensive. However, while a sea defence structure protecting the coast requires a minimization of the overtopping rates for extreme wave conditions, an OWEC should be designed to maximize the overtopping rates (usually

for operational wave conditions) and therefore the electricity output. This is only possible for ranges of geometries for sea defence structures previously unexplored in the scientific literature.

Kofoed (2002) developed further the idea of using the overtopping research initially focusing on sea defence structures for application for OWEC research. Based on physical model tests of fixed OWECs with a limited draft, a uniform slope and a single reservoir, he obtained correction factors for the overtopping prediction formula published in the EurOtop (2007) manual. With these correction factors, the range of the prediction formula is extended towards ranges of slope angles and crest freeboards more suitable for OWECs.

Victor and Troch (2012b) studied the performance of wave overtopping with respect to the OWEC geometry and characteristics. It was stated that the most convenient range would be for slope angles α from mild to vertical walls ($6 \geq \cot \alpha \geq 0$), as the wave breaking for this range of slopes is limited, not reducing the energy of the waves and therefore the run-up and overtopping. For relative crest freeboards R_c/H_{m0} (where R_c is the crest freeboard and H_{m0} the incident spectral wave height at the toe of the structure) the most suitable range would be for small relative crest freeboards up to the zero freeboard case ($R_c/H_{m0} < 1.5$), as the overtopping rate increases for lower R_c/H_{m0} . A range of structures with interest for OWECs is formed by steep low-crested structures as for this range the overtopping is maximized due to the very small freeboards. Figure 1.6 shows this range of steep low-crested structures as a subset of the optimal range for OWECs suggested by Victor and Troch (2012b). An accurate overtopping prediction for steep low-crested structures is necessary to avoid an underdesign (leading to a reduced operational time) or overdesign (leading to an increase of costs) of the device.

For the various OWEC prototypes mentioned in this section, wave overtopping studies have been published. Tedd and Kofoed (2009) studied the overtopping rates on a Wave Dragon prototype installed in Denmark, obtaining flow time series and individual overtopping distributions. Vicinanza et al. (2012) performed 2D small-scale physical model tests to study the overtopping rates and the hydraulic efficiency of the SSG, while Zanuttigh et al. (2009) studied the wave reflection from the same device. Vicinanza et al. (2017) studied the overtopping rates and the structural response of the OBREC, both in 2D small-scale physical model tests and in a full-scale prototype built in Naples (Italy). Numerical models have also been developed to predict the overtopping rates for OWECs (Liu et al., 2008) and for specific prototypes such as the OBREC (Di Lauro et al., 2017).

All these overtopping studies were performed for specific OWEC prototypes, and they are not valid for a more general prediction of the overtopping

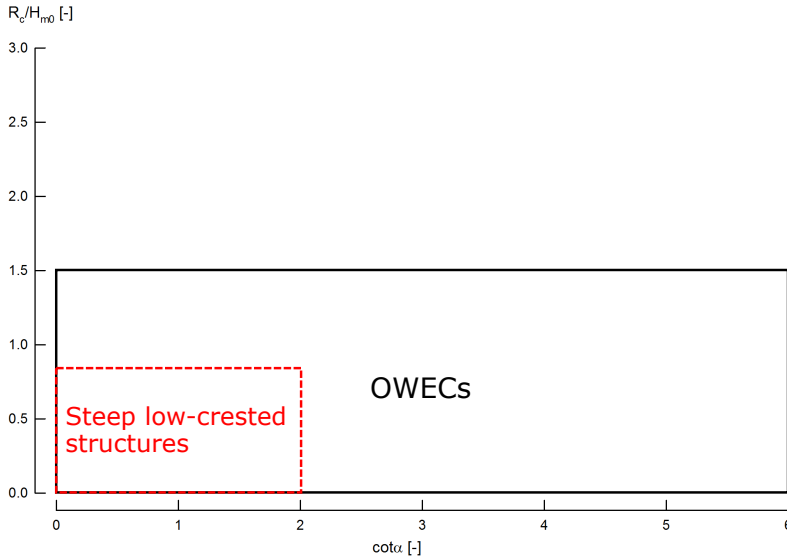


Figure 1.6: Range of slope angles $\cot \alpha$ and relative crest freeboards R_c/H_{m0} for OWECs according to Victor and Troch (2012b) and steep low-crested structures.

rates as the wave conditions and geometries tested are specific for each device. From these studies it is not possible to extrapolate a general prediction of the overtopping rates for different wave and structural conditions. However, the research of wave overtopping for sea defence structures offers a large number of wave overtopping prediction formulae suitable for a wide range of structural and wave conditions.

1.3 Research Objectives

The objectives of this research are described in this section and are addressing the presented knowledge gaps in Section 1.2. These objectives should be taken as general objectives. Specific objectives based on the main objectives will be determined in Section 2.5 after a literature study is made. The four main research objectives are:

Increase knowledge on wave overtopping performance for steep low-crested structures.

As outlined during this chapter, the main objective is to increase the knowledge on wave overtopping by filling the gaps for steep low-crested structures

with impermeable slopes. This type of structures are of use as coastal structures, as the sea level rise is lowering the available crest freeboard of existing coastal structures, into the range of low-crested structures. Another use of these structures is for overtopping wave energy converters (OWECs), as the steep low-crested structures maximize energy production due to the larger overtopping produced by these structures.

Analysis of average overtopping rates for steep low-crested structures.

The average overtopping rate is a key design parameter of coastal structures. The parameters that rule the overtopping process (Figure 1.1) affect differently the average overtopping rates depending on the ranges considered. For OWECs it is also important to know the average overtopping rates to correctly design the device for the appropriate energy production according to the wave climate. For steep low-crested structures, the knowledge available is scarce, and therefore its analysis can be of added value to the scientific literature.

Analysis of individual overtopping volumes for steep low-crested structures.

The knowledge of the distribution of the individual overtopping volumes of a storm event allows to design safer coastal structures that can withstand the extreme events in each storm. The individual overtopping distribution is affected by the same parameters (Figure 1.1) as the average overtopping rates. However, the influence of these parameters on the individual overtopping distribution has not been thoroughly studied in literature, especially for steep low-crested structures. A study of the individual overtopping distributions for these structures will improve the knowledge available and be of use for the design and assessment of coastal structures and OWECs.

Improvement of the accuracy of existing prediction formulae.

Literature presents several prediction formulae both for the average overtopping rates and the individual overtopping distributions. These formulae are widely used to predict the average overtopping rates or the parameters that define the individual volumes distribution. These formulae use to be semi-empirical, i.e., fitted through measured data obtained in physical model tests or in prototype experiments. The empirical origin of most of the formulae means that only specific wave and structural parameter ranges are covered by

them, leaving other ranges for which the formulae are not validated, therefore not being applicable, or for which the accuracy of the prediction is low.

One of these ranges is for steep low-crested structures, for which a small number of prediction formulae are available, with a limited accuracy as the number of model tests available for this type of structures is low. New predictions for steep low-crested structures can be obtained with an improved accuracy.

1.4 Outline

The four objectives mentioned in Section 1.3 to increase the knowledge of wave overtopping on steep low-crested structures are addressed in this dissertation. The dissertation consists of seven chapters, each of them covering a specific part of the research.

Chapter 2 reviews the scientific literature available about wave overtopping, with a special focus on wave overtopping for steep low-crested structures. The various prediction formulae for average and individual overtopping are analysed and compared with each other, identifying the knowledge gaps that will be filled by this research. At the end of the chapter, a re-definition of the main research objectives is made, detailing more specific objectives.

Chapter 3 defines the methodology followed in the design of the experimental phase of the research, which is to perform 2D hydraulic model tests in a wave flume. Chapter 4 explains the experimental setup used to perform the experiments and the test programme followed during the research as designed in the methodology of the experiments.

Chapter 5 presents the average overtopping results of the experiments, analysing them with respect to various parameters and comparing them with the average overtopping prediction formulae available in literature. As an improvement of these predictions is possible, a new prediction is fitted through the new data acquired within this research, and it is described in this chapter.

Chapter 6 presents the distribution of the individual overtopping volumes and the parameters that describe it. The parameters are analysed and compared to the existing prediction formulae. New predictions are proposed to improve their accuracy for steep low-crested structures.

Finally, Chapter 7 presents the conclusions of the research and gives suggestions on how to continue further the research.

Chapter 2

Literature Review on Wave Overtopping

The scientific literature available on wave overtopping prediction is very extensive. This chapter summarizes the literature about wave overtopping for steep low-crested structures, including the overtopping prediction formulae available. The focus is both on average and individual overtopping. The literature about stepped revetments is also reviewed and presented in this chapter.

2.1 Wave Overtopping Prediction in Perspective

Overtopping is one of the main parameters that define the safety and the design of coastal structures. Therefore, it is necessary to accurately predict the wave overtopping rates. Since the early stages of coastal engineering research, the overtopping prediction was defined by empirical formulae, as the chaotic behaviour of overtopping is impossible to predict with analytical methods, except for idealized wave theories and structures. These formulae are empirical, based on data acquired on physical model tests that reproduce coastal structures on small scale, conducted on research facilities such as wave flumes (for 2D tests) and wave basins (for 3D tests).

One of the first examples of such research was performed by Saville and Caldwell (1953) and Saville (1955), who conducted physical model tests on various scales (1:30 and 1:17) in a wave flume, measuring wave run-up and wave overtopping on smooth slopes, composite slopes and stepped slopes under regular waves. Weggel (1976) used these data to propose an overtopping prediction formula for regular waves, including an estimation of scale effects

as both small-scale and large-scale tests were performed. Various authors (Tsuruta and Goda, 1968; Goda, 1971; Battjes, 1974; Ahrens, 1977) extrapolated the overtopping data of regular waves to predict the wave overtopping generated by irregular waves, using the procedure called by Tsuruta and Goda (1968) "linear summation". This procedure assumes that an irregular sea state can be described by a summation of the individual waves belonging to different regular sea states.

Novel physical model tests with irregular waves were conducted by Goda and Kishira (1975) for vertical structures. Further analysis allowed to determine the effects of the foreshore geometry and the wave steepness on the overtopping rates, and to compare the new overtopping data with the extrapolation made from regular waves in Goda (1971). Owen (1980) and Owen (1982) also performed small-scale overtopping tests (scale 1:25) with irregular waves on seawalls with different geometries, obtaining an overtopping prediction formula with an exponential relationship, although only valid for plunging (i.e., breaking) waves.

Douglass (1984) and Douglass (1986) made an overview of the different overtopping predictions available at that time and concluded that more overtopping data for irregular waves were necessary, as the accuracy of the existing formulae was difficult to determine. The need of overtopping prototype measurements or large-scale model tests was also suggested for a better estimation of the scale effects on wave overtopping.

Over the next decade the physical model research on wave overtopping moved towards expanding the knowledge for various wave conditions (e.g., shallow water, short crested waves, oblique waves, etc.) and structural conditions (e.g., roughness of the slope, influence of a berm, etc.) De Waal and Van der Meer (1992) performed physical model tests introducing these factors to assess a possible influence on the overtopping rates. The authors presented a novel overtopping prediction formula for non-breaking waves relating the crest freeboard R_c with the 2% run-up on a non-overtopped slope $R_{u2\%}$.

Van der Meer and Janssen (1994) presented two different overtopping prediction formulae depending on breaking or non-breaking wave conditions. These formulae would be widely used in the coming years, with the average overtopping rate being dependent on the incident spectral wave height H_{m0} and the crest freeboard R_c . The authors also investigated the individual overtopping volumes of each test, presenting a probability distribution function of the individual volumes following a three-parameter Weibull distribution, the maximum volume of a single wave and a formula to predict the number of overtopping waves.

Franco et al. (1994) presented a physical model dataset —started by de Ger-

loni et al. (1991)— about wave overtopping on vertical and composite breakwaters for both average rates and individual events. A new average prediction formula for the case of vertical walls in relatively deep water conditions was presented. This dataset was continued later by Franco and Franco (1999) extending it with 3D overtopping tests to measure the effect of oblique and short-crested waves. Allsop et al. (1995) and McBride et al. (1995) also investigated overtopping on a vertical breakwater, proposing a prediction formula for relatively shallow water conditions and introducing the parameter h^* to assess the impulsiveness of the waves on vertical structures. Besley et al. (1998) also presented a overtopping prediction formula for vertical structures under impulsive conditions in shallow foreshores. For very shallow foreshores, Van Gent (1999) conducted experimental model tests and proposed a prediction formula, later complemented by the concept of equivalent slope by Altomare et al. (2016) to solve the prediction inaccuracies for certain very shallow foreshores.

Between 2002 and 2004, the CLASH project, an European Union research project coordinated by Ghent University (De Rouck et al., 2009; van der Meer et al., 2009) was developed to study the wave overtopping process for various types of structures and wave conditions. One of the major achievements was to obtain a database consisting of more than 10,000 overtopping tests on all kinds of coastal structures, each one described by 31 wave and structural parameters, such as the water depth, incident wave conditions, slope angles of the structure, etc. The focus of the project was to generate a homogeneous overtopping database formed by tests of existing projects, to fill overtopping knowledge gaps on missing parameters and structures. The CLASH database contained not only physical model tests on small and large scales, but also field overtopping measurements in Ostia, Italy (Franco et al., 2009), Zeebrugge, Belgium (Geeraerts et al., 2009) and Samphire Hoe, UK (Pullen et al., 2009). Special attention was also placed in the socio-economic impact of wave overtopping (Bouma et al., 2009), the overtopping performance of different armour units for rubble mound breakwaters (Bruce et al., 2009), and the 3D effects of wave overtopping (Lykke Andersen and Burcharth, 2009). The CLASH project was also complemented with overtopping numerical modelling (Ingram et al., 2009).

From the CLASH project and the large amount of overtopping tests contained in it, various research was developed. Various wave overtopping prediction formulae were based on CLASH data (Victor and Troch, 2012b; Van der Meer and Bruce, 2014; Goda, 2009), and neural networks to predict wave overtopping were also developed, introducing a new concept in wave overtopping prediction. In her PhD thesis, Verhaeghe (2005) developed a two-phases neural network trained with the CLASH database, predicting whether

overtopping would occur in a specific case, and the value of the average overtopping rate (Verhaeghe et al., 2008). Van Gent et al. (2007) also developed a neural network trained with CLASH overtopping data, and more recently Zanuttigh et al. (2016) presented a new neural network trained with an extended CLASH dataset.

The overtopping neural networks are widely used to predict the average overtopping rates of coastal structures with various complex geometries. The Verhaeghe et al. (2008) and the Van Gent et al. (2007) neural networks are, however, not applicable for structures with zero freeboard, as this case is outside the range of application of both neural networks. Also, for structures with very small relative freeboards these neural networks are not giving a good prediction of the overtopping rates. As the zero freeboard case and the very small relative freeboards are a substantial part of this research, it was decided not to use neural networks as a comparison tool.

In recent years, the overtopping research has been focused on filling the knowledge gaps that the CLASH project left in the literature. During his PhD research, Victor (2012) obtained a new overtopping dataset on steep low-crested structures which was used in the fitting of the Victor and Troch (2012b) and Van der Meer and Bruce (2014) overtopping prediction formulae for this type of structures. Victor et al. (2012) and Hughes et al. (2012) presented predictions of the probability distribution of individual overtopping volumes also for steep low-crested structures.

The literature review presented in this chapter is not intended to provide a full review of all the published research related to wave overtopping. Instead, the focus is on the most relevant overtopping research and prediction formulae related to the topic of this dissertation on steep low-crested structures.

2.2 Wave Overtopping Manuals

The literature on overtopping and other aspects of coastal engineering has been summarised and presented in the form of manuals. These manuals are very convenient to use by researchers and professionals in the coastal engineering field as they gather in a concise and schematized form all the knowledge available. The aim of the manuals range from a wide theoretical study of coastal engineering to the more specific aspects of wave overtopping applied to the design of coastal structures.

The first manual available was the Shore Protection Manual (SPM) (US Army Corps of Engineers, 1973), presenting all the coastal engineering knowl-

edge available at the time, and specifically a method to estimate wave overtopping due to irregular waves based on the research carried out by the US Army Corps of Engineers Coastal Engineering Research Center. Four editions of the Shore Protection Manual were published from 1973 through 1984. Years later, the Coastal Engineering Manual (CEM) (US Army Corps of Engineers, 2002) was presented as an update of the SPM. The CEM is divided in six parts, dealing with all aspects of coastal engineering (wave theories, wave actions, wave transformation processes, hydrodynamics, sediment transport, etc.). It is the reference manual in the field of coastal engineering with a very extended use. The Rock Manual (CIRIA et al., 2007) is also a reference manual for rubble mound breakwater design, containing an overview of overtopping influence factors depending on the different types of armour units considered.

Different manuals dealing specifically with wave overtopping were published in Europe. In the UK, Besley (1999) presented the Environment Agency Manual on Overtopping, which contains an overview of different research related to wave overtopping on smooth and rough coastal structures, including the research of Owen (1980) and Van der Meer and Janssen (1994). In The Netherlands, TAW (2002) presented the Technical Report Wave Run-up and Wave Overtopping at Dikes. The manual summarizes the Dutch research of the previous years on wave run-up and wave overtopping. In Germany, EAK (2002) published guidelines and recommendations for the design of coastal structures. In a comparable effort to the CEM, the EAK (2002) covers a wide range of knowledge around coastal engineering, including wave overtopping (EAK, 2002, chapter 4).

With the goal of gathering all the overtopping knowledge obtained by European researchers, the EurOtop (2007) manual was published. The manual provides guidance on the analysis and prediction of wave overtopping for sea defence structures attacked by wave action. It is not intended to provide full guidelines on how to design and construct sea defence structures as other manuals do (e.g., CIRIA et al., 2007). The publication of the EurOtop (2007) manual revises and updates the British, Dutch and German manuals aforementioned (Besley, 1999; TAW, 2002; EAK, 2002). The formulae contained in the EurOtop (2007) manual assess the overtopping for different types of structures –smooth slopes, rough slopes, vertical walls, composite breakwaters, (very) shallow foreshore– and wave conditions –breaking and non-breaking, oblique wave attack, short-crested waves–. A 2nd edition of the EurOtop manual was published in 2016 including new research on wave overtopping published on the last ten years (EurOtop, 2016).

This dissertation contributes to further improve the existing wave overtopping manuals by filling the knowledge gaps on wave overtopping for steep low-crested structures for average and individual overtopping.

2.3 Average Overtopping Rate Prediction Formulae

One of the main parameters to consider to design a sea defence structure and assess its level of safety is the average overtopping rate —i.e., the volume of water passing over the structure per unit of time—. The research about wave overtopping has been focused on determining the average rates for various types of structures. The main prediction formulae available in the scientific literature are presented in this section divided by type of structure.

The mean value approach of the prediction formulae is given throughout this section and the rest of this chapter. In this approach, the coefficients are considered as stochastic parameters with a normal distribution around an average value μ with a standard deviation σ (also referred to as standard error of the estimate σ_{est}). In some cases, a coefficient of variation σ' is given instead, where $\sigma' = \sigma/\mu$.

The prediction band is an estimate of the interval in which future observations will fall with a certain probability, based on what has been already observed. The 90% prediction band is calculated. The 90% prediction band (5% exceedance lines) of a prediction formulae can be calculated by the expression $\mu \pm 1.64 \sigma$ for each of the stochastic parameters.

The prediction formulae reviewed in this section do not account for the increase in average overtopping rates due to wind action. However, the influence of the wind on the overtopping results, although common in nature, does not have a big influence on the average overtopping rates. The EurOtop (2016) manual quantifies this influence by a factor between 3–4, although the research leading to these values seems to be greatly overestimating the influence of the wind on the average overtopping rates. Instead, the influence of the wind can be accounted for by the uncertainty of the prediction formulae.

2.3.1 Sloping Structures

A coastal structure featuring a mild seaward slope is referred to as a sloping structure. There is no criterion on the definition of sloping structures in the scientific literature, as different authors give various ranges of slope angles α considered as sloping structures.

Van der Meer and Janssen (1994) presented the most used overtopping prediction for sloping structures. The formula was included in the EurOtop (2007) manual and the TAW (2002) manual. The mean value approach of the

average overtopping prediction formulae for sloping structures is presented in Eq. 2.1 (breaking waves) and Eq. 2.2 (non-breaking waves):

$$\frac{q}{\sqrt{gH_{m0}^3}} = \frac{0.067}{\sqrt{\tan \alpha}} \gamma_b \xi_{m-1,0} \exp \left(-4.75 \frac{R_c}{\xi_{m-1,0} H_{m0} \gamma_b \gamma_f \gamma_\beta \gamma_v} \right) \quad (2.1)$$

with a maximum of

$$\frac{q}{\sqrt{gH_{m0}^3}} = 0.2 \exp \left(-2.6 \frac{R_c}{H_{m0} \gamma_f \gamma_\beta} \right) \quad (2.2)$$

In this equation q is the average overtopping rate, H_{m0} is the incident spectral wave height at the toe of the structure and R_c is the crest freeboard, α the slope angle of the structure, and $\xi_{m-1,0}$ the surf similarity parameter (also called Iribarren number). The parameters γ_b , γ_f , γ_β and γ_v are different influence factors for the presence of a berm, roughness of the slope, oblique wave attack and presence of a vertical wall, respectively. The coefficients 4.75 and 2.6 of Eqs. 2.1 and 2.2 are a normally distributed stochastic parameters with an associated standard deviation of $\sigma = 0.5$ and $\sigma = 0.35$ respectively.

The range of application of Eqs. 2.1 and 2.2 is for slope angles α between $1 \leq \cot \alpha \leq 4$ and for relative crest freeboards R_c/H_{m0} between $0.5 \leq R_c/H_{m0} \leq 3.5$. This range is limited to the more conventional geometries (mild slopes with large relative crest freeboards), while for very steep slopes and vertical walls with very small and zero freeboards (i.e., steep low-crested structures) this formula should not be used. This equation is valid for surf similarity parameters $\xi_{m-1,0} \leq 5$ (EurOtop, 2007; TAW, 2002).

Van der Meer and Janssen (1994) fitted the formulae through datasets from different sources formed by tests on various types of structures and wave conditions. The different overtopping influence factors γ were fitted using these data. EurOtop (2007) contains formulae defining these influence factors (see Section 2.3.6).

2.3.2 Influence of Shallow Foreshores on Wave Overtopping

A foreshore in front of the structure (dike) may influence the incident wave conditions at the toe of the dike—and therefore, the overtopping behaviour—causing heavy breaking due to depth limitation when the waves propagate from deep water. Goda (2009) defines as foreshore the section in front of the dike that is horizontal or up to maximum slope of 1:10 (i.e., $\cot \theta > 10$), being θ the angle of the foreshore slope. The Rock Manual (CIRIA et al., 2007)

and the Coastal Engineering Manual (US Army Corps of Engineers, 2002) use different definitions of foreshore related to the different local water levels.

Van Gent (1999) proposed a criterion to characterize the water depth at the toe of the dike and therefore determine whether the foreshore is influencing the wave conditions. This criterion is shown in Table 2.1, where $H_{m0,deep}$ is the incident spectral wave height on deep water, and h is the water depth at the toe of the structure.

Table 2.1: Water depth conditions according to Van Gent (1999).

Depth condition	$H_{m0,deep}/h$ [-]
Very shallow	$H_{m0,deep}/h > 1.5$
Shallow	$1.5 > H_{m0,deep}/h > 0.75$
Intermediate	$0.75 > H_{m0,deep}/h > 0.4$
Deep	$H_{m0,deep}/h < 0.4$

A different criterion is proposed by Nørgaard et al. (2014). The authors consider deep water conditions when $H_{m0}/h \leq 0.2$ and shallow water conditions when $H_{m0}/h \geq 0.5$, while in between values $0.2 < H_{m0}/h < 0.5$ are considered transitional water depth conditions. A similar criterion is proposed by Hofland et al. (2017), using the same parameters as Nørgaard et al. (2014) although with different ranges to define the shallow water conditions. At first sight the Nørgaard et al. (2014) criterion may seem contradictory with the one suggested by Van Gent (1999) in Table 2.1, although both are applicable for structures with low reflection coefficients like dikes and rubble mound breakwaters. However, there are two main differences in these criteria.

The most significant difference is that Van Gent (1999) had always a foreshore slope present (1:10 step, followed by a 1:100 or 1:250 slope) in the experimental tests, while Nørgaard et al. (2014) had a horizontal foreshore. This indicates that, on the one hand, the criterion by Van Gent (1999) is for wave conditions with an influence of the foreshore –i.e., due the geometric characteristics of the foreshore there is not enough water depth available, causing the waves to break– leading to values of the surf similarity parameter $\xi_{m-1,0} < 2-3$. On the other hand, the criterion by Nørgaard et al. (2014) is for wave conditions without any influence of the foreshore, indicating that the waves transform due to the depth limitation without breaking, leading to values of the surf similarity $\xi_{m-1,0} > 2-3$. Also, Van Gent (1999) uses the incident spectral wave height in deep water conditions $H_{m0,deep}$ in the criterion, while Nørgaard et al. (2014) uses the incident spectral wave height at the toe of the dike H_{m0} .

Data show that the heavy wave breaking on (very) shallow foreshores

will cause a drastic increase in the wave period $T_{m-1,0}$, implying a change in the shape of the energy spectrum (Altomare et al., 2016). Due to the very low values of wave steepness $s_{m-1,0}$ at the toe of the dike, the Iribarren number $\xi_{m-1,0}$ (Eq. 1.3) can become very large for the cases of (very) shallow foreshores for mild sloping structures ($\cot \alpha > 2$). For the case of steep and very steep slopes ($0 < \cot \alpha < 2$) the values of the surf similarity parameter can also be very large, although due to the very large values of $\tan \alpha$ (very small values of $\cot \alpha$) of this type of structures. Even though the surf similarity parameter can be similar in these two cases, the wave breaking behaviour is very different. For very shallow foreshores, the waves break while propagating on the foreshore, while for (very) steep slopes the waves are surging (non-breaking).

The EurOtop (2016) manual proposes to use the wave steepness $s_{m-1,0}$ value as criterion for shallow foreshores. The same criterion was applied by Altomare et al. (2016), who suggested that a foreshore can be considered shallow (or very shallow) when the wave steepness at the toe of the dike is $s_{m-1,0} \leq 0.01$ for dikes with slope angles $2 < \cot \alpha < 8$.

Van Gent (1999) proposed an overtopping prediction formula for (very) shallow foreshores, with its mean value approach shown in Eq. 2.3:

$$\frac{q}{\sqrt{gH_{m0}^3}} = 10^c \exp\left(-\frac{R_c}{\xi_{m-1,0} H_{m0} \gamma_f \gamma_\beta (0.33 + 0.022 \xi_{m-1,0})}\right) \quad (2.3)$$

The parameter c is a normally distributed stochastic parameter with a mean value of $c = -0.92$ and a standard deviation $\sigma = 0.24$. Eq. 2.3 is only valid for Iribarren numbers $\xi_{m-1,0} \geq 7$, although the experimental data used by Van Gent (1999) to fit this formula include values of the surf similarity parameter smaller than $\xi_{m-1,0} \leq 5$, raising concerns about the use of this parameter as a criterion to assess the influence of the foreshore in wave overtopping.

Altomare et al. (2016) proposed a new calculation approach –based on considering an equivalent slope by combining the foreshore slope and the dike slope– for the case of very shallow foreshores, as the Van Gent (1999) formula (Eq. 2.3) was overpredicting the results. Given these different definitions of shallow foreshores available in literature, caution is advised when characterizing a foreshore or the water depth conditions.

2.3.3 Steep Low-Crested Structures

As explained in Chapter 1, the definition of steep low-crested structures cover a range of coastal structures with slope angles α from steep ($\cot \alpha < 2$) up

to the limit case of vertical walls ($\cot \alpha = 0$), with relative crest freeboards R_c/H_{m0} from small ($R_c/H_{m0} < 0.8$) up to the limit zero freeboard case ($R_c/H_{m0} = 0$).

Traditionally, the average overtopping prediction formulae available in the scientific literature were not applicable to this range of slope angles α and relative crest freeboards R_c/H_{m0} . However, more recently two different overtopping prediction formulae valid for the range of steep low-crested structures were presented by Victor and Troch (2012b) and Van der Meer and Bruce (2014).

During the PhD research of Victor (2012) on overtopping wave energy converters a new wave overtopping prediction formula was needed which included the operational conditions of these devices that behave as low-crested structures. To fill the knowledge gap for overtopping on this type of structures, he obtained a new overtopping dataset for steep low-crested structures, the so-called 'UG10' dataset (see Table 4.2 in Chapter 4). Victor and Troch (2012b) developed new average overtopping prediction formulae based on the dataset UG10, and the CLASH database for plain vertical walls under non-impulsive conditions with a relative crest freeboard $R_c/H_{m0} < 0.8$ (subsets 106 for small crest freeboards, 107 for zero crest freeboards and 402 for large crest freeboards).

The formulae are divided into 4 different zones (Z1, Z2, Z3, Z4) depending on the values of slope angle α and relative crest freeboard R_c/H_{m0} (Figure 2.1). This provides a high physical insight of wave overtopping, allowing a clear visualization of the physical meaning of the formulae and leading to a better understanding of the dependence of wave overtopping on the slope angle α and relative crest freeboard R_c/H_{m0} . Eq. 2.4 shows the formula to predict the dimensionless average overtopping rate $q/\sqrt{gH_{m0}^3}$ and Table 2.2 shows the expressions for the a and b coefficients as a function of the slope angle α and relative crest freeboard R_c/H_{m0} . The formula in Eq. 2.4 maintains the shape of the EurOtop (2007) formula for non-breaking conditions (Eq. 2.2), with the relative crest freeboard R_c/H_{m0} as governing parameter of the wave overtopping prediction. However, as opposed to Eq. 2.2, the overtopping prediction resulting from Eq. 2.4 is also influenced by the slope angle α .

$$\frac{q}{\sqrt{gH_{m0}^3}} = a_{Victor} \cdot \exp\left(-b_{Victor} \frac{R_c}{H_{m0}}\right) \quad (2.4)$$

For slopes $0 \leq \cot \alpha \leq 1.5$ and (very) small relative crest freeboards $0 \leq R_c/H_{m0} \leq 0.8$ (zone Z1) the effect of the slope angle α on wave overtopping is significant, while for large relative crest freeboards $0.8 \leq R_c/H_{m0} \leq 2$

Table 2.2: Coefficients of Victor and Troch (2012b) formulae (Eq. 2.4) as a function of the slope angle α and relative crest freeboard R_c/H_{m0} .

		Relative crest freeboard R_c/H_{m0}	
		$0 \leq R_c/H_{m0} \leq 0.8$	$0.8 \leq R_c/H_{m0} \leq 2$
cot α	$0 \leq \cot \alpha \leq 1.5$	Z1 $a_{\text{Victor}} = 0.033 \cdot \cot \alpha + 0.062$ $b_{\text{Victor}} = 3.45 - 1.08 \cdot \cot \alpha$	Z2 $a_{\text{Victor}} = 0.2$ $b_{\text{Victor}} = 4.88 - 1.57 \cdot \cot \alpha$
	$1.5 \leq \cot \alpha \leq 2.75$	Z3 $a_{\text{Victor}} = 0.11$ $b_{\text{Victor}} = 1.85$	Z4 $a_{\text{Victor}} = 0.2$ $b_{\text{Victor}} = 2.6$

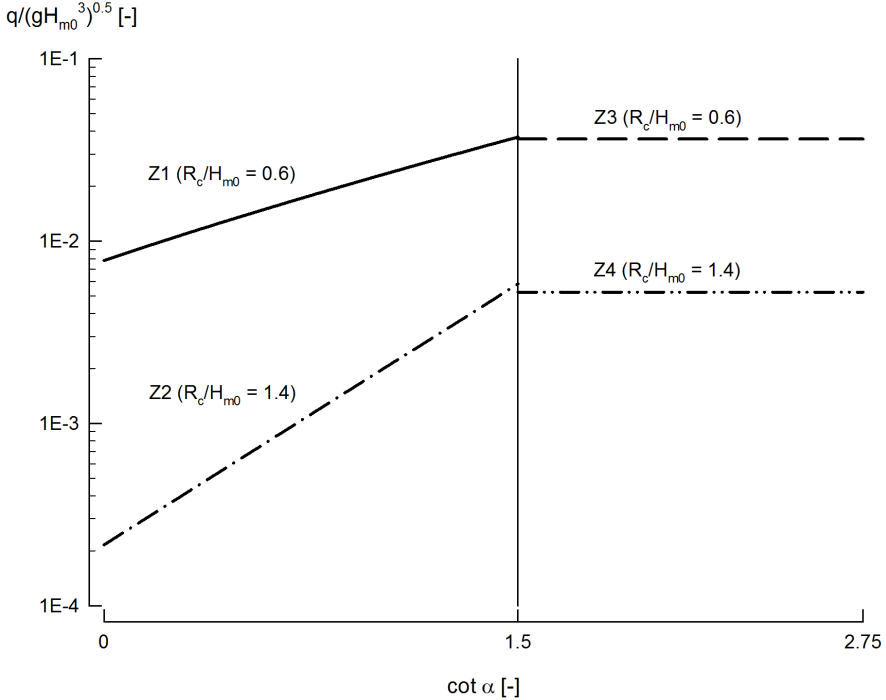


Figure 2.1: Zones of the Victor and Troch (2012b) formulae (Eq. 2.4) as a function of $\cot \alpha$ for the selected values relative crest freeboard $R_c/H_{m0} = 0.6$ and $R_c/H_{m0} = 1.4$.

(zone Z2) this effect is even stronger than in the zone Z1 (see Figure 2.1). When considering slopes $1.5 \leq \cot \alpha \leq 2.75$, for both (very) small relative crest freeboards ($0 \leq R_c/H_{m0} \leq 0.8$; zone Z3) and large relative crest freeboards ($0.8 \leq R_c/H_{m0} \leq 2$; zone Z4) the effect of the slope angle α on wave overtopping is negligible and therefore not considered in the coefficients. The zone Z4 of this formula is equal to the EurOtop (2007) overtopping prediction formula for non-breaking wave conditions (Eq. 2.2).

To obtain the 90% confidence band of the overtopping prediction, Victor

and Troch (2012b) apply an overtopping discharge factor based on the root mean square error (RMSE) of the tests through which the formulae were fitted. The overtopping discharge factor for the zone Z1 is 1.25; for the zone Z2 is 1.47; and for the zone Z3 is 1.18. To obtain the upper limit of 90% confidence band, the predicted overtopping value should be multiplied by the overtopping discharge factor; while to obtain the lower limit 90% confidence band, it should be divided by the overtopping discharge factor. The overtopping prediction in the zone Z4 is equal to Eq. 2.2 and therefore the standard deviation σ given with the equation is still valid.

Using the same UG10 dataset, Van der Meer and Bruce (2014) presented another overtopping prediction set of formulae valid for the range of steep low-crested structures for non-breaking conditions. The mean value approach of these formulae are presented in Eqs. 2.5 – 2.8:

$$\frac{q}{\sqrt{gH_{m0}^3}} = a_{V\&B} \cdot \exp \left[- \left(b_{V\&B} \frac{R_c}{H_{m0} \gamma_f \gamma_\beta} \right)^{c_{V\&B}} \right] \quad (2.5)$$

with the following expressions for the coefficients a , b and c :

$$a_{V\&B} = 0.09 - 0.01(2 - \cot \alpha)^{2.1} \text{ and } a_{V\&B} = 0.09 \text{ for } \cot \alpha > 2 \quad (2.6)$$

$$b_{V\&B} = 1.5 + 0.42(2 - \cot \alpha)^{1.5} \text{ with a maximum of } b_{V\&B} = 2.35; \quad (2.7)$$

$$\text{and } b_{V\&B} = 1.5 \text{ for } \cot \alpha > 2$$

$$c_{V\&B} = 1.3 \quad (2.8)$$

This prediction has an extended range of application with respect to Eq. 2.2 towards steep, very steep slopes and vertical walls ($\cot \alpha \geq 0$), with very small and zero freeboard ($R_c/H_{m0} \geq 0$). For the range of validity of the EurOtop (2007) formula, the Van der Meer and Bruce (2014) formulae give a similar prediction of average wave overtopping although providing a deeper insight of the overtopping process. The Van der Meer and Bruce (2014) formulae are included in the EurOtop (2016) manual as the reference overtopping prediction for structures with steep slopes up to vertical walls.

Compared to Eq. 2.2, Eq. 2.5 adds two coefficients $a_{V\&B}$ and $b_{V\&B}$ which are a function of the slope angle α . The coefficient $a_{V\&B}$ (Eq. 2.6) determines the overtopping value when the value of the x-axis in a $q/\sqrt{gH_{m0}^3}$ versus R_c/H_{m0} plot is equal to zero (i.e., in the case of zero relative crest freeboards $R_c = 0$). The coefficient $b_{V\&B}$ (Eq. 2.7) determines the shape of the equation for the entire range of R_c/H_{m0} .

The prediction also adds a power $c_{V\&B}$ (with a constant value) inside the exponential function (Eq. 2.8) indicating that the prediction follows a Weibull distribution. This exponent c results in a curved shape of the prediction in a log-linear plot.

The reliability of Eq. 2.5 is described by a coefficient of variation $\sigma' = \sigma/\mu$ for the coefficients $a_{V\&B}$ and $b_{V\&B}$, with the values $\sigma'(a_{V\&B}) = 0.15$ and $\sigma'(b_{V\&B}) = 0.10$.

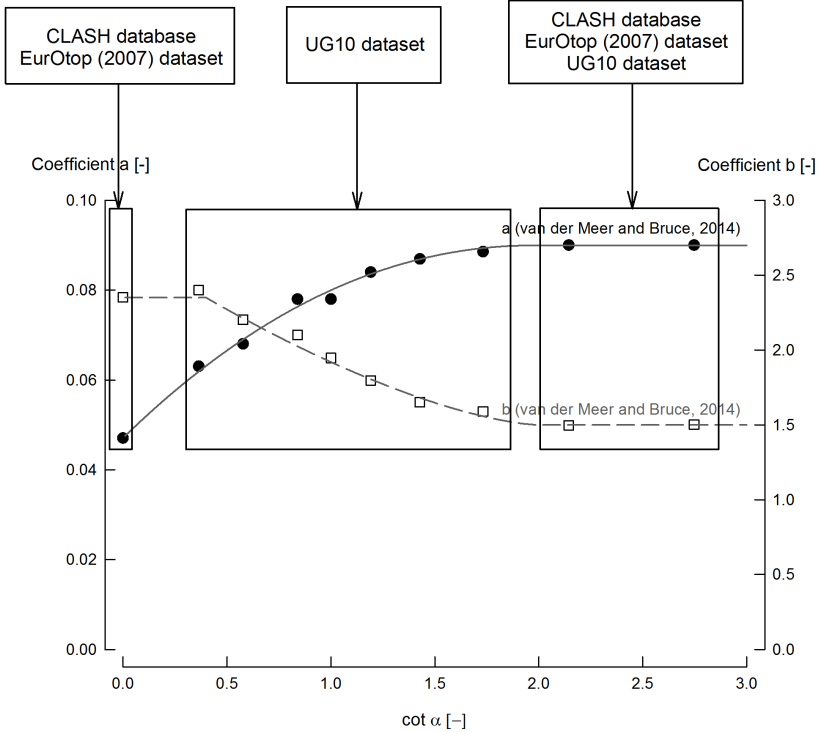


Figure 2.2: Best fit per slope angle α of the a and b coefficients for the UG10 dataset and selected tests of the CLASH database, with the Van der Meer and Bruce (2014) formulae expressions for $a_{V\&B}$ (Eq. 2.6) and $b_{V\&B}$ (Eq. 2.7).

The expressions for the $a_{V\&B}$ and $b_{V\&B}$ coefficients of Eq. 2.5 were fitted by Van der Meer and Bruce (2014) using wave overtopping results for specific slope angles α and relative crest freeboards R_c/H_{m0} from different sources shown in Figure 2.2. This figure also shows the a and b coefficients per slope angle that were used to fit $a_{V\&B}$ and $b_{V\&B}$, with a data gap for very steep slopes that the overtopping datasets of this research fill.

For the mild slope range ($\cot \alpha > 2$) the fit of the coefficients of the prediction formulae was performed through the UG10 dataset, the EurOtop

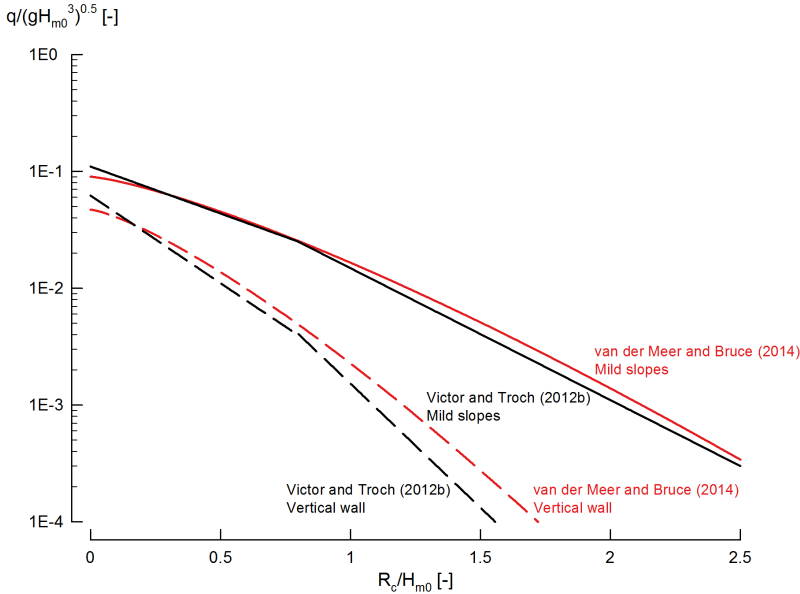


Figure 2.3: Comparison of overtopping prediction between Victor and Troch (2012b) (Eq. 2.4 and Table 2.2) and Van der Meer and Bruce (2014) (Eqs. 2.5 – 2.8) for mild slopes ($\cot \alpha > 2$) and vertical structures ($\cot \alpha = 0$).

(2007) dataset and the CLASH subsets 102 (with small crest freeboards) and 108 (with zero freeboard), taking these coefficients of the mild slope limit case as asymptotic values for steeper slopes with $\cot \alpha < 2$. In the range of steep slopes ($2 > \cot \alpha > 0.27$) only the UG10 dataset results were used to fit the expressions of the coefficients, as the CLASH database lacks of overtopping data for this range of slopes. For very steep slopes ($0.27 \geq \cot \alpha > 0$) no data were used to fit the formulae, however the overtopping prediction is still considered valid which raises concerns about the accuracy of the formulae on this range of slope angles. For the case of the vertical wall ($\cot \alpha = 0$), the UG10 dataset also lacked overtopping data. Therefore, the fit of the coefficients was performed through 9 subsets of the CLASH database for vertical walls (subsets 106 for small freeboards; 107 for zero freeboards; 113, 228, 229, 315, 351, 380 and 914), and the EurOtop (2007) dataset.

Figure 2.3 compares the Victor and Troch (2012b) overtopping prediction formula (Eq. 2.4 and Table 2.2; black lines) with the Van der Meer and Bruce (2014) formula (Eqs. 2.5 – 2.8; red lines) for the case of mild slopes $\cot \alpha > 2$ (solid lines) and vertical walls $\cot \alpha = 0$ (dashed lines). Both formulae give similar overtopping prediction, although Eq. 2.5 gives a slightly higher prediction for the case of vertical walls except for zero freeboards. The shape of

the formulae are different even though they are both exponential. Eq. 2.4 are straight lines on a log-linear plot while Eq. 2.5 are curved lines due to the coefficient $c_{V\&B}$. For very small and zero relative crest freeboards, Eq. 2.4 gives a higher overtopping prediction than Eq. 2.5. However, neither of the two formulae have been fitted with overtopping data in this range of relative crest freeboards and therefore the questions about the accuracy of the overtopping prediction raise.

2.3.4 Vertical Structures

The wave-structure interaction plays an important role in assessing wave overtopping for vertical structures, as the overtopping behaviour is different for non-impulsive (pulsating) or impulsive conditions.

Non-impulsive conditions occur when the ratio between the incident spectral wave height H_{m0} and the local water depth h is relatively small, with a low wave steepness. In this situation the foreshore (or a structure toe) is not influencing the overtopping behaviour, resulting in green overtopping and smoothly-varying loads on the structure (EurOtop, 2016).

Impulsive conditions occur at vertical or steep structures with a relatively large incident spectral wave height H_{m0} with respect to the local water depth h . Some waves will break against the wall producing a violent up-rushing (vertical) jet of water, with impact forces 10 to 40 times higher than the ones caused by non-impulsive conditions (EurOtop, 2016).

There is no clear methodology to determine the impulsiveness of the wave conditions. An approach used in the literature (EurOtop, 2007) was to determine the impulsiveness parameter h_* as defined in Eq. 2.9, based on the water depth at the toe of the structure h :

$$h_* = 1.35 \frac{h^2}{H_{m0}} \frac{2\pi}{g T_{m-1,0}^2} \quad (2.9)$$

Non-impulsive conditions dominate the vertical structure when $h_* > 0.3$, while impulsive conditions occur when $h_* < 0.2$ (EurOtop, 2007). In the transition $0.2 \leq h_* \leq 0.3$ the overtopping prediction for both conditions should be calculated and the largest value assumed.

Using the impulsiveness parameter h_* , the EurOtop (2007) manual proposed two different prediction formulae. The mean value approach prediction formula for non-impulsive conditions ($h_* > 0.3$) is shown in Eq. 2.10:

$$\frac{q}{\sqrt{gH_{m0}^3}} = 0.04 \cdot \exp\left(-2.6 \frac{R_c}{H_{m0}}\right) \quad (2.10)$$

This prediction is valid in a range of relative crest freeboards $0.1 < R_c/H_{m0} < 3.5$, with the coefficient 2.6 having an associated standard deviation of $\sigma = 0.8$.

However, the EurOtop (2016) manual introduced a new method to determine the wave overtopping behaviour on a vertical wall, not using the impulsiveness parameter h_* as a classifier. After a careful analysis of tests of the CLASH database for vertical and battered structures (i.e., steep or very steep structures), Van der Meer and Bruce (2014) found a clear distinction in the overtopping behaviour of vertical structures with and without sloping foreshore. Overtopping was higher for structures with a sloping foreshore. For structures without a sloping foreshore, there was no significant difference between caisson-type structures (i.e., with a toe) and plain vertical walls. Based on these findings, a new decision chart to choose the right wave overtopping prediction formula depending on the type of vertical structure considered was suggested in the EurOtop (2016) manual, although it was first presented in Van der Meer and Bruce (2014) with some modifications.

For vertical structures without a foreshore, the EurOtop (2016) manual suggests the use of the general Van der Meer and Bruce (2014) prediction formula (Eqs. 2.5 – 2.8) for the case of vertical structures ($\cot \alpha = 0$), which is presented in Eq. 2.11 (mean value approach, with the standard deviations of the coefficients being $\sigma(0.047) = 0.007$ and $\sigma(2.35) = 0.23$):

$$\frac{q}{\sqrt{gH_{m0}^3}} = 0.047 \cdot \exp \left[- \left(2.35 \frac{R_c}{H_{m0}} \right)^{1.3} \right] \quad (2.11)$$

This prediction formula is valid for the whole range of positive relative crest freeboards ($R_c/H_{m0} \geq 0$).

Van der Meer and Bruce (2014) did not include their newly developed overtopping prediction formula in the decision chart presented in the paper. Instead, they suggest to use the prediction formula by Allsop et al. (1995) in the case of lower relative freeboards ($R_c/H_{m0} < 0.91$), presented in Eq. 2.12 (standard deviation of the coefficient 2.78 is $\sigma = 0.17$):

$$\frac{q}{\sqrt{gH_{m0}^3}} = 0.05 \cdot \exp \left(-2.78 \frac{R_c}{H_{m0}} \right) \quad (2.12)$$

For the case of higher relative freeboards ($R_c/H_{m0} > 0.91$), the suggested prediction formula is the one by Franco et al. (1994) presented in Eq. 2.13 (standard deviation of the coefficient 4.3 is $\sigma = 0.6$):

$$\frac{q}{\sqrt{gH_{m0}^3}} = 0.2 \cdot \exp \left(-4.3 \frac{R_c}{H_{m0}} \right) \quad (2.13)$$

Both formulae performed well for their range of application, although the different behaviour of the prediction for large relative freeboards is still unexplained. However, in the decision chart of the EurOtop (2016) the suggestion of using the Franco et al. (1994) prediction is removed, and Allsop et al. (1995) prediction is suggested instead to be used for vertical (or composite vertical) structures with an influence of the foreshore and without possible breaking. This change in criteria about when to use the Allsop et al. (1995) and Franco et al. (1994) deepens the question about the different use and behaviour of these two predictions.

The Victor and Troch (2012b) prediction formulae (Eq. 2.4 and Table 2.2) were considered neither by the chart of Van der Meer and Bruce (2014) nor by the EurOtop (2016) manual, although the prediction is fully applicable to vertical structures ($\cot \alpha = 0$) without the influence of a foreshore. The particularization for this case is shown in Eq. 2.14 and Eq. 2.15 (see Section 2.3.3 to assess the reliability of these formulae):

$$\frac{q}{\sqrt{gH_{m0}^3}} = 0.062 \cdot \exp\left(-3.45 \frac{R_c}{H_{m0}}\right) \text{ for } 0 \leq R_c/H_{m0} \leq 0.8 \quad (2.14)$$

$$\frac{q}{\sqrt{gH_{m0}^3}} = 0.2 \cdot \exp\left(-4.88 \frac{R_c}{H_{m0}}\right) \text{ for } 0.8 \leq R_c/H_{m0} \leq 2 \quad (2.15)$$

Figure 2.4 shows a comparison of the wave overtopping prediction formulae for vertical structures without the influence of a foreshore slope. Allsop et al. (1995) (Eq. 2.12, dot dashed blue line) shows a higher prediction for large relative freeboards, while for small relative freeboards it is similar to Van der Meer and Bruce (2014) (Eq. 2.11, dashed red line) and Victor and Troch (2012b) (Eqs. 2.14 - 2.15, black solid line). The prediction of Franco et al. (1994) (Eq. 2.13, double-dot dashed green line) is larger for small relative freeboards than the other 3 formulae, revealing the still unexplained prediction differences between the formulae.

2.3.5 Zero Freeboard

The available scientific literature is limited for the case of coastal structures with zero freeboards ($R_c = 0$). Only a few prediction formulae deal with sloping or vertical structures under this condition, while the datasets available including zero freeboard overtopping data are scarce.

Schüttrumpf (2001) developed two prediction formulae for zero freeboard depending on the surf similarity parameter $\xi_{m-1,0}$. These formulae are pre-

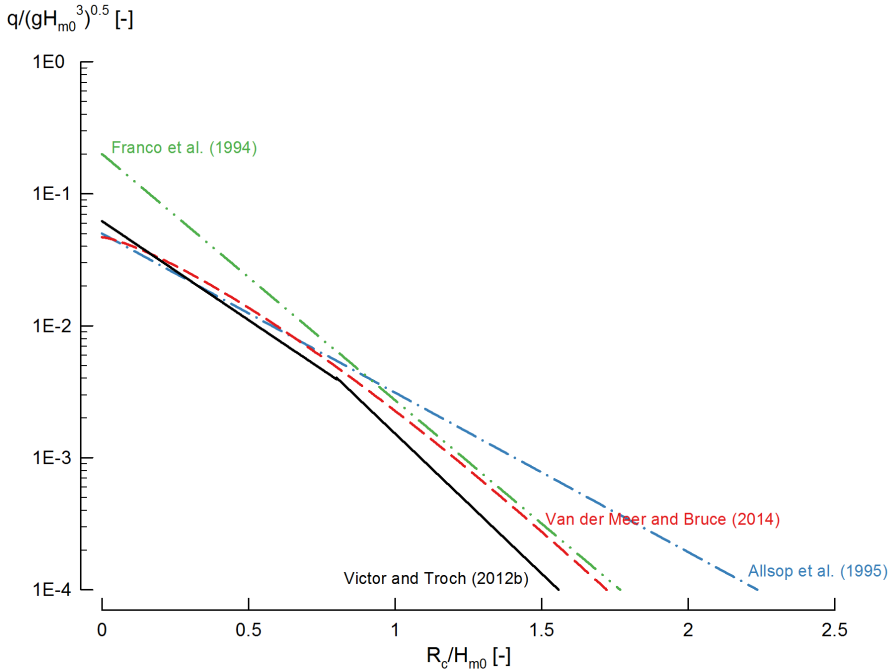


Figure 2.4: Comparison of the wave overtopping prediction formulae for vertical structures by Allsop et al. (1995) (Eq. 2.12), Franco et al. (1994) (Eq. 2.13), Van der Meer and Bruce (2014) (Eq. 2.11) and Victor and Troch (2012b) (Eqs. 2.14 - 2.15).

sented in Eq. 2.16 for $\xi_{m-1,0} < 2$ and Eq. 2.17 for $\xi_{m-1,0} \geq 2$ as reported in the EurOtop (2007) manual:

$$\frac{q}{\sqrt{gH_{m0}^3}} = 0.0537 \cdot \xi_{m-1,0} \text{ for } \xi_{m-1,0} < 2 \quad (2.16)$$

$$\frac{q}{\sqrt{gH_{m0}^3}} = \left(0.136 - \frac{0.226}{\xi_{m-1,0}^3} \right) \text{ for } \xi_{m-1,0} \geq 2 \quad (2.17)$$

The use of the Iribarren number as an independent parameter in the prediction complicates the comparison with other prediction formulae with R_c/H_{m0} as independent variable. For large values of the surf similarity parameter ($\xi_{m-1,0} > 10$), as is for the case of steep low-crested structures –due to the steep slopes–, Eq. 2.17 tends to a constant value of $q/\sqrt{gH_{m0}^3} \approx 0.136$.

It is also possible to particularize the various prediction formulae described in Sections 2.3.3 and 2.3.4 for the specific case of zero freeboards ($R_c = 0$).

The particularization of the Victor and Troch (2012b) prediction formulae (Eq. 2.4 and Table 2.2) for $R_c = 0$ is shown in Eq. 2.18 and Eq. 2.19 (see Section 2.3.3 to assess the reliability of these formulae):

$$\frac{q}{\sqrt{gH_{m0}^3}} = 0.033 \cdot \cot \alpha + 0.062 \text{ for } 0 \leq \cot \alpha \leq 1.5 \quad (2.18)$$

$$\frac{q}{\sqrt{gH_{m0}^3}} = 0.11 \text{ for } 1.5 \leq \cot \alpha \leq 2.75 \quad (2.19)$$

For the Van der Meer et al. (2013) formulae, the particularization for the zero freeboard case is shown in Eq. 2.20, with a reliability based on the coefficient of variation $\sigma' = 0.15$. This prediction corresponds to the coefficient $a_{V\&B}$ of Eq. 2.5, as the exponential part of the equation is 1 when $R_c = 0$:

$$\frac{q}{\sqrt{gH_{m0}^3}} = 0.09 - 0.01(2 - \cot \alpha)^{2.1} \text{ and } \frac{q}{\sqrt{gH_{m0}^3}} = 0.09 \text{ for } \cot \alpha > 2 \quad (2.20)$$

For vertical walls ($\cot \alpha = 0$) with zero crest freeboard ($R_c = 0$), Smid (2001) proposed a constant average overtopping rate for non-impulsive wave conditions (Eq. 2.21) which was based on experimental tests. Victor and Troch (2012b) considered this constant value by Smid (2001) and fixed the value of their prediction formula (Eqs. 2.14 and 2.15) for the case of vertical walls with zero freeboard according to Eq. 2.21:

$$\frac{q}{\sqrt{gH_{m0}^3}} = 0.062 \pm 0.0062 \quad (2.21)$$

Also for vertical walls with zero freeboards ($\cot \alpha = 0$ and $R_c = 0$) it is possible to particularize the Allsop et al. (1995) and the Franco et al. (1994) prediction formulae (Eqs. 2.12 and 2.13) for zero freeboards. With this particularization, Eq. 2.12 gives a constant prediction of $q/\sqrt{gH_{m0}^3} = 0.05$ and Eq. 2.13 a constant prediction of $q/\sqrt{gH_{m0}^3} = 0.2$, which is one order of magnitude higher than the former, highlighting the different behaviour of the prediction for small freeboards already stated in Section 2.3.4.

Figure 2.5 shows the various overtopping prediction formulae for the case of zero freeboard $R_c = 0$ described in this section. The prediction by Victor and Troch (2012b) (black solid line, Eqs. 2.18-2.19) is higher than the prediction by Van der Meer and Bruce (2014) (red dashed line, Eq. 2.20) for the whole range of $\cot \alpha$. Smid (2001) prediction (blue cross, Eq. 2.21) is only valid for vertical structures ($\cot \alpha = 0$) and was taken by Victor and Troch (2012b) as a limit case for their prediction.

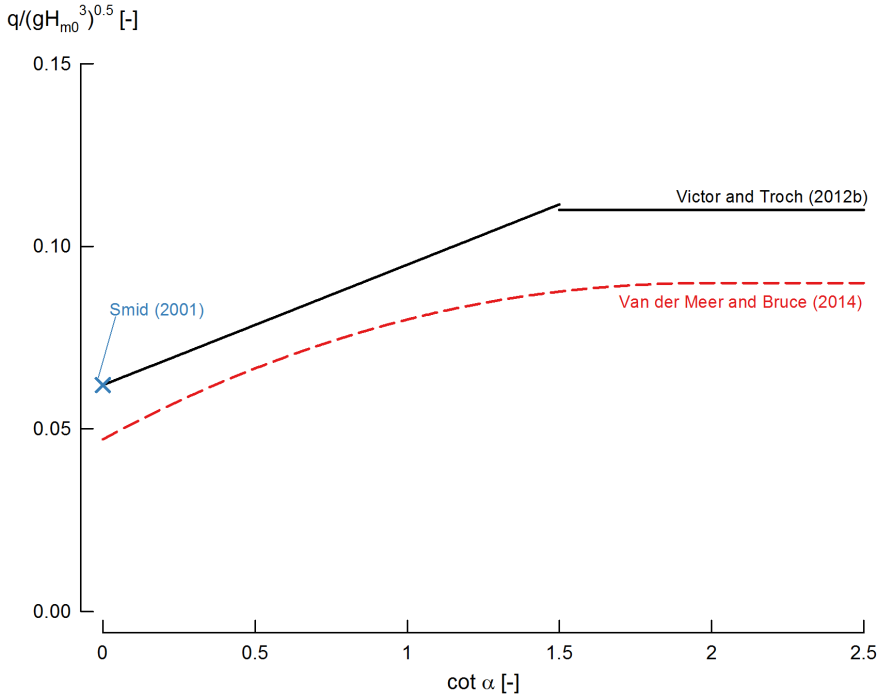


Figure 2.5: Comparison of the wave overtopping prediction formulae for the zero freeboard case ($R_c = 0$) by Victor and Troch (2012b) (Eqs. 2.18-2.19), Van der Meer and Bruce (2014) (Eq. 2.20) and Smid (2001) (Eq. 2.21).

A different approach for predicting average overtopping rates for zero freeboards ($R_c = 0$) is to consider the prediction for the negative freeboard ($R_c < 0$), i.e., when the water level is higher than the crest of the coastal structure. In this case, the EurOtop (2007) manual considers that the overtopping is formed by superposition of two states: a part corresponding to the overflow of water over the structure, and a part attributed to the overtopping for the zero freeboard case. The overflow part can be calculated following the different weir formulae depending on the shape of the crest, while for the overtopping part the EurOtop (2007) suggests to use the Schüttrumpf (2001) prediction for zero freeboards (Eqs. 2.16 and 2.17). In the EurOtop (2016) the superposition of the two states (overflow and overtopping for the zero freeboard case) is also suggested, although changing the prediction formulae for the zero freeboard case to Eq. 2.20.

Reeve et al. (2008) used a numerical model to predict the overtopping for negative freeboards for mild slopes between $6 > \cot \alpha > 3$, which gave values for the overtopping for $R_c = 0$ of $q/\sqrt{gH_{m0}^3} = 0.233$, one order of magnitude higher than the predictions in Eqs. 2.18 and 2.20. Hughes and

Nadal (2009) performed physical modelling of a mild slope $\cot \alpha = 4.25$ with negative freeboards, obtaining an empirical prediction formula for this conditions. The particularization for $R_c = 0$ give values of $q/\sqrt{gH_{m0}^3} = 0.034$. Pan et al. (2013) also performed physical model tests for negative freeboards, suggesting an empirical prediction formula, however, being undefined for $R_c = 0$ values.

Table 2.3 presents an overview of the most important average wave overtopping prediction formulae presented in this section for mild slopes, steep low-crested structures and vertical structures.

Table 2.3: Summary of the overtopping prediction formulae overviewed in this section and their range of application.

Equation	Reference	Range of $\cot \alpha$	Range of R_c/H_{m0}
2.2	EurOtop (2007) mild slopes non-breaking	$1 \leq \cot \alpha \leq 4$	$0.5 \leq R_c/H_{m0} \leq 3.5$
2.4	Victor and Troch (2012b)	$0 \leq \cot \alpha \leq 2.75$	$0 \leq R_c/H_{m0} \leq 2$
2.5	Van der Meer and Bruce (2014)	$\cot \alpha \geq 2.75$	$R_c/H_{m0} \geq 0$
2.10	EurOtop (2007) vertical walls	$\cot \alpha = 0$	$0.1 < R_c/H_{m0} < 3.5$
2.21	Smid (2001)	$\cot \alpha = 0$	$R_c/H_{m0} = 0$

2.3.6 Effect of Roughness on Wave Overtopping

The roughness of the structure slope is a key reduction factor of overtopping. This factor is simbolized as γ_f in most of the overtopping prediction formulae, such as Van der Meer and Bruce (2014) (Eqs. 2.5 - 2.8). The roughness of a slope can be reached by the material of the slope —i.e., grass, asphalt, concrete, natural block revetments, etc.— or by artificial roughness elements —i.e., blocks, ribs, stepped revetments—. The γ_f factor also includes the influence of the permeability of the structure on the overtopping rates.

The UG16 overtopping dataset obtained at Ghent University featured artificial roughness elements to analyse the overtopping reduction derived from the presence of these elements. The scientific literature available for blocks, ribs and stepped revetments is reviewed in this section.

Blocks and Ribs

Blocks and ribs (or battens) create a turbulent water flow on the structure slope, increasing the energy dissipation and therefore, decreasing the overtopping rates.

The EurOtop (2016) defines the most efficient shape of blocks and ribs on embankments (i.e., on mild slopes) on reducing the overtopping. Optimum

values are given for the width (f_b) and the height of the element (f_h), and the distance between the elements (f_L).

The optimal ratio between the width and height of the blocks is reported in EurOtop (2016) as $f_b/f_h = 5 - 8$. However, this ratio would lead to very slender blocks that are not feasible to install on mild slopes to reduce the overtopping rates. This recommendation seems to be an error, as its origin can be traced back to Van der Meer (1998) (who re-analysed data from Szymkiewitz et al. (1994)) and does not report such a ratio. Instead, Van der Meer (1998) recommends that the optimal distance between ribs is $f_L/f_b = 7$ with an area of application $f_L/f_b = 5 - 8$, which is also reported by EurOtop (2016). Smaller f_L/f_b would reduce the macro roughness, dissipating less energy. The optimal ratio between the height of the block and the incident wave height is $f_h/H_{m0} = 0.15$. A larger block or rib height than this value does not further reduce the overtopping rates. Table 2.4 shows the minimum roughness influence factors $\gamma_{f,\min}$ per area covered by blocks or ribs and $f_h/H_{m0} = 0.15$.

According to the EurOtop (2016) manual, the effect of roughness elements is negligible $0.25R_{u2\%,\text{smooth}}$ under the SWL and $0.5R_{u2\%,\text{smooth}}$ above the SWL. Therefore, if an overtopping reduction is wanted, it is recommended to install the roughness elements in the area of influence.

Table 2.4: Minimum influence factors due to roughness $\gamma_{f,\min}$ if the total area is covered by blocks or ribs and $f_h/H_{m0} = 0.15$ (EurOtop, 2016).

Condition	$\gamma_{f,\min}$
Block, 1/25 of total surface covered	0.85
Block, 1/9 of total surface covered	0.80
Ribs, $f_L/f_b = 7$	0.75

There are no scientific publications studying the effects of blocks or ribs on reducing wave overtopping on (very) steep low-crested structures.

Stepped Revetments

Various authors studied wave run-up and wave overtopping for stepped revetments, such as Saville (1955), Van Steeg et al. (2012), Chuenchai et al. (2014) and more recently Kerpen et al. (2014) and Kerpen (2017). An overview of the scientific research published for stepped revetments is presented by Kerpen and Schlurmann (2016).

Physical modelling was carried out for different step sizes and slope angles. However, the steepest slope tested was $\cot \alpha = n = 1$ by Kerpen (2017),

where $n = S_w/S_h$ being S_w the width of the step and S_h the height of the step. There is no research on the overtopping behaviour of stepped structures with (very) steep slopes. Considering that the stepped revetments have two limit cases for smooth slopes ($S_h = 0$) and vertical walls ($S_h = \infty$), the very steep stepped slope behaviour would be similar to the vertical structure. However, this assumption still needs to be validated with overtopping physical modelling.

In his research, Kerpen (2017) performed overtopping physical model tests for three slope angles ($\cot \alpha = n = 1, 2, 3$) with two different step heights ($S_h = 0.05$ m and $S_h = 0.3$ m). Wave loads were also measured. Individual overtopping measurements could not be obtained due to the excessive length of the overtopping chute. Smooth slopes overtopping tests with the same test setup were also performed for comparison. The results of the smooth tests indicate a higher overtopping than the one predicted by Van der Meer and Bruce (2014), probably due to the absence of active wave absorption during the experiments.

After analysing the overtopping results, Kerpen (2017) found that the reduction of wave overtopping of a stepped revetment compared to a smooth slope depends on the relative step height H_{m0}/S_h and the surf similarity parameter $\xi_{m-1,0}$. For cases where the step height is larger than the wave height ($H_{m0}/S_h < 1$) the overtopping reduction is 10–30%, while for $H_{m0}/S_h < 0.5$ the reduction in overtopping is not significant (2–10%). The most effective overtopping reduction was for $H_{m0}/S_h = 2$ (40–60%). The relative position of the SWL with respect to the nearest step edge is relevant on reducing the overtopping for $0.5 < H_{m0}/S_h < 2$. In this case, the highest overtopping reduction is produced when the SWL is close to the step edge.

As for the surf similarity parameter $\xi_{m-1,0}$, the reduction in overtopping is smaller for larger $\xi_{m-1,0}$, with no overtopping reduction for $\xi_{m-1,0} > 7$. For plunging waves the overtopping reduction is most effective (40–60%) due to the macro roughness of the stepped revetment that induces wave breaking. Therefore, the overtopping reduction for collapsing and surging waves is smaller (10–30%).

Kerpen (2017) fits an exponential prediction formula through the smooth overtopping data, and calculates roughness influence factors γ_f for the tested stepped revetments based on that overtopping prediction. The influence factors are also analysed with respect the characteristic step diameter (defined by $k_h = \cos \alpha \cdot S_h$), finding a correlation described with a hyperbolic tangent. It is possible that the calculated γ_f are not applicable to other prediction formulae, hence caution is advised when applying the influence factors.

2.4 Individual Overtopping Volumes

The individual overtopping volumes are a key design parameter for coastal structures, as a single wave overtopping event can affect the structural stability of dikes, sea walls or even buildings and other constructions located near the coast. Also, single events can threaten the safety of people near the coast during a storm event. There is a direct link between the individual volume and the wave force for the same event. The consideration of these forces and the related pressures in the coastal structure design is key for determining the structural safety of a structure.

However, the references dealing with the prediction of the probability distribution of the individual overtopping volumes and the probability of overtopping are scarce in scientific literature, as most of the research was focused in the prediction of average overtopping rates. The EurOtop (2007) manual includes a simple estimation of the probability distribution of the individual volumes for sloping structures, although this estimation is not valid for the range of steep low-crested structures. In recent years, authors such as Hughes et al. (2012), Victor et al. (2012) and Zanuttigh et al. (2013) extended the research on individual overtopping volumes and their probability distribution towards steep low-crested structures and negative freeboards. Nørgaard et al. (2014) studied the individual overtopping rates for rubble mound breakwaters with a focus on the shallow water effects on the probability distribution of the individual volumes.

Van der Meer et al. (2010) and Hughes et al. (2012) investigated the flow thickness and flow velocities of the individual overtopping events which are of use when designing wave overtopping simulators (see Section 1.2.1). Hughes and Thornton (2016) studied the time variation of the wave-per-wave discharge, which the authors fitted through a two-parameter Weibull distribution with $B = 2$ (i.e., Rayleigh distribution) as best fit. The individual overtopping volumes used for the research were analysed using a supervised method described in Hughes (2015).

2.4.1 Probability Distribution of Individual Overtopping Volumes

The individual overtopping volumes are distributed following a two-parameter Weibull distribution as found by Franco et al. (1994) and Van der Meer and Janssen (1994). The exceedance probability P_v of each overtopping volume V

is described by Eq. 2.22, where A is the scale factor and B is the shape factor:

$$P_v = [V_i \geq V] = \exp\left(-\left(\frac{V}{A}\right)^B\right) \quad (2.22)$$

The scale factor A is proportional to the average overtopping discharge per wave. Larger individual volumes V_i correspond to larger values of the factor A . The shape factor B determines the shape of the probability distribution. For small values of B , the average overtopping rate q is determined by a small number of very large overtopping volumes. A small B value corresponds also to larger maximum volumes. When B becomes larger, the average overtopping rate q is formed by more similar individual volumes as the volumes are more equally distributed. A special case of the Weibull distribution corresponds to $B = 2$ which is a Rayleigh distribution.

The scale factor A (Eq. 2.27) is derived by considering the measured mean overtopping volumes \bar{V}_{meas} to be fully characterized by a Weibull distribution. First, it is necessary to define the average overtopping rate as the ratio between the total overtopped volume V_0 (the sum of the individual volumes V_i) and the sum T_0 of the wave periods of each wave in the wave train T_i (Eq. 2.23), which is rewritten as Eq. 2.24 when divided by the number of overtopping waves N_{ow} :

$$q = \frac{V_0}{T_0} = \frac{\sum V_i}{\sum T_i} = \frac{\sum V_i}{N_w T_m} \quad (2.23)$$

$$\frac{q N_w T_m}{N_{ow}} = \frac{\sum V_i}{N_{ow}} \quad (2.24)$$

The measured mean overtopping volume \bar{V}_{meas} (Eq. 2.25) is the ratio between the sum of the individual overtopping volumes V_i and the number of overtopping waves N_{ow} , and it is equal to the right hand side of Eq. 2.24. The theoretical mean overtopping volume (\bar{V}_{theor} , Eq. 2.26) follows a two-parameter (A and B) Weibull where Γ is the mathematical gamma function:

$$\bar{V}_{meas} = \frac{\sum V_i}{N_{ow}} = \frac{q N_w T_m}{N_{ow}} \quad (2.25)$$

$$\bar{V}_{theor} = E[V]_{Weibull} = A \Gamma\left(1 + \frac{1}{b}\right) \quad (2.26)$$

By making equal the measured and the theoretical mean individual overtopping volumes $\bar{V}_{meas} = \bar{V}_{theor}$ (Franco and Franco, 1999), the coefficient A

is defined (Eq. 2.27), which is possible to simplify with the use of a parameter A' (Eq. 2.28):

$$A = A' \frac{qN_w T_m}{N_{ow}} \quad (2.27)$$

$$A' = \frac{1}{\Gamma\left(1 + \frac{1}{B}\right)} \quad (2.28)$$

To simplify the use of A' , Victor et al. (2012) suggest to approximate Eq. 2.28 by using a hyperbolic tangent fit with the shape factor B as variable (Eq. 2.29). This approximation has a coefficient of determination r^2 of 0.96, proving to be very accurate in describing A' :

$$A' = 1.13 \tanh(1.132 B) \quad (2.29)$$

2.4.2 Estimation of Shape Factor B

Various authors have studied the probability distribution of the individual overtopping volumes, suggesting estimations for the shape factor B for various types of structures.

Mild Sloping Structures

Van der Meer and Janssen (1994) and Franco et al. (1994) found that the shape factor for smooth sloping structures is not dependent on the wave steepness or the slope angle of the structure. The authors suggested an average value of $B = 0.75$ (with an associated $A' = 0.84$ according to Eq. 2.29), which was later adopted in the TAW (2002) manual and the EurOtop (2007) manual. Bruce et al. (2009) found a very similar average value of $B = 0.74$ valid for smooth sloping structures and for rubble mound structures with rock and concrete armour. The scatter of the data used by Van der Meer and Janssen (1994), Franco et al. (1994) and Bruce et al. (2009) was relatively large indicating a possible effect of a wave or structural parameter in the shape factor B . However, the authors decided to provide an average value of B for all wave and structural tested conditions to simplify the prediction of the individual volumes distribution.

Besley (1999), however, found that the offshore peak wave steepness s_{0p} has an influence on the B value. For a wave steepness of $s_{0p} = 0.02$ the value suggested is $B = 0.76$, and for $s_{0p} = 0.04$ the value increases to $B = 0.92$ (with a linear interpolation between the s_{0p} values). He also found an effect

of the slope angle α but determined and it was unclear and did not include this effect when suggesting B values.

Steep Low-Crested Structures

The shape factor B predictions suggested by Van der Meer and Janssen (1994), Franco et al. (1994), Besley (1999) and Bruce et al. (2009) were obtained after analysing individual overtopping data on sloping structures outside the range of steep low-crested structures ($2 > \cot \alpha \geq 0$; $0.8 > R_c/H_{m0} \geq 0$). The question whether a constant prediction of B is still valid for the range of steep low-crested structures remained unanswered until Victor et al. (2012) analysed the individual overtopping volumes of the dataset UG10 for steep low-crested structures. For this dataset, the authors found an effect of the slope angle α and the relative crest freeboard R_c/H_{m0} on the shape factor B , although no effect of the wave steepness. Victor et al. (2012) suggested a new prediction formula (Eq. 2.30) for B fitted through all the best fit b values of each UG10 test (364 tests):

$$B = \exp\left(-2\frac{R_c}{H_{m0}}\right) + (0.56 + 0.15 \cot \alpha) \quad (2.30)$$

For each test, B was fitted through the individual volumes with $V_i > \overline{V}_{meas}$. The range of application of Eq. 2.30 is for slope angles $\cot \alpha \leq 2.75$ and relative crest freeboards $R_c/H_{m0} \leq 1.7$. The reliability of Eq. 2.30 is expressed by a root mean square error value of $RMSE = 0.10$.

Hughes et al. (2012) used the same data from the UG10 dataset (364 tests) to fit a new shape factor B prediction formula, also adding new individual overtopping data (27 tests) for smooth structures with negative freeboard ($R_c < 0$) from Hughes and Nadal (2009), and data with very large relative crest freeboards (14 tests) from Van der Meer and Janssen (1995). For each test, B was fitted through the upper 10% of values to better represent the largest volumes although reducing the accuracy of the fitting for the lowest volumes. The resulting prediction formula (Eq. 2.31) is only depending on the relative crest freeboard R_c/H_{m0} and is valid for a range of R_c/H_{m0} from negative to $R_c/H_{m0} < 4$:

$$B = \left[\exp\left(-0.6\frac{R_c}{H_{m0}}\right) \right]^{1.8} + 0.64 \quad (2.31)$$

Zanuttigh et al. (2013) investigated the shape factor B for rough and permeable structures compared to smooth and impermeable structures. The authors used individual overtopping data from the DELOS project (Van der

Meer et al., 2005a; Kramer et al., 2005) for rubble mound breakwaters, including low-crested and zero freeboard structures, and from the CLASH project (see Section 2.1) for both rubble mound breakwaters and smooth impermeable sloping structures, including negative freeboards (R_c/H_{m0}). The slope angles α considered in the data are mild slopes, and not in the range of steep or very steep slopes. However, the R_c/H_{m0} of the data range from small to zero, allowing a comparison with the B predictions valid for steep low-crested structures. For smooth structures, the prediction of the shape factor B by Zanuttigh et al. (2013) is shown in Eq. 2.32, and it is dependent on the average overtopping rate q , the incident spectral wave height at the toe of the structure H_{m0} and the wave period $T_{m-1,0}$. This prediction formula is included in the EurOtop (2016) manual for mild sloping structures:

$$B = 0.73 + 55 \left(\frac{q}{gH_{m0}T_{m-1,0}} \right)^{0.8} \quad (2.32)$$

Figure 2.6 compares the shape factor B prediction by the EurOtop (2007) manual $B = 0.75$ (blue line) as suggested by Van der Meer and Janssen (1994), Franco et al. (1994) and Besley (1999), by Victor et al. (2012) for different values of the slope angle α (black line for $\cot \alpha = 2$, red line for vertical walls $\cot \alpha = 0$), and by Hughes et al. (2012) (green line). For negative freeboards $R_c = 0$, neither the EurOtop (2007) prediction nor Victor et al. (2012) prediction are valid, although the latter is shown in dashed lines for this range in order to allow a comparison with Hughes et al. (2012). Zanuttigh et al. (2013) is excluded from this figure because it is not dependent on R_c/H_{m0} , making difficult a direct comparison between Eq. 2.30, Eq. 2.31 and 2.32.

As the Victor et al. (2012) prediction depends on the slope angle α , Figure 2.6 shows the two limit values for steep low-crested structures: $\cot \alpha = 2$ and the vertical wall case ($\cot \alpha = 0$). As shown, the B value prediction decreases for increasing values of $\cot \alpha$ (for steeper slopes). However, the influence of α in the prediction is rather limited in the range of steep low-crested structures compared to the influence of the relative crest freeboard R_c/H_{m0} . R_c/H_{m0} affects exponentially the prediction of B , reaching an asymptotic value when $R_c/H_{m0} \approx 2$ which is close to the value $B = 0.75$ predicted by the EurOtop (2007) manual for sloping structures. Hughes et al. (2012) gives a prediction in between $\cot \alpha = 2$ and $\cot \alpha = 0$ for this figure for positive R_c/H_{m0} , although it does not depend on α . When $R_c/H_{m0} > 2$ the prediction of Hughes et al. (2012) is also similar to $B = 0.75$.

The different shape factor B predictions may seem contradictory at first sight, but a close analysis of the behaviour of the various formulae and values shows that an integrated approach towards B prediction is possible. For

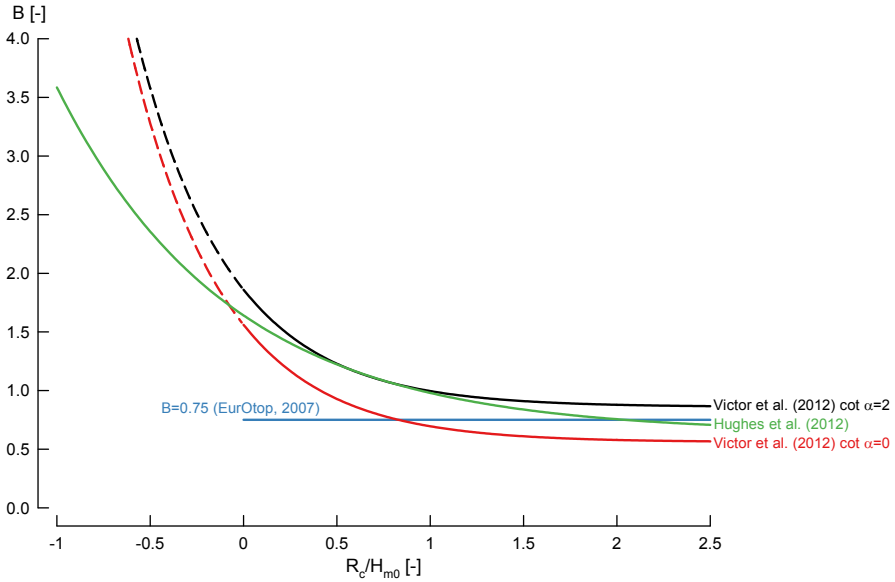


Figure 2.6: Comparison the shape factor B prediction formulae for mild sloping and steep low-crested structures by EurOtop (2007), Victor et al. (2012) (Eq. 2.30) for $\cot \alpha = 2$ and $\cot \alpha = 0$, and Hughes et al. (2012) (Eq. 2.31).

structures with mild slopes ($\cot \alpha > 2$) and relatively large crest freeboards ($R_c/H_{m0} > 2$), the prediction by EurOtop (2007) of $B = 0.75$ proves to be valid. For steep low-crested structures the predictions by Victor et al. (2012) and Hughes et al. (2012) are similar, although Victor et al. (2012) it is supposedly giving a more accurate prediction of B as it also depends on the slope angle α .

Besides Hughes et al. (2012) and Zanuttigh et al. (2013), also Hughes and Nadal (2009) and Pan et al. (2015) proposed shape factor B values for the case of negative freeboards ($R_c/H_{m0} < 0$). The zero freeboard case ($R_c = 0$) can be studied as a limit case for negative freeboards. Hughes and Nadal (2009) and Pan et al. (2015) suggest values within the range of $B = 1 - 4$ for negative freeboards, meaning that the for zero and small freeboards B is expected to be larger than the value of $B = 0.75$ suggested by EurOtop (2007), confirming the aforementioned statement that $B = 0.75$ is only valid for large values of R_c/H_{m0} .

Vertical Structures

Franco et al. (1994) found that the same constant value of $b = 0.75$ suggested by Van der Meer and Janssen (1994) was valid for vertical structures, with no influence of any wave or structural parameters. However, Franco and Franco (1999) found an effect of the wave steepness on B . The same authors also reported various B values for vertical structures (caissons) with noses and perforations, and for long-crested and short-crested waves as they included 3D overtopping tests in the research. The range of B for all the conditions tested is $B = 0.66 - 0.86$.

Besley (1999) also found that the wave steepness and the impulsiveness of the waves at the toe of the structure (see Section 2.3.4) has an affect on B for vertical structures. For vertical structures and non-impulsive waves the author suggests $B = 0.66$ for $s_{0p} = 0.02$ and $b = 0.82$ for $s_{0p} = 0.04$ (with a linear interpolation between these values of s_{0p}); while for vertical structures and impulsive waves the author suggests $B = 0.85$ for any value of wave steepness s_{0p} . These values of B are included in the EurOtop (2016) manual for vertical structures.

The particularization for vertical structures ($\cot \alpha = 0$) of the Victor et al. (2012) prediction formula (Eq. 2.30) gives the limit case for this prediction as shown in Figure 2.6. This particularization is not possible for the prediction formulae of Hughes et al. (2012) (Eq. 2.31) as the formulae are not dependent on the slope angle α , although the prediction is still valid for vertical structures. For these two predictions the value is dependent on the relative crest freeboard R_c/H_{m0} .

The spreading of the B values for vertical structures suggested in literature is the result of the variety of wave and structural parameters that authors report to have an effect on the shape parameter B (wave steepness, impulsiveness and relative crest freeboard). As a consequence, it is difficult to suggest an integrated approach for the B values of vertical structures and to estimate the accuracy of the predictions. The most recent predictions by Victor et al. (2012) and Hughes et al. (2012) agree with the predictions by Franco et al. (1994), Franco and Franco (1999) and Besley (1999) for relative crest freeboards $R_c/H_{m0} > 2$ in giving B predictions $B \leq 1$. For values $R_c/H_{m0} < 2$ Victor et al. (2012) and Hughes et al. (2012) proved that the B values were $B > 1$. Therefore for low-crested structures it is more reasonable to use these two predictions.

Table 2.5 shows an overview of the various shape factor B prediction values prediction formulae presented in this section for mild sloping, steep low-crested and vertical structures.

Table 2.5: Summary of the shape factor B prediction formulae presented in this section, with their reference and structure type validity.

Shape factor B	Reference	Structure type
0.75	Franco et al. (1994), Van der Meer and Janssen (1994), EurOtop (2007)	Mild sloping
0.76 for $s_{op} = 0.02$ 0.92 for $s_{op} = 0.04$	Besley (1999)	Mild sloping
0.74	Bruce et al. (2009)	Mild sloping
Eq. 2.30	Victor et al. (2012)	Steep low-crested
Eq. 2.31	Hughes et al. (2012)	Steep low-crested
Eq. 2.32	Zanuttigh et al. (2013), EurOtop (2016)	Low-crested
0.75	Franco et al. (1994)	Vertical
0.66 – 0.86	Franco and Franco (1999)	Vertical
0.66 for $s_{op} = 0.02$ 0.82 for $s_{op} = 0.04$	Besley (1999)	Vertical, non-impulsive waves
0.85	Besley (1999)	Vertical, impulsive waves

2.4.3 Probability of Overtopping P_{ow}

The probability of overtopping P_{ow} is defined by Eq. 2.33, in which N_{ow} is the number of overtopping waves and N_w is the number of incident waves at the toe of the structure. Van der Meer and Janssen (1994) and Franco et al. (1994) stated that the run-up heights distribution follows a Rayleigh distribution, giving the theoretical probability of overtopping P_{ow} described by Eq. 2.34, where the coefficient χ (Eq. 2.35) is related to the relative 2% run-up height $R_{u2\%}/H_{m0}$ when run-up heights are Rayleigh distributed. The relation presented between P_{ow} and $R_{u2\%}/H_{m0}$ is based on knowledge of structures with a limited amount of overtopping, and hence, questions raise about the validity of this relation for structure with large overtopping rates, like steep low-crested structures.

The theoretical limit values of the probability of overtopping P_{ow} are 1 for the case of zero freeboard (all waves overtop the crest of the structure) and 0 for the case of very large relative crest freeboards (no waves overtop the structure):

$$P_{ow} = \frac{N_{ow}}{N_w} \quad (2.33)$$

$$P_{ow} = \exp\left(-\left(\frac{1}{\chi} \cdot \frac{R_c}{H_{m0}}\right)^2\right) \quad (2.34)$$

$$\chi = \frac{R_{u2\%}}{H_{m0}} \frac{1}{\sqrt{-\ln(0.02)}} \approx 0.51 \frac{R_{u2\%}}{H_{m0}} \quad (2.35)$$

Mild Sloping Structures

Various authors suggested values for the relative 2% run-up height $R_{u2\%}/H_{m0}$ or the probability of overtopping P_{ow} . Van der Meer and Janssen (1994) suggested to use Eq. 2.36, with a maximum for non-breaking waves presented in Eq. 2.37, to predict $R_{u2\%}/H_{m0}$ for smooth sloping structures:

$$\begin{aligned}\frac{R_{u2\%}}{H_{m0}} &= 1.5 \cdot \gamma_h \gamma_f \gamma_\beta \gamma_b \xi_p \\ \chi &= 0.76 \cdot \gamma_h \gamma_f \gamma_\beta \gamma_b \xi_p\end{aligned}\quad (2.36)$$

with a maximum of

$$\begin{aligned}\frac{R_{u2\%}}{H_{m0}} &= 3.0 \cdot \gamma_h \gamma_f \gamma_\beta \\ \chi &= 1.53 \cdot \gamma_h \gamma_f \gamma_\beta\end{aligned}\quad (2.37)$$

In these equations, $\gamma_h, \gamma_f, \gamma_\beta$ and γ_b are influence factors taking into account the effect of shallow foreshores, slope roughness, oblique wave attack and a berm, respectively; and ξ_p is the peak surf similarity parameter. The equations also show the resulting value of the coefficient χ following Eq. 2.35. The probability of overtopping (P_{ow}) that is derived from Eq. 2.37 for non-breaking waves is shown in Eq. 2.38:

$$P_{ow} = \exp\left(-\left(0.65 \frac{R_c}{H_{m0}}\right)^2\right)\quad (2.38)$$

The TAW (2002) manual suggested a different expression for $R_{u2\%}/H_{m0}$ using the surf similarity parameter $\xi_{m-1,0}$ based on the mean spectral wave period $T_{m-1,0}$. The expression is shown in Eq. 2.39, with the maximum for non-breaking waves shown in Eq. 2.40:

$$\begin{aligned}\frac{R_{u2\%}}{H_{m0}} &= 1.65 \cdot \gamma_h \gamma_f \gamma_\beta \gamma_b \xi_{m-1,0} \\ \chi &= 0.84 \cdot \gamma_h \gamma_f \gamma_\beta \gamma_b \xi_{m-1,0}\end{aligned}\quad (2.39)$$

$$\frac{R_{u2\%}}{H_{m0}} = 1.0 \cdot \gamma_f \gamma_\beta \gamma_b \left(4 - \frac{1.5}{\sqrt{\xi_{m-1,0}}}\right)\quad (2.40)$$

The range of application of this prediction for the parameters $\gamma_\beta \xi_{m-1,0}$ is $0.5 < \gamma_\beta \xi_{m-1,0} < 8-10$, and the reliability is expressed with a variation coefficient of $\sigma' = 0.07$. Eqs. 2.39 and 2.40 are included in the EurOtop (2007) and the EurOtop (2016) manuals to predict the values of the relative 2% run-up $R_{u2\%}/H_{m0}$ for smooth sloping structures.

When applying the $R_{u2\%}/H_{m0}$ expressions to Eq. 2.34, the probability of overtopping P_{ow} is dependent on the relative crest freeboard R_c/H_{m0} and the surf similarity parameter (either ξ_p or $\xi_{m-1,0}$). For non-breaking waves, Eq. 2.37 suggests a constant value for the relative 2% run-up $R_{u2\%}/H_{m0}$, while the prediction for $R_{u2\%}/H_{m0}$ increases for increasing values of the surf similarity parameter $\xi_{m-1,0}$ in Eq. 2.40. These predictions are only valid for mild sloping structures given that the range of application associated with the surf similarity parameter $\xi_{m-1,0}$ is similar to the $\xi_{m-1,0}$ values obtained for this type of structures. A steep low-crested structure would have a larger $\xi_{m-1,0}$ with vertical structures as the limit case, for which $\xi_{m-1,0}$ is mathematically undefined.

Vertical Structures

For vertical structures, a theoretical value of the relative 2% run-up $R_{u2\%}/H_{m0}$ can be calculated. A non-overtopped vertical structure has a theoretical 100% wave reflection. Therefore, the run-up height is equal to the incident wave height, and $R_{u2\%} = H_{2\%}$ in the case of linear waves with pulsating behaviour. If the wave heights are Rayleigh distributed, the theoretical $R_{u2\%}/H_{m0}$ expression for vertical structures is shown in Eq. 2.41, which gives the probability of overtopping (P_{ow}) shown in Eq. 2.42:

$$\frac{R_{u2\%}}{H_{m0}} = \frac{H_{2\%}}{H_{m0}} = 1.4 \quad (2.41)$$

$$P_{ow} = \exp\left(-\left(1.4 \frac{R_c}{H_{m0}}\right)^2\right) \quad (2.42)$$

Franco et al. (1994) found the value for vertical structures $R_{u2\%}/H_{m0} = 1.78$ ($\chi = 0.91$), which is slightly larger than the theoretical value for vertical structures (Eq. 2.41). These values of $R_{u2\%}/H_{m0}$ for vertical structures are lower than the values suggested in literature for mild sloping structures in Eqs. 2.39 and 2.40. The probability of overtopping P_{ow} by Franco et al. (1994) is presented in Eq. 2.43:

$$P_{ow} = \exp\left(-\left(1.1 \frac{R_c}{H_{m0}}\right)^2\right) \quad (2.43)$$

From analysing only the former expressions for mild sloping structures it could be expected that for steep low-crested structures the values of $R_{u2\%}/H_{m0}$ would remain constant when $\xi_{m-1,0} > 8-10$. However, for vertical structures—which are the limit case of steep low-crested structures—, $R_{u2\%}/H_{m0}$

is lower than for mild sloping structures. This suggests a different behaviour of the wave run-up for steep low-crested structures than the one suggested by the traditional formulation of Eqs. 2.39 and 2.40.

Steep Low-Crested Structures

Victor et al. (2012) investigated the steep low-crested structures with the dataset UG10 and found that indeed the relative 2% run-up $R_{u2\%}/H_{m0}$ was decreasing for steep low-crested structures until reaching approximately the theoretical value for vertical structures. Moreover, the values of the surf similarity parameter $\xi_{m-1,0}$ in the UG10 dataset are not constant for $2 < \xi_{m-1,0} < 8-10$ as suggested by Eqs. 2.39 and 2.40 but behave as steep low-crested structures and decrease. The authors found also a dependency of $R_{u2\%}/H_{m0}$ on the slope angle α of the structure.

The probability of overtopping suggested by Victor et al. (2012) is shown in Eq. 2.44:

$$P_{ow} = \exp \left[- \left((1.4 - 0.3 \cot \alpha) \frac{R_c}{H_{m0}} \right)^2 \right] \quad (2.44)$$

The range of application of Eq. 2.44 is for slope angles $0 \leq \cot \alpha \leq 2.5$ and relative crest freeboards $R_c/H_{m0} > 0.4$. The coefficient inside of the exponential expression has a minimum value of 0.65. The authors decided to take into the prediction the theoretical value of P_{ow} for vertical structures (Eq. 2.42) as the limit case for vertical structures ($\cot \alpha = 0$) and the Van der Meer and Janssen (1994) prediction (Eq. 2.38) as the limit case for $\cot \alpha = 2.5$. If $\cot \alpha > 2.5$ the authors suggest to use Eq. 2.38 instead. Eq. 2.45 is the relative 2% run-up $R_{u2\%}/H_{m0}$ by Victor et al. (2012) based on Eq. 2.44:

$$\frac{R_{u2\%}}{H_{m0}} = \frac{1}{0.71 - 0.15 \cot \alpha} \quad (2.45)$$

As mentioned at the beginning of this Section, the use of the relation between P_{ow} and $R_{u2\%}/H_{m0}$ showed in Eqs. 2.34 and 2.35 should be questioned for structures with large overtopping rates, as it is the case for steep low-crested structures. Victor et al. (2012) stated that in this case, the relation between Eqs. 2.44 and 2.45 is still valid because the prediction was only fitted through tests with $R_c/H_{m0} > 0.4$ with rather low overtopping rates.

Figure 2.7 shows the probability of overtopping P_{ow} predictions by Van der Meer and Janssen (1994) (blue solid line, Eq. 2.38), the theoretical prediction for vertical structures (red solid line, Eq. 2.42) and the prediction by

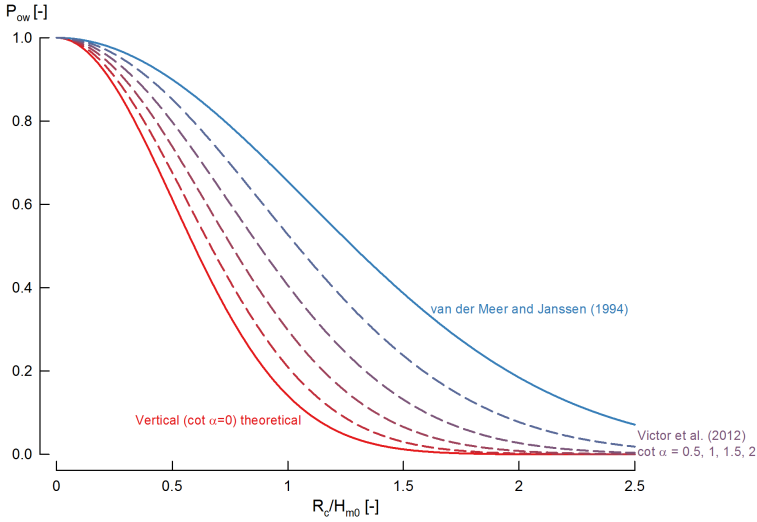


Figure 2.7: Comparison the probability of overtopping P_{ow} prediction formulae by Van der Meer and Janssen (1994) (Eq. 2.38), the theoretical prediction for vertical structures (Eq. 2.42) and Victor et al. (2012) for $\cot \alpha = 0.5, 1, 1.5, 2$.

Victor et al. (2012) for the values $\cot \alpha = 0.5, 1, 1.5, 2$ (red to blue graded dashed lines, Eq. 2.44). As aforementioned, the vertical theoretical P_{ow} prediction and the prediction by Van der Meer and Janssen (1994) are the limit cases for Victor et al. (2012) for $\cot \alpha = 0$ and $\cot \alpha = 2.5$. Franco et al. (1994) prediction (Eq. 2.43) for vertical walls is the same as Victor et al. (2012) for $\cot \alpha = 1$, indicating that the Franco et al. (1994) prediction of P_{ow} for vertical structures is lower in the case of Victor et al. (2012).

Table 2.6 shows an overview of the various probability of overtopping P_{ow} prediction formulae presented in this section for mild sloping, steep low-crested and vertical structures.

Table 2.6: Summary of the probability of overtopping P_{ow} prediction formulae presented in this section, with their reference and structure type validity.

Probability of overtopping P_{ow}	Reference	Structure type
Eq. 2.38	Van der Meer and Janssen (1994)	Mild sloping
Eq. 2.42	Theoretical	Vertical
Eq. 2.43	Franco et al. (1994)	Vertical
Eq. 2.44	Victor et al. (2012)	Steep low-crested ($R_c/H_{m0} > 0.4$)

2.4.4 Maximum Volume V_{\max}

The maximum individual overtopping volume V_{\max} of a series of waves is estimated by Eq. 2.46 if the individual overtopping volumes follow a two-parameter Weibull distribution. V_{\max} depends on the scale factor A , the shape factor B and the number of overtopping waves N_{ow} . Reordering Eq. 2.33, $N_{ow} = P_{ow}N_w$, and hence, V_{\max} can be estimated by combining the predictions of B (see Section 2.4.2) and of P_{ow} (see Section 2.4.3). The maximum volume V_{\max} is then proportional to the number of incident waves N_w which depends on the duration of a storm event.

$$V_{max} = A [\ln(N_{ow})]^{\frac{1}{B}} \quad (2.46)$$

For conditions with only one overtopping wave $N_{ow} = 1$, the result according to Eq. 2.46 is $V_{max} = 0$, which is not true. Lykke Andersen and Burcharth (2009) addressed this problem by prescribing the ratio between V_{max} and the total overtopped volume in relation to the scale factor A and the shape factor B . Their new expression also improves the estimation of the maximum volumes with $N_{ow} < 10$.

2.5 Summary

After a thorough review of the literature available for wave overtopping on steep low-crested structures for average and individual overtopping, the following knowledge gaps on the data are identified:

- overtopping data for very steep slopes ($0.27 \geq \cot \alpha > 0$) for complete range of relative crest freeboards R_c/H_{m0} ;
- overtopping data for zero freeboards ($R_c = 0$) and very small relative freeboards ($0.11 > R_c/H_{m0} > 0$) for the complete range of slope angles α ;
- overtopping data for relatively shallow water conditions and non-breaking waves; and
- overtopping data for stepped revetments with steep slopes.

By covering these knowledge gaps with new overtopping data, the overtopping process can be better described and analysed. The objectives of this dissertation are then redefined to be more specific than the ones defined in Section 1.3. These specific objectives are:

- determination of the average overtopping rates for the steep low-crested structures used in the experiments;

- improvement of the average overtopping prediction formulae on the range of very steep slopes to vertical structures with very small to zero freeboards;
- determination of the effects of relatively shallow water conditions on the average overtopping;
- determination of the individual overtopping volumes distribution for steep low-crested structures, obtaining the scale factor A , the shape factor B and the probability of overtopping P_{ow} ;
- improvement of the prediction formulae for B and P_{ow} on the range of very steep slopes to vertical structures with very small to zero freeboards;
- determination of the relatively shallow water effects on the individual volumes distribution;
- determination of the average overtopping for stepped revetments with steep slopes and small relative freeboards; and
- determination of the individual overtopping distribution for stepped revetments with steep slopes and small relative freeboards.

These knowledge gaps and the redefined objectives are considered in order to design and set up the methodology for this research described in Chapter 3.

Chapter 3

Research Methodology

This chapter describes what was done to investigate wave overtopping on steep low-crested structures and the methods used to obtain and analyse the new overtopping data acquired to fill the knowledge gaps in wave overtopping scientific literature.

The main objectives are outlined in Section 1.3. The main objectives are redefined by more specific objectives based on a literature review in Section 2.5.

3.1 Methodology Outline

The methodology used to meet the objectives of the research is experimental. The knowledge increase of the wave overtopping process for steep low-crested structures is achieved by performing hydraulic model tests that increase the experimental wave overtopping data available in the scientific literature. The acquired data are analysed and results are obtained, interpreted and incorporated in the scientific knowledge available on the wave overtopping process.

Two-dimensional hydraulic experimental model tests were performed at the wave flume of the Department of Civil Engineering at Ghent University. The design of the test programme that was followed for the model tests is explained in Section 3.2. The raw data of the wave overtopping and the wave parameters were processed (see Section 4.3), obtaining the incident wave conditions and overtopping parameters (both for average and individual overtopping) for all the tests performed.

The obtained results were analysed regarding the various wave and structural parameters to obtain significant relations that explain and describe the

overtopping process for steep low-crested structures. The results were compared to the existing overtopping prediction formulae, analysing the accuracy of the prediction for various ranges of the most significant wave and structural parameters, with special focus on the overtopping prediction for the range of steep low-crested structures. The accuracy of the predictions are measured by the root mean square error (RMSE) and the bias, both explained in Section 3.4.

If prediction inaccuracies were detected for the existing prediction formulae available in literature, new formulas were derived adding the new data acquired in this research to existing overtopping data of the scientific literature when available. The new prediction formulae obtained focus on improving the prediction for steep low-crested structures while maintaining the accuracy for the rest of structural types.

3.2 Design of Hydraulic Model Tests

To meet the specific research objectives detailed in Section 2.5, the main wave and structural parameters (see Figure 1.1) that influence the overtopping process were identified. The parameters are the relative crest freeboard (defined by R_c/H_{m0} , Section 3.2.1), the structure slope angle (defined by α , Section 3.2.2), the relative water depth (defined by H_{m0}/h , see Section 3.2.3) and the roughness of the slope (see Section 3.2.4).

The study of these four parameters based on the aforementioned specific objectives allowed to design the experimental test programme of the hydraulic model tests that form the wave overtopping datasets. The parameter values were varied in order to meet the specific objectives, therefore focusing on covering the complete range of steep low-crested structures, for relatively deep and relatively shallow water conditions. Roughness on the slope of the structure is added to study the differences in the overtopping behaviour compared to smooth slopes. The influence of the wind has not been considered in the hydraulic model tests, as it was not possible to simulate it in the 2D facility used to perform the tests.

The UG10 overtopping dataset, previously obtained at Ghent University, was also considered in the design of the design of the hydraulic model tests. The UG10 dataset features smooth structures data for mild and steep slopes with large and small freeboards. The new datasets are obtained for slope angles and relative freeboards that were not considered in the UG10 dataset.

3.2.1 Relative Crest Freeboard R_c/H_{m0}

The structural parameter R_c/H_{m0} is the main parameter that defined the amount of overtopping on coastal structures. A steep low-crested structure is defined (see Table 1.2) by small ($0.8 > R_c/H_{m0} \geq 0.11$), very small ($0.11 > R_c/H_{m0} > 0$) and zero ($R_c = 0$) relative crest freeboards. The limit case with large relative crest freeboards ($R_c/H_{m0} \geq 0.8$) is also included in the design test programme to have an understanding of the overtopping for the complete range of relative freeboards.

The relative crest freeboard is the ratio between the crest freeboard R_c and the incident spectral wave height H_{m0} . Therefore, values of R_c and target H_{m0} are chosen to meet the wanted values of R_c/H_{m0} . To select the values of R_c the only limitation is the total height of the structure, which is either 0.53 m or 0.57 m (see Section 4.1). To select the values of H_{m0} , the limitation is the physical capabilities of the wave generation system of the wave flume at Ghent University where the research was carried out (see Section 4.1.1).

3.2.2 Slope Angle α

The slope angle α is a structural parameter that influences the wave overtopping for steep low-crested structures. According to the definition made in Section 1.2 and Table 1.1, a steep low-crested structures is formed by steep slopes ($2 > \cot \alpha > 0.27$) and very steep slopes ($0.27 \geq \cot \alpha > 0$) up to the limit with vertical structures ($\cot \alpha = 0$). To have a complete understanding of the behaviour of the overtopping process, it is decided to perform also model tests for the limit cases of mild slopes ($\cot \alpha \geq 2$) and vertical structures ($\cot \alpha = 0$). To know the overtopping behaviour for these limit cases it is important to set a benchmark to compare the results obtained for the target structure types. The range of tested slope angles is $2.14 \geq \cot \alpha \geq 0$.

The resolution of the slope angles tested should be high enough so that the variations in the overtopping process due to small changes in the slope angle α are detected, but low enough so that those variations indeed exist. It is decided to perform physical model tests with a resolution of $\alpha = 10^\circ$ for mild and steep slopes, increasing to a resolution of $\alpha = 5^\circ$ for the very steep slopes range.

The extension ranges of relative crest freeboard R_c/H_{m0} and slope angle α are divided in three different zones Z1*, Z2* and Z3* according to Victor and Troch (2012b) (Table 3.1).

Table 3.1: Definition of the extension zones Z1*, Z2* and Z3* as a function of the slope angle α and relative crest freeboard R_c/H_{m0} according to Victor and Troch (2012b) .

		Relative crest freeboard R_c/H_{m0}	
		$0 \leq R_c/H_{m0} < 0.11$	$0.8 \leq R_c/H_{m0} \leq 2$
$\cot \alpha$	$0 \leq \cot \alpha \leq 0.27$	Z1*	Z2*
	$1.5 \leq \cot \alpha \leq 2.75$	Z3*	N/A

3.2.3 Relative Water Depth H_{m0}/h

The relative water depth H_{m0}/h is a wave parameter that is directly linked to the relative crest freeboard R_c/H_{m0} , as the local water depth at the toe of the structure h is the difference between the height of the structure and the crest freeboard R_c . The variation in relatively water depth is linked to the specific objective of improving the knowledge of the influence of relatively shallow water conditions on the overtopping for non-breaking conditions.

The relatively deep water conditions $H_{m0}/h < 0.2$, the relatively shallow water conditions $H_{m0}/h > 0.5$ and the transitional zone between them $0.2 < H_{m0}/h < 0.5$ were covered by the model tests. The results of the relatively deep water conditions were compared to the results of increasing relatively shallow water conditions (increasing H_{m0}/h) to study the influence of the relatively shallow water conditions on wave overtopping.

3.2.4 Roughness of the Slope

An increase of the roughness on the slope reduces the average overtopping rates. For steep low-crested structures this overtopping reduction has not been studied in detail. The model tests within this research are designed to study the effect of adding roughness to the structure slope and compare it with tests for smooth slopes with similar slope angle and relative crest freeboard conditions. The roughness of the slope is determined by the influence factor γ_f , which indicates the reduction on the overtopping rates due to roughness compared to the reference case of a smooth slope.

It is decided to add blocks as roughness element on the slope. However, the first results prove that blocks had little reduction of the overtopping due to the small surface coverage and therefore small increase of energy dissipation of the incident waves. The blocks are converted into ribs, which increase the area coverage, the energy dissipation and the overtopping reduction.

The stepped revetments are also included in the research, as a second type of roughness elements with a more practical application as sea defence structures. The stepped revetments were designed based on existing literature which is limited, and non-existent for steep structures. Therefore, it is decided to investigate the overtopping behaviour for stepped revetments with steep slopes.

3.3 Wave Overtopping Datasets

The hydraulic model tests are divided into four different datasets, obtained in consecutive years: UG13, UG14, UG15 and UG16. Each of the datasets focused on specific ranges of the four parameters relative crest freeboard R_c/H_{m0} , slope angle α , relative water depth H_{m0}/h and slope roughness (see Sections 3.2.1 to 3.2.4).

UG13 features tests on a smooth structure for mild, steep, very steep slopes and vertical structures, with relative crest freeboards from large to zero, and relatively deep water conditions. UG14 and UG15 features tests on a smooth slope for steep, very steep slopes and vertical structures, with relative crest freeboards from large to zero. The UG14 dataset covers entirely the transitional zone of relative water depths, while the UG15 dataset covers part of the transitional zone and the relatively shallow water conditions. The UG16 dataset features tests with roughness elements on the slope for steep slopes with relative crest freeboards from small to large and for relatively deep water conditions.

Figure 3.1 shows a sketch plot of the slope angle $\cot \alpha$ versus the relative crest freeboard R_c/H_{m0} indicating the range of the tests of the UG13, UG14, UG15 and UG16 dataset, including the UG10 dataset for comparison. As shown, the UG13, UG14 and UG15 datasets cover the gap of very steep slopes and vertical structures with very small and zero relative freeboards left by UG10. The UG16 dataset only includes data for two different slope angles with roughness elements, therefore, not covering the complete range of steep low-crested structures.

Figure 3.2 shows a sketch plot of the slope angle α versus the relative wave height H_{m0}/h that indicates the range of the datasets UG13, UG14, UG15 and UG16 on these two parameters, including the UG10 dataset for comparison. The UG10 and the UG13 datasets are focused on wave overtopping for relatively deep water conditions, while the UG14 and UG15 dataset cover the relatively shallow water conditions and the transitional zone. The UG16 featured tests mostly for relatively deep water conditions.

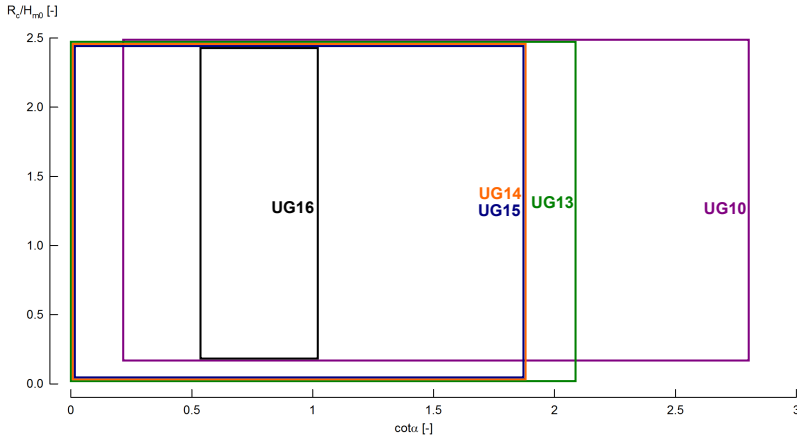


Figure 3.1: Sketch plot of the slope angle $\cot \alpha$ versus the relative crest freeboard R_c/H_{m0} of the datasets UG10, UG13, UG14, UG15 and UG16.

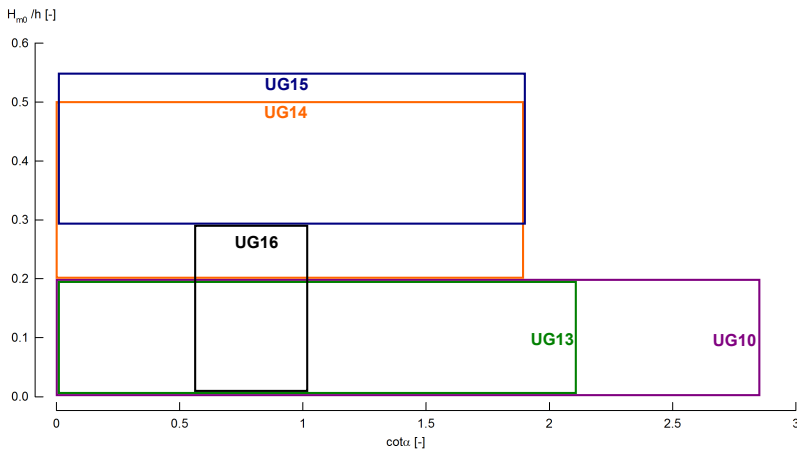


Figure 3.2: Sketch plot of the slope angle $\cot \alpha$ versus the relative wave height H_{m0}/h of the datasets UG10, UG13, UG14, UG15 and UG16.

The design of the datasets suffered later small modifications due to various factors including physical limitations of the facility and time available to perform the tests. Section 4.2 shows the final range of values of the tests performed for all the datasets.

3.4 Assessment of the Accuracy of a Prediction

To assess the accuracy of the prediction formulae, the root mean square error (RMSE) will be used, following Eq. 3.1, while the bias of the prediction is shown in Eq. 3.2:

$$\text{RMSE} = \sqrt{\frac{1}{N_{\text{test}}} \sum_{n=1}^{N_{\text{test}}} \left[\frac{q_{\text{pred}_n}}{\sqrt{gH_{m0}^3}} - \frac{q_{\text{meas}_n}}{\sqrt{gH_{m0}^3}} \right]^2} \quad (3.1)$$

$$\text{Bias} = \frac{1}{N_{\text{test}}} \sum_{n=1}^{N_{\text{test}}} \left[\frac{q_{\text{pred}_n}}{\sqrt{gH_{m0}^3}} - \frac{q_{\text{meas}_n}}{\sqrt{gH_{m0}^3}} \right] \quad (3.2)$$

In Eq. 3.1, N_{test} is the total number of data used to calculate the RMSE, q_{pred_n} the absolute average overtopping predicted for the test n , and q_{meas_n} the absolute average overtopping measured for the test n . A smaller RMSE value for a specific set of data means a more accurate prediction than a larger RMSE value. The comparison between RMSE values from different predictions is only possible for the same set of data. The bias of the prediction (Eq. 3.2) is calculated to assess if there is underprediction or overprediction of the measured overtopping values. A positive value of bias indicates that the overtopping is overpredicted for the considered data, while a negative value of bias indicates underprediction.

The root mean square logarithmic error (RMSLE) is shown in Eq. 3.3. The expression is comparable to Eq. 3.1 although calculating the decimal logarithm of the predicted and measured dimensionless average overtopping rates. Also, the coefficient c of a Weibull-type prediction of the dimensionless average overtopping rates (see Section 2.3.3) is included in the expression to account for cases with $c \neq 1$.

$$\text{RMSLE} = \sqrt{\frac{1}{N_{\text{test}}} \sum_{n=1}^{N_{\text{test}}} \left[\left(-\log \left(\frac{q_{\text{pred}_n}}{\sqrt{gH_{m0}^3}} \right) \right)^{1/c} - \left(-\log \left(\frac{q_{\text{meas}_n}}{\sqrt{gH_{m0}^3}} \right) \right)^{1/c} \right]^2} \quad (3.3)$$

The RMSLE is also considered as a tool to assess the accuracy of average overtopping prediction. The main difference between the RMSE and the RMSLE is the weight that the two expressions apply to the relative error between the prediction and the measurement. The RMSE applies a larger weight on the relative errors of larger values of the dimensionless average overtopping rate, while the RMSLE applies the same weight for equal relative errors. However,

the experimental overtopping data show a larger scatter of the average overtopping rates for lower values (large relative freeboards) than for larger values (small relative freeboards). Also most of the existing average overtopping predictions like Eq. 2.2 and Eq. 2.5 have smaller prediction uncertainties for larger overtopping rates than for smaller overtopping rates. Therefore, the weight of the relative errors should be linked to the absolute value of the dimensionless average overtopping rate, as does the RMSE. Moreover, one of the objectives of this research is to assess the overtopping prediction for zero and very small relative freeboards, which have larger average overtopping rates. For these reasons, the RMSE is used instead of the RMSLE to assess the accuracy of the prediction formulae.

Chapter 4

Experimental Setup and Test Programme

In this chapter, a description of the experimental setup and the test programme of the 2D physical model tests carried out within this research are presented. The wave parameters and wave overtopping measurement systems are described, and the processing of the data is explained in detail.

4.1 Experimental Setup

The experimental setup is described in this section. The model tests are carried out at the wave flume of Ghent University, measuring wave parameters and wave overtopping. For each dataset a test setup is defined for various slope angles and water depths, defining the complete range of steep low-crested structures.

4.1.1 Wave Flume at Ghent University

The wave flume of Ghent University (Figures 4.1a and 4.1b) is located at the Department of Civil Engineering, and it is operational since March 2003. It has a length of 30 m, a width of 1 m and a height of 1.2 m, with a design water depth of 0.8 m and a maximum wave height of about 0.35 m (Dept. of Civil Engineering Ghent University, 2010). The wave flume walls are made of reinforced concrete except for a 15 m section of one side wall which is made of 30-mm-thick glass supported by a steel frame. This section is located at one end of the wave flume, opposite to the wave paddle, to allow a direct view on

the tested models. It is also possible to generate currents with an electrical pump and manual valves to regulate flow and direction.

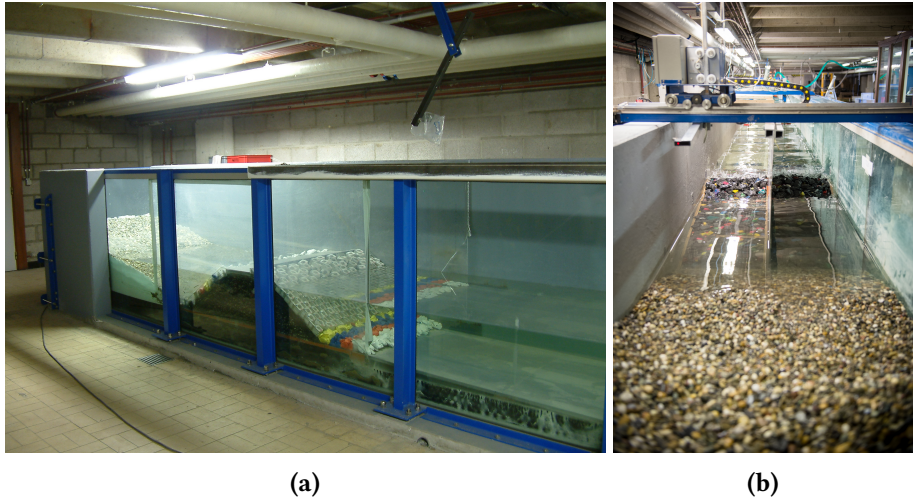


Figure 4.1: Different views of the wave flume at Ghent University while testing rubble mound breakwaters: (a) from the glass window, and (b) from the inside of the wave flume.

Wave Paddle

The wave flume is equipped with a piston type wave paddle with a maximum stroke length of 1.5 m (Figure 4.2a). It is fixed to a moving open framework and moves on linear bearings. The distance of the wave paddle at its zero position to the back of the flume is 3.15 m. The paddle displacement is driven by an electro servo motor in step mode connected to a real time controller. The generation system is able to generate both regular and 1st order irregular waves, using an in-house software developed in LabVIEW™ environment (National Instruments, 2003) and coupled with the data acquisition system (DAQ). The calculated wave time series are transformed into paddle movements by the Biésel transfer function (Lykke Andersen and Frigaard, 2008).

Active Wave Absorption System (AWA)

The generation system is equipped with an active wave absorption system (AWA) that allows the wave paddle to absorb the reflected waves and simultaneously generate the desired wave time series. The AWA implemented is an in-house LabVIEW™ (National Instruments, 2003) software based on Frigaard and Christensen (1994) and Frigaard and Brorsen (1995).

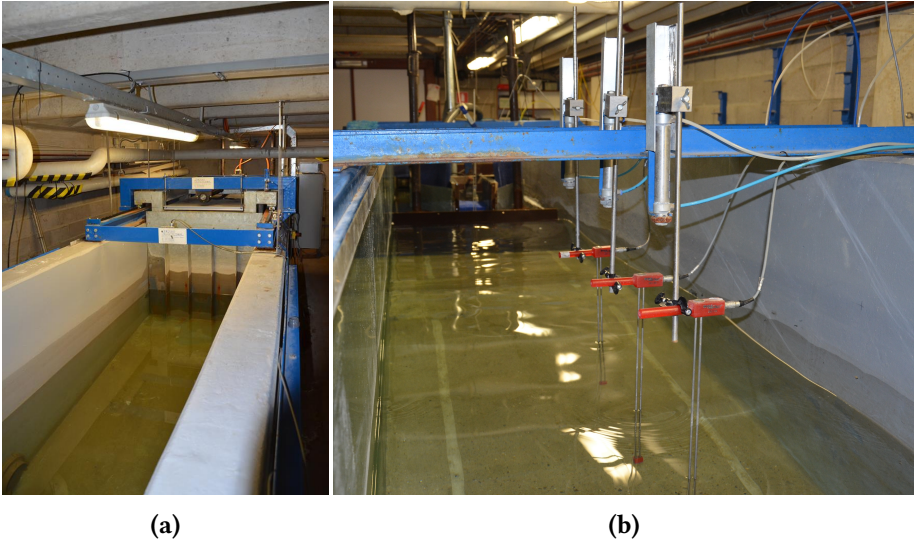


Figure 4.2: View of the (a) wave paddle and (b) wave gauges of the wave flume at Ghent University.

This AWA method requires the placement of two wave gauges (WG) in front of the wave paddle —although out of the near wave field, i.e., more than approximately three water depths from the wave paddle— and the design of two digital filters, which are able to separate the incident and reflected wave components in real time. The filtered surface elevations are superposed and added to the incident wave signal. As a result, the reflected wave is absorbed by the wave paddle (Dept. of Civil Engineering Ghent University, 2010). The design of the filter requires setting low-pass (with an associated high cut-off frequency f_{HC} between 1–1.6 Hz) and high-pass (with an associated low cut-off frequency f_{LC} between 0.25–0.35 Hz) filters which are selected to include the major part of the wave energy of the spectrum. This results in 5–10% of the peak frequency value f_p being left out from signal analysis. In Section 4.1.2 a further explanation of the distances between the active wave absorption wave gauges ($\Delta x_{AWA1,AWA2}$) is presented.

The AWA system available at the Ghent University wave flume consisting of two WGs in front of the wave paddle in combination with the first order wave generation, makes it very difficult to absorb waves in the low frequency range (i.e., infragravity waves with large wave periods). Therefore, it is not possible to absorb low frequency waves due to resonance (i.e., seiches). These waves may artificially increase the overtopping rates, especially for the low-freeboard conditions of this research. The experimental setup has a natural frequency between 0.035–0.055 Hz and therefore, a peak on the energy spec-

trum should be expected if resonance waves are occurring. When analysing the energy spectrum of the incident waves at an offshore position (see Section 4.1.2 for a description of the position of the WGs) very low values of spectral energy were found around the natural frequency. Therefore, no important contribution of seiche waves is expected on the overtopping rates.

4.1.2 Measurement Systems

During the physical model experiments carried out at Ghent University, the overtopping rates and the water surface elevations (i.e., wave heights and wave periods) were measured for all the tests.

Wave Parameters Measurements

The elevation of the water surface during the experiments is measured by resistive wave gauges (WG), model DHI 202 (Figure 4.2b), with a total length of 0.5 m, an acquisition rate of 40 Hz and a resolution < 0.001 m. The installed WGs are connected to a wave amplifier type DHI 102E. This type of WG consists of two electrodes (metal bars) situated partially under the water surface. The resistance value between the two bars is linearly proportional to the elevation of the water surface, and it is influenced by the conductivity of the water. The total wave height and the wave period can be calculated by analysing the signal from the WGs.

A source of errors in the measured WGs signal is the change of conductivity of the water due to temperature or alkalinity changes. The temperature of the water may change due to the addition of new water at a lower temperature. The alkalinity may change due to freshly placed cement (to build a foreshore or a structure in the wave flume), the appearance of algae in stagnant water if the water has been left in the wave flume for too long, or due to dust and dirt from previous experimental setups. The change of conductivity of the water was not compensated during the experiments, although it is possible to activate it at the expense of a lower measurement accuracy. Instead, when the reading of the WGs was differing ± 2 mm from the zero reading (at the SWL), or when the signal was drifting with calm water in between tests, a recalibration of the WGs was made to assure accurate and reliable water surface measurements. Also, extra care was taken when new water was added into the wave flume, after the construction of a new foreshore requiring cement. For the same reason, when the experiments had to be stopped for a long time period, the wave flume was emptied and the water was stored in reservoirs with no direct sunlight to avoid algae

growth. The WGs were maintained weekly to clean off the limescale that may accumulate in the metal bars of the WGs.

It is necessary to calibrate the WGs to have the correct relation between the resistance and the water surface elevation, i.e., to obtain the offset and the gain factor of the linear relation. The calibration is done by measuring the resistance values for two different known height positions of the WG: at the still water level (SWL) as the zero reference, and +0.1 m from the SWL, simulating a change in the water level. The height position of the WGs is changed by a compressed air system. To compensate for possible drifts in the signal, the WGs are calibrated for the overtopping tests in this research. The whole calibration process is fast and effortless for the wave flume operator, and therefore, it was performed as many times as necessary in between each test to guarantee a consistent reading from the WGs.

For all the tests, two arrays of 3 WGs were installed at two different locations of the wave flume to measure the incident and reflected waves. The first array (WG1, WG2 and WG3) is located in deep water (i.e., offshore position), with distances $\Delta x_{WG1,WG2}$ between WG1 and WG2, and $\Delta x_{WG1,WG3}$ between WG1 and WG3. The second array (WG4, WG5 and WG6) is located near the toe of the structure, with distances $\Delta x_{WG4,WG5}$ between WG4 and WG5, and $\Delta x_{WG4,WG6}$ between WG4 and WG6. To detect individual overtopping events, an additional wave gauge (WG7) is located at the crest of the structure. The different wave gauges are numbered in descending order from their relative position to the wave paddle, i.e., WG1 is the closest to the wave paddle and WG6 is the farthest to the wave paddle.

The distances in between the WGs in an array of 3 are based on the recommendations by Mansard and Funke (1980), which are shown in Eq. 4.1:

$$\begin{aligned} \Delta x_{WG1,WG2} &= \frac{L_p}{10} \\ \frac{L_p}{6} &< \Delta x_{WG1,WG3} < \frac{L_p}{3} \\ \Delta x_{WG1,WG3} &\neq \frac{L_p}{5} \text{ and } \Delta x_{WG1,WG3} \neq \frac{3L_p}{10} \end{aligned} \quad (4.1)$$

The distances are dependent on the peak wave length L_p . This recommendations are based on studies using monochromatic waves, and intend to avoid indeterminations on the reflection calculations that occur when $\Delta x_{WG1,WG2} = L_p/2$ and $\Delta x_{WG1,WG3}$ is an integer multiple of $\Delta x_{WG1,WG2}$. To apply the distance recommendations to the second array of WGs, WG1, WG2 and WG3 are equivalent to WG4, WG5 and WG6, respectively.

Another important parameter is the distance of the WGs from the reflective structure ($\Delta x_{WG6,toe}$). According to Klopman and Van der Meer (1999),

the distance should be $\Delta x_{\text{WG6,toe}} \geq 0.4L_p$ from the intersection of the reflecting structure with the still water level (SWL).

The WGs of the active wave absorption system (AWA) are installed in an array of 2, being the wave gauge AWA1 located at a fixed distance of 3 m from the wave paddle (out of the near wave field, see Section 4.1.1). The distance between AWA1 and AWA2 ($\Delta x_{\text{AWA1,AWA2}}$) follows the Goda and Suzuki (1976) criterion for reflection analysis $0.05L_{\text{max}} \leq \Delta x_{\text{AWA1,AWA2}} \leq 0.45L_{\text{min}}$, where L_{max} and L_{min} are the wave lengths corresponding respectively to the lower (f_{LC}) and upper (f_{HC}) limits of the effective frequency range.

Wave Overtopping Measurements

In scientific literature, three wave overtopping measurement techniques are described. All of them are based on the principle of measuring the evolution over time of the overtopped water, which is collected in a reservoir installed behind the structure. The first technique is to measure the water elevation of the reservoir by wave gauges. This system is commonly used to measure wave overtopping although the oscillations of the water inside the reservoir due to the impacts of the new overtopping events creates noise in the signal as the measurement is only on one point. These oscillations can be eliminated by installing an array of wave gauges in the reservoir and averaging the signals. A second technique is to install a pressure sensor at the bottom of the reservoir, which provides the pressure of the water column inside the reservoir. Similar to the wave gauge technique, the oscillations of the mass of water create noise in the signal. Moreover, the installation of pressure sensors inside the reservoir may be difficult. The third technique is to measure the mass of the water contained in the reservoir by weigh cells installed beneath it. The output signal is only affected by the average oscillations of the total volume of water inside the reservoir, and therefore the signal is more robust. Within the CLASH database (see Section 2.1), Van der Meer et al. (2005b) concluded that for small scale model tests, a wave overtopping measurement system based on the weigh cell technique is about two orders of magnitude more accurate than a system based on the wave gauge technique.

Victor (2012) developed a so-called overtopping box, which is presented in Victor and Troch (2010). The overtopping box was designed taking into account the requirements needed to measure wave overtopping for steep low-crested structures: large average overtopping rates and a combination of small and large wave-by-wave overtopping volumes. The former will create large oscillations of the water mass inside the reservoir, and the latter will require a system to measure with a high accuracy both conditions. To meet the requirements, Victor (2012) decided to measure wave overtopping using

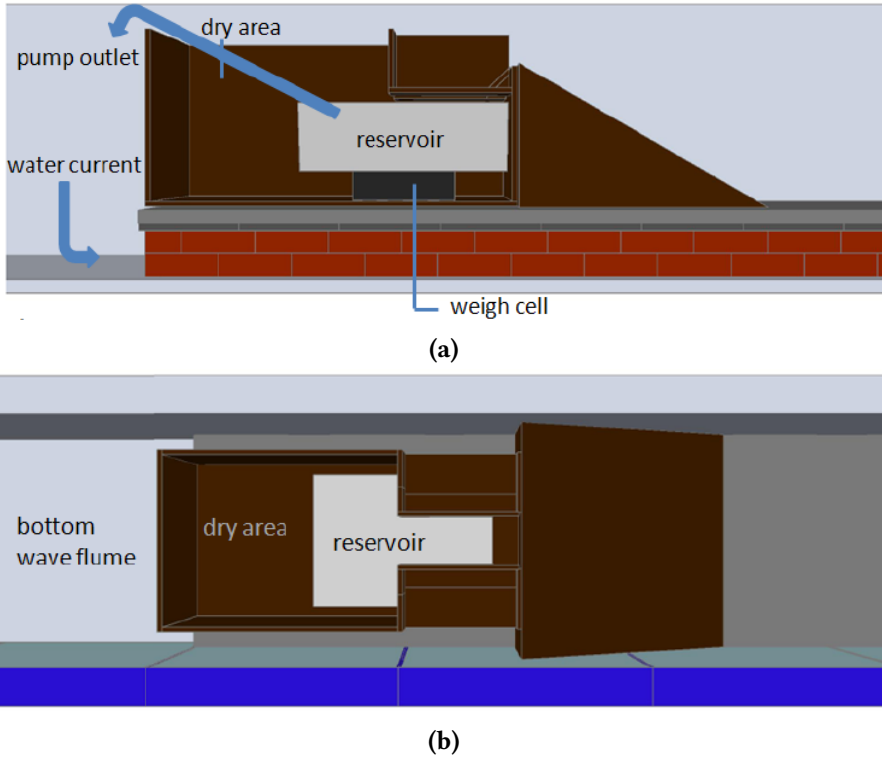


Figure 4.3: Drawing of the (a) cross section and (b) top view of the overtopping box in the wave flume (Victor, 2012).

the weigh cell technique as it is not affected by large oscillations of the mass of water in the reservoir (i.e., sloshing) and is more accurate than any other technique. To be able to measure with a high accuracy the wave-by-wave overtopping volumes, the box is designed to have a very short chute that connects the crest of the structure with the reservoir (Figures 4.3a and 4.3b). In this design, the overtopped water is almost instantly reaching the reservoir, and therefore, the increase of water mass is instantaneously measured by the weigh cell when the overtopping event occurs. The overtopping box is designed to contain the reservoir to collect the overtopped water, a weigh cell beneath it to measure the mass of the water, and a pump that returns the overtopped water to the wave flume.

The box is made of plywood panels, with its joints sealed with silicone to make the box watertight. It is placed inside the wave flume and behind the structure, and it has a smaller width than the wave flume to avoid water flowing into the box from the sides of the structure model. Figure 4.4a shows a picture of the overtopping box with all its parts marked, and Figure 4.4b

shows a front view of the structure and the chute, being B_q the width of the chute. The water that overtops the crest of the structure is carried by a (very short) chute of a certain width (either 0.1 m or 0.2 m, depending on the expected amount of overtopping), and collected in the reservoir installed inside the box. For the post-processing of the individual overtopping events it is necessary to know the time of the overtopping event. For this purpose, a WG (WG7) is installed at the crest of the structure, in front of the chute leading to the reservoir. The reservoir has a maximum capacity of 100 l which in practice is reduced to approximately 32 l, as a minimum water level inside it has to be assured at all times to guarantee that the pump works always on load and without suctioning any air, which may damage it. Beneath the reservoir, the weigh cell constantly measures the mass of the water in it. The weigh cell has a non-constant acquisition rate of around 5 Hz, and an accuracy of ± 0.005 kg. Inside the reservoir, the pump is installed (submerged and without any contact with the bottom of the reservoir) to return the water back into the wave flume. The pump is activated every time the weigh cell reaches a threshold value, which can be selected on the generation system software, as well as the duration of the pumping event.

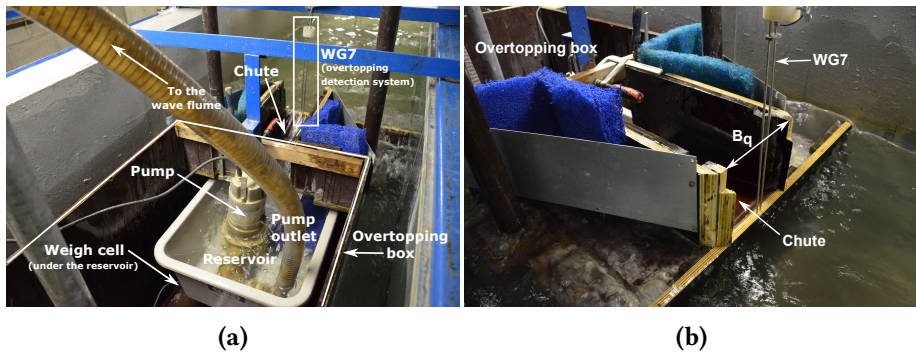


Figure 4.4: (a) Overtopping box used in the experiments and developed by Victor and Troch (2010); (b) front view of the structure and the chute.

The reservoir has to be calibrated for every dataset. The water creates an uplift force on the pump when it is partially submerged, resulting in an added weight on the weigh cell. To calibrate the reservoir, a known water volume of around 1 l is added into it, and the value of the weigh cell after adding the volume is written down. This procedure is performed repeatedly until reaching a value higher than the threshold value selected on the generation system software. There is a linear relation between the absolute mass added to the reservoir M_{abs} and the relative mass measured in the weigh cell $M_{rel,cell}$, as seen in Figure 4.5. The $\Delta M_{abs} = \Delta M_{rel,cell}$ line indicates the situation of

equal increase of mass between M_{abs} and $M_{\text{rel,cell}}$ (1 kg of added water into the reservoir equals 1 kg of water measured by the weigh cell).

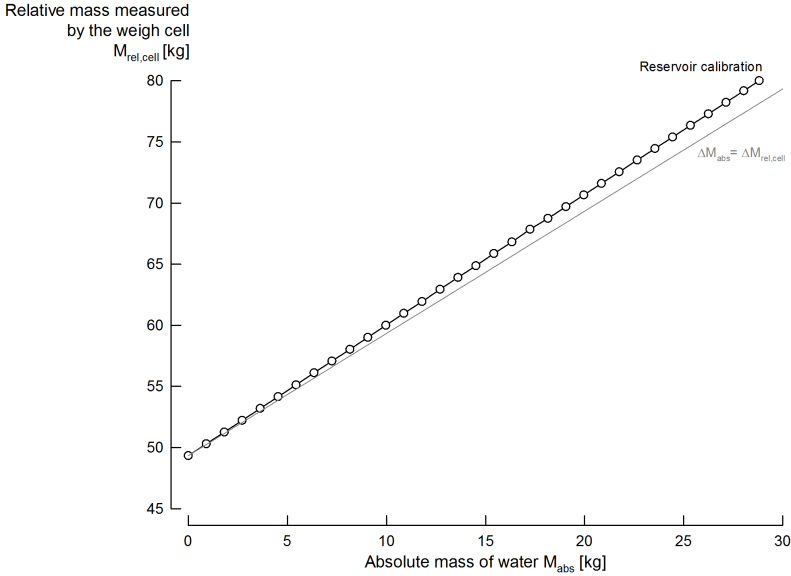


Figure 4.5: Calibration of the reservoir of the UG13 dataset, showing the absolute mass added to the reservoir (M_{abs}) versus the relative mass measured by the weigh cell ($M_{\text{rel,cell}}$), compared to the line indicating equal increase of mass for M_{abs} and $M_{\text{rel,cell}}$.

Also the pump has to be calibrated for every dataset. According to Victor (2012), the pump has a start-up phase of about 0.4 s (the pump is on, but the suction of water has not yet started), and a cool-down phase of about 2 s (the pump is off, but the inertia of the moving parts of the pump makes that the pump is still emptying the reservoir). The cooling-down phase varies for every pump action, meaning that the total mass of water pumped back into the wave flume is different in every pump action. To solve this, an average pump curve of the relative pumped mass versus time is calculated from ten different pumping events. Figure 4.6 shows the characteristic pump curve (average pump curve) in a black line and the ten different pump curves in grey lines. The variation of relative mass from the characteristic pump curve for different pumping events was calculated to be ± 0.09 kg for the UG10 dataset (Victor, 2012). The same value is assumed for the datasets obtained within this research. The characteristic pump curve is used in the post-processing of the data to calculate the average overtopping rates and the individual overtopping volumes.

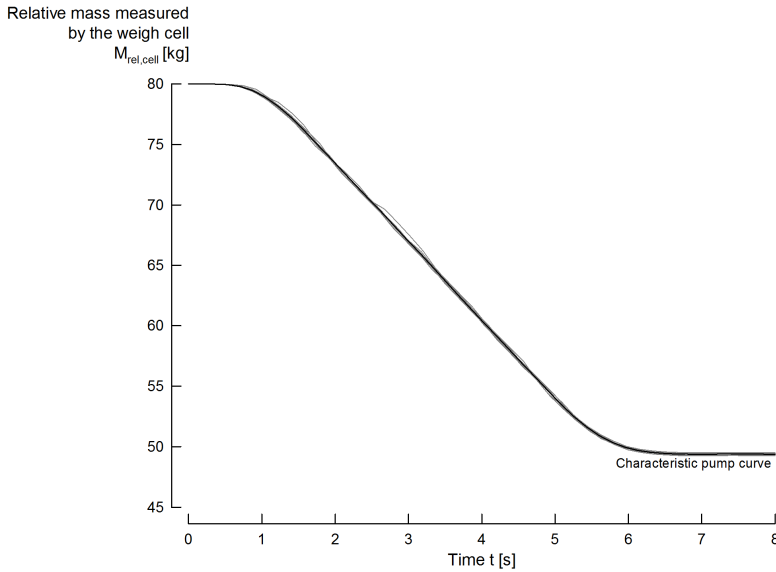


Figure 4.6: Characteristic pump curve (black line) of 10 pump curves (grey lines) of the UG13 dataset over time t .

4.1.3 Experimental Setup of Datasets

The four datasets obtained within this PhD research have a similar test setup, consisting of a foreshore at the bottom of the wave flume, the test structure at the end of the foreshore and the overtopping box (see Section 4.1.2) behind it. The main differences between datasets are the configuration of the foreshore and the model structure tested. The foreshores are considered mildly sloping and not influencing the incident wave conditions as wave breaking is not induced. The purpose of the foreshore is to elevate the model structure inside the wave flume for practical reasons, and to allow a return flow channel beneath the foreshore.

The model structure in the experimental setup consisted of a smooth impermeable plywood panel forming a given slope angle α with the foreshore (Figure 4.7). In the UG16 dataset, the model structure either had rough elements or was a stepped dike. The top part of the model structure supports the plywood panel acting as a hinge on which the plywood panel rotates to form a slope angle α with the foreshore. The height of the model structure over the foreshore is 0.53 m (except for the UG13 dataset, which is 0.57 m). Behind the test section the overtopping box was placed, so that the overtopped water is instantly collected by the reservoir. At the toe of the structure the water depth is h , and the distance between the still water level and the crest of the structure is the crest freeboard R_c .

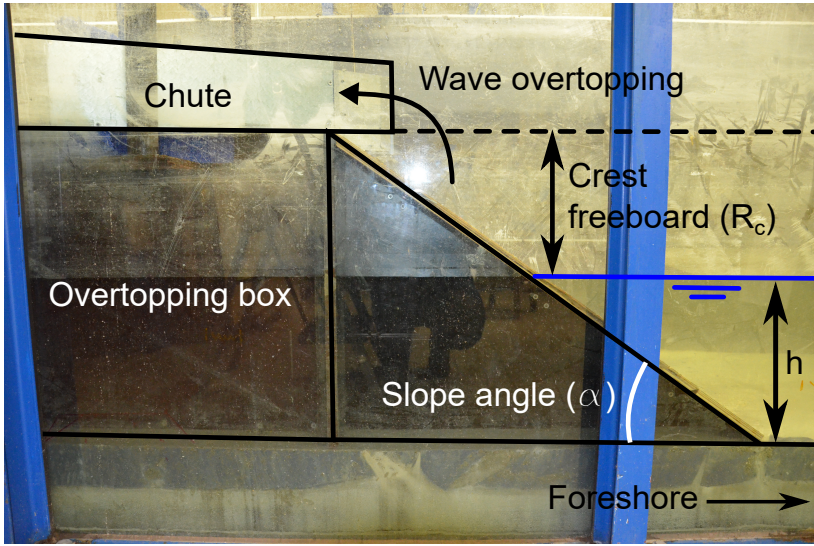


Figure 4.7: Cross section of the model structure.

All the experimental setups featured a so-called return flow channel, which consisted of a 0.2 m high channel constructed beneath the foreshore to allow the overtopped water to return to the central section of the flume in order to maintain a constant water level during the tests. This channel is wide enough to assure a low velocity flow that does not affect the incoming waves.

Wave conditions were measured at two different characteristic locations of the wave flume (deep water and near the toe of the structure, see Section 4.1.2) by two arrays of wave gauges. The distance between WG6 and the toe of the structure $\Delta x_{\text{WG6,toe}}$ is 2 m except for the UG13 dataset (see the paragraph corresponding to the UG13 dataset in this section). The wave gauges corresponding to the active wave absorption system were installed as the AWA was active for all the tests in all the datasets. The wave gauge acting as the overtopping detection system (WG7) was also installed for all the tests, to allow the calculation of the individual overtopping volumes in the post-processing.

As aforementioned, the number of waves analysed for each test was 1000. Therefore, during the experiments, more than 1000 irregular waves per test were generated to take into account the warm-up and cool-down periods that were not included in the wave analysis. First order waves were generated using a JONSWAP spectrum defined by H_s and T_p with a shape parameter of $\gamma = 3.3$.

UG13 Dataset

The test setup of the physical model tests corresponding to the UG13 dataset is shown in Figure 4.8a. The bottom of the wave flume featured a 1:20 concrete foreshore slope that was developed over 3 m, starting at a 10 m distance from the wave paddle and reaching a height of 0.27 m (including the return flow channel). It then continued as a horizontal foreshore for 9.5 m until the front of the model structure.

WG6 was installed at a constant distance of 2 m from the crest (and not the toe) of the model structure, which meets the requirement set by Klopman and Van der Meer (1999). For the UG13 dataset, the width of the overtopping chute was $B_q = 0.2$ m.

UG14 and UG15 Datasets

The test setup of the physical model tests corresponding to the UG14 and UG15 datasets is shown in Figure 4.8b. The bottom of the wave flume featured a 1:100 concrete foreshore slope which is based on the foreshore of the Nørgaard et al. (2014) experiments. The foreshore was developed over 15 m, starting at 7.6 m from the wave paddle and reaching a height of 0.2 m for the UG14 dataset and of 0.32 m for the UG15 dataset in front of the overtopping box (including the return flow channel), where a horizontal part of 0.75 m was located to have a constant toe height for all the slope angles. WG3 was located at the start of the 1:100 foreshore slope.

For the UG14 dataset, the width of the overtopping chute was $B_q = 0.1$ m, except for the first tests that were performed for which $B_q = 0.2$ m. The reduction of B_q was due to the excessive amount of overtopping that was causing the pump to overwork. A repeatability study was performed to analyse the influence of different B_q widths in the average overtopping rates. The data showed no influence of this parameter, and therefore a narrower width of $B_q = 0.1$ m was chosen to be able to measure large amounts of overtopping.

The test setup of the physical model tests corresponding to the UG15 dataset is identical to the setup of the UG14 dataset shown in Figure 4.8b. For all the tests in the UG15 dataset, the width of the overtopping chute was $B_q = 0.1$ m.

UG16 Dataset

The test setup of the physical model tests corresponding to the UG16 dataset is shown in Figure 4.8c. The bottom of the wave flume featured a 1:7.5 concrete

foreshore slope. The foreshore was developed over 1.5 m starting at 7.5 m from the wave paddle and reaching a height of 0.2 m (including the return flow channel) 13.5 m from the crest of the model structure. WG3 was located 2 m from the start of the 1:7.5 foreshore slope. For the UG16 dataset, the width of the overtopping chute was $B_q = 0.2$ m.

Three different types of roughness were analysed in this dataset: 5-step revetments (Figure 4.9a), 10-step revetments and artificial rough elements (Figure 4.9b).

The artificial roughness elements selected were individual blocks (smooth cubes with a 5 cm side) installed in a staggered pattern (Figure 4.10a). The width of the block in the direction of wave propagation is $f_b = 5$ cm, the height of the block is $f_h = 5$ cm and the distance between the centre of the blocks in the direction of wave propagation is $f_L = 10.2$ cm. Therefore, the ratio of the distance between blocks and the width is $f_L/f_b = 2.04$, while the recommendation is a range between 5–8 with an optimal at 7. If the recommended ratio values were followed, only a small number of rows with blocks could have been installed, therefore it was decided to increase the number of rows by reducing the distance ratio between them. The covering ratio of the total surface is 1/9. The maximum reduction of overtopping takes place for the ratio of the block height and the incident wave height $f_h/H_{m0} = 0.15$, and for all the tested wave heights the ratio is always higher, meaning that a larger block height f_h would not further reduce the overtopping.

It was observed after the experiments with the slope angle $\cot \alpha = 1$ ($\alpha = 45^\circ$) that this configuration of the individual blocks had a very small effect on the overtopping process. It was decided not to perform any test with individual blocks for the slope angle $\cot \alpha = 0.58$ ($\alpha = 60^\circ$), and to transform the blocks into ribs in the upper part of the slope (where the wave run-up is taking place), as shown in Figure 4.10b. The ribs are formed by adding the same 5 cm cubes to the left and right of the existing individual blocks. The block height and width remains the same ($f_h = f_b = 5$ cm), as does the distance between ribs $f_L = 10.2$ cm, although the covering ratio of the total surface is larger than for the block setup.

Stepped revetments are highlighted in literature to effectively reduce the overtopping for mild structures, although an analysis of stepped seawalls with steeper angles is not present in the literature (see Section 2.3.6). The stepped revetment is designed with two different step heights ($S_h = 0.106$ m and $S_h = 0.053$ m) to analyse the influence of S_h on the overtopping. The width of the step S_w is defined by the ratio $n = S_w/S_h$ which is equivalent to $n = \cot \alpha$. Figures 4.11a–4.11d show the four different stepped revetments

tested in the UG16 dataset.

Table 4.1 shows a comparison between the test setups of the UG13, UG14, UG15 and UG16 datasets, remarking the most important differences between them, which are the height of the structure and the cross section of the foreshore (see Figures 4.8a, 4.8b and 4.8c).

Table 4.1: Comparison between the test setups of the UG13, UG14, UG15 and UG16 datasets.

Dataset	Structure height (m)	Foreshore cross section
UG13	0.57	Short 1:20 slope and horizontal
UG14 and UG15	0.53	1:100 slope
UG16	0.53	Short 1:7.5 slope and horizontal

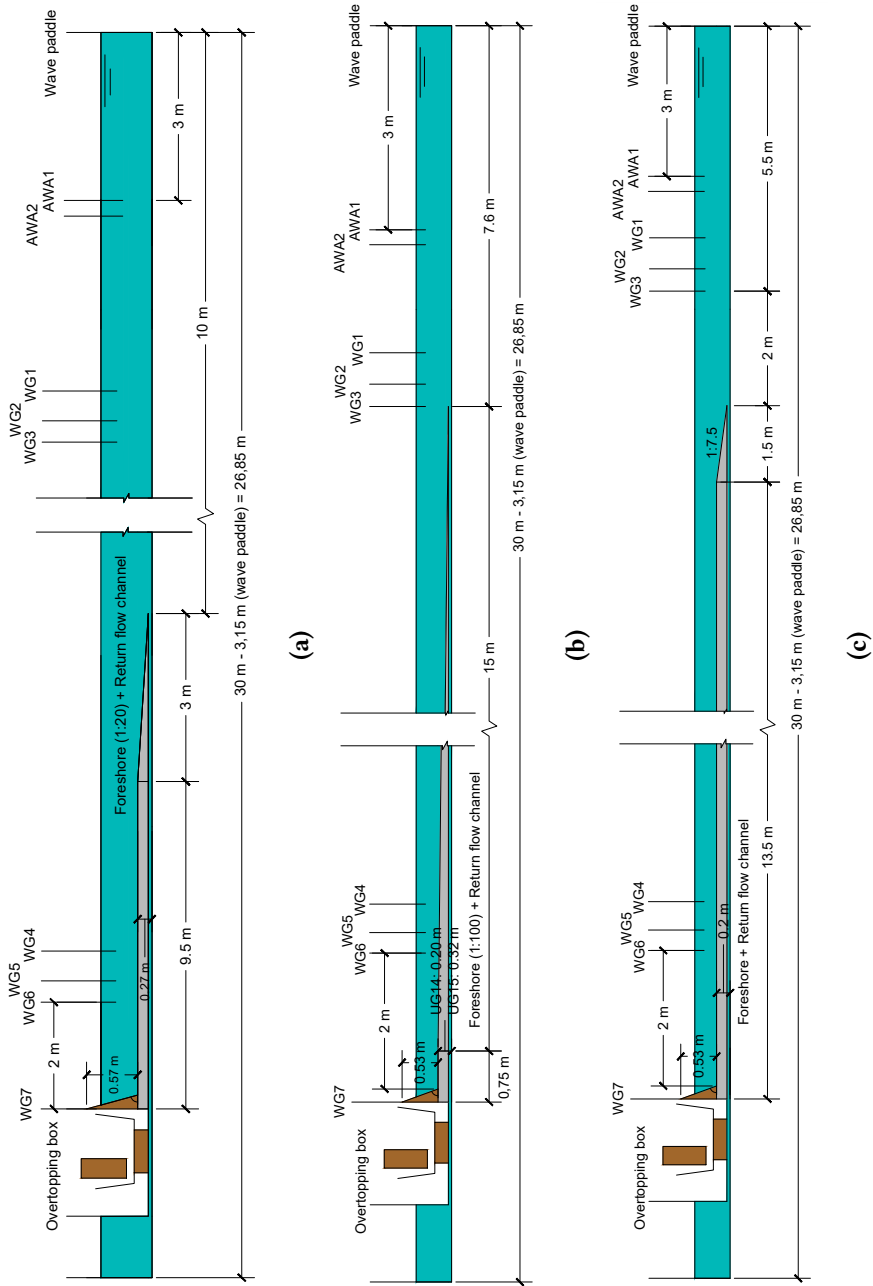


Figure 4.8: Test setup of the (a) UG13 dataset, (b) UG14 and UG15 datasets, and (c) UG16 dataset. Drawings not to scale.

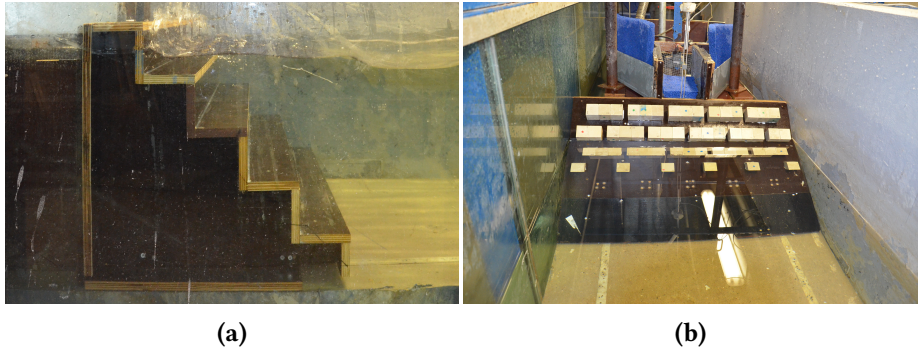


Figure 4.9: Model structures tested in the UG16 dataset: (a) 5-steps revetment, $\cot \alpha = 1$ ($\alpha = 45^\circ$), (b) ribs as artificial rough elements.

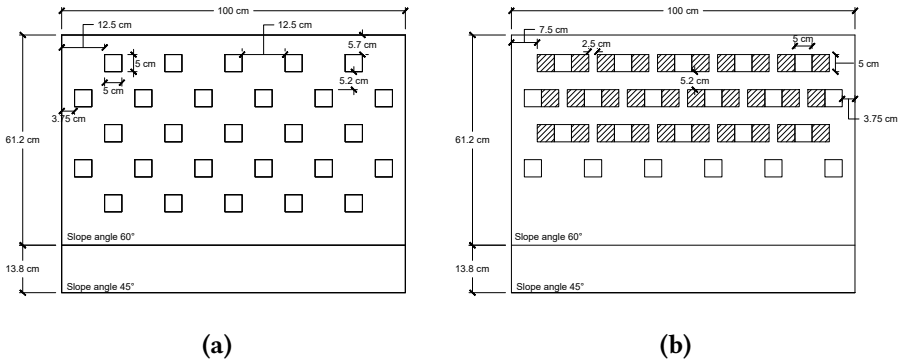


Figure 4.10: Model structure tested in the UG16 dataset with (a) individual blocks, and (b) ribs.

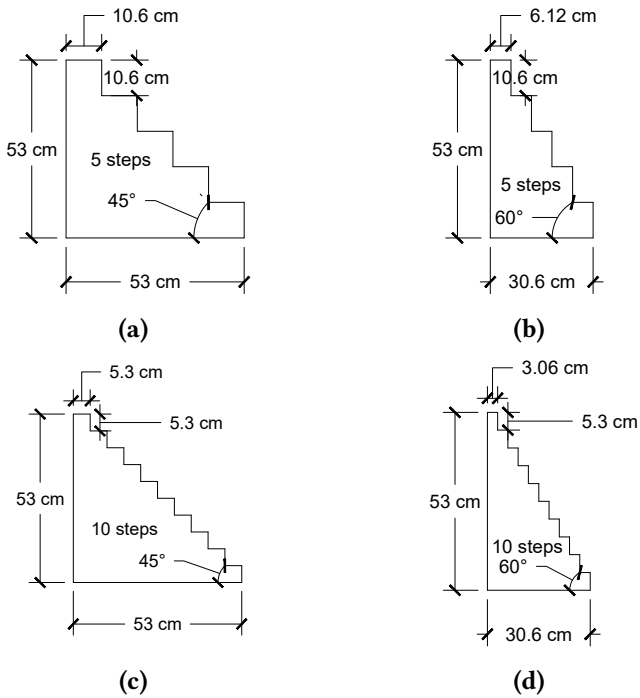


Figure 4.11: Model structures tested in the UG16: (a) 5 steps, $n=1$, $S_h = 0.106$ m ; (b) 5 steps, $n=0.58$, $S_h = 0.106$ m; (c) 10 steps, $n=1$, $S_h = 0.053$ m; and (d) 10 steps, $n=0.58$, $S_h = 0.053$ m.

4.2 Test Programme

Section 3.2 describes the design of the dataset within the methodology of the research. A study of the objectives of the research led to the identification of the four main parameter (relative crest freeboard R_c/H_{m0} , slope angle α , relative wave height H_{m0}/h and roughness of the slope) that were varied to achieve all the objectives. Figures 3.1 and 3.2 show a sketch the design values of all the datasets.

The new datasets obtained have as a starting point the UG10 dataset and continue to extend the overtopping knowledge of steep low-crested structures towards the limit case with the vertical structure and with the zero freeboard (UG13 dataset). The study of the shallow water effects on overtopping for this type of structures is then included in the research with the UG14 and UG15 datasets. UG16 focuses on the effect on wave overtopping of roughness in steep low-crested structures.

Table 4.2 shows the test programme of the UG13, UG14, UG15 and UG16, and the UG10 dataset for comparison. Figures 4.12, 4.13 and 4.14 show a comparison of the parameters tested in the datasets UG13, UG14 and UG15, which were obtained for smooth slopes. The parameters compared are the cotangent of the slope angle $\cot \alpha$, the relative crest freeboard R_c/H_{m0} and the relative wave height H_{m0}/h . The figures show that the complete range of steep low-crested structures is covered by the new datasets, both for relatively deep water and shallow water conditions. In these figures, the symbols have been shifted artificially around the real values of $\cot \alpha$ for a better visualization. In Figure 4.14 the curved pattern of the data corresponds to the discreet values of the tested crest freeboards R_c as the parameters R_c/H_{m0} and H_{m0}/h are related.

4.2.1 UG13 Dataset

The UG13 dataset is a continuation of the UG10 dataset (Victor and Troch, 2012a), extending the tested slope angles α towards the limit vertical wall case ($0.27 \geq \cot \alpha \geq 0$); and the crest freeboards R_c towards the limit zero freeboard case ($0.1 \geq R_c/H_{m0} \geq 0$). Twelve per cent of the UG13 tests are on the same slope angles α and relative crest freeboard R_c/H_{m0} range as the UG10 dataset for comparability. The model structure tested is smooth and impermeable. The total number of tests obtained is 307.

The UG13 dataset is considered almost entirely (except 10 tests) in the non-breaking waves region. Most of the tests of the UG13 dataset featured relative wave height values in the range of deep water conditions according

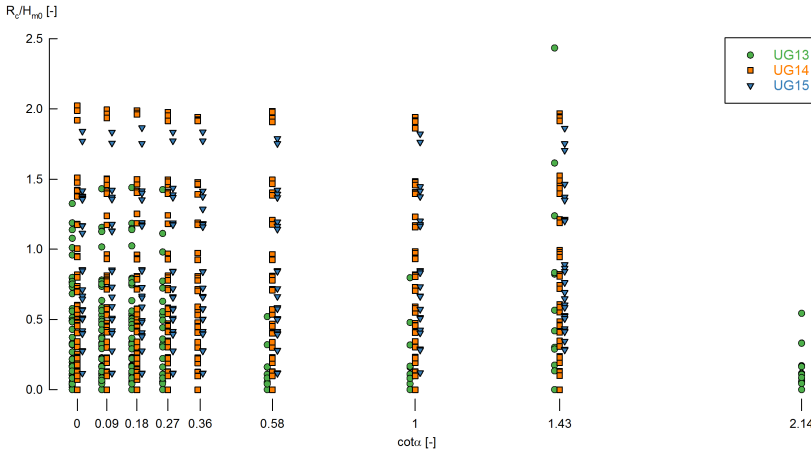


Figure 4.12: $\cot \alpha$ of the model structure compared to the relative crest freeboard R_c/H_{m0} for all the tests of the UG13, UG14 and UG15 datasets.

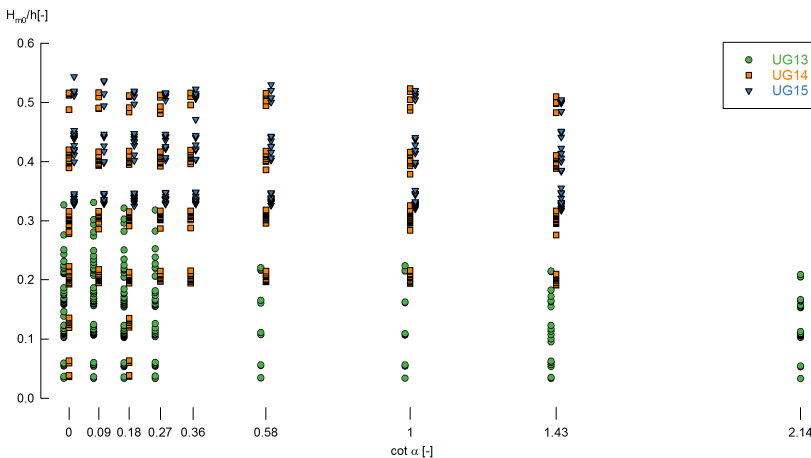


Figure 4.13: $\cot \alpha$ of the model structure compared to the relative wave height H_{m0}/h for all the tests of the UG13, UG14 and UG15 datasets.

to Nørgaard et al. (2014). However, 21% of the tests featured values in the range of shallow or transitional water conditions ($H_{m0}/h > 0.2$).

4.2.2 UG14 and UG15 Datasets

While the UG10 and UG13 datasets were obtained in relatively deep water conditions, it is also important to characterize wave overtopping for relatively shallow water conditions. The UG14 dataset was designed to fill the knowl-

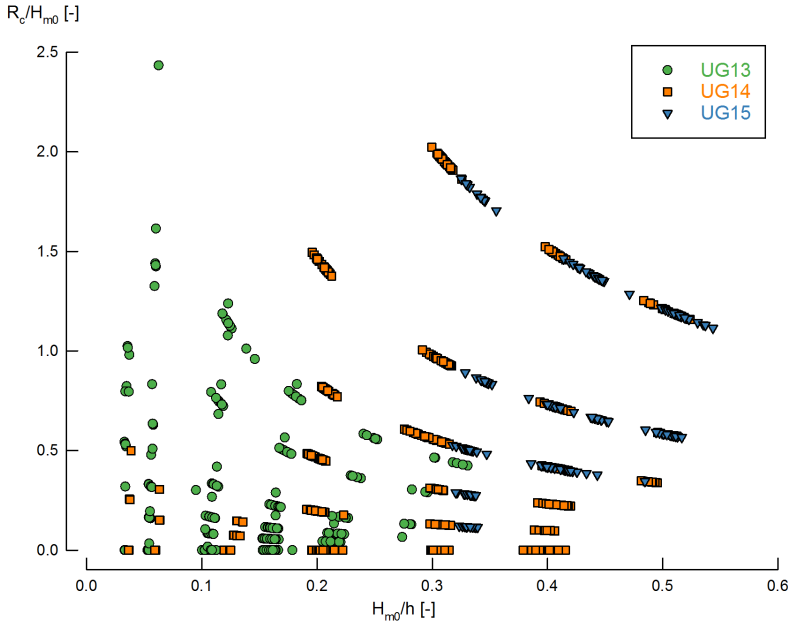


Figure 4.14: Relative wave height H_{m0}/h compared to the relative crest freeboard R_c/H_{m0} for all the tests of the UG13, UG14 and UG15 datasets.

edge gap of wave overtopping for steep low-crested structures in shallow water conditions. On this dataset, the focus is on characterizing the overtopping for the transitional conditions between deep water and shallow water conditions ($0.2 < H_{m0}/h < 0.5$), although 6% of the tests were performed for deep water conditions ($H_{m0}/h < 0.2$), as repetition tests of the UG13 dataset were required. The UG15 dataset is a continuation of the UG14 dataset. More tests are performed with a target relative wave height of $H_{m0}/h = 0.5$ to increase the number of tests available with overtopping data for shallow water conditions. The dataset also includes additional tests in the transitional zone between relatively deep and shallow water conditions ($0.2 < H_{m0}/h < 0.5$).

As explained in Section 2.3.2, various authors follow different criteria to characterize water depth conditions based on the relative wave height H_{m0}/h or the wave steepness $s_{m-1,0}$. The criterion by Nørgaard et al. (2014) seems suitable for the UG datasets, as the wave conditions were not influenced by the presence of a foreshore. Moreover, the foreshore featured by Nørgaard et al. (2014) is very similar to the foreshore featured in the UG14 and UG15 datasets.

The model structures tested in the UG14 dataset are smooth and impermeable, and the range of slope angles α and relative crest freeboards R_c/H_{m0}

tested is similar to UG13 ($1.43 \geq \cot \alpha \geq 0$, $2.92 \geq R_c/H_{m0} \geq 0$). For the dataset UG15, the slope angles α are the same as for the UG14 dataset, however the very small and zero relative crest freeboards ($0.1 \geq R_c/H_{m0} \geq 0$) could not be tested as the overtopping rate was too large and the pump of the overtopping measurement system was not able to cope with the small interval between pumping events that was necessary to empty the overtopping reservoir. The UG14 and UG15 datasets are considered entirely in the non-breaking waves region as the Van der Meer and Bruce (2014) prediction applicable is the non-breaking one. The total number of tests in the UG14 dataset is 435, while in the UG15 dataset is 197.

4.2.3 UG16 Dataset

The UG16 dataset introduced the influence of roughness in the overtopping behaviour of steep low-crested structure. From a physical consideration, it is known that the effect of roughness on wave overtopping decrease for steeper slopes, as the run-up length of waves on the structure is smaller than for milder slopes. For the same crest freeboard R_c , the overtopping rate on a vertical structure is less influenced by the roughness of the structure than on a mild slope. For the same reason, the effect of roughness is also very limited for small R_c . The overtopping rate on a mild structure with a zero freeboard $R_c = 0$ is not influenced by the roughness of its slope as the run-up length on the slope is very small. However, it has not been determined in the scientific literature which is the limit value of the slope angle α and relative crest freeboard R_c/H_{m0} for which the influence of roughness on overtopping is negligible.

To obtain meaningful results that determine the influence of roughness on overtopping, and to find the limit of the influence for steep low-crested structures, the tested structures should be mild or steep slopes with small and large relative crest freeboards. The slope angles $\cot \alpha = 1$ ($\alpha = 45^\circ$) and $\cot \alpha = 0.58$ ($\alpha = 60^\circ$) are tested in the UG16 dataset for values of the relative crest freeboard $R_c/H_{m0} \geq 0.1$. The total number of tests with roughness elements in the UG16 dataset is 238.

Also, smooth structures with slope angles $\cot \alpha = 1$ ($\alpha = 45^\circ$) and $\cot \alpha = 0.58$ ($\alpha = 60^\circ$) were tested in order to check the accuracy of the test setup within the UG16 dataset and to compare to the other Ghent University datasets (UG10, UG13, UG14 and UG15). Tests were carried out for same-seed and different-seed time series of waves. The total number of tests with smooth slopes in the UG16 dataset is 34 (see Section 4.4).

Table 4.2: Test programmes of the UG10, UG13, UG14, UG15 and UG16 datasets.

Parameter	UG10	UG13	UG14	UG15	UG16
Number of tests (-)	366	307	435	197	272
Slope angle α (°)	20, 25, 30, 35, 40, 45, 50, 60, 70	25, 35, 45, 60, 75, 80, 85, 90	35, 45, 60, 70, 75, 80, 85, 90	35, 45, 60, 70, 75, 80, 85, 90	45, 60 (Smooth, 5-steps revetment, 10-steps revetment, artificial roughness elements)
$\cot \alpha$ (-)	2.75, 2.14, 1.73, 1.43, 1.19, 1, 0.84, 0.58, 0.36	2.14, 1.43, 1, 0.58, 0.27, 0.18, 0.09, 0	1.43, 1, 0.58, 0.36, 0.27, 0.18, 0.09, 0	1.43, 1, 0.58, 0.36, 0.27, 0.18, 0.09, 0	1, 0.58
Crest freeboard R_c (m)	0.02, 0.045, 0.070	0, 0.005, 0.01, 0.02, 0.045, 0.07	0, 0.02, 0.045, 0.076, 0.12, 0.2	0.02, 0.045, 0.076, 0.12, 0.2	0.01, 0.03, 0.05, 0.07, 0.1, 0.13, 0.15
Foreshore slope at the toe of the structure m (-)	0	0	1:100	1:100	0
Incident spectral wave height at the toe H_{m0} (m)	0.023-0.19	0.018-0.16	0.061-0.225	0.107-0.22	0.04-0.13
Relative crest freeboard R_c/H_{m0} (-)	0.11-1.69	0-2.43	0-2.92	0.11-1.87	0.11-3.25
Relative wave height at the toe of the structure H_{m0}/h (-)	0.03-0.33	0.04-0.38	0.2, 0.3, 0.4, 0.5	0.3, 0.4, 0.5	0.07-0.32
Target peak wave period T_p (s)	1.000-2.000	1.022-2.045	1.022, 1.534, 2.045	1.534, 2.045, 2.534	1.000, 1.300, 1.500
Wave steepness at the toe of the structure $s_{m-1.0}$ (-)	0.016-0.056	0.014-0.047	0.01-0.06	0.01-0.05	0.01-0.05
Surf similarity parameter at the toe of the structure $\xi_{m-1.0}$ (-)	2-21.5	2.28-95	2.8-90	3.3-82	3.95-14.7

4.3 Processing of Data

The data from the wave gauges are processed to obtain the incident wave parameters (i.e., wave height, wave period, etc.) at the toe of the structures. Also the data from the weigh cell are post-processed to obtain the average wave overtopping rates and the individual overtopping volumes. An integrated analysis of incident wave parameters and overtopping data is then performed for a complete understanding of how the various wave and structural parameters affect the overtopping process.

4.3.1 Incident Wave Parameters Processing

The water surface measurements are obtained in two locations of the wave flume (deep water and close to the toe of the structure, see Section 4.1.2) by two arrays of three WGs each. The raw data obtained is the total wave height, which is the sum of incident and reflected wave heights. For wave overtopping analysis it is necessary to separate the incident and the reflected wave heights as the average overtopping rates are usually presented by a dimensionless parameter which depends on the incident spectral wave height at the toe of the structure, H_{m0} . A reflection analysis separates the total wave height into its incident and reflected components, calculating also a reflection coefficient C_r for the wave frequencies considered in the analysis.

The reflection analysis is performed in this research with the software WaveLab (Dept. of Civil Engineering Aalborg University, 2013) following the separation method by Zelt and Skjelbreia (1992), which is an extension for N-gauges of the three-gauges method by Mansard and Funke (1980). This method uses a fast Fourier transform (FFT) to divide the analysed wave signal into its frequency components in the frequency domain. The wave build-up process at the beginning of each test and the cool-down at the end of each test are not considered in the reflection analysis. To this purpose, the first 55 seconds and the last 170 s of each test are excluded from the analysis (although it may vary between tests), analysing around 1000 waves. A band-pass filtering is also applied, between the frequencies $0.33f_p$ and $3f_p$. The number of data in the FFT blocks of the reflection analysis is selected according to each test, although for most of the tests the value is 1024 or 2048, which provides a sufficient resolution of the energy spectrum. The reflection analysis is also performed in the time domain.

The separation method by Zelt and Skjelbreia (1992) is only valid for linear waves. For nonlinear waves, the errors when separating the incident and the reflected waves are high. Tests with relatively shallow water conditions in the UG14 and UG15 datasets may have nonlinear waves as a result

of depth-limited wave breaking caused by the foreshore. To account for the nonlinearities in the wave field, the model structure is removed and tests with an absorbing beach at the end of the flume are performed. The absorbing beach is made of pebbles, and it has a parabolic shape, with the minimum curvature of the parabola around the SWL. The absorbing beach has reflection coefficients between 10%–20%, which are low enough to consider that the chosen separation method does not influence the incident wave obtained. By comparing tests with the same wave time series (same seeding number) for the absorbing beach and for the model structure, the error of the Zelt and Skjelbreia (1992) separation method for nonlinear waves can be estimated. The results indicate that the estimated incident waves with the presence of the model structure are maximum a 10% higher than the incident waves with an absorbing beach. This error is small and therefore, it is considered that the Zelt and Skjelbreia (1992) separation method is sufficiently accurate for the nonlinear waves in this research.

The output of the reflection analysis is an energy spectrum on the frequency domain, from which various characteristics are derived (e.g., incident spectral wave height H_{m0} , incident peak wave period T_p and incident spectral wave period $T_{m-1,0}$). The output on the time domain are also wave characteristics such as significant wave height H_s and the mean wave period T_m . The reflection coefficient C_r is also an output from WaveLab, as well as the energy spectrum in the frequency domain analysis, and a time series of the total, incident and reflected wave heights in the time domain.

4.3.2 Wave Overtopping Processing

The average overtopping rates q and the individual overtopping volumes V_i are obtained by post-processing the acquired data in MATLAB[®] (Mathworks, 2015), with scripts developed by Victor (2012) and improved further during this research. This section is based on the explanations of the scripts provided by Victor (2012).

Average Overtopping Rates Processing

The average overtopping rate can be calculated from the output signals of the weigh cell, which give the mass of water inside the reservoir of the overtopping box. The variation of the relative mass measured by the weigh cell $M_{\text{rel,cell}}$ for the complete duration of test 285 of the UG13 dataset is shown in Figure 4.15. At four different occasions the pump is activated when the weigh cell measures $M_{\text{rel,cell}} = 80$ kg, producing a fast decrease of $M_{\text{rel,cell}}$ (vertical

lines in Figure 4.15). Based on the calibration of the reservoir previously performed (Figure 4.5), the relative mass in the reservoir $M_{\text{rel,cell}}$ is transformed in absolute mass M_{abs} .

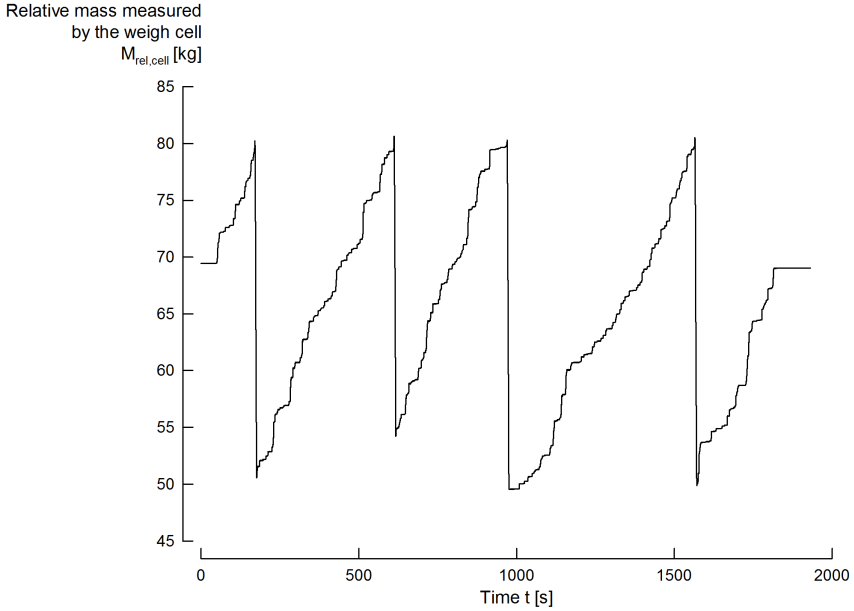


Figure 4.15: Relative mass measured in the weigh cell $M_{\text{rel,cell}}$ over time t of test 285, UG13 dataset.

The pumping events in Figure 4.15 are compensated by the integration of the characteristic pump curve (Figure 4.6) converted to absolute masses M_{abs} (Figure 4.5) into every pumping event, obtaining the pumped mass of water in each pumping event. This pumped mass of water is added to the curve of absolute mass in the reservoir over time (Figure 4.15), obtaining the cumulative mass of water M_{cul} over time, as shown in Figure 4.16.

The average overtopping rate q is the difference between the final and initial cumulative mass ($M_{\text{cul,end}}$ and $M_{\text{cul,start}}$, respectively) on the analysed time window, divided by the density of the water ρ , the width of the overtopping chute B_q (see Figure 4.4b) and the duration of the analysed time window T_0 , as shown in Eq 4.2. This expression is related to the average slope angle of the cumulative curve in Figure 4.16. The time window is the same as considered for the incident wave height analysis (see Section 4.3.1), therefore the first 55 s and the last 170 s of each test are not considered in the analysis.

$$q = \frac{M_{\text{cul,end}} - M_{\text{cul,start}}}{\rho B_q T_0} \quad (4.2)$$

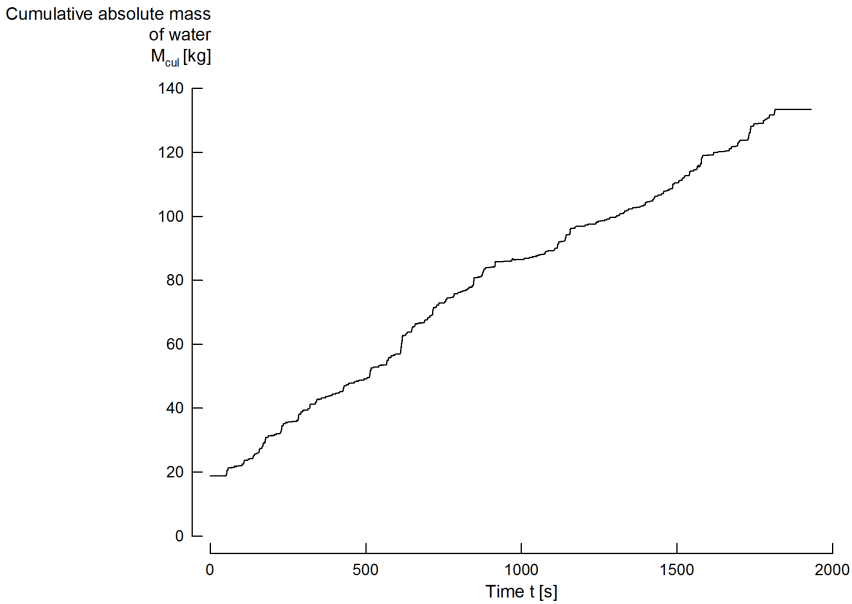


Figure 4.16: Cumulative absolute mass of water M_{cul} over time t of test 285, UG13 dataset.

Individual Overtopping Volumes Processing

Each time a wave overtops the crest of the structure, there is an increase in the cumulative mass of the reservoir (Figure 4.16). To detect when an overtopping event is produced, the output signal from the WG7, acting as an overtopping detection system (see Figure 4.4a), is analysed. Around the times when the overtopping event is produced, the script analyses the output signal of the weigh cell (Figure 4.15) to detect horizontal parts that indicate when there is no increase of M_{cul} , i.e., a period between two consecutive overtopping events.

Therefore, the differences in cumulative mass M_{cul} between two consecutive horizontal sections of the cumulative curve correspond to the individual overtopping masses M_i (Figure 4.17), which are converted into individual overtopping volumes V_i by Eq. 4.3. The average overtopping rate q can also be calculated as the sum of all the individual overtopping volumes V_i over the analysed time window divided by the duration of the window T_0 (Eq. 4.4). This method was used by Franco et al. (1994), Pearson et al. (2002) and Pullen et al. (2009) among others.

$$V_i = \frac{M_i}{\rho B q} \quad (4.3)$$

$$q = \frac{\sum V_i}{T_0} \quad (4.4)$$

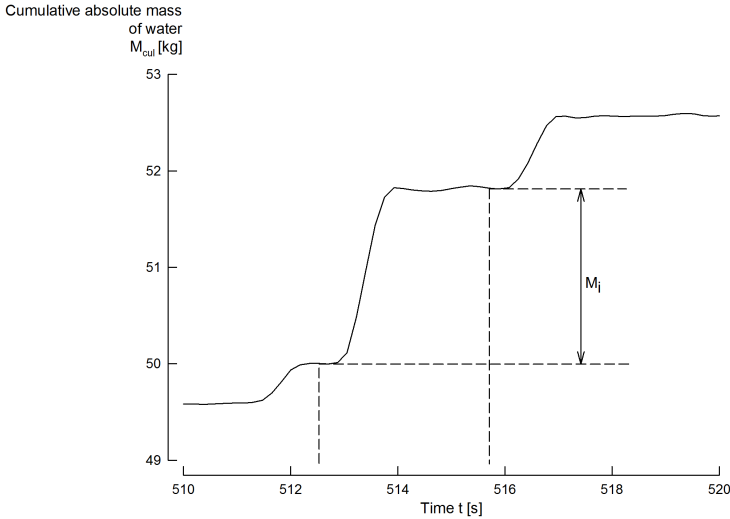


Figure 4.17: Detail of the cumulative absolute mass of water M_{cul} over time t of test 285, UG13 dataset, with the identification an individual overtopping event made by the MATLAB[®] script.

The pumping events are also taken into account when post-processing the data and calculating the individual overtopping volumes. The compensation of the pumping events is performed as aforementioned for average overtopping rates. However, the accuracy of the individual volumes V_i calculation is different depending on whether the overtopping event occurs during a pumping event or not.

Victor (2012) reported that for overtopping events occurring when there is no pumping event, the minimum accuracy of the calculated volumes V_i is defined by the accuracy of the weigh scale used in the experiment (± 0.005 kg, see Section 4.1.2). This accuracy is independent of the absolute value of V_i . Assuming the worst-case scenario of an accuracy of ± 0.005 kg, for an error in the calculation of V_i of 5%, only volumes lower than $V_i = 0.1$ l can have larger errors.

For overtopping events occurring during a pumping event, the minimum accuracy of V_i is defined by the spreading of the pump curves with respect to the characteristic pump curve (Figure 4.6), which for the UG10 dataset was calculated to be ± 0.09 kg, and for the datasets obtained within this research is assumed to be similar. This accuracy is also independent of the absolute value of V_i . Assuming the worst-case scenario of an accuracy of ± 0.09 kg for an

error in the calculation of V_i of 5%, volumes lower than $V_i = 1.8$ l could have larger errors. If the overtopping occurs during a pumping event, the smallest V_i are not calculated with enough accuracy, while the largest volumes are still calculated with a good accuracy. To prove whether this accuracy calculation was correct, Victor (2012) tested the addition of different known volumes of water to the overtopping reservoir and compared them with the calculated volumes by the script. For overtopping occurring during a pumping event, the largest observed difference was ± 0.057 l, lower than the theoretical ± 0.09 l, which means that the accuracy of the calculation of the overtopping volumes occurring during a pumping event may be higher than assumed.

4.4 Repeatability of the Overtopping Parameters

In physical modelling, the measured overtopping parameters have a natural variability caused by a variability in wave sequences. There are infinite number of wave sequences that can be generated from one energy spectrum. By changing the seeding number used to assign the starting phases of the components in the Random Phase Method (RPM, Tuah and Hudspeth (1982)), a different wave sequence—and therefore elevation time series—is generated (Romano et al., 2015). Two tests with the same seeding number have the same wave sequence, while two tests with a different seeding number have a different wave sequence but the same energy spectrum (i.e., the same generated spectral wave height H_{m0} and peak wave period T_p). The variability of the measured overtopping parameters was studied by Kortenhaus et al. (2004) and Romano et al. (2015) among others.

Kortenhaus et al. (2004) studied the uncertainty and model effects of overtopping physical model tests by performing repetition tests with the same and different seeding number. Table 4.3 shows the coefficient of variation $\sigma' = \sigma/\mu$ (assuming that the parameter is normally distributed with an average μ and a standard deviation σ) obtained by Kortenhaus et al. (2004) for the average overtopping q and spectral incident wave height H_{m0} of same seeding and different seeding overtopping experiments. The variation of different seeding number tests is a factor two higher than the variation for same seeding number tests.

Romano et al. (2015) found that the variation of average overtopping rate increases for increasing relative crest freeboards, from a 20% variability for $R_c/H_{m0} < 1.2$ up to one order of magnitude variability for $R_c/H_{m0} > 1.4$.

The accuracy of the experimental setup is determined by performing repeatability tests on smooth slopes within the UG16 dataset (see Section 4.2). The tests are performed for the slope angles $\cot \alpha = 1$ ($\alpha = 45^\circ$) and

Table 4.3: Overview of the uncertainty of the average overtopping rate q and the spectral incident wave height H_{m0} obtained by Kortenhaus et al. (2004).

Parameter	Same seeding	Different seeding
	σ' (%)	σ' (%)
q (l/s/m)	12.9	33.0
H_{m0} (m)	3.0	6.1

$\cot \alpha = 0.58$ ($\alpha = 60^\circ$), with a crest freeboard $R_c = 0.05$ m, a target spectral wave height $H_{m0,\text{target}} = 0.07$ m and a peak wave period $T_p = 1.5$ s. These values are chosen to be representative of the complete research.

The parameters studied are the average overtopping rate q , the spectral incident wave height at the toe of the structure H_{m0} , the dimensionless average overtopping rate $q/\sqrt{gH_{m0}^3}$, the shape factor B of the Weibull distribution of the individual volumes, and the probability of overtopping P_{ow} . The parameters are considered normally distributed with an average value μ (with the same dimensions as the parameter), a standard deviation σ (with the same dimensions as the parameter) and a coefficient of variation $\sigma' = \sigma/\mu$ (as a percentage). Table 4.4 shows the results for same seeding number tests. For the slope angle $\cot \alpha = 1$ ($\alpha = 45^\circ$) 12 tests were performed, while for the slope angle $\cot \alpha = 0.58$ ($\alpha = 60^\circ$) nine tests were performed.

The repeatability of the measured overtopping parameters for same seeding number tests is very high. The coefficient of variation σ' values of q and H_{m0} are one order of magnitude smaller than obtained by Kortenhaus et al. (2004) (see Table 4.3). The shape factor B has the largest variation, due to the fitting of the Weibull distribution through the largest 10% of volumes (see Section 6.1). The fittings performed through more extreme events present a larger variability than fittings performed for less extreme events.

Table 4.5 shows the results for different seeding number tests. For the slope angle $\cot \alpha = 1$ ($\alpha = 45^\circ$) 11 tests were performed, while for the slope angle $\cot \alpha = 0.58$ ($\alpha = 60^\circ$) four tests were performed. The variability of the parameters for different seeding number tests is larger that for same seeding number tests, as expected. The repeatability of the measured overtopping parameters is also high. The coefficients of variation of q and H_{m0} are again smaller than the ones obtained by Kortenhaus et al. (2004) for different seeding number tests (see Table 4.3). As it is the case for same seeding number tests, the shape factor B is the less repeatable of the overtopping parameters.

The overtopping results obtained using the experimental setup described in Section 4.1 are very repeatable, which prove that the results are trustworthy. As indicated by Romano et al. (2015), the repeatability of the overtopping

Table 4.4: Average value μ , standard deviation σ and coefficient of variation σ' of the overtopping parameters for tests with same seeding number and $R_c = 0.05$ m, $H_{m0,target} = 0.07$ m and $T_p = 1.5$ s.

Slope angle	Parameter	μ	σ	σ' (%)
$\cot \alpha = 1$	q (l/s/m)	0.819	0.012	1.5
	H_{m0} (m)	0.065	0.0005	0.7
	$q/\sqrt{gH_{m0}^3}$ (-)	0.016	0.0003	2.1
	B (-)	1.143	0.057	5.0
	P_{ow} (-)	0.550	0.010	1.9
$\cot \alpha = 0.58$	q (l/s/m)	0.406	0.005	1.1
	H_{m0} (m)	0.066	0.00005	0.1
	$q/\sqrt{gH_{m0}^3}$ (-)	0.008	0.0001	1.2
	B (-)	1.005	0.132	13.1
	P_{ow} (-)	0.411	0.006	1.3

Table 4.5: Average value μ , standard deviation σ and coefficient of variation σ' of the overtopping parameters for test with different seeding number and $R_c = 0.05$ m, $H_{m0,target} = 0.07$ m and $T_p = 1.5$ s.

Slope angle	Parameter	μ	σ	σ' (%)
$\cot \alpha = 1$	q (l/s/m)	0.791	0.036	4.6
	H_{m0} (m)	0.065	0.0007	1.1
	$q/\sqrt{gH_{m0}^3}$ (-)	0.015	0.0005	3.3
	B (-)	0.999	0.119	11.9
	P_{ow} (-)	0.531	0.015	2.9
$\cot \alpha = 0.58$	q (l/s/m)	0.400	0.008	2.1
	H_{m0} (m)	0.065	0.001	1.3
	$q/\sqrt{gH_{m0}^3}$ (-)	0.008	0.0001	1.6
	B (-)	0.804	0.054	6.7
	P_{ow} (-)	0.403	0.016	3.9

results is expected to be lower for large relative freeboards than for small relative freeboards. Therefore, caution is advised when comparing the coefficient of variation values presented in this section to other values obtained for larger relative crest freeboards, as the values might not be representative of the uncertainty for larger freeboards.

4.5 Summary

Hydraulic model tests have been performed with the experimental setup described in Section 4.1. The chosen wave and structural parameters cover the complete range of steep low-crested structures, from mild slopes to the limit case with vertical structures, for large relative freeboards to the limit case of zero freeboard. This range of structures is designed to address all the specific objectives defined in Section 2.5 by obtaining the UG13, UG14, UG15 and UG16 datasets.

The repeatability tests performed (Section 4.4) show that the experimental setup is able to obtain very repeatable results that can be extrapolated to improve the scientific knowledge about wave overtopping.

Chapter 5

Data Analysis of Average Wave Overtopping Rates of Steep Low-Crested Structures

Three new overtopping datasets featuring smooth slopes were obtained in this research: UG13, UG14 and UG15 (see Chapter 4). These new datasets focused on wave overtopping for steep low-crested structures up to the limit case of vertical walls and zero freeboards, covering the range between relatively deep and shallow water conditions. A different dataset (UG16) was obtained to analyse the influence of roughness on wave overtopping. This chapter presents the resulting average overtopping rates corresponding to these datasets, compares the results with predictions from existing overtopping prediction formulae and suggests a new average overtopping prediction formula for smooth slopes in the range of steep low-crested structures.

5.1 Average Overtopping Results

The datasets featuring model tests for smooth impermeable slopes were UG13, UG14 and UG15. The UG13 dataset focused on relatively deep water conditions ($H_{m0}/h < 0.2$), while the UG14 and UG15 datasets focused on the transition zone ($0.2 < H_{m0}/h < 0.5$) and relatively shallow water conditions ($H_{m0}/h \geq 0.5$). An analysis of the effect of the relatively shallow water conditions on the average overtopping rates will be presented in Section 5.3.

The dimensionless average overtopping rates $q/\sqrt{gH_{m0}^3}$ versus the relative crest freeboards R_c/H_{m0} for the 939 tests of these datasets are presented in Figure 5.1. In this figure, the UG13 dataset is represented by green circles, the UG14 dataset by orange squares and the UG15 by blue inverted triangles. $q/\sqrt{gH_{m0}^3}$ increases when R_c/H_{m0} decreases. The data have more scatter for large relative crest freeboards than for small relative crest freeboards. Therefore, the scatter is larger for the smaller average overtopping rates.

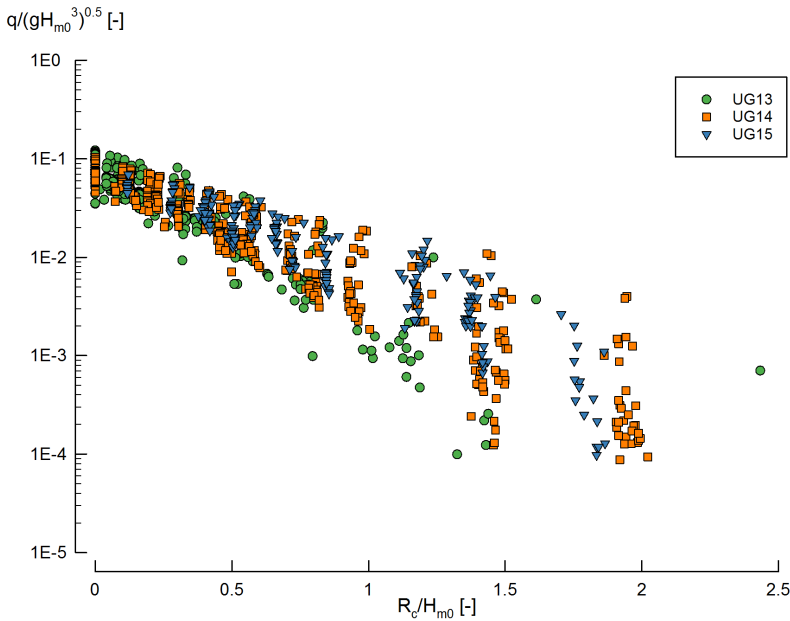


Figure 5.1: Dimensionless average overtopping rate $q/\sqrt{gH_{m0}^3}$ versus relative crest freeboard R_c/H_{m0} of the complete UG13, UG14 and UG15 datasets.

Figure 5.2 shows the same data as Figure 5.1 although classified per slope angle according to Table 1.1. In this figure, the green squares indicate the subset of mild slopes ($\cot \alpha \geq 2$); the red triangles indicate steep slopes ($2 > \cot \alpha > 0.27$); the blue diamonds indicate very steep slopes ($0.27 \geq \cot \alpha > 0$); and the white circles indicate the vertical wall ($\cot \alpha = 0$). The average overtopping rate $q/\sqrt{gH_{m0}^3}$ decreases for decreasing values of $\cot \alpha$ (increasing slope angle α , steeper slopes). The effect of the slope angle on the average wave overtopping will be discussed throughout the chapter.

There is no influence on the dimensionless average overtopping rates of the wave period $T_{m-1,0}$, wave steepness $s_{m-1,0}$ and surf similarity parameter $\xi_{m-1,0}$. This is in line with what is reported in the literature about the influence of these parameters, including the reports of Victor and Troch (2012b)

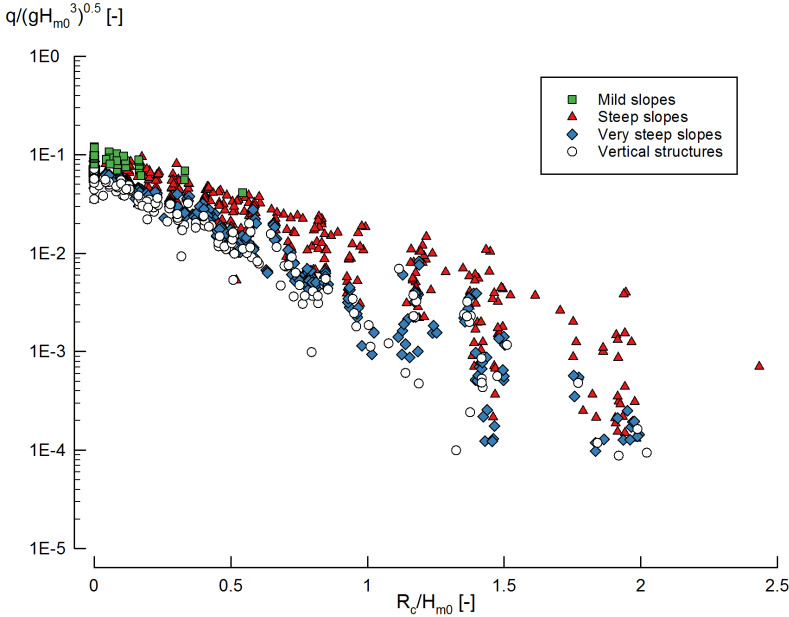


Figure 5.2: Dimensionless average overtopping rate $q/\sqrt{gH_{m0}^3}$ versus relative crest freeboard R_c/H_{m0} of the complete UG13, UG14 and UG15 datasets divided per slope angle classification according to Table 1.1.

about the UG10 dataset.

Figure 5.3 shows the dimensionless average overtopping rate $q/\sqrt{gH_{m0}^3}$ as a function of $\cot \alpha$ for very small and zero relative freeboards ($0.11 > R_c/H_{m0} \geq 0$) of the UG13 and UG14 datasets. The UG15 dataset does not contain overtopping data for this range of relative crest freeboards. This figure shows four groups of relative crest freeboards ($R_c/H_{m0} = 0$ in white diamonds; $0.05 > R_c/H_{m0} > 0$ in yellow circles; $0.08 > R_c/H_{m0} > 0.05$ in orange triangles; and $0.11 > R_c/H_{m0} > 0.08$ in red squares). All these overtopping data form the new zones Z1* (for $\cot \alpha < 1.5$) and Z3* ($\cot \alpha > 1.5$) that were not tested in the UG10 dataset.

An influence of the slope angle α on the dimensionless overtopping rates is present in the data for very small and zero relative crest freeboards. For mild ($\cot \alpha \geq 2$) and steep slopes ($2 > \cot \alpha > 0.27$), the dimensionless average overtopping rate decreases for steeper slopes. However, in the range of very steep slopes ($0.27 \geq \cot \alpha > 0$) this influence seems to be negligible as the overtopping rates are constant. The influence of the slope angle is again present when moving towards the vertical wall limit ($\cot \alpha = 0$) as the overtopping rates decrease. The behaviour described is the same within each

of the four groups of R_c/H_{m0} shown in Figure 5.3. Therefore, a vertical wall ($\cot \alpha = 0$) performs better than a very steep slope when reducing average wave overtopping on very low-crested conditions.

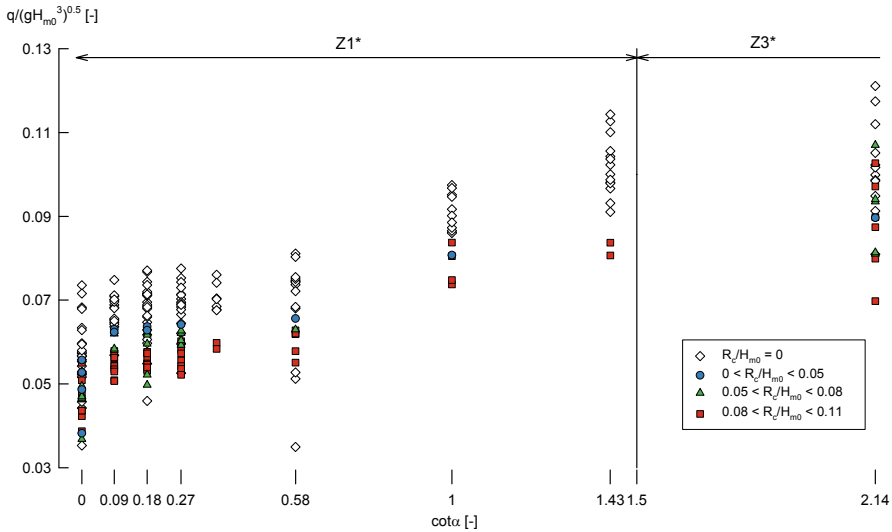


Figure 5.3: Dimensionless average overtopping rate $q/\sqrt{gH_{m0}^3}$ versus the slope angle ($\cot \alpha$) for very small and zero relative crest freeboards ($0.11 > R_c/H_{m0} \geq 0$).

5.2 Comparison with Average Overtopping Prediction Formulae

The existing wave overtopping prediction formulae can be analysed for the new UG13, UG14 and UG15 datasets. By comparing the prediction formulae with the overtopping data of these datasets, the accuracy of the prediction can be validated for their range of application.

The Van der Meer and Bruce (2014) prediction formula (Eq. 2.5) is chosen as the reference case since it is included in the EurOtop (2016) manual as the reference prediction for steep low-crested structures.

5.2.1 Sloping Structures

As stated in Section 2.3.1, the EurOtop (2007) average overtopping prediction formula (Eq. 2.1 with a maximum for non-breaking waves on Eq. 2.2) has a range of application for non-breaking waves that is partially overlapping

with the new datasets UG13, UG14 and UG15 for slope angles $\cot \alpha \leq 1$ and relative crest freeboards $R_c/H_{m0} > 0.5$.

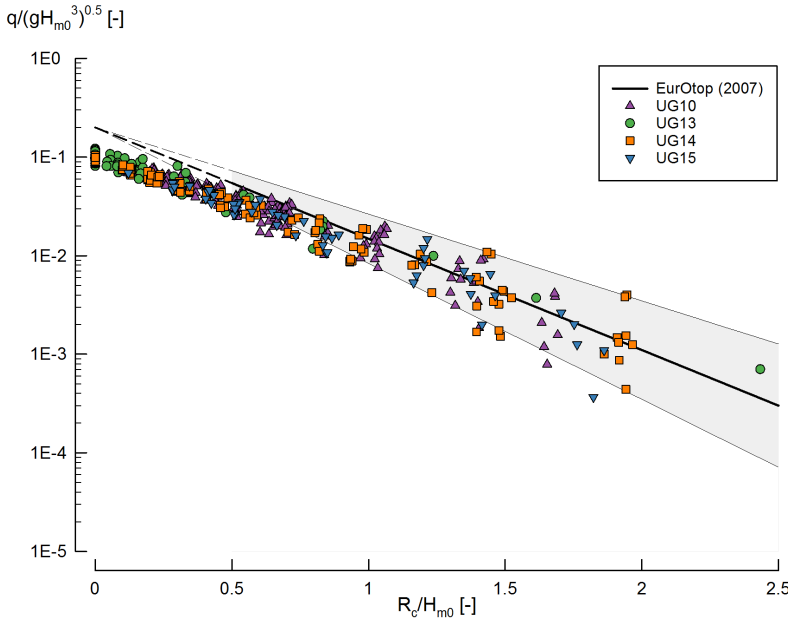


Figure 5.4: Dimensionless average overtopping rate $q/\sqrt{gH_{m0}^3}$ versus relative crest freeboard R_c/H_{m0} of the UG10, UG13, UG14 and UG15 datasets for $\cot \alpha > 1$, compared to EurOtop (2007) prediction for non-breaking waves (Eq. 2.2) with its 90% prediction band.

Figure 5.4 shows the non-breaking overtopping data of the UG10, UG13, UG14 and UG15 datasets within the range of application of Eq. 2.2 (solid line). An extension of Eq. 2.2 for $0.5 > R_c/H_{m0} > 0$ (dashed line) and the overtopping data in this range of the new datasets are also added for an integrated comparison of the complete range of crest freeboards. Eq. 2.2 is predicting with good accuracy the overtopping rates for relative crest freeboards $R_c/H_{m0} > 1$. For lower relative freeboards the shape of the data is slightly curved and Eq. 2.2 is overpredicting the overtopping, even though its range of application is up to $R_c/H_{m0} = 0.5$. It is possible to improve the prediction for the range of relative crest freeboards $0.5 < R_c/H_{m0} < 1$ by using the new UG13, UG14 and UG15 datasets to fit a new prediction formula.

5.2.2 Step Low-Crested Structures

To predict the average overtopping rates for steep low-crested structures, Victor and Troch (2012b) presented Eq. 2.4 and Van der Meer and Bruce

(2014) presented Eq. 2.5, which is the reference prediction for sloping and steep low-crested structures in the EurOtop (2016) manual. Both of them were fitted through the UG10 dataset and selected subsets of the CLASH database. The accuracy of these predictions has not been validated for very steep slopes ($0.27 \geq \cot \alpha > 0$) and very small and zero relative freeboards ($0.11 > R_c/H_{m0} \geq 0$), as the UG10 dataset does not contain overtopping data in these ranges. However, both predictions claim to be valid for the whole range steep low-crested structures. By comparison with the new UG13, UG14 and UG15 overtopping datasets, it is possible to analyse and validate the accuracy of Eq. 2.4 and Eq. 2.5.

Table 5.1: RMSE values (Eq. 3.1) and bias (Eq. 3.2) of the UG13 dataset in different ranges of relative crest freeboard R_c/H_{m0} and slope angle α .

Equation	Eq. 2.4		Eq. 2.5	
	RMSE (-)	Bias (-)	RMSE (-)	Bias (-)
UG13 (All tests)	0.0075	7.9×10^{-4}	0.0094	-3.8×10^{-3}
Zero freeboard ($R_c = 0$)	0.0114	4.4×10^{-3}	0.0156	-1.1×10^{-2}
$0 < R_c/H_{m0} < 0.05$	0.0078	2.3×10^{-3}	0.0090	-6.5×10^{-3}
$0.05 < R_c/H_{m0} < 0.08$	0.0072	9.1×10^{-7}	0.0096	-7.5×10^{-3}
$0.08 < R_c/H_{m0} < 0.11$	0.0066	-7.1×10^{-4}	0.0077	-5.0×10^{-3}
$0.11 < R_c/H_{m0} < 0.8$	0.0054	-6.4×10^{-4}	0.0057	3.9×10^{-4}
$R_c/H_{m0} > 0.8$	0.0012	2.2×10^{-4}	0.0014	-1.0×10^{-4}
Mild slopes	0.0119	6.2×10^{-3}	0.0123	-5.9×10^{-3}
Steep slopes	0.0116	5.6×10^{-3}	0.0126	-2.6×10^{-3}
Very steep slopes	0.0044	-2.6×10^{-3}	0.0085	-5.1×10^{-3}
Vertical structures	0.0060	2.5×10^{-3}	0.0061	-4.1×10^{-4}

Tables 5.1, 5.2 and 5.3 show the RMSE (Eq. 3.1) and bias (Eq. 3.2) values of the Victor and Troch (2012b) prediction (Eq. 2.4) and the Van der Meer and Bruce (2014) prediction (Eq. 2.5) for the UG13, UG14 and UG15 datasets, respectively. The relative crest freeboards R_c/H_{m0} ranges are based on Table 1.2 and Figure 5.3), while the slope angle α ranges are based on Table 1.1.

For the UG13 and UG14 datasets, Eq. 2.4 has smaller RMSE values than Eq. 2.5 in all the R_c/H_{m0} and slope ranges considered. Specifically, for the entire UG13 dataset the RMSE value of Eq. 2.4 is a 21% smaller and for the zero freeboard case ($R_c = 0$) is a 26% smaller. For the entire UG14 dataset, the RMSE value of Eq. 2.4 is a 21% smaller and for the zero freeboard case ($R_c = 0$) is a 41% smaller. However, for the UG15 dataset the behaviour is the opposite: the RMSE values are smaller for Eq. 2.5 than for Eq. 2.4 (20% smaller). The bias values indicate that Eq. (2.5) is consistently underpredicting the results (negative values of bias) for most of the ranges considered, while Eq. 2.4 does

Table 5.2: RMSE values (Eq. 3.1) and bias (Eq. 3.2) of the UG14 dataset in different ranges of relative crest freeboard R_c/H_{m0} and slope angle α .

Equation	Eq. 2.4		Eq. 2.5		
	Item	RMSE (-)	Bias (-)	RMSE (-)	Bias (-)
UG14 (All tests)		0.0045	-3.1×10^{-4}	0.0056	-2.2×10^{-3}
Zero freeboard ($R_c = 0$)		0.0071	3.8×10^{-3}	0.0120	-1.0×10^{-2}
$0.05 < R_c/H_{m0} < 0.08$		0.0050	3.4×10^{-3}	0.0039	-1.6×10^{-3}
$0.08 < R_c/H_{m0} < 0.11$		0.0064	-3.5×10^{-3}	0.0078	-6.9×10^{-3}
$0.11 < R_c/H_{m0} < 0.8$		0.0044	-1.2×10^{-3}	0.0035	-4.4×10^{-5}
$R_c/H_{m0} > 0.8$		0.0017	-6.8×10^{-4}	0.0017	-7.0×10^{-4}
Steep slopes		0.0038	7.0×10^{-4}	0.0042	-1.4×10^{-3}
Very steep slopes		0.0049	-1.6×10^{-3}	0.0062	-2.8×10^{-3}
Vertical structures		0.0051	-3.3×10^{-4}	0.0074	-2.9×10^{-3}

Table 5.3: RMSE values (Eq. 3.1) and bias (Eq. 3.2) of the UG15 dataset in different ranges of relative crest freeboard R_c/H_{m0} and slope angle α .

Equation	Eq. 2.4		Eq. 2.5		
	Item	RMSE (-)	Bias (-)	RMSE (-)	Bias (-)
UG15 (All tests)		0.0051	-2.7×10^{-3}	0.0041	-2.0×10^{-3}
$0.11 < R_c/H_{m0} < 0.8$		0.0063	-3.4×10^{-3}	0.0049	-2.3×10^{-3}
$R_c/H_{m0} > 0.8$		0.0030	-1.7×10^{-3}	0.0028	-1.7×10^{-3}
Steep slopes		0.0049	-1.2×10^{-3}	0.0040	-1.2×10^{-3}
Very steep slopes		0.0056	-4.2×10^{-3}	0.0045	-3.0×10^{-3}
Vertical structures		0.0048	-3.9×10^{-3}	0.0035	-2.6×10^{-3}

not show a clear trend in underpredicting or overpredicting the three datasets.

For both datasets, the prediction for very small and zero relative freeboards ($0 < R_c/H_{m0} \leq 0.11$) by Eq. 2.4 is more accurate than the prediction by Eq. 2.5. As Eq. 2.4 divides the full range of R_c/H_{m0} in two zones (see Table 2.2), the shape of the prediction adapts better to the shape of the data than Eq. 2.5, which is dominated by the coefficient $c_{V\&B} = 1.3$ causing an underprediction of the overtopping for very small and zero relative freeboards. For small ($0.11 < R_c/H_{m0} < 0.8$) and large ($R_c/H_{m0} > 0.8$) relative crest freeboards, Eq. 2.5 has a similar accuracy to Eq. 2.4 on the three datasets, as both prediction formulae were fitted through the UG10 dataset, which contained overtopping data in this range.

Mild slopes ($\cot \alpha \geq 2$) were covered in the UG10 dataset and again in the UG13 dataset with an extension to the zero freeboard limit forming the new

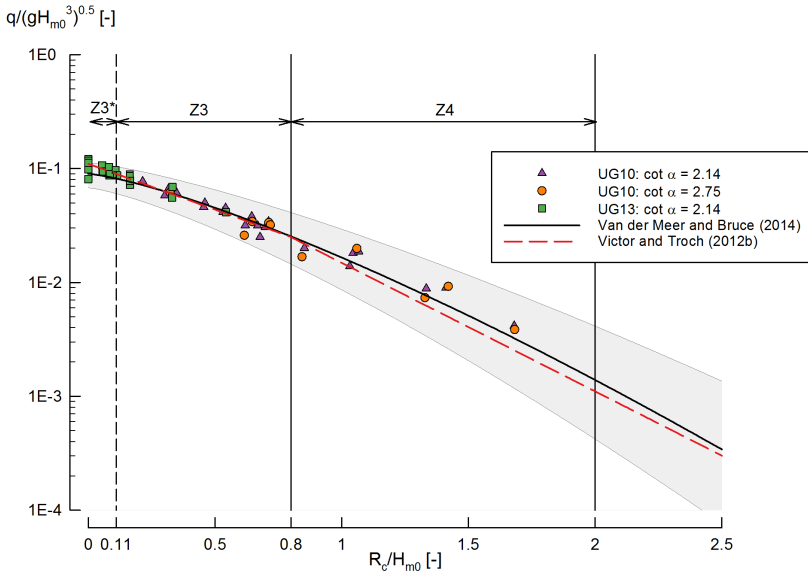


Figure 5.5: Dimensionless average overtopping rate $q/\sqrt{gH_{m0}^3}$ versus relative crest freeboard R_c/H_{m0} for mild slopes ($\cot \alpha = 2.14$ and $\cot \alpha = 2.75$) of the UG10 and UG13 datasets, compared to Victor and Troch (2012b) (Eq. 2.4) and Van der Meer and Bruce (2014) (Eq. 2.5) with its 90% prediction band.

zone $Z3^*$ ($1.5 \leq \cot \alpha \leq 2.75$, $R_c/H_{m0} < 0.11$). The UG14 and UG15 do not feature tests for mild slopes. Figure 5.5 shows the non-breaking overtopping data for the mild slopes ($\cot \alpha \geq 2$) of both datasets ($\cot \alpha = 2.14$ in purple triangles for UG10 and green squares for UG13, and $\cot \alpha = 2.75$ in orange circles for UG10), compared to Eq. 2.4 (dashed red line) and Eq. 2.5 for mild slopes (solid black line) with its 90% prediction band (grey area). The wave overtopping data of the UG13 dataset with very small relative crest freeboards define a new zone $Z3^*$ with a range of R_c/H_{m0} not tested in the UG10 dataset. In general, both predictions have a good agreement with the UG10 and UG13 dataset. In the extension zone $Z3^*$, Eq. 2.5 is slightly underpredicting the dimensionless average overtopping rate (with a RMSE = 0.0137) probably due to the fact that the prediction has not been fitted through overtopping data on that range.

For steeper slopes ($\cot \alpha \leq 1.5$), Victor and Troch (2012b) described two zones: $Z1$ for $R_c/H_{m0} < 0.8$ and $Z2$ for $R_c/H_{m0} > 0.8$. Figure 5.6 shows the UG10 (purple triangles), UG13 (green circles), UG14 (orange squares) and UG15 (blue inverted triangles) data of dimensionless average wave overtopping $q/\sqrt{gH_{m0}^3}$ as a function of the relative crest freeboard R_c/H_{m0} for the steep slope $\cot \alpha = 1$ ($\alpha = 45^\circ$), compared to Eq. 2.4 (red dashed line) and Eq.

2.5 (black solid line) with its 90% prediction band.

In the zone Z1, there is a good agreement of the prediction formulae with the datasets. In the zone Z2, however, the datasets UG14 and UG15 are underpredicted for $R_c/H_{m0} > 1$ by both equations, with five of the data points outside the 90% prediction band. The zone Z1* is composed by new overtopping data on steep slopes with very small relative freeboards which are not considered in the fitting of the existing overtopping prediction formulae. In the zone Z1*, Eq. 2.5 underpredicts the dimensionless overtopping rates, following the general trend of underprediction for very small and zero freeboards. Both Eq. 2.4 and Eq. 2.5 give very similar predictions for the whole range of R_c/H_{m0} , except for the zero freeboard case ($R_c = 0$). In this case, Eq. 2.4 gives a slightly higher prediction, predicting with a higher accuracy the overtopping values.

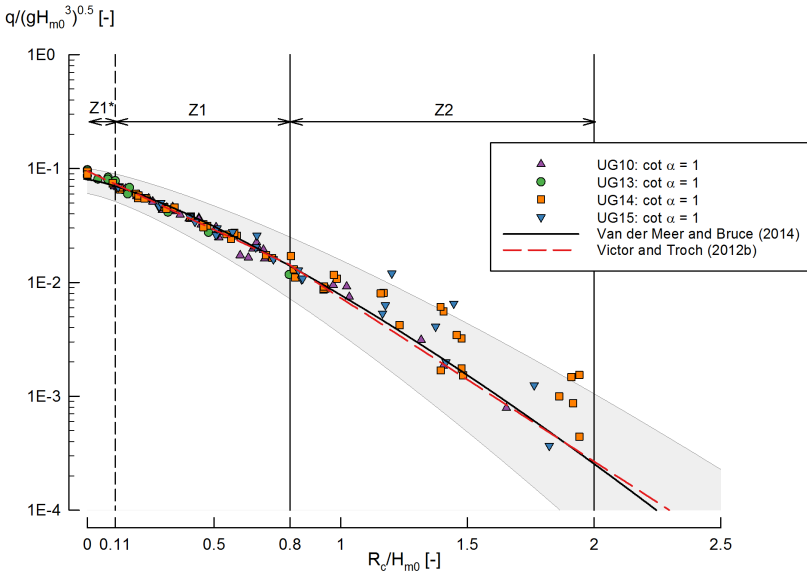


Figure 5.6: Dimensionless average overtopping rate $q/\sqrt{gH_{m0}^3}$ versus relative crest freeboard R_c/H_{m0} for $\cot \alpha=1$ (steep slope, $\alpha=45^\circ$) of the UG10, UG13, UG14 and UG15 datasets, compared to Victor and Troch (2012b) (Eq. 2.4) and Van der Meer and Bruce (2014) (Eq. 2.5) with its 90% prediction band.

For very steep slopes ($0.27 \geq \cot \alpha > 0$), the new datasets fill a knowledge gap in the scientific literature. The new zones Z1* ($0.27 \geq \cot \alpha \geq 0$, $0.8 > R_c/H_{m0} \geq 0$) and Z2* ($0.27 \geq \cot \alpha \geq 0$, $2 \geq R_c/H_{m0} \geq 0.8$) are defined where the UG10 dataset range is extended by UG13, UG14 and UG15. Figure 5.7 shows the UG13 (green circles), UG14 (orange squares) and UG15 (blue inverted triangles) data for the very steep slope of $\cot \alpha = 0.18$ ($\alpha =$

80°). The new data now defined in the zones Z1* and Z2* are compared to the predictions of Eq. 2.4 (red dashed line) and Eq. 2.5 (black solid line) with its 90% prediction band.

The accuracy of both predictions in the zone Z1* is good although for relative crest freeboards $R_c/H_{m0} \leq 0.25$ the trend of the data diverges from the prediction of Eq. 2.5, resulting in an underprediction of the overtopping values. This is in agreement with the underprediction for very small and zero relative crest freeboards already proved for mild and steep slopes, and shown in the overview of RMSE values (Tables 5.1, 5.2 and 5.3). Eq. 2.4 adapts better to the shape of the data in the zone Z1* for very small and zero freeboards. In the zone Z2*, both predictions are underestimating the overtopping rates of the UG14 and UG15 datasets, as was observed for the steep slope $\cot \alpha = 1$ (Figure 5.6).

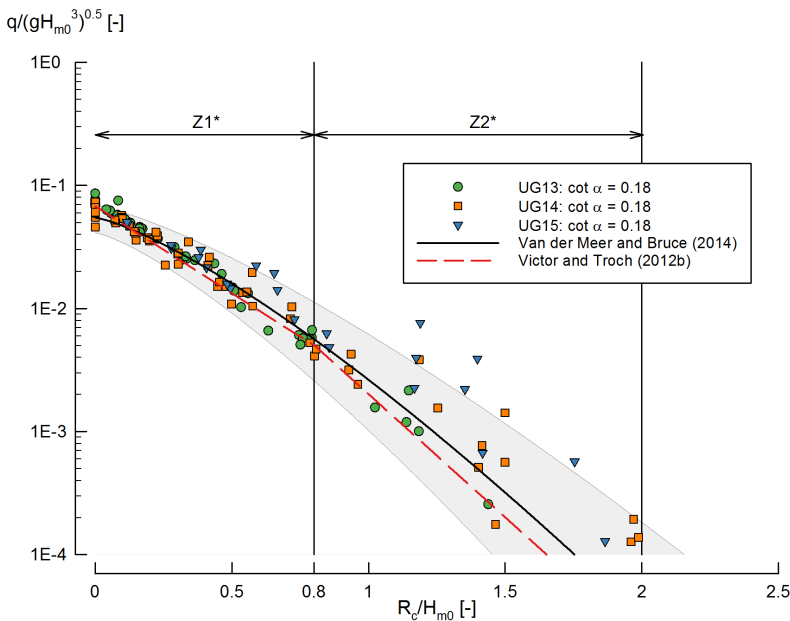


Figure 5.7: Dimensionless average overtopping rate $q/\sqrt{gH_{m0}^3}$ versus relative crest freeboard R_c/H_{m0} for $\cot \alpha=0.18$ (very steep slope, $\alpha=80^\circ$) of the UG13, UG14 and UG15 datasets, compared to Victor and Troch (2012b) (Eq. 2.4) and Van der Meer and Bruce (2014) (Eq. 2.5) with its 90% prediction band.

5.2.3 Vertical Structures

For vertical walls, UG13, UG14 and UG15 also add new data to the zones Z1* ($0.27 \geq \cot \alpha \geq 0, 0.8 > R_c/H_{m0} \geq 0$) and Z2* ($0.27 \geq \cot \alpha \geq 0,$

$2 \geq R_c/H_{m0} \geq 0.8$) where the UG10 dataset had a gap. Figure 5.8 shows the UG13 (green circles), UG14 (orange squares) and UG15 (blue inverted triangles) data for vertical structures $\cot \alpha = 0$ compared to the predictions for this type of structures by Eq. 2.14 and Eq. 2.15 (red dashed line) and Eq. 2.11 (black solid line) with its 90% prediction band.

In the zone $Z1^*$, Eq. 2.11 is again underpredicting the overtopping values for very small and zero freeboards, while Eqs. 2.14 and 2.15 predict with a higher accuracy the data for this range. In the zone $Z2^*$, both predictions are underestimating the values of the UG14 and UG15 datasets, as was the case for steep and very steep slopes (see Section 5.2.2).

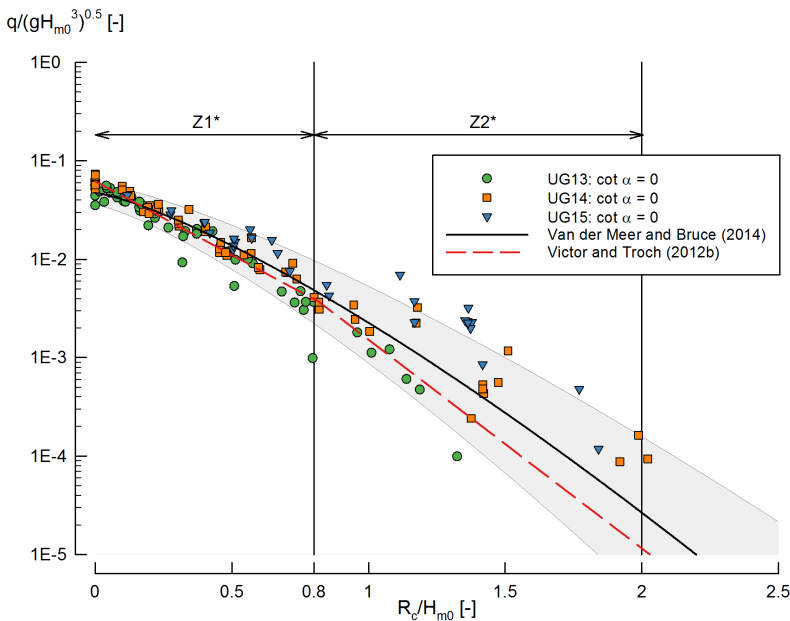


Figure 5.8: Dimensionless average overtopping rate $q/\sqrt{gH_{m0}^3}$ versus relative crest freeboard R_c/H_{m0} for $\cot \alpha=0$ (vertical structures, $\alpha=90^\circ$) of the UG13, UG14 and UG15 datasets, compared to Victor and Troch (2012b) (Eqs. 2.14 and 2.15) and Van der Meer and Bruce (2014) (Eq. 2.11) with its 90% prediction band.

5.2.4 Zero Freeboard

Across all the datasets, and for all the slopes considered (mild, steep, very steep slopes and vertical structures) a consistent underprediction of the overtopping values for very small and zero relative crest freeboards is seen. This is also confirmed by Figure 5.9 which shows the UG13 (green circles) and UG14

(orange squares) zero freeboard ($R_c = 0$) data compared to the prediction by Eq. 2.21 (black cross), Eqs. 2.18 and Eq. 2.19 (red dashed line) and Eq. 2.20 (black solid line) with its 90% prediction band.

Almost all the overtopping values are underpredicted by Eq. 2.20. Moreover, as seen in Table 5.4, 45.2% of the UG13 tests (from a total of 73 tests) and 25.4% (from a total of 67 tests) of the UG14 tests with zero freeboard are predicted outside the 90% prediction band. By definition, only 10% of the tests should be predicted outside the 90% prediction band (considering a sufficiently large dataset). Also for $0 < R_c/H_{m0} < 0.05$ (inside the range of very small freeboards defined in Table 1.2) 16.7% of the UG13 tests are predicted outside the 90% prediction band. For small ($0.11 < R_c/H_{m0} < 0.8$) and large ($R_c/H_{m0} > 0.8$) relative crest freeboards, the percentage is lower than (or around) 10% for the UG13, UG14 and UG15 datasets.

Table 5.4: Percentage of UG13, UG14 and UG15 tests outside the 90% prediction band of the Van der Meer and Bruce (2014) prediction formulae (Eq. 2.5) for various ranges of relative crest freeboards R_c/H_{m0} .

Percentage of Tests Outside 90% Prediction Band			
Range	UG13	UG14	UG15
All tests	15.6	10.1	23.4
Zero freeboard ($R_c = 0$)	45.2	25.4	N/A
$0 < R_c/H_{m0} < 0.05$	16.7	N/A	N/A
$0.05 < R_c/H_{m0} < 0.08$	9.5	0	N/A
$0.08 < R_c/H_{m0} < 0.11$	0	11.1	N/A
$0.11 < R_c/H_{m0} < 0.8$	6.5	0.5	10.0
$R_c/H_{m0} > 0.80$	7.7	17.3	40.2

For large relative crest freeboards ($R_c/H_{m0} > 0.8$), 17.3% of the UG14 tests in this range and 40.2% of the UG15 tests in this range are outside the 90% prediction band of Eq. 2.5. However, for the UG13 dataset, only 7.7% of the tests in this range are outside the band. This result confirms the conclusions from a graphical analysis of underprediction of large R_c/H_{m0} , possibly related to the effect of relatively shallow water conditions.

5.2.5 Discussion

Between the Victor and Troch (2012b) formulae (Eq. 2.4 and Table 2.2) and the Van der Meer and Bruce (2014) formulae (Eqs. 2.5–2.8), there is a special interest in the latter, as they are recommended in the EurOtop (2016) manual as the reference prediction for very steep slopes to vertical walls with very

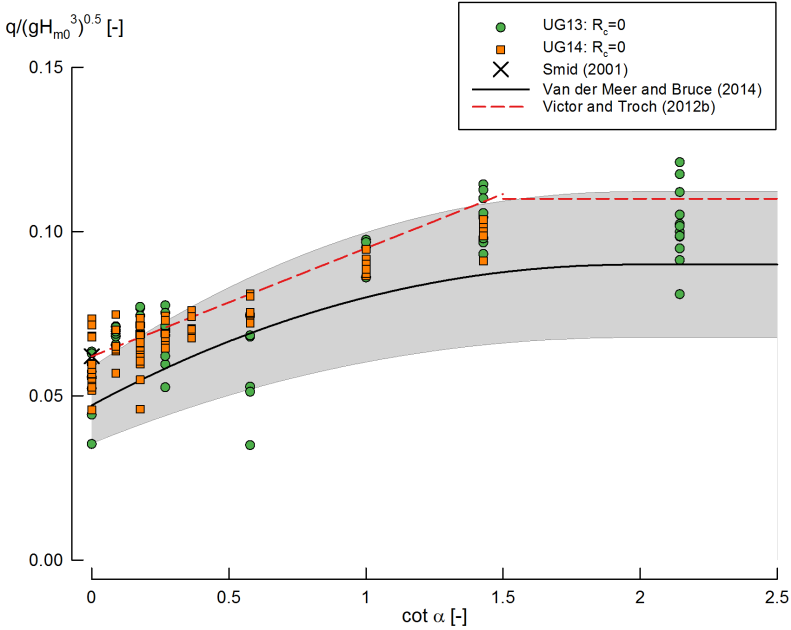


Figure 5.9: Dimensionless average overtopping rate $q/\sqrt{gH_{m0}^3}$ versus $\cot \alpha$ of the UG13 and UG14 datasets, compared to Smid (2001) (Eq. 2.21), Victor and Troch (2012b) (Eqs. 2.18 and 2.19), and Van der Meer and Bruce (2014) (Eq. 2.20) with its 90% prediction band.

small and zero freeboard. However, the prediction formulae by Victor and Troch (2012b) are in general more accurate (i.e., smaller RMSE values for the same set of data) in predicting the overtopping values of the UG13, UG14 and UG15 dataset than the Van der Meer and Bruce (2014) formulae.

None of the predictions were validated explicitly by data for very steep slopes to vertical structures, and very small to zero freeboards (i.e., steep low-crested structures). UG13, UG14 and UG15 can be used to check the accuracy of the prediction in this range, previously a knowledge gap in the literature. For these conditions, the new zones Z1* ($0.27 \geq \cot \alpha \geq 0$, $0.8 > R_c/H_{m0} \geq 0$), Z2* ($0.27 \geq \cot \alpha > 0$, $2 \geq R_c/H_{m0} \geq 0.8$) and Z3* ($2.75 \geq \cot \alpha \geq 1.5$, $R_c/H_{m0} < 0.11$) are defined with the extension data of the new datasets. Van der Meer and Bruce (2014) formulae have a good accuracy for mild slopes and steep slopes (Figures 5.5 and 5.6), while for very steep slopes (Figure 5.7) and vertical structures (Figure 5.8) the trend of the data is slightly different than the prediction, causing a small overprediction for relative crest freeboards $R_c/H_{m0} \geq 0.25$ and a small underprediction for $R_c/H_{m0} \leq 0.25$.

For very small and zero relative crest freeboards ($0 \leq R_c/H_{m0} \leq 0.11$) there is a consistent underprediction across all the slope angles by the Van der Meer and Bruce (2014) formulae. This is confirmed graphically by Figure 5.9, by the RMSE values for various ranges of relative crest freeboards (Tables 5.1 and 5.2) and by the large percentage of UG13 and UG14 data for zero freeboard outside the 90% prediction band of the prediction (Table 5.4).

For large relative crest freeboards, the UG14 and UG15 overtopping data is consistently underpredicted by the Victor and Troch (2012b) and Van der Meer and Bruce (2014) formulae. As these datasets feature tests with transitional ($0.2 < H_{m0}/h < 0.5$) and relatively shallow water conditions ($H_{m0}/h \geq 0.5$), it is possible that this underprediction is caused by an increase of the dimensionless average overtopping rates for large relative freeboards due to the effect of relatively shallow water conditions. This hypothesis is discussed in Section 5.3.

The accuracy of the prediction by Van der Meer and Bruce (2014) can improve by adding the UG13, UG14 and UG15 datasets to the previous UG10 dataset and CLASH data and refitting the a , b and c coefficients in Eq. 2.5. This is possible through the complete range of slope angles ($\cot \alpha \geq 0$) and relative crest freeboards ($R_c/H_{m0} \geq 0$). With this updated fit, the accuracy will increase for very steep slopes towards vertical walls, and for very small relative freeboards towards the zero freeboard case, while maintaining the achieved accuracy for the more conventional ranges (see Section 5.4).

5.3 Influence of Shallow Water Conditions on Non-Breaking Overtopping

As stated in Section 2.3.2, relatively deep water conditions occur for $H_{m0}/h < 0.2$, relatively shallow water conditions for $H_{m0}/h > 0.5$, and transitional conditions for in between values $0.2 < H_{m0}/h < 0.5$. The UG14 and UG15 datasets mostly contain overtopping data for transitional and relatively shallow water conditions, to increase the knowledge of shallow water effects on wave overtopping for non-breaking wave conditions.

In Section 5.2.2 a possible increase of the dimensionless average overtopping rates for large R_c/H_{m0} due to shallow water effects is commented. By dividing the data into different ranges of relative wave height H_{m0}/h it is possible to assess this effect. For mild slopes there is not enough data in the UG13, UG14 and UG15 datasets to determine this effect.

Figure 5.10 shows the overtopping data of the UG10, UG13, UG14 and UG15 datasets corresponding to $\cot \alpha = 0.18$ (very steep slope, $\alpha = 80^\circ$), com-

pared to Eq. 2.5 with its 90% prediction band. The data are divided in five ranges of H_{m0}/h for relatively deep water conditions, transitional conditions and relatively shallow water conditions. Figure 5.11 show the same type of plot for vertical structures ($\cot \alpha=0$, $\alpha=90^\circ$), adding Eq. 2.12 and Eq. 2.13.

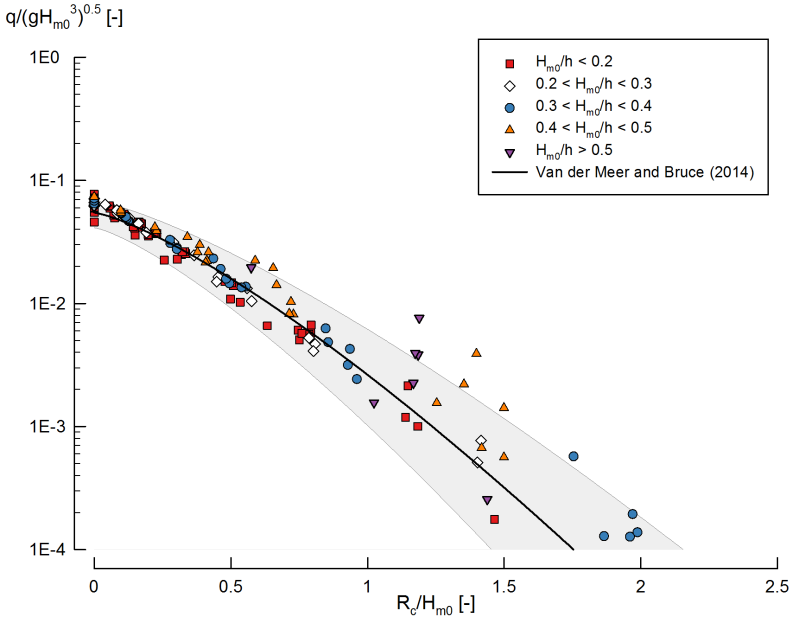


Figure 5.10: Dimensionless average overtopping rate $q/\sqrt{gH_{m0}^3}$ versus relative crest freeboard R_c/H_{m0} divided per H_{m0}/h for the very steep slope $\cot \alpha=0.18$ ($\alpha=80^\circ$) of the UG13, UG14 and UG15 datasets, compared to Van der Meer and Bruce (2014) (Eq. 2.5) with its 90% prediction band.

In these figures, the influence of relatively shallow water conditions is non-existent for zero, very small and small relative crest freeboards ($0 \leq R_c/H_{m0} < 0.11$). The data of the various ranges of H_{m0}/h align with the prediction by Eq. 2.5 showing a low scatter, with the prediction inaccuracies stated in Section 5.2.2.

However, for relative crest freeboards $R_c/H_{m0} > 1$, there is an increase of the average overtopping for shallower water conditions. The average overtopping is consistently larger for increasing values of H_{m0}/h . This is also observed by comparing the overtopping data with the prediction by Eq. 2.5, which is underpredicting the rates for this relative freeboard range. In fact, part of the data for transitional conditions ($0.2 < H_{m0}/h < 0.5$) and relatively shallow water conditions ($H_{m0}/h > 0.5$) is outside the 90% prediction band (see Table 5.4).

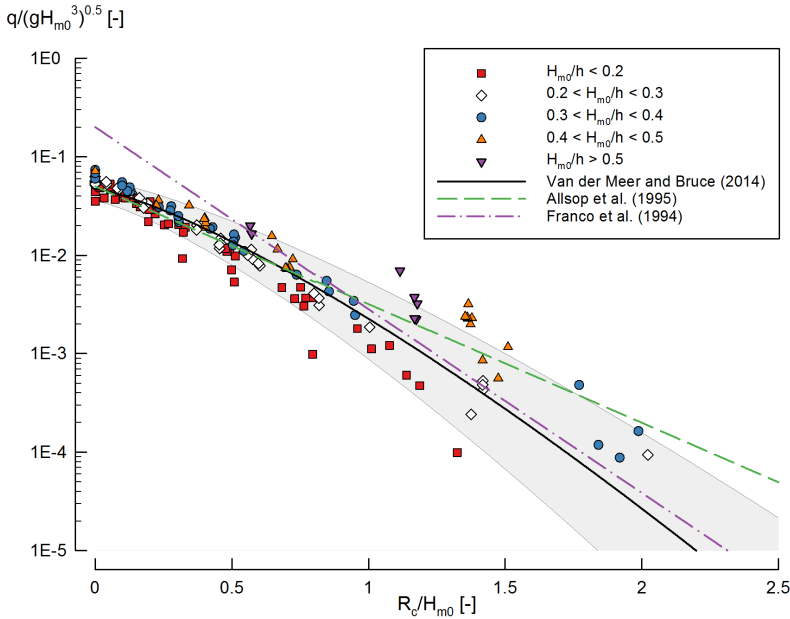


Figure 5.11: Dimensionless average overtopping rate $q/\sqrt{gH_{m0}^3}$ versus relative crest freeboard R_c/H_{m0} divided per H_{m0}/h for vertical structures $\cot \alpha=0$ ($\alpha=90^\circ$) of the UG10, UG13, UG14 and UG15 datasets, compared to Van der Meer and Bruce (2014) (Eq. 2.11) with its 90% prediction band, Allsop et al. (1995) (Eq. 2.12) and Franco et al. (1994) (Eq. 2.13).

For vertical walls, the EurOtop (2016) manual suggests to use Allsop et al. (1995) prediction (Eq. 2.12) to predict non-breaking overtopping influenced by the foreshore. However, the definition of an influencing foreshore is not clearly stated in EurOtop (2016), where only a qualitative definition of a no influencing foreshore is given. One approach would be to assimilate the relatively shallow water conditions to an influencing foreshore. Figure 5.11 shows this approach with the UG13, UG14 and UG15 data. Eq. 2.12 is predicting with a higher accuracy than Eq. 2.11 the overtopping rates of transitional and relatively shallow water conditions for $R_c/H_{m0} > 1$.

An increase in the H_{m0}/h values indicates that for the same water depth at the toe of the structure h , there is an increase in the incident spectral wave height H_{m0} . If the foreshore had an influence on the wave overtopping, this influence would be a function of h , and for equal values of h the foreshore would influence similarly the overtopping rates. This is in contradiction with the fact that H_{m0} is the main influencing parameter. Therefore, it would be advised to drop the terminology referring to an influencing foreshore for further consideration in the selection of the most appropriate non-breaking wave

overtopping prediction as it leads to a misunderstanding of the overtopping process.

Figure 5.8 also answers the question posed in Section 2.3.4 about the different use of the predictions by Allsop et al. (1995) (Eq. 2.12) and Franco et al. (1994) (Eq. 2.13). For relative freeboards $R_c/H_{m0} > 1$, Eq. 2.12 is valid for tests with relatively shallow water conditions, and Eq. 2.13 is valid for tests with relatively deep water conditions. For relative freeboards $R_c/H_{m0} < 1$, Eq. 2.12 is predicting the overtopping rates similar to Eq. 2.5, while Eq. 2.13 is overpredicting the overtopping rates by a factor three.

The increase of the average overtopping rates due to shallow water conditions is not significant enough to be considered apart from the natural scatter of the average overtopping for large relative crest freeboards. Although Allsop et al. (1995) is correctly predicting the overtopping rates for relatively shallow water conditions, its use is increasing the complexity of the overtopping prediction decision tree for vertical structures.

Moreover, the same effect of increasing average overtopping rates for relatively shallow water conditions is also found in steep and very steep slopes. However, for that range of slopes the only recommendation is to use the prediction by Van der Meer and Bruce (2014). It would make sense to have a consistent approach to the overtopping prediction for very steep slopes and vertical structures, as the latter are the limit case of the former. This would also be in line with the simplification effort of the overtopping prediction initiated in the EurOtop (2016) manual. To include the effect of relatively shallow water conditions in the prediction of the overtopping, it would be advised to increase the uncertainty of the prediction for relative crest freeboards $R_c/H_{m0} > 1$, instead of suggesting the use of a different prediction formula or fitting a new prediction.

5.4 Update of the Overtopping Prediction for Steep Low-Crested Structures

As stated in Section 5.2.5, it is possible to update the a , b and c coefficients of Eq. 2.5 to include the new overtopping datasets UG13, UG14 and UG15 in the fitting of the prediction. In particular, a higher prediction accuracy is wanted for:

- i. vertical walls ($\cot \alpha = 0$);
- ii. very steep slopes ($0.27 \geq \cot \alpha > 0$); and
- iii. very small and zero relative freeboards ($0.11 > R_c/H_{m0} \geq 0$).

The update of the prediction should maintain the accuracy achieved by Victor and Troch (2012b) and Van der Meer and Bruce (2014) for steep slopes ($2 > \cot \alpha > 0.27$) and mild slopes ($\cot \alpha \geq 2$) with small ($0.8 > R_c/H_{m0} \geq 0.11$) and large ($R_c/H_{m0} \geq 0.8$) relative crest freeboards.

5.4.1 Selection of Overtopping Data to Update the Prediction

The overtopping data considered for their inclusion in the fit of the coefficients update belong to the UG10, UG13, UG14 and UG15 datasets, the CLASH database and overtopping data for vertical walls reported in the EurOtop (2016) manual. However, not all the tests are suitable to be included in the fit due to various reasons. To have a consistent overtopping dataset to fit the updated coefficients, only tests with similar setup and wave conditions should be chosen.

The criteria and the reasons to select tests to be included in the fitting of the coefficients update are:

1. Foreshore at the toe of the structure milder than 1:100, to avoid any possible influence of the foreshore in the overtopping process, and to match the mild foreshores of all the datasets obtained at Ghent University.
2. No complex cross sections, as the presence of a toe or a berm influences the overtopping rates. The only exception is for vertical structures without influencing foreshore, as the EurOtop (2016) classification states that in this case the overtopping is not influenced by the presence of a toe or a berm.
3. Smooth and impermeable structures ($\gamma_f = 1$), as the effect of rough slopes and permeable structures should be excluded for the analysis of the overtopping at this stage.
4. Perpendicular wave attack ($\beta = 0^\circ$), to exclude from the analysis the effect of oblique wave attack on the overtopping rates.
5. Slope angle $\cot \alpha \leq 4$, as the purpose is to update the steep low-crested overtopping prediction formula.
6. Tests with non-breaking waves, as the prediction formula to update is for non-breaking conditions. Tests with a surf similarity parameter $\xi_{m-1,0} < 2$, and tests which are described by the non-breaking prediction formula by Van der Meer and Bruce (2014) are excluded from the fit.
7. Relatively deep water conditions ($H_{m0}/h < 0.2$) and transitional conditions ($0.2 < H_{m0}/h < 0.4$). As discussed in Section 5.3, relatively shallow water conditions have an effect on the overtopping rates. Therefore, tests with $H_{m0}/h > 0.4$ are excluded from the fit. The limit value of

$H_{m0}/h = 0.4$ is taken to match the values of H_{m0}/h tested in the UG10 dataset.

8. No tests with zero overtopping or with average overtopping $q < 1 \times 10^{-6} \text{ m}^3/\text{s}/\text{m}$, following the approach of the authors of several neural networks (Verhaeghe et al., 2008; Van Gent et al., 2007; Zanuttigh et al., 2016).

By applying these criteria, a total of 1410 tests of the following datasets are selected to fit the update of the coefficients of the overtopping prediction formula:

- UG10 dataset: 311 tests.
- UG13 dataset: 297 tests.
- UG14 dataset: 322 tests.
- UG15 dataset: 91 tests.
- CLASH: 322 tests.
 - Subsets (most of them partially): 028, 102, 103, 106, 107, 113, 218, 220, 221, 222, 226, 228, 229, 315, 351, 380, 402, 510, 703, 914.
- Tests reported in Figure 7.7 of the EurOtop (2016) manual on vertical structures without influencing foreshore: 67 tests, obtained by personal communication with Jentsje van der Meer.

A comment is necessary about the CLASH subset 108 by Smid (2001) on zero freeboard (20 tests) and $R_c/H_{m0} > 0.5$ (37 tests) for $\cot \alpha = 1.5$. This subset was classified in the CLASH database with a so-called reliability factor (RF) (see Steendam et al., 2004) of $\text{RF} = 4$, which according to Van der Meer et al. (2013) is due to inconsistencies on the measured wave periods. Van der Meer and Bruce (2014) included the subset 108 in the fitting of the formulae Eq. 2.5 arguing that the wave period is not influencing the overtopping for non-breaking conditions. However, it was excluded from the fit of the updated coefficients as the data show an unusual spreading of the dimensionless average overtopping rates, which reaffirms the concerns about the reliability of the data stated in the CLASH database.

5.4.2 Update of the Coefficients

The average overtopping prediction formula for non-breaking conditions is the Weibull-type seen in Eq. 5.1 and used by Van der Meer and Bruce (2014), with a , b and c coefficients with the same physical meaning as explained in Section 2.3.3. The resulting update after the fit of the coefficients a , b and c are shown in Eqs. 5.2, 5.3 and 5.4, respectively:

$$\frac{q}{\sqrt{gH_{m0}^3}} = a_{\text{update}} \cdot \exp \left[- \left(b_{\text{update}} \frac{R_c}{H_{m0} \gamma_f \gamma_\beta} \right)^{c_{\text{update}}} \right] \quad (5.1)$$

with the following expressions for the coefficients a , b and c :

$$a_{\text{update}} = 0.109 - 0.035 (1.5 - \cot \alpha) \text{ and } a_{\text{update}} = 0.109 \text{ for } \cot \alpha \geq 1.5 \quad (5.2)$$

$$b_{\text{update}} = 2 + 0.56 (1.5 - \cot \alpha)^{1.3} \text{ and } b_{\text{update}} = 2 \text{ for } \cot \alpha \geq 1.5 \quad (5.3)$$

$$c_{\text{update}} = 1.1 \quad (5.4)$$

The uncertainty related to a_{update} is defined by a standard error of the estimate $\sigma_{\text{est}} = 0.01$, and the uncertainty related to b_{update} is defined by a standard error of the estimate $\sigma_{\text{est}} = 0.66$. The range of application of the formula is for slope angles $0 \leq \cot \alpha \leq 4$ and relative crest freeboards $R_c/H_{m0} \geq 0$.

Eq. 5.1 includes the roughness influence factor γ_f and the oblique wave attack influence factor γ_β in the prediction. The various γ_f and γ_β expressions published in literature (e.g., in the EurOtop (2016) manual) are assumed to be valid in the updated prediction, although this validity has not been confirmed by new physical model tests. The effect on the influence factors of a prediction with a coefficient c different from 1 is negligible, as the natural scatter of the overtopping process compensates for the different value that should be used to account for a $c > 1$ coefficient.

Coefficient c_{update}

A nonlinear regression is performed with the software SPSS (IBM, 2016) to find the best fit of the a , b and c coefficients per slope angle by minimizing the residual sum of squares (RSS, as shown in Eq. 5.5) and using a sequential quadratic programming algorithm as the iterative method. The RSS has a similar formulation to the RMSE (Eq. 3.1). The reasons to choose to minimize the RSS instead of a version with the logarithm of the measured and predicted values are the same as explained in Section 3.4 for the RMSE.

$$\text{RSS} = \sum_{n=1}^{N_{\text{test}}} \left[\frac{q_{\text{meas}_n}}{\sqrt{gH_{m0}^3}} - \frac{q_{\text{pred}_n}}{\sqrt{gH_{m0}^3}} \right]^2 \quad (5.5)$$

The data do not show a dependence of c on the slope angle, therefore, it is decided to have a constant c coefficient. The best fit of the c coefficient is found to be $c_{\text{update}} = 1.1$ (Figure 5.12).

Battjes (1974) presented an analytical overtopping prediction formula for mild slopes with breaking wave conditions. While most of the existing predictions feature an exponential formula which on a log-linear plot is a straight

line, this prediction features a bivariate Rayleigh distribution which is a curve on a log-linear plot. Two reformulations of the Battjes (1974) prediction were made: a first one in the TAW (1989) manual, and a second one made by Van der Meer et al. (2013) to match the EurOtop (2007) overtopping prediction for breaking waves (Eq. 2.1). Combining both reformulations Van der Meer et al. (2013) found that Battjes (1974) was adapting well to the CLASH data for large freeboards and, surprisingly, also to zero freeboard data (CLASH subset 102 by Smid (2001)).

Indeed, the curved shape of the prediction in a log-linear plot fits the data for zero freeboard of the CLASH subset 102, which a straight line prediction would greatly overpredict. The same principle is followed by Van der Meer and Bruce (2014) in the fitting of their prediction: a curved line on a log-plot would accurately predict the overtopping for large relative crest freeboard and the very small and zero freeboards. The three-parameter Weibull distribution is chosen by Van der Meer and Bruce (2014) with a $c = c_{V\&B} = 1.3$ (Eq. 2.8).

The data per slope angle show that a $c = 1.3$ coefficient is overestimating the best c for all the slope angles considered. As it is explained in Van der Meer et al. (2013), the value $c_{V\&B} = 1.3$ is both valid for breaking and non-breaking conditions although it is not the best fit for the non-breaking tests. As the proposed updated coefficients are not fitted through breaking wave conditions overtopping data, on the trade-off between keeping the same c coefficient for both breaking and non-breaking conditions and improving the accuracy of the non-breaking prediction, the latter is chosen. Therefore, it is decided to disassociate the non-breaking from the breaking overtopping prediction formulae to increase the accuracy of the non-breaking prediction.

The obtained values of c for each slope angle (Figure 5.12) also suggest that the shape of overtopping data for the complete range of relative crest freeboards is closer to a line in a log-linear plot than estimated by Van der Meer et al. (2013) and Van der Meer and Bruce (2014). This inaccurate estimation is maybe due to lack of a significant number of overtopping data available for zero and very small freeboards at the time of both publications. This closer to linear shape was already observed in the data when comparing UG13, UG14 and UG15 with Eq. 2.5 (see Section 5.2.2). The value selected for c in the update of the coefficients $c_{\text{update}} = 1.1$ yields a prediction trend close to a straight line in a log-linear plot, matching better the shape of the data.

Coefficient a_{update}

The best fit of the a coefficients (Figure 5.13) is found among the zero freeboard data ($R_c = 0$) to assure the most accurate prediction for these con-

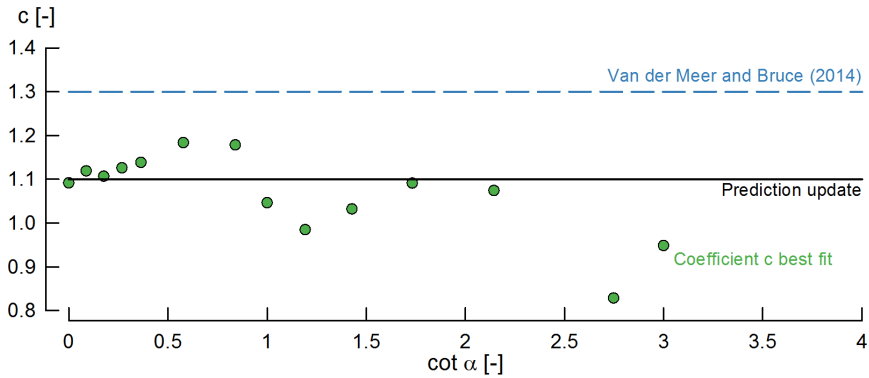


Figure 5.12: Best fit of the c coefficient per slope angle and updated value $c_{\text{update}} = 1.1$ compared to Van der Meer and Bruce (2014) (Eq. 2.8).

ditions, resulting in Eq. 5.2. The value of a corresponding to $\cot \alpha = 4$ shown in the figure is calculated from only one test and therefore it is not representative of that slope angle. The a coefficients show a dependence on the slope angle, although only for values $\cot \alpha < 1.5$. This limit differs from Van der Meer and Bruce (2014) who found a limit on $\cot \alpha = 2$ but is the same value found by Victor and Troch (2012b). The updated a coefficient has a similar expression to Eq. 2.6 although with a linear shape, reaching a constant value at $\cot \alpha = 1.5$. The resulting expression for a is larger for the updated prediction than for Van der Meer and Bruce (2014).

Coefficient b_{update}

A linearisation is applied to the data by calculating the natural logarithm \ln of both sides of Eq. 5.1. On this step, the values of c_{update} and a_{update} are fixed according to Eq. 5.4 and 5.2, respectively. The best fit power law with the same shape as Eq. 2.7 with a limit on $\cot \alpha = 1.5$ is calculated through the linearised b values per slope angle, resulting in Eq. 5.3 (Figure 5.14). Compared to Eq. 2.7, Eq. 5.3 does not have a constant maximum value of b for very steep slopes as the data show increasing values of b at this range of slopes. The influence of slope angle α is found to be until $\cot \alpha = 1.5$, matching Victor and Troch (2012a) and diverging from Van der Meer and Bruce (2014), as was the case for the coefficient a .

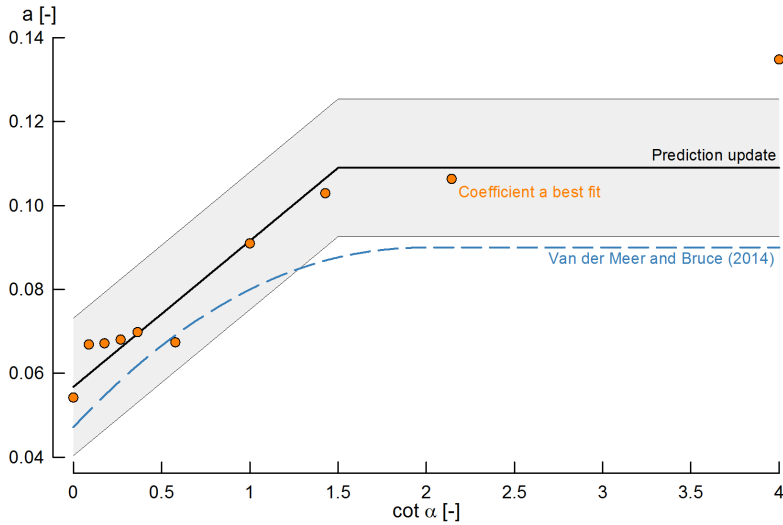


Figure 5.13: Best fit of the a coefficient (Eq. 5.2 with its 90% prediction band) for tests with $R_c = 0$ compared to Van der Meer and Bruce (2014) (Eq. 2.6).

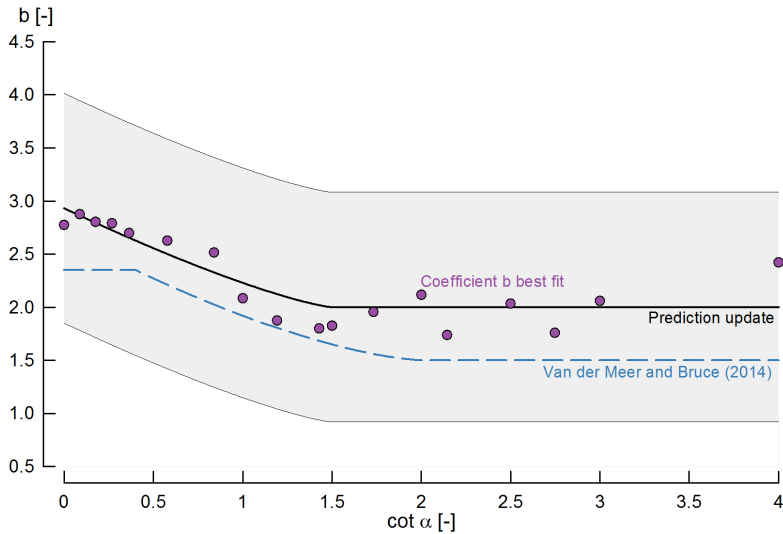


Figure 5.14: Best fit of the b coefficient (Eq. 5.3 with its 90% prediction band) compared to Van der Meer and Bruce (2014) (Eq. 2.7).

5.4.3 Uncertainty of the Prediction Update

EurOtop (2016) described the uncertainty of the Van der Meer and Bruce (2014) prediction by a coefficient of variation $\sigma' = \sigma/\mu$ of $a_{V\&B}$ and $b_{V\&B}$ (where σ is the standard deviation and μ the average value of the coefficient for a specific slope angle). However, for the prediction update it is decided that the uncertainty is described by a single value of the standard error of the estimate σ_{est} for the coefficients a_{update} and b_{update} . To suggest a coefficient of variation σ' instead of the standard error of the estimate σ_{est} implies that the uncertainty is larger for larger values of the considered coefficient, whereas the data show no influence of the slope angle α on the uncertainty of the prediction.

The uncertainty of the a_{update} coefficient (Eq. 5.2) is obtained by calculating the standard error of the estimate a of all the $R_c = 0$ tests, which resulted in $\sigma_{\text{est}}(a_{\text{update}}) = 0.01$. The scatter of the data for vertical structures ($\cot \alpha = 0$) is dominating the value of $\sigma_{\text{est}}(a_{\text{update}})$, artificially increasing the uncertainty for other slope angles. The 90% prediction band of a_{update} is calculated by $a_{\text{update}} \pm 1.64 \sigma_{\text{est}}(a_{\text{update}})$, assuming that a_{update} is a normally distributed stochastic parameter.

The uncertainty of the b_{update} coefficient (Eq. 5.3) is obtained by calculating the standard error of the estimate b for all the tests, which results in $\sigma_{\text{est}} = 0.66$. This uncertainty is more than a factor two larger than the calculated for Eq. 2.7 in the EurOtop (2016) manual. However, a re-analysis of the UG10 dataset per slope angle yields values of $\sigma(b)$ from 1.2 to 2 times larger than the $\sigma(b)$ suggested by EurOtop (2016), meaning that the uncertainty of the Van der Meer and Bruce (2014) prediction is greatly underestimated.

The data used to fit Eq. 5.3 show a large scatter of the b values when a and c are fixed, therefore the uncertainty of the prediction derived from the data is also large. Especially, for vertical structures ($\cot \alpha = 0$) the scatter of the data is larger than for other slope angles, increasing the final value of $\sigma_{\text{est}}(b_{\text{update}})$ and overestimating the uncertainty for other slope angles. The inclusion in the data of overtopping tests for composite vertical structures without influencing foreshore and the difficulties in identifying tests influencing foreshores creates this larger scatter of the data.

The 90% prediction band of b_{update} is calculated by $b_{\text{update}} \pm 1.64 \sigma_{\text{est}}(b_{\text{update}})$, assuming that b_{update} is a normally distributed stochastic parameter.

5.4.4 Comparison of Predictions and Discussion

In Figure 5.15, the updated prediction (Eq. 5.1) is compared to the Van der Meer and Bruce (2014) prediction (Eq. 2.5) for mild slopes (including $\cot \alpha \geq 1.5$ in the case of the updated prediction) and the very steep slope $\cot \alpha = 0.09$. Eq. 5.1 gives a larger prediction than Eq. 2.5 for zero freeboards ($R_c = 0$) as a result of a_{update} being larger than $a_{V\&B}$ for the complete range of slope angles. The higher predicted value for $R_c = 0$ solves the prediction inaccuracy by Van der Meer and Bruce (2014) for this case stated in Section 5.2.4.

For larger relative freeboards, both predictions are similar in the case of mild slopes ($\cot \alpha \geq 2$), with the EurOtop (2007) prediction (Eq. 2.2) applicable in this range and predicting accurately the overtopping rates for $R_c/H_{m0} > 1$ (see Figure 5.4). For steeper slopes, the updated prediction yields larger overtopping rates than the Van der Meer and Bruce (2014) prediction due to the smaller coefficient $c_{\text{update}} = 1.1$ of the updated prediction as it adapts better to the shape of the data.

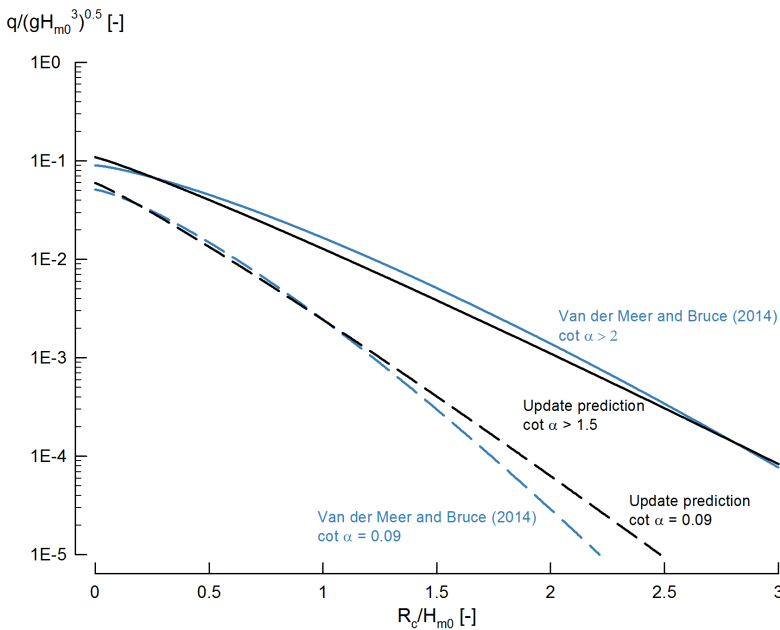


Figure 5.15: Comparison between the updated prediction (Eq. 5.1) and Van der Meer and Bruce (2014) (Eq. 2.5) for mild slopes ($\cot \alpha > 2$) and the very steep slope $\cot \alpha = 0.09$.

Figure 5.16 shows the vertical structures overtopping data used to fit the updated prediction. The data is compared to Eq. 5.1 with its 90% prediction band, Eq. 2.11 and Eq. 2.12.

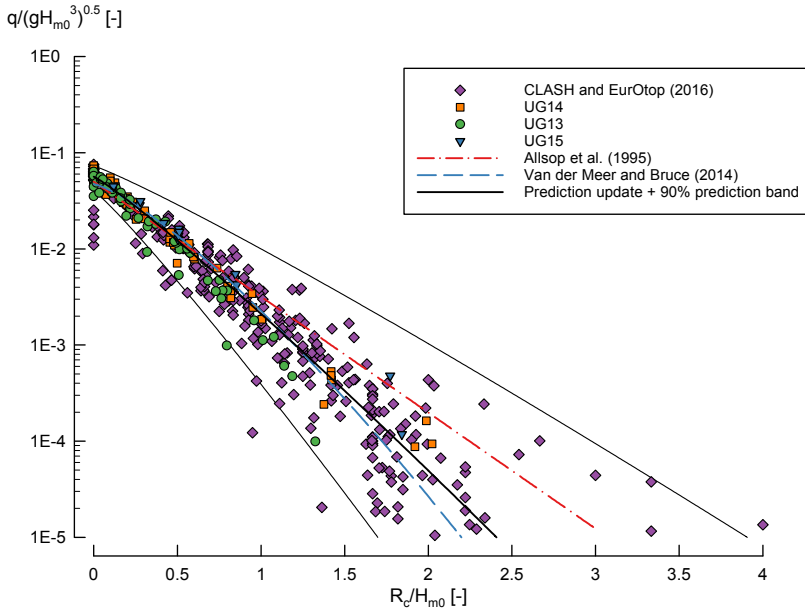


Figure 5.16: Vertical structures overtopping data compared to the updated prediction (Eq. 5.1) with its 90% prediction band, Van der Meer and Bruce (2014) (Eq. 2.11) and Allsop et al. (1995) (Eq. 2.12).

Whereas Eq. 2.5 is recommended to be used only to predict overtopping with no influencing foreshores, the updated prediction takes the scatter of the data that accounts for shallower water conditions — a possible presence of an influencing foreshore— in the uncertainty determination (see Section 5.4.2). Eq. 2.12 is included in the 90% prediction band of the updated prediction. Therefore, a distinction between tests with and without influencing foreshore is no longer necessary if Eq. 5.1 is used. The decision tree of which overtopping prediction for vertical structures to select would be simplified with Eq. 5.1.

One of the objectives of updating the prediction is to improve the accuracy of the prediction by Van der Meer and Bruce (2014) for the zero freeboard case ($R_c = 0$), which was underpredicting consistently for all the slope angles the average overtopping rates for this case. Figure 5.17 shows the updated prediction compared to the Van der Meer and Bruce (2014) for the zero freeboard case. The updated prediction shows a great improve of the accuracy of the prediction, as it adapts better than the Van der Meer and Bruce (2014) prediction to the data.

Table 5.5 shows the RMSE (Eq. 3.1) and bias (Eq. 3.2) values of Eq. 2.5 and Eq. 5.1 for the 1410 tests that were used to fit the prediction update. Eq. 5.1 is

5.4 Update of the Overtopping Prediction for Steep Low-Crested Structures

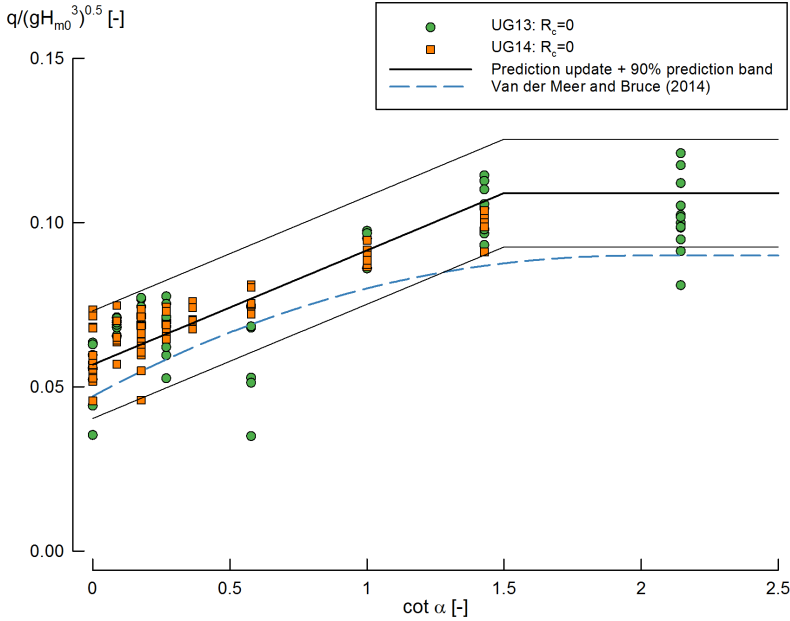


Figure 5.17: Zero freeboard ($R_c = 0$) overtopping data compared to the updated prediction (Eq. 5.1) with its 90% prediction band, Van der Meer and Bruce (2014) (Eq. 2.5) and Allsop et al. (1995) (Eq. 2.12).

Table 5.5: RMSE values (Eq. 3.1) and bias (Eq. 3.2) of the 1410 tests used to fit Eq. 5.1, for different ranges of relative crest freeboard R_c/H_{m0} and slope angle α .

Equation	Eq. 2.5		Eq. 5.1		
	Item	RMSE (-)	Bias (-)	RMSE (-)	Bias (-)
All tests		0.0064	-1.4×10^{-3}	0.0051	-1.7×10^{-4}
Zero freeboard ($R_c = 0$)		0.0155	-1.0×10^{-2}	0.0114	2.8×10^{-4}
$0 < R_c/H_{m0} < 0.05$		0.0094	-6.9×10^{-3}	0.0070	-9.2×10^{-4}
$0.05 < R_c/H_{m0} < 0.08$		0.0089	-7.1×10^{-3}	0.0054	-1.7×10^{-3}
$0.08 < R_c/H_{m0} < 0.11$		0.0074	-5.7×10^{-3}	0.0053	-1.9×10^{-3}
$0.11 < R_c/H_{m0} < 0.8$		0.0042	4.4×10^{-4}	0.0041	4.6×10^{-5}
$R_c/H_{m0} > 0.8$		0.0020	-2.8×10^{-4}	0.0019	-3.5×10^{-4}
Mild slopes		0.0091	-2.5×10^{-3}	0.0058	-1.2×10^{-3}
Steep slopes		0.0052	-8.9×10^{-4}	0.0046	3.1×10^{-4}
Very steep slopes		0.0071	-3.5×10^{-3}	0.0044	-1.9×10^{-3}
Vertical structures		0.0066	-3.2×10^{-4}	0.0061	6.8×10^{-4}

reducing the RMSE value of Eq. 2.5 by 20%, consistently reducing the RMSE values for all the relative crest freeboard and slope angle ranges considered

in Table 5.5. Particularly, the reduction of RMSE for zero freeboard ($R_c = 0$) tests is 26%, for very small relative freeboards ($0 < R_c/H_{m0} < 0.11$) between 25% and 39%, and for very steep slopes ($0.27 \geq \cot \alpha > 0$) the reduction is of 38%. For vertical structures there is a slight reduction of the RMSE value (9%). The bias values suggest a consistent underprediction of the overtopping rates by Eq. 2.5 (negative values of the bias, as explained in Section 5.2.2), while Eq. 5.1 does not show a clear influence of the relative crest freeboard or slope angle in underpredicting or overpredicting the overtopping rates.

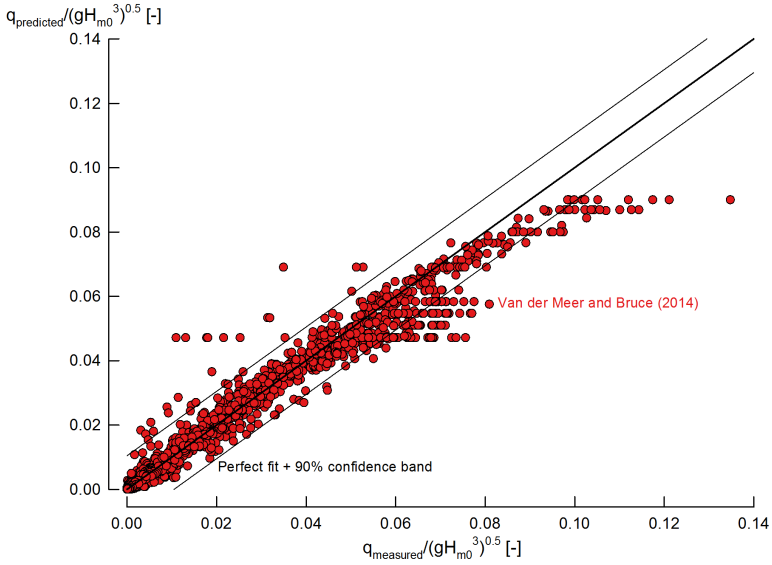
This indicates that Eq. 5.1 is predicting more accurately than Eq. 2.5 the overtopping rates of these 1410 tests. However, it is obvious that the overtopping rates of a set of tests will be better predicted by an equation that has been fitted through the set than by an equation which has not been fitted through it. Instead, the strength of Eq. 5.1 as an update of the overtopping prediction for steep low-crested structures is the size of the dataset used to fit the prediction and the use of new data (the Ghent University datasets) that are novel and that allow a better prediction of the overtopping on relative crest freeboard and slope angle ranges which before were a knowledge gap in the literature.

Figure 5.18a and Figure 5.18b show the comparison of the measured and predicted dimensionless average overtopping rates for Eq. 2.5 and Eq. 5.1) respectively. It is decided to show linear plots instead of logarithmic plots for a better visualization of the large overtopping rates. The line of perfect fit is shown in both figures, together with the 90% confidence band of the predictions. The data points below the perfect fit line are underestimated by the prediction, while the data points above the perfect fit line are overestimated by the prediction.

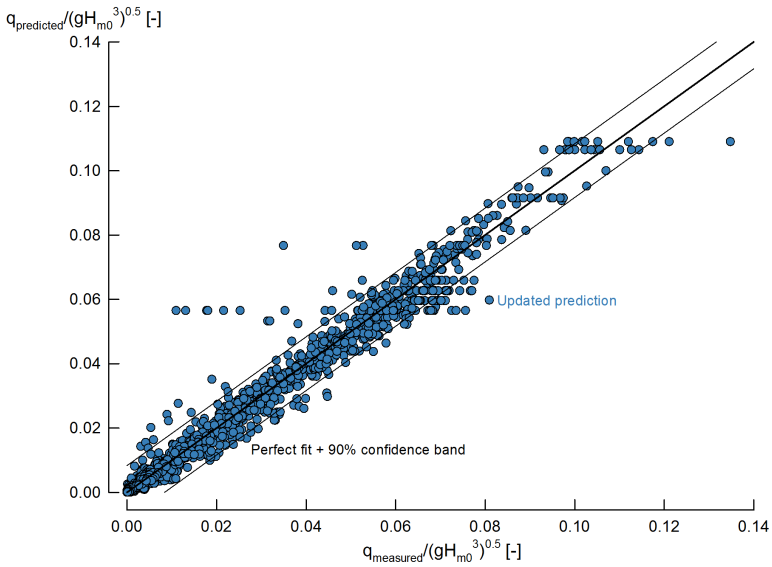
Eq. 2.5 shows a clear underestimation (in some cases outside the 90% confidence band) for the largest dimensionless overtopping rates which correspond to zero and very small relative freeboards, confirming the results discussed along this chapter. The overtopping rates for these conditions are better predicted by Eq. 5.1, with most of the values inside the 90% confidence band. For larger relative crest freeboards both Eq. 2.5 and Eq. 5.1 are predicting correctly the overtopping rates, even though there are some outliers in the data.

Eq. 5.1 is an update of the Eq. 2.5 prediction for non-breaking conditions, fitted through new overtopping data which was not available in literature. The result is an improvement of the prediction for the complete range of relative crest freeboards ($R_c/H_{m0} \geq 0$) and slope angles ($\cot \alpha \geq 0$). The prediction improvement is specially significant for zero freeboards ($R_c = 0$), very small ($0 < R_c/H_{m0} < 0.11$) and small ($0.11 < R_c/H_{m0} < 0.8$)

5.4 Update of the Overtopping Prediction for Steep Low-Crested Structures



(a)



(b)

Figure 5.18: Dimensionless average measured overtopping rate of the 1410 tests used to fit the updated prediction, compared with the dimensionless average predicted overtopping rate of (a) Van der Meer and Bruce (2014) (Eq. 2.5) and (b) the updated prediction (Eq. 5.1)

relative crest freeboards, and for very steep slopes ($0.27 \geq \cot \alpha > 0$). For vertical structures, the prediction of Eq. 5.1 is valid for tests with or without influencing foreshores, and for complex structures, simplifying the decision tree for vertical structures suggested in the EurOtop (2016) manual.

5.5 Average Wave Overtopping Results for Tests with Roughness Elements

The average overtopping results of the tests performed within the UG16 dataset with blocks, ribs, 5-steps revetments and 10-steps revetments are presented and discussed in this section.

5.5.1 Blocks and Ribs

Blocks and ribs were tested as artificial roughness elements to reduce the overtopping rates (see Section 4.2). The average overtopping rates of $\cot \alpha = 1$ ($\alpha = 45^\circ$) for blocks and ribs and $\cot \alpha = 0.58$ ($\alpha = 60^\circ$) for ribs are presented in Figure 5.19. The results are compared to smooth slopes overtopping data from datasets UG10, UG13, UG14 and UG15, choosing the best fit per slope angle of the a , b and c coefficients in Eq. 5.6 (Table 5.6). The roughness reduction factors γ_f are calculated for each case. The γ_f values are obtained by minimizing the RMSLE (Eq. 3.3) of the overtopping data for each case compared to the best fit for smooth slopes. As opposed to what is decided for smooth slopes (see Section 3.4), the calculation of γ_f is made using the RMSLE, as the differences between the overtopping prediction for smooth slopes and the average overtopping results with roughness elements are small. These differences would be even further reduced if they are linked to the absolute value of the dimensionless average overtopping rates as RMSE does.

$$\frac{q}{\sqrt{gH_{m0}^3}} = a_{\text{smooth}} \cdot \exp \left[- \left(b_{\text{smooth}} \frac{R_c}{H_{m0} \gamma_f \gamma_\beta} \right)^{c_{\text{smooth}}} \right] \quad (5.6)$$

Table 5.6: Best fit of the a_{smooth} , b_{smooth} and c_{smooth} coefficients in Eq. 5.6 for smooth slopes with $\cot \alpha = 1$ and $\cot \alpha = 0.58$.

$\cot \alpha$ (-)	a_{smooth} (-)	b_{smooth} (-)	c_{smooth} (-)
1	0.091	2.21	1.05
0.58	0.067	2.32	1.18

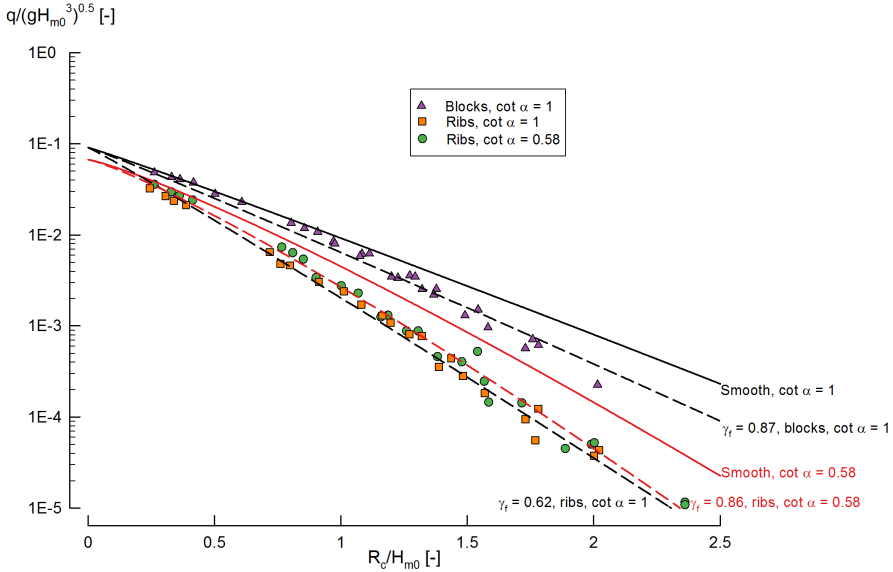


Figure 5.19: Blocks and ribs as artificial roughness elements for tests with $\cot \alpha = 1$ and $\cot \alpha = 0.58$ in the UG16 dataset, compared to the best fit for smooth slopes and the calculated γ_f according to Table 5.7.

The results of γ_f are shown in Table 5.7. The γ_f of blocks on the slope $\cot \alpha = 1$ ($\alpha = 45^\circ$) is $\gamma_f = 0.87$, which is very close to 1, meaning that the overtopping reduction caused by the blocks is very small and only present for $R_c/H_{m0} > 1$. As for a steeper slope angle it was expected that γ_f is even closer to 1, it was decided not to perform tests with blocks on the $\cot \alpha = 0.58$ ($\alpha = 60^\circ$) slope and install ribs on the model to increase the reduction on the overtopping rates due to roughness. According to EurOtop (2016) the reduction factor for a 1/9 coverage should be $\gamma_f = 0.8$ (see Section 2.3.6), which is not reached in the experiments. The blocks are designed for the optimum block height, although the distance between blocks is smaller than the optimal, which could explain the lower overtopping reduction.

Table 5.7: Results of the roughness reduction factor compared to the best fit for smooth slopes (Table 5.6) for blocks and ribs in the UG16 dataset.

$\cot \alpha$ (-)	Artificial roughness element	γ_f (-)
1	Blocks	0.87
	Ribs	0.62
0.58	Ribs	0.86

For ribs the overtopping reduction is larger than for blocks, as the covered slope area is larger. The slope $\cot \alpha = 1$ ($\alpha = 45^\circ$) has a lower γ_f compared to the steeper slope $\cot \alpha = 0.58$ ($\alpha = 60^\circ$) which is almost negligible and very similar to the overtopping reduction by blocks on $\cot \alpha = 1$. This could indicate that the overtopping reduction effect of ribs is decreasing for steeper slopes. However, more overtopping data for slope angles in between the two values tested in the UG16 dataset would be necessary to be confident about this conclusion.

The reduction factor suggested for ribs with optimum dimensions by the EurOtop (2016) manual is $\gamma_f = 0.75$, which is larger than the γ_f for $\cot \alpha = 1$ but smaller than the γ_f for $\cot \alpha = 0.58$. This indicates an effect of the slope angle on the effectiveness of ribs when reducing the overtopping (less reduction for steeper slopes). However, as seen in Section 4.2, the dimensions of the ribs are not optimum as the distance between ribs is $f_L/f_b = 2.04$ and not the recommended value of $f_L/f_b = 7$ (with a range between 5–8). Therefore, it is possible that the γ_f values could be lower if the distance between ribs were closer to the optimum as this would increase the macro roughness of the slope and the energy dissipation. As it was the case for blocks, more overtopping data for more steep slopes would be needed to be confident about these conclusions.

There is no influence of the surf similarity parameter $\xi_{m-1,0}$ on the overtopping reduction neither for blocks nor for ribs.

5.5.2 Stepped Revetments

The overtopping data for stepped revetments acquired within the UG16 dataset is analysed in this section. The results are analysed per relative step height H_{m0}/S_h and surf similarity parameter $\xi_{m-1,0}$, following Kerpen (2017). d_{st} is defined as the position of the SWL relative to the nearest lower step edge (Figure 5.20). This definition is different from Kerpen (2017) for convenience when analysing the results. The ratio d_{st}/S_h can be defined by values between 0 (SWL at the lower step edge) and 1 (SWL at the higher step edge). When referring to the steps, the 1st step is the closest step to the crest of the structure.

Figure 5.21 and Figure 5.22 show the dimensionless average overtopping compared to the best fit of the smooth tests in the UG10, UG13, UG14 and UG15 datasets (Table 5.6) for the $\cot \alpha = n = 1$ ($\alpha = 45^\circ$) slope and $\cot \alpha = n = 0.58$ ($\alpha = 60^\circ$), respectively. In these figures, the data is divided in various ranges of the relative step height H_{m0}/S_h following the conclusions reached by Kerpen (2017) about the reduction in overtopping depending on H_{m0}/S_h (see Section 2.3.6).

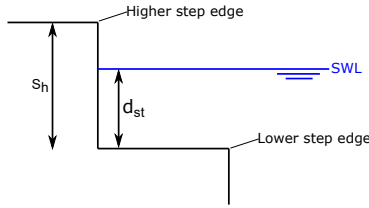


Figure 5.20: Definition sketch of d_{st} .

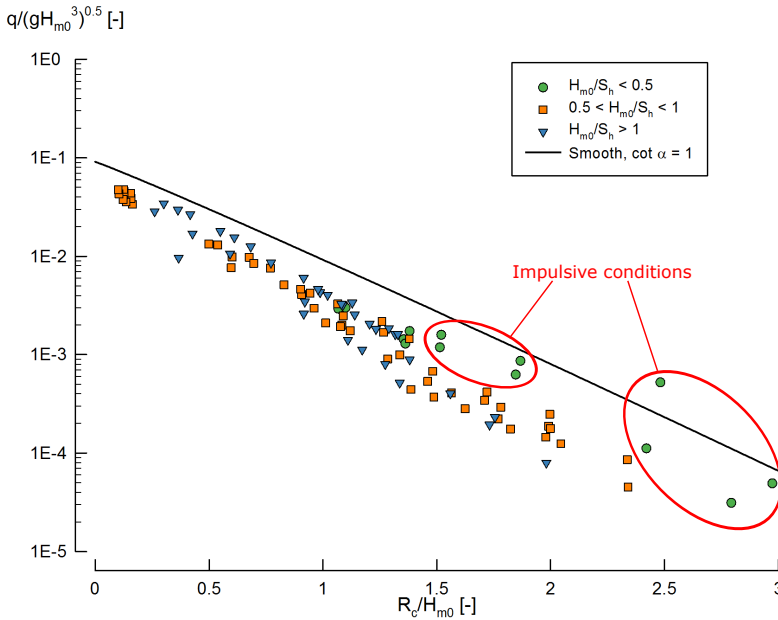


Figure 5.21: Stepped revetment overtopping data with $\cot \alpha = 1$ ($\alpha = 45^\circ$) divided per H_{m0}/S_h compared to the best fit for smooth slope.

For $\cot \alpha = n = 1$ (Figure 5.21), there is a reduction in overtopping for the complete range of relative crest freeboards R_c/H_{m0} . There are eight outliers that deviate from the data trend, marked with red circles in Figure 5.21. These outliers are identified as tests with impulsive wave conditions, i.e., with an impulsiveness parameter $h_* < 0.3$ (Eq. 2.9). The impulsive conditions are occurring for incident wave heights smaller than half of the step height ($H_{m0}/S_h < 0.5$), and for tests with d_{st} on the 1st step or with $d_{st}/S_h \approx 1$ on the 2nd step. This behaviour is not present for $\cot \alpha = n = 0.58$ (Figure 5.22). The geometry is causing the waves to break on the 1st step of the structure causing impulsive conditions that increase the overtopping for equal R_c/H_{m0} . A larger incident wave height (leading to $H_{m0}/S_h > 0.5$) causes that the waves behave as surging waves therefore not breaking.

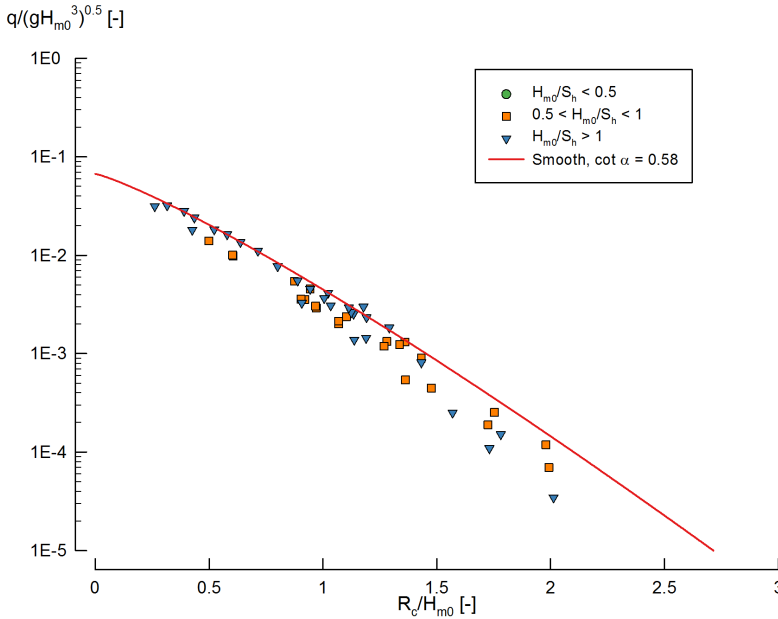


Figure 5.22: Stepped revetment overtopping data with $\cot \alpha = 0.58$ ($\alpha = 60^\circ$) divided per H_{m0}/S_h compared to the best fit for smooth slope.

According to Kerpen (2017), the overtopping reduction on stepped revetments is dependent on the surf similarity parameter $\xi_{m-1,0}$, which is not visible in these figures. The effect of $\xi_{m-1,0}$ on the roughness influence factor γ_f is analysed in Figure 5.23. Table 5.8 shows the expressions of γ_f that describe the overtopping data with respect to $\xi_{m-1,0}$. These expressions are valid for values of the surf similarity parameter $\xi_{m-1,0} < 8$.

For $\cot \alpha = n = 1$ the increase in $\xi_{m-1,0}$ leads to larger values (decreasing overtopping reduction) of the roughness reduction factor for $\cot \alpha = n = 1$, $\gamma_{f,1}$. There is no effect of the various ranges of H_{m0}/S_h considered. For $\cot \alpha = n = 0.58$ the overtopping reduction does not depend on $\xi_{m-1,0}$, being the average value for all the tests $\gamma_{f,0.58} = 0.91$ (where $\gamma_{f,0.58}$ is the roughness reduction factor for $\cot \alpha = n = 0.58$) which is around the maximum value observed for $\cot \alpha = n = 1$. Kerpen (2017) (Eq. 5.7) overestimates the value of the UG16 γ_f values:

$$\gamma_f = 0.1 \xi_{m-1,0} + 0.3 \quad (5.7)$$

Moreover, he did not find in the data a different behaviour depending on the slope angle. A possible explanation is that Kerpen (2017) tested milder values of slope angles (see Section 2.3.6) in a range where γ_f may not be

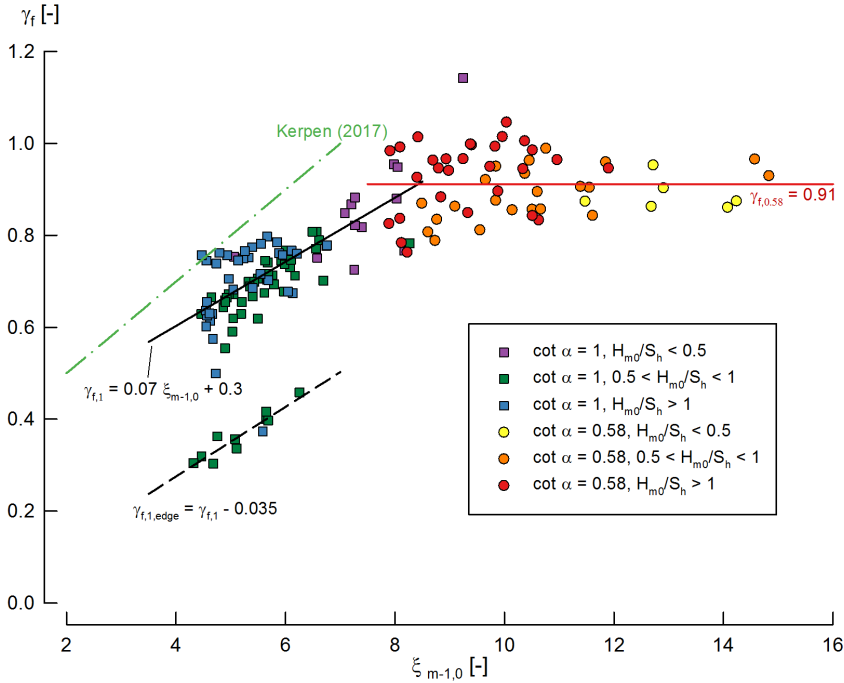


Figure 5.23: Roughness influence factor γ_f as a function of the surf similarity parameter $\xi_{m-1,0}$ for stepped revetments in the UG16 dataset, with the expressions describing the data in Table 5.8 compared to Kerpen (2017) (Eq. 5.7).

influenced by the small differences in step size that different slopes have in the range of mild slopes.

The effect of stepped revetments on the overtopping rates seems to be dependent on the slope angle, with the overtopping reduction tending to zero (values of γ_f tending to 1) for steeper slopes. More hydraulic model tests are needed for steep slopes in between $\cot \alpha = n = 1$ and $\cot \alpha = n = 0.58$, and beyond this value to be confident about this conclusion. More data will allow to fully understand the overtopping behaviour of stepped revetments for steep structures, and to know the range of slope angle α for which the influence of stepped revetments is negligible and behaves as a smooth slope.

Eleven tests with $\cot \alpha = n = 1$ and with relative step heights $0.5 < H_{m0}/S_h < 1$ (except one test) have a lower γ_f for the same $\xi_{m-1,0}$ than the rest of the data. This further decrease of γ_f is caused by the influence of the edge step. For all these tests, the SWL is on the 1st step and very close to the crest of the structure, with $R_c/H_{m0} \approx 0.1$ and $d_{st}/S_h \approx 0.9$. The best fit

trend for these tests (roughness reduction factor of $\cot \alpha = n = 1$ due to the effect of a step edge $\gamma_{f,1,edge}$ in Table 5.8) has the same slope as the general trend $\gamma_{f,1}$, being possible to describe $\gamma_{f,1,edge}$ by subtracting a constant value from $\gamma_{f,1}$.

Table 5.8: Roughness influence factor from the best fit for smooth slopes (Table 5.6) for stepped revetments in the UG16 dataset.

$\cot \alpha$ (-)	Type	γ_f (-)
1	General	$\gamma_{f,1} = 0.07 \xi_{m-1,0} + 0.3$
	Step edge	$\gamma_{f,1,edge} = \gamma_{f,1} - 0.035$
0.58	General	$\gamma_{f,0.58} = 0.91$

As the crest of the structure is acting as the higher step edge of the 1st step, it is possible that the waves are interacting with this step edge. The incident wave interacts with the reflected wave from the 1st step, creating high turbulence increasing energy dissipation and reducing γ_f . This effect of the step edge on the overtopping reduction was also described by Kerpen (2017) (see Section 2.3.6). However, Kerpen (2017) found this effect to be consistent for all the step edges, whereas in the UG16 dataset this effect is only occurring on the 1st step, and not for other steps. More model tests are needed to fully describe this effect.

The influence of the parameter defined by Kerpen (2017) as the characteristic step diameter (k_h) has also been studied for the UG16 dataset. However, unlike Kerpen (2017), no effect was found on describing the overtopping reduction.

5.6 Summary

The average overtopping data for steep low-crested structures obtained in the datasets UG13, UG14, UG15 and UG16 datasets have been analysed and compared with the existing prediction formulae. The formulae show an underprediction of the average overtopping rates for very small and zero relative freeboards, and for very steep slopes with large freeboards.

The effect of relatively shallow water conditions has been evaluated by comparing the results of the UG10 and UG13 datasets for relatively deep water conditions to the results of the UG14 and UG15 datasets for relatively shallow water conditions and the transitional zone. An increase of the average overtopping rates for large relative freeboards on relatively shallow water conditions is found. However, this increase is within the prediction bands of

the prediction formulae and therefore, it is possible to account for this effect in the uncertainty of the prediction.

An update of the prediction formula for steep low-crested structures has been fitted through the new datasets obtained in this research and existing overtopping data. The updated prediction improves the accuracy of the prediction for very small and zero relative freeboards, while maintaining the accuracy for the other ranges.

The overtopping reduction caused by artificial roughness elements on the structure slope decreases for steeper slopes. In the case of stepped revetments, the overtopping reduction depends on the surf similarity parameter $\xi_{m-1,0}$ although the effect is reduced for steeper slopes. An extra overtopping reduction is achieved when the SWL is close to the step edge on the highest step of the revetment.

Chapter 6

Data Analysis of Individual Overtopping

The individual overtopping is characterized and analysed in this chapter for the new datasets UG13, UG14, UG15 and UG16. The scale factor A and the shape factor B determine the probability distribution of the individual overtopping volumes, and the probability of overtopping P_{ow} determines the number of waves that overtop a coastal structure. These coefficients are analysed with respect to various wave and structural parameters and compared with prediction formulae on the literature. New prediction formulae for B and P_{ow} are suggested based on the new datasets.

6.1 Probability Distribution of Individual Overtopping Volumes

As explained in Section 2.4.1, the probability distribution of the individual overtopping volumes follows a two-parameter Weibull distribution (Eq. 2.22) with a scale factor A and a shape factor B .

For each test of the Ghent University datasets, the best fit of a Weibull distribution is found through the upper 10% of individual volumes V_i to better represent the largest volumes, although reducing the accuracy of the fitting for the lowest volumes. This value was also selected by Hughes et al. (2012), while Victor et al. (2012) fitted the Weibull distribution through the volumes higher than the average individual volume of each test. As a result, A and B values are obtained for each test. The difference in the percentage of individual volumes used to fit the Weibull distribution may lead to a larger

scatter of the factors for similar conditions, as the variation of the factors is larger when the distribution is fitted through the most extreme volumes.

Figure 6.1 shows the exceedance probability P_v of the individual overtopping volumes V_i corresponding to the tests number 260 of the UG13 dataset, which features a vertical structure ($\cot \alpha = 0$, $\alpha = 90^\circ$) with $H_{m0} = 0.088$ m, $R_c = 0.045$ m, $R_c/H_{m0} = 0.51$ and $T_{m-1,0} = 1.201$ s. The resulting best fit of the Weibull parameters is $A = 0.0018$ m³/m and $B = 0.87$. In this figure, the x-axis follows a Rayleigh scale, on which the Rayleigh distribution—a special case of the Weibull distribution with $B = 2$ —is linear. For this test, the best fit of B is smaller than the Rayleigh distribution, meaning that the average overtopping rate is determined by a few larger volumes, while for larger values of B —including the Rayleigh distribution ($B = 2$)—the average overtopping rate is determined by more similar volumes. The value of A is determining the value of the individual volumes in the Weibull distribution. A different test with the same B but a larger A would have the same probability distribution shape with the magnitude of the individual volumes scaled up.

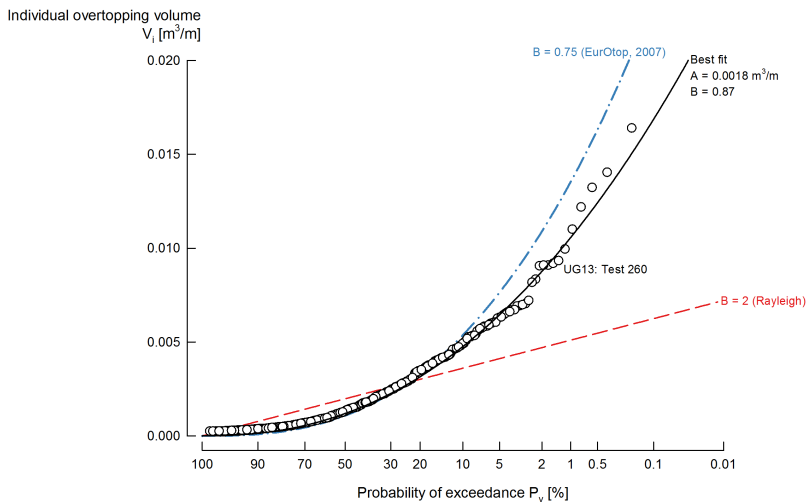


Figure 6.1: Probability of exceedance (P_v) of the individual volumes (V_i) for the test 260 of the UG13 dataset, compared to its best two-parameter Weibull distribution fit, the Rayleigh distribution and the EurOtop (2007) suggested $b = 0.75$ value.

By generating a Weibull plot it is possible to graphically check whether the Weibull distribution describes the theoretical exceedance probability P_v of the individual volumes V_i . Rewriting Eq. 2.22, the expression of the individual volumes V_i shown in Eq. 6.1 is obtained, and then the expression is

transformed into Eq. 6.2 by taking the logarithm of both sides:

$$V_i = A(-\ln P_v)^{\frac{1}{B}} \quad (6.1)$$

$$\log V_i = \log A + \frac{1}{B} \log(-\ln P_v) \quad (6.2)$$

The theoretical exceedance probability (P_v) is approximated by the empirical exceedance probability (\hat{P}_v), which is defined by Eq. 6.3. An exceedance probability is calculated for every i -th volume of a total of N . The equivalent expression to Eq. 6.2 for empirical values is Eq. 6.4, where $\lambda = \log A$ is the intercept and $\psi = 1/B$ is the slope of a linear equation describing the relation between $\log(-\ln \hat{P}_v)$ and $\log V_i$. The A and B coefficients are obtained by a linear regression following the linearization of the coefficients in Eq. 6.4:

$$\hat{P}_v = \frac{i}{N + 1} \quad (6.3)$$

$$\log V_i = \lambda + \psi \log(-\ln \hat{P}_v) \quad (6.4)$$

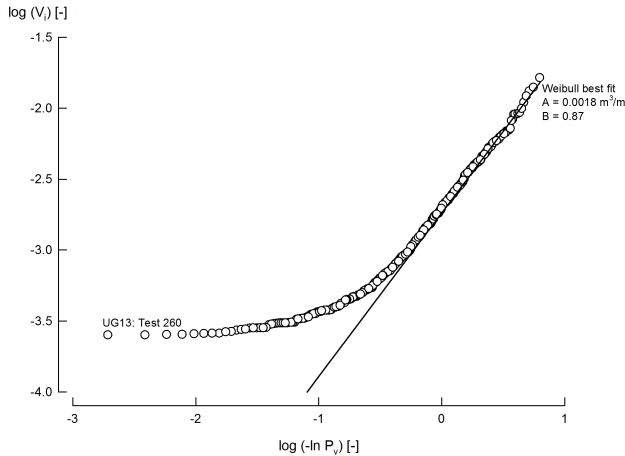


Figure 6.2: Weibull plot of the test number 260 of the UG13 dataset compared to the best fit of a two-parameter Weibull distribution with $A = 0.0018 \text{ m}^3/\text{m}$ and $B = 0.87$.

A Weibull plot is a plot of the empirical volumes (Eq. 6.4) with $\log(-\ln P_v)$ as the x-axis and $\log V_i$ as the y-axis. Figure 6.2 shows the Weibull plot of the test number 260 of the UG13 dataset shown in Figure 6.1. The data

that follow a linear trend on a Weibull plot is described by a two-parameter Weibull distribution, as it is the case of the individual volumes V_i in Figure 6.2.

The long left tail of the data with respect to the best fit of the Weibull distribution is a direct consequence of fitting the distribution through the largest 10% of the volumes. The smaller volumes are not correctly represented by the Weibull distribution, forming the left tail. As seen in Figure 6.1, this misrepresentation of the smallest volumes by the Weibull distribution is negligible as these volumes (with the highest exceedance probabilities) are close to $0 \text{ m}^3/\text{m}$.

6.2 Shape Factor B

The shape factor B is one of the two-parameter Weibull probability distribution that the individual overtopping volumes follow. It determines whether the average overtopping is formed by a small number of large individual volumes (small values of B) or by more similar individual volumes (large values of B) as seen in Section 2.4. In this section, the results of the shape factor B from the datasets UG13, UG14 and UG15 are analysed and compared to the prediction formulae by Victor et al. (2012) (Eq. 2.30), Hughes et al. (2012) (Eq. 2.31) and Zanuttigh et al. (2013) (Eq. 2.32). A new prediction formula based on the Ghent University overtopping datasets is suggested.

6.2.1 Results

The shape factor B of the individual overtopping volumes Weibull probability distribution is analysed for the UG13, UG14 and UG15 datasets. For the analysis of the B values, tests with a number of overtopping waves $N_{ow} \leq 30$ have been excluded from the analysis as fit a two-parameter Weibull distribution through a smaller number of overtopping waves is not statistically significant. This criteria was also followed by Victor et al. (2012). Three tests of the UG14 dataset with a number of overtopping waves $30 < N_{ow} < 80$ are excluded as the calculated best fit B values are outliers ($B > 3$) from the general trend.

Figure 6.3 shows the shape factor B of the UG13, UG14 and UG15 datasets divided per slope angle range according to Table 1.1. The shape factor values have an average on $B = 1.5$ for very small relative crest freeboards, decreasing for larger relative freeboards until reaching an asymptotic value for $R_c/H_{m0} > 1.5$. This influence of the relative crest freeboard R_c/H_{m0} was also observed by Victor et al. (2012) and Hughes et al. (2012). However, other authors such as Van der Meer and Janssen (1994), Franco et al. (1994)

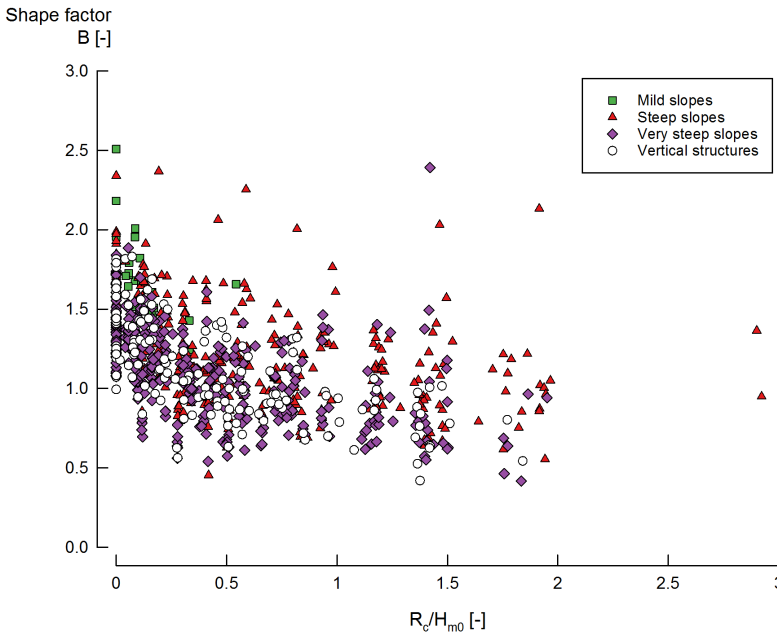


Figure 6.3: Shape factor B as a function of the relative crest freeboard R_c/H_{m0} for mild, steep, very steep slopes and vertical structures of the datasets UG13, UG14 and UG15.

and Besley (1999) did not report an influence of R_c/H_{m0} on B , although their research was based on overtopping data with large relative freeboards which do not influence the B values.

The shape factor B is also influenced by the slope angle α . Figure 6.4 and Figure 6.5 show the shape factor B versus $\cot \alpha$ for zero freeboard ($R_c = 0$) and very small ($0.11 > R_c/H_{m0} > 0$) relative freeboards; and small ($0.8 > R_c/H_{m0} > 0.11$) and large ($R_c/H_{m0} > 0.8$) relative freeboards, respectively.

The B values decrease for smaller $\cot \alpha$ (steeper slopes) for equal R_c/H_{m0} , which is the same behaviour reported by Victor et al. (2012). This influence, however, is negligible for very steep slopes and vertical walls, as B does not decrease further for $\cot \alpha < 0.5$. This behaviour is present for all the ranges of R_c/H_{m0} considered, although for small and large relative freeboards this behaviour seems to be less significant. Hughes et al. (2012) and Zanuttigh et al. (2013) did not include the effect of α in the B prediction formulae.

For steeper slopes the reflection of the waves on the structure increase, reducing the energy available for the run-up and overtopping process. Therefore, only the largest waves overtop the structure and, as a consequence, the shape factor B decreases.

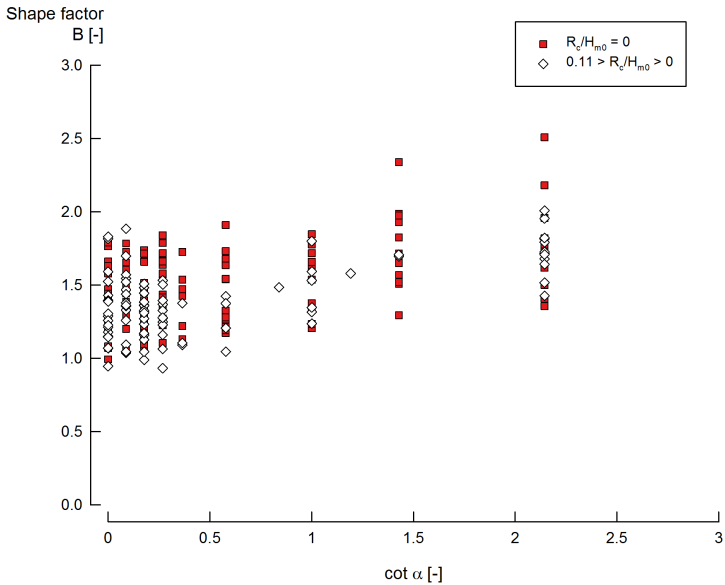


Figure 6.4: Shape factor B as a function of the relative crest freeboard R_c/H_{m0} for the datasets UG10, UG13, UG14 and UG15 for zero ($R_c = 0$) and very small ($0 < R_c/H_{m0} < 0.11$) relative freeboards.

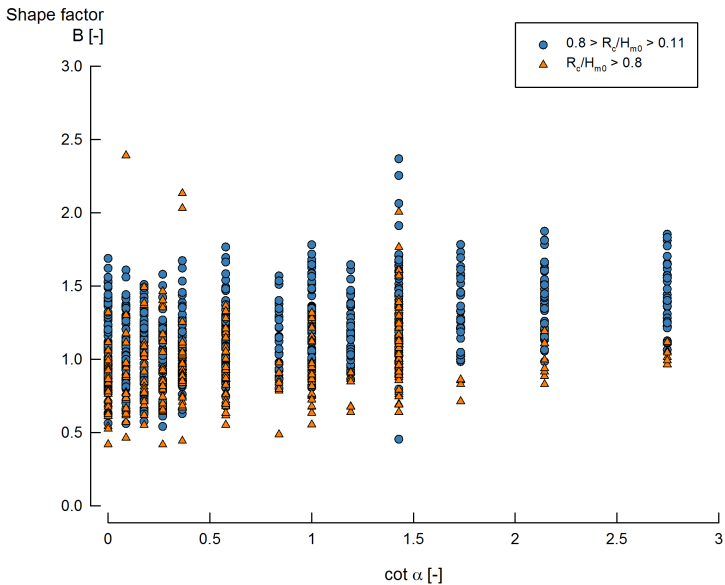


Figure 6.5: Shape factor B as a function of the relative crest freeboard R_c/H_{m0} for the datasets UG10, UG13, UG14 and UG15 for small ($0.11 < R_c/H_{m0} < 0.8$) and large ($R_c/H_{m0} > 0.8$) relative freeboards.

Effect of Relatively Shallow Water Conditions on B

The UG14 and UG15 overtopping datasets allow a study of the effect of relatively shallow water conditions on the shape factor B . Figure 6.6 shows the shape factor B as a function of the relative wave height H_{m0}/h for zero ($R_c = 0$), very small ($0.11 > R_c/H_{m0} > 0$), small ($0.8 > R_c/H_{m0} > 0.11$) and large ($R_c/H_{m0} > 0.8$) relative crest freeboards.

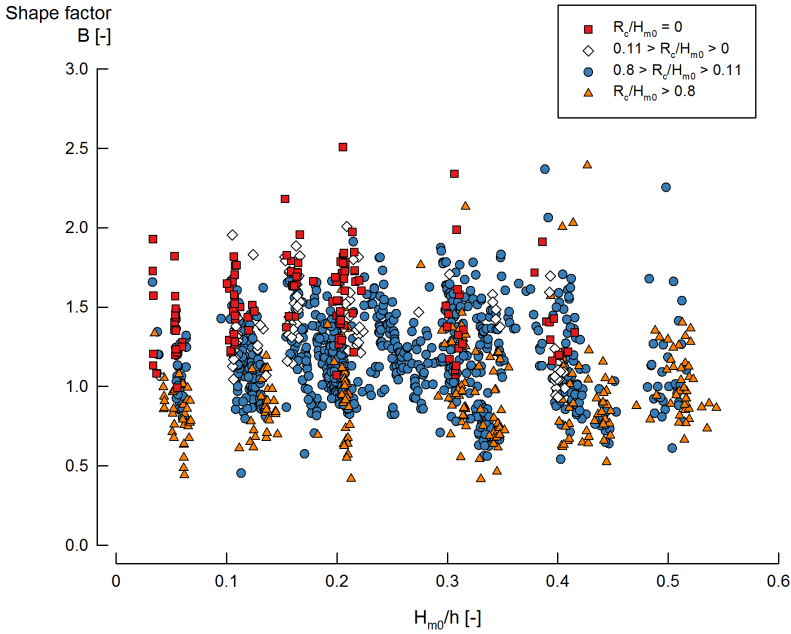


Figure 6.6: Shape factor B as a function of the relative wave height H_{m0}/h for the datasets UG10, UG13, UG14 and UG15, divided per range of relative crest freeboard R_c/H_{m0} according to Table 1.2.

The scatter of the B values can be explained by the relative crest freeboard R_c/H_{m0} . However, no effect of H_{m0}/h is seen in the shape factor B . For the same range of R_c/H_{m0} , the B values remain approximately constant for increasing H_{m0}/h .

The relatively shallow water wave conditions can also be studied if instead of the relative wave height H_{m0}/h , the distribution of the incident wave heights is considered. According to Battjes and Groenendijk (2000), the incident significant wave height at the toe of the structure on deep water conditions H_s are distributed following a Rayleigh distribution, while on shallow water conditions the H_s are not distributed following a Rayleigh distribution. Following this criteria to classify the tests of the UG10, UG13, UG14 and UG15 datasets, the B values are analysed.

There is no difference between the Rayleigh and non-Rayleigh distributed H_s on the shape factor B . This result is in contrast with Victor et al. (2012), who found larger values of B for non-Rayleigh distributed tests on the same range of relative crest freeboards.

Both results of the analysis of the shape factor B compared to the relative wave height H_{m0}/h and the distribution of the incident wave heights indicate that there is no influence of relatively shallow water conditions on the shape factor B values.

6.2.2 Comparison with Prediction Formulae

The shape factor B of the UG13, UG14 and UG15 datasets are compared to the predictions by Victor et al. (2012) (Eq. 2.30) and Hughes et al. (2012) (Eq. 2.31). Table 6.1 shows the RMSE (Eq. 3.1) and bias (Eq. 3.2) values of these two predictions for the mentioned datasets. The data are divided in the slope angle ranges shown in Table 1.1 and the relative crest freeboard ranges shown in Table 1.2.

The shape factor B prediction formula by Victor et al. (2012) (Eq. 2.30) is taken as the reference case. This prediction is the only one that includes the effect of the slope angle α in the prediction, which according to the analysis of the results in Section 6.2.1 is also observed in the datasets acquired in this research.

Table 6.1: RMSE values (Eq. 3.1) and bias (Eq. 3.2) of the UG13, UG14 and UG15 datasets dataset for the shape factor B , in different ranges of relative crest freeboard R_c/H_{m0} and slope angle α .

Equation	Eq. 2.30		Eq. 2.31	
	RMSE (-)	Bias (-)	RMSE (-)	Bias (-)
All tests	0.51	-0.06	0.52	0.08
Zero freeboard ($R_c = 0$)	0.27	0.14	0.29	0.13
$0 < R_c/H_{m0} < 0.05$	0.20	0.05	0.24	0.10
$0.05 < R_c/H_{m0} < 0.08$	0.20	0.07	0.26	0.13
$0.08 < R_c/H_{m0} < 0.11$	0.25	0.14	0.33	0.22
$0.11 < R_c/H_{m0} < 0.8$	0.26	-0.01	0.33	0.19
$R_c/H_{m0} > 0.8$	0.92	-0.36	0.88	-0.19
Mild slopes	0.24	0.05	0.26	-0.13
Steep slopes	0.73	-0.15	0.71	-0.05
Very steep slopes	0.28	0.004	0.33	0.19
Vertical structures	0.39	-0.05	0.41	0.17

The RMSE results show a very similar accuracy of Eq. 2.30 and Eq. 2.31 for all the tests, and for all the relative crest freeboards and slope angle ranges considered. Although the bias value indicates a certain underprediction of B in the case of Eq. 2.30 and an overprediction in the case of Eq. 2.31, there is no clear trend when dividing the data in the various ranges. For large relative crest freeboards ($R_c/H_{m0} > 0.8$), both predictions have larger RMSE values than for other ranges of R_c/H_{m0} , and according to the bias values in both cases it consists of an underprediction of B .

Figure 6.7 show the shape factor B for mild and steep slopes, compared to the predictions by Victor et al. (2012) (for $\cot \alpha = 1$), Hughes et al. (2012) and the value of $B = 0.75$ suggested by EurOtop (2007). Both Victor et al. (2012) and Hughes et al. (2012) predict correctly the B values for small relative freeboards. The value $B = 0.75$ is underpredicting B for small relative freeboards. For larger relative freeboards, the data tend towards a value higher than $B = 0.75$, which is not correctly predicted neither by Hughes et al. (2012) nor by Victor et al. (2012) as both predictions yield values slightly smaller than $B = 0.75$.

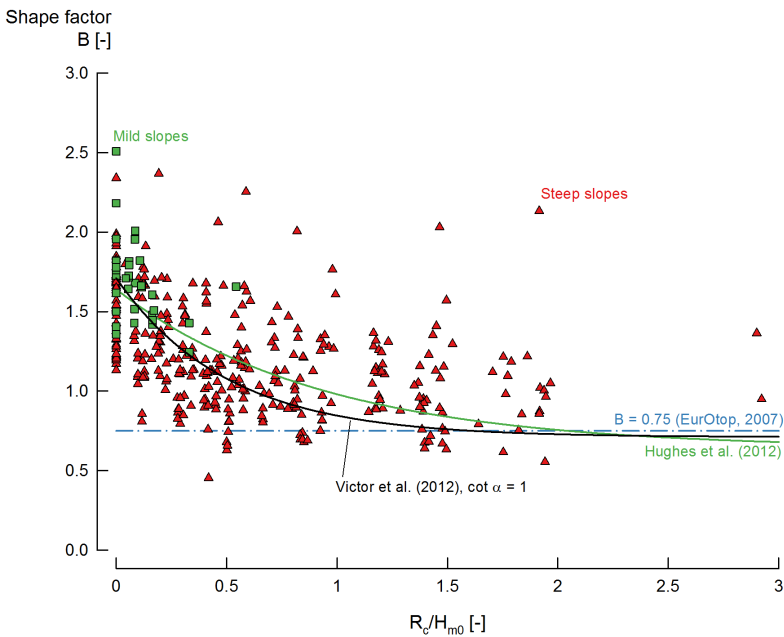


Figure 6.7: Shape factor B as a function of the relative crest freeboard R_c/H_{m0} for mild and steep slopes of the datasets UG13, UG14 and UG15, compared to Victor et al. (2012) (Eq. 2.30), Hughes et al. (2012) (Eq. 2.31) and $B = 0.75$ (EurOtop, 2007).

The B values for very steep slopes and vertical structures are shown in

Figure 6.8 and Figure 6.9, respectively. The values are compared also to Victor et al. (2012) (for $\cot \alpha = 0.18$), Hughes et al. (2012) and $B = 0.75$ (EurOtop, 2007). For very steep slopes and vertical structures, Victor et al. (2012) is predicting correctly the B values, although underpredicting the values for relative crest freeboards $R_c/H_{m0} > 1$. Hughes et al. (2012) is consistently overpredicting the values for the complete range of R_c/H_{m0} , most probably because the prediction does not include the effect of the slope angle α . The value $B = 0.75$ is smaller than the average B for large relative crest freeboards. The predictions by Franco et al. (1994) ($B = 0.75$), Franco and Franco (1999) ($B = 0.66 - 0.86$) and Besley (1999) for non-impulsive conditions ($B = 0.66$ for a wave steepness $s_{op} = 0.02$ and $B = 0.82$ for a wave steepness $s_{op} = 0.04$) are similar to the B values of the analysed datasets although only for large relative freeboards.

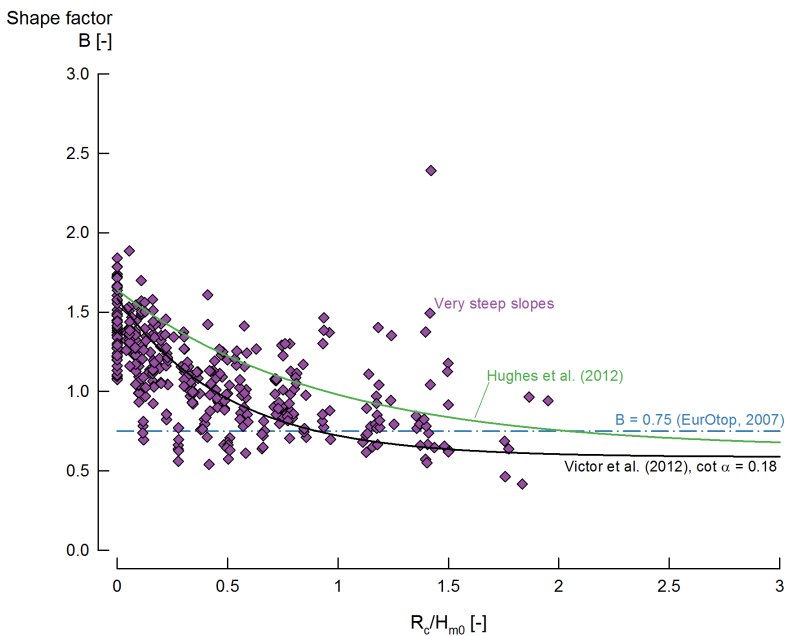


Figure 6.8: Shape factor B as a function of the relative crest freeboard R_c/H_{m0} for very steep slopes of the datasets UG13, UG14 and UG15, compared to Victor et al. (2012) (Eq. 2.30), Hughes et al. (2012) (Eq. 2.31) and $B = 0.75$ (EurOtop, 2007).

Both Victor et al. (2012) and Hughes et al. (2012) predictions were fitted through the same overtopping dataset (UG10), although Hughes et al. (2012) included extra tests with negative freeboards and large freeboards. However, the behaviour of the predictions is different, due to the decision made by the authors of including (Victor et al., 2012) or not (Hughes et al., 2012) the effect

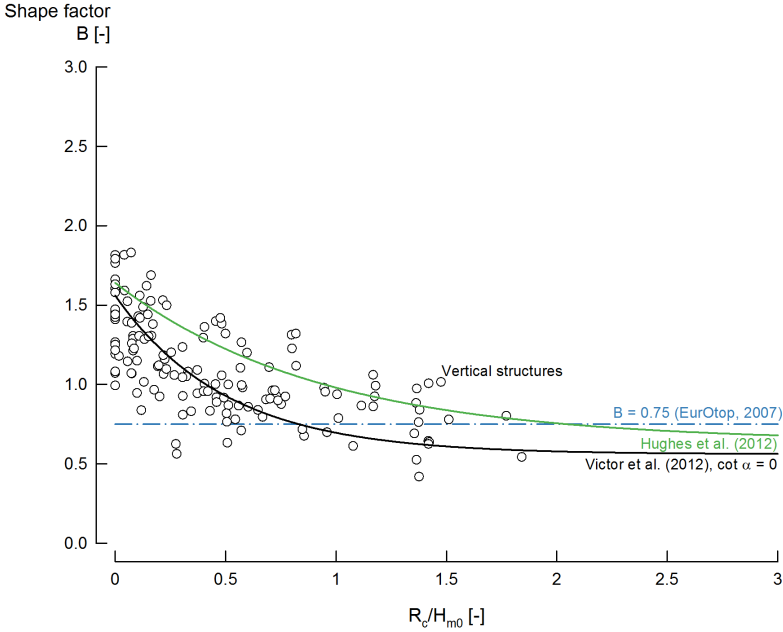


Figure 6.9: Shape factor B as a function of the relative crest freeboard R_c/H_{m0} for vertical structures of the datasets UG13, UG14 and UG15, compared to Victor et al. (2012) (Eq. 2.30), Hughes et al. (2012) (Eq. 2.31) and $B = 0.75$ (EurOtop, 2007).

of the slope angle α on the shape factor B . Victor et al. (2012) adapts better to the B values of the UG13, UG14 and UG15 datasets, proving that α has indeed an effect on B , even considering the large scatter of the values.

Comparing Figures 6.7, 6.8 and 6.9, it is seen that for the zero freeboard case ($R_c = 0$), the B values decrease for decreasing $\cot \alpha$ (steeper slopes), as well as the B values for very small relative freeboards ($0 < R_c/H_{m0} < 0.11$). However, for relative freeboards $R_c/H_{m0} > 1.5$, the B values are not influenced by the slope angle α as for all the slope angle ranges considered the shape factor is between $0.6 < B < 1.4$. This justifies the large value of RMSE for large relative crest freeboards calculated for both predictions shown in Table 6.1, which already indicated an underprediction of B on this range of relative freeboards.

Zanuttigh et al. (2013) took a different approach by suggestion a prediction with the shape factor B being dependent on the average overtopping rate q . To represent the average overtopping q , the authors selected the dimensionless parameter $q/gH_{m0}T_{m-1,0}$, instead of the more common $q/\sqrt{gH_{m0}^3}$ as the data showed a smaller scatter in the former than in the latter. By using the dimensionless overtopping rate, the effect on B of other parameters such

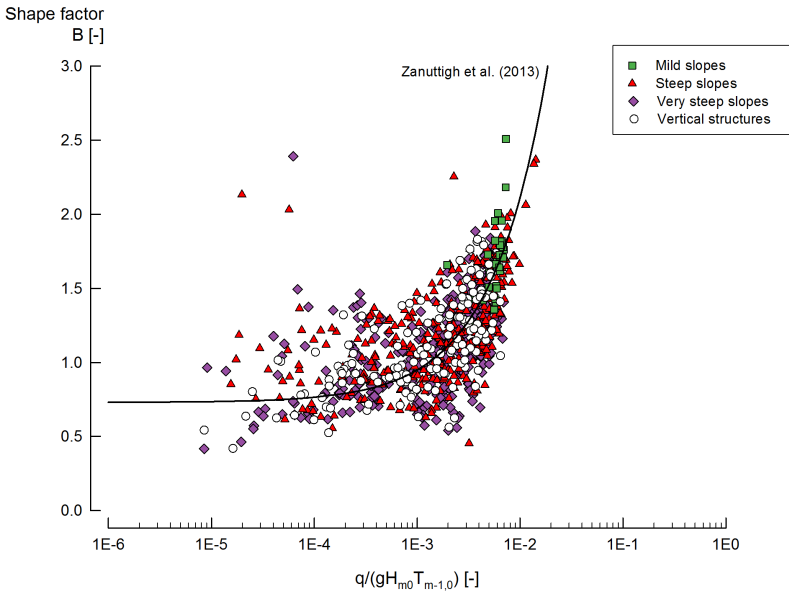


Figure 6.10: Shape factor B as a function of the dimensionless average overtopping rate $q/gH_{m0}T_{m-1,0}$ for mild, steep, very steep slopes and vertical structures of the datasets UG13, UG14 and UG15, compared to Zanuttigh et al. (2013) (Eq. 2.32).

as the relative crest freeboard, wave steepness or slope angle is implicitly included.

Figure 6.10 shows the shape factor B versus the mentioned dimensionless average overtopping rate $q/gH_{m0}T_{m-1,0}$ of the datasets UG13, UG14 and UG15, compared to the prediction by Zanuttigh et al. (2013) (Eq. 2.32). The shape factor B is constant for low values of the dimensionless average overtopping, and increasing for increasing dimensionless overtopping until reaching a value around $q/gH_{m0}T_{m-1,0} = 1 \times 10^{-2}$. This value corresponds to tests with zero freeboard which give larger values of B as seen in Figure 6.3. Larger values of $q/gH_{m0}T_{m-1,0}$ correspond to tests with negative freeboards. For $q/gH_{m0}T_{m-1,0} < 1 \times 10^{-3}$, the data present a large scatter which results on Eq. 2.32 underpredicting B for that range. For $q/gH_{m0}T_{m-1,0} > 1 \times 10^{-3}$, Eq. 2.32 follows the shape of the data with a good prediction of the higher B values.

Zanuttigh et al. (2013) gives an accurate prediction of the shape factor B . However, the use of $q/gH_{m0}T_{m-1,0}$ as a parameter hides the physical insights of the influence of other parameters such as the relative crest freeboard R_c/H_{m0} and the slope angle α on B , even hiding the influence of the latter when plotting the data in a log-linear plot.

6.2.3 New Prediction Formula

As seen in Section 6.2.2, the existing prediction formulae of the shape factor B based on the relative crest freeboard R_c/H_{m0} as main parameter have a lack of accuracy for certain conditions.

On the one hand, the Hughes et al. (2012) prediction does not fully adapt to the shape of the data as it does not consider the slope angle α as an influence parameter of the B values. This results in an overprediction of the data for very steep slopes and vertical structures. On the other hand, Victor et al. (2012) prediction considers α as an influencing parameter of B . However, the predicted B values for zero freeboards and large relative freeboards are not predicted with accuracy, with B being underpredicting in both cases. Moreover, for large relative freeboards the formula assumes that B is influenced by the slope angle α , although the data show that B for this range of relative freeboards is constant and not dependent on α .

The datasets UG13, UG14 and UG15 fill the gap for zero and very small relative freeboards, and very steep and vertical structures that the UG10 dataset had. As both Hughes et al. (2012) and Victor et al. (2012) predictions were fitted though UG10, it is possible to improve the accuracy of both predictions for the range of relative freeboards and slope angles where UG10 lacks of overtopping data.

Shape of the Prediction

To improve the accuracy of the existing predictions it is necessary to address the inaccuracies aforementioned. The expression presented in Eq. 6.5 is suggested to be used in the new prediction formula:

$$B = w \exp\left(-x \frac{R_c}{H_{m0}}\right) + y \quad (6.5)$$

The selected shape is similar to Victor et al. (2012) and Hughes et al. (2012), and not to Zanuttigh et al. (2013) because the former predictions give a stronger physical insight than the latter. Eq. 6.5 has an exponential shape with three coefficients: w , x and y . The coefficient y is the B prediction for very large relative freeboards. Approximately, B reaches the value of y for relative freeboards $R_c/H_{m0} \geq 2$. Contrary to Eq. 2.30 and Eq. 2.31, y does not determine the value of the prediction for zero freeboards in Eq. 6.5.

The coefficient w is added compared to the predictions by Victor et al. (2012) (Eq. 2.30) and Hughes et al. (2012) (Eq. 2.31). w is the value of the intercept of the prediction with the y -axis, i.e., it determines the prediction

of B for the zero freeboard case. In the case of Eq. 2.30 and Eq. 2.31, the prediction for zero freeboards depends on the y coefficient of the formula and the value is always $1 + y$. With the addition of w to the formula it is possible to adapt the B prediction of zero freeboards to the differences per slope angle seen in the data (see Section 6.2.2).

The coefficient x affects the exponential expression of the prediction and changes its shape on a linear plot. The possibility of adding a power to the exponential expression is also analysed, following the Hughes et al. (2012) approach on Eq. 2.31. However, the influence of such a power is rather limited on the shape of the prediction and it does not improve the accuracy of the prediction.

Selection of the Overtopping Data

The set of tests selected to fit the new shape factor B prediction formula is formed by tests of the UG10, UG13, UG14 and UG15 datasets, covering from mild slopes to vertical structures with relative crest freeboards from large to zero. The tests also cover the range from relatively deep to relatively shallow water conditions (see Chapter 4 for a description of the datasets).

Only tests with a number of overtopping waves $N_{ow} > 30$ are included in the fit of the formula, to assure that the fit of a two-parameter Weibull distribution through the volumes is statistically significant. In total, 17 tests have been excluded because of this reason. Six more tests were excluded as the B values were outliers. No selection of tests based on the relative wave height H_{m0}/h is made, as the analysis of the results reported no relatively shallow water effects on B .

The total number of tests through which the new B prediction formula is fitted is 1223. This number compares to the 364 tests of the UG10 dataset used by Victor et al. (2012) and the 405 tests from UG10 and other sources used by Hughes et al. (2012) to fit the predictions, which is a factor three increase.

Fit of the Coefficients

Using a nonlinear regression analysis, the best fit of the w , x and y coefficients of Eq. 6.5 per slope angle is found by minimizing the residual sum of squares (Eq. 5.5) and using a sequential quadratic programming algorithm as iterative method. The expressions of w , x and y are seen in Eq. 6.6, Eq. 6.7 and Eq. 6.8:

$$w = 0.59 + 0.23 \cot \alpha \quad (6.6)$$

$$x = 2.2 \quad (6.7)$$

$$y = 0.83 \quad (6.8)$$

Combining the previous equations with Eq. 6.5, the new formula to predict the shape factor B is Eq. 6.9:

$$B = (0.59 + 0.23 \cot \alpha) \exp \left(-2.2 \frac{R_c}{H_{m0}} \right) + 0.83 \quad (6.9)$$

Figure 6.11 shows the best fit of the w coefficient per slope angle of the tests selected to fit the new prediction. The value of w increases for increasing $\cot \alpha$ (milder slopes), indicating that the B values for the zero freeboard case increase for milder slopes. This behaviour confirms the analysis performed of the UG13, UG14 and UG15 B data in Figures 6.7, 6.8 and 6.9. The linear best fit of the w values is presented in Eq. 6.6 and is also plotted in Figure 6.11.

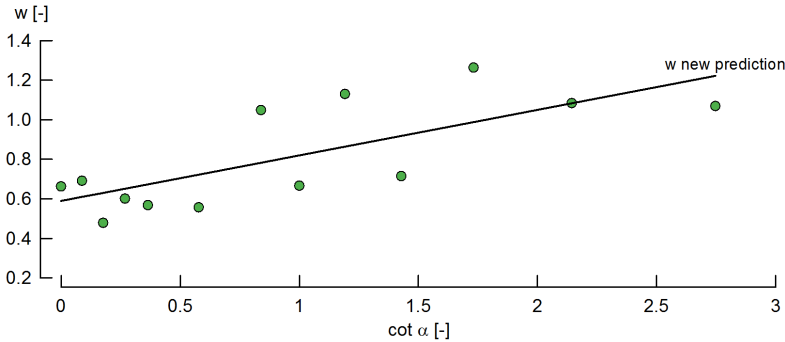


Figure 6.11: Best fit of the coefficient w per slope angle and expression of w for the new prediction (Eq. 6.6).

Figure 6.12 shows the best fit of the x coefficient per slope angle of the tests selected to fit the new prediction. The x values do not show a dependence on $\cot \alpha$, therefore, a constant value of $x = 2.2$ equal to the average value of x for all the slopes is suggested. Also constant values of the coefficient inside the exponential expression were also chosen by Victor et al. (2012) and Hughes et al. (2012) for their predictions.

Figure 6.13 shows the best fit of the y coefficient per slope angle of the tests selected to fit the new prediction. The y values do not show a dependence on $\cot \alpha$, therefore, a constant value of $y = 0.83$ equal to the average

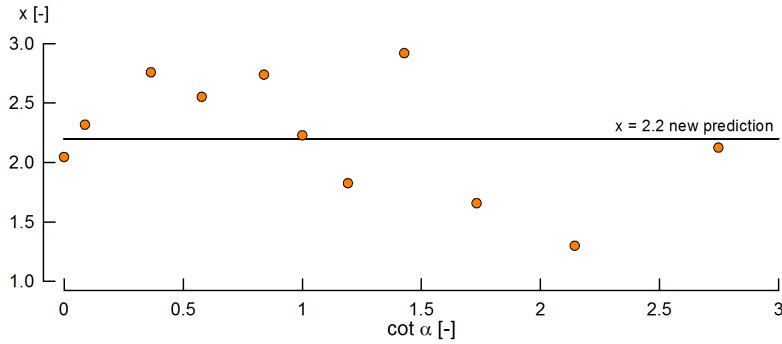


Figure 6.12: Best fit of the coefficient x per slope angle and expression of x for the new prediction (Eq. 6.7).

value of y for all the slopes is suggested. This value is similar to $B = 0.75$ suggested by the EurOtop (2007) manual, which confirms the analysis of the data shown in Figures 6.7, 6.8 and 6.9 stating that for large relative freeboards the B values were slightly higher than $B = 0.75$.

Victor et al. (2012) found that y was dependent on $\cot \alpha$. However, as Victor et al. (2012) did not include a coefficient w in the prediction, the true dependence of B on the slope angle occurs for zero and very small relative freeboards and not for large relative freeboards, as w and y for the new prediction indicates.

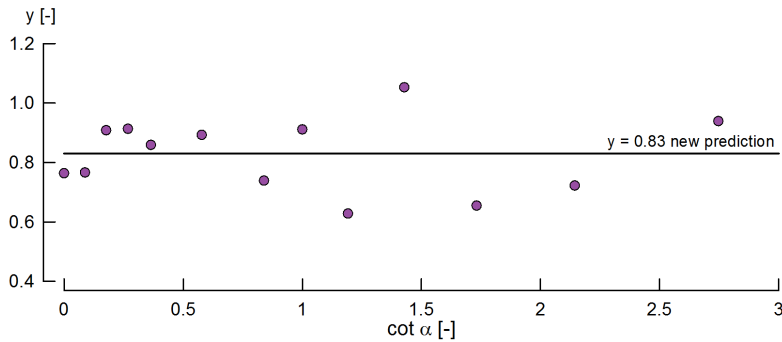


Figure 6.13: Best fit of the coefficient y per slope angle and expression of y for the new prediction (Eq. 6.8).

The RMSE (Eq. 3.1) of Eq. 6.9 is 0.217, and the bias (Eq. 3.2) is 0.010. The reliability of the prediction can be expressed with this value of RMSE. The 90% prediction interval is determined by $B \pm 1.64 \cdot \text{RMSE}$.

Figure 6.14 shows the measured B values of the fitting set compared to the predicted B values by the new prediction (Eq. 6.9), with the perfect fit line and the 90% confidence band based on the aforementioned RMSE value. The values are aligned with the perfect fit line with some scatter that is accounted by the reliability of the prediction.

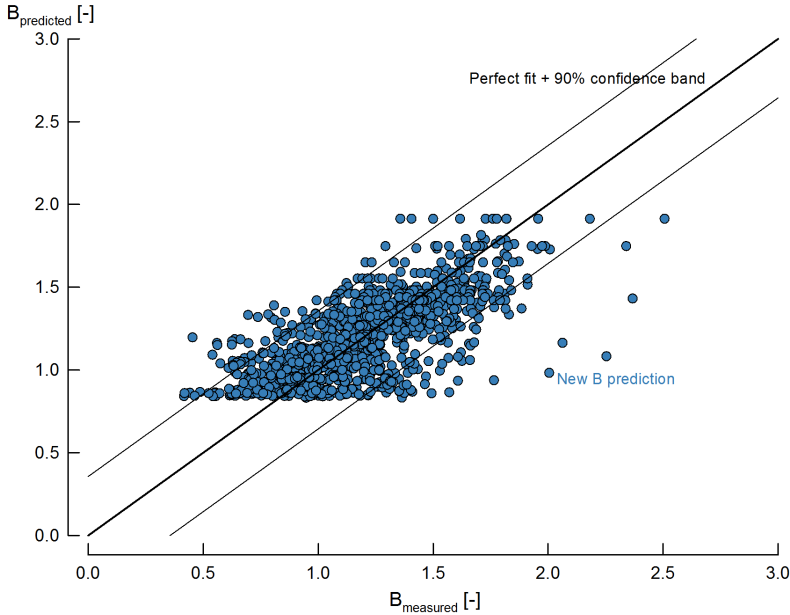


Figure 6.14: Shape factor B measured compared to the predicted B by Eq. 6.9, with the perfect fit line and the 90% confidence band.

Figure 6.15 and Figure 6.16 add to Figure 6.8 and Figure 6.9 respectively the new B prediction (Eq. 6.9), to allow a comparison with the Victor et al. (2012) prediction and the value $B = 0.75$ suggested by EurOtop (2007). As already mentioned, the B prediction for zero freeboards of the new formula is higher than the prediction by Victor et al. (2012) and depends on the slope angle as a result of the new coefficient w , which adapts better to the average of the values for this conditions.

Also for large relative freeboards the new prediction is higher, however it does not depend on the slope angle α , as the coefficient γ was found not to be dependent on the slope angle of the structure. The prediction for this range of relative freeboards is slightly higher than $B = 0.75$, indicating that the EurOtop (2007) is still valid for large relative freeboards and all slope angles.

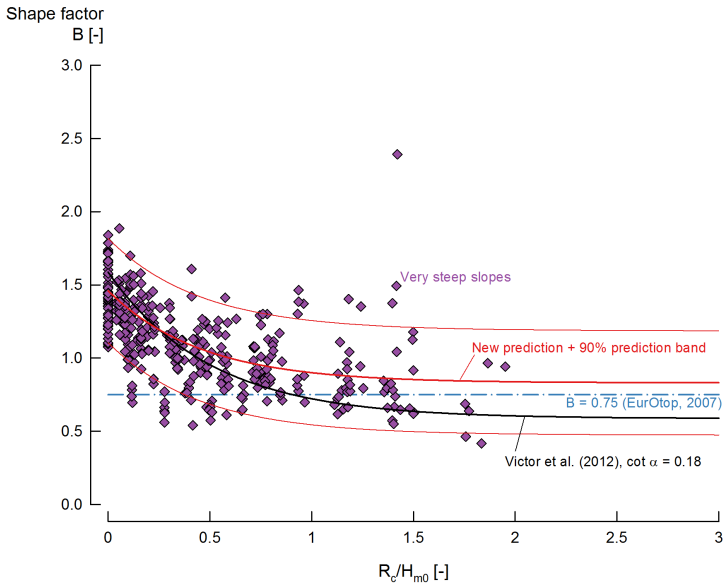


Figure 6.15: Shape factor B as a function of the relative crest freeboard R_c/H_{m0} for very steep slopes of the datasets UG13, UG14 and UG15, compared to Victor et al. (2012) (Eq. 2.30), $B = 0.75$ (EurOtop, 2007) and the new B prediction (Eq. 6.9) with its 90% prediction band.

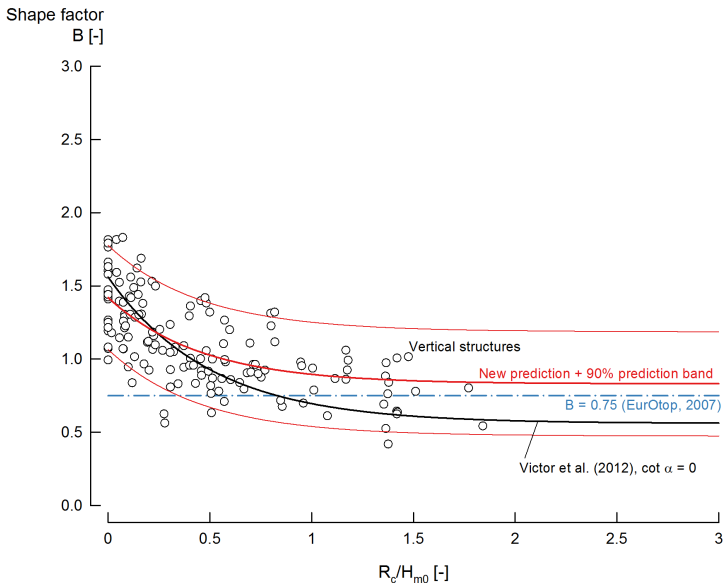


Figure 6.16: Shape factor B as a function of the relative crest freeboard R_c/H_{m0} for vertical structures of the datasets UG13, UG14 and UG15, compared to Victor et al. (2012) (Eq. 2.30), $B = 0.75$ (EurOtop, 2007) and the new B prediction (Eq. 6.9) with its 90% prediction band.

6.3 Probability of Overtopping P_{ow}

The probability of overtopping P_{ow} is described by the ratio between the number of overtopping waves N_{ow} and the number of incident waves N_w (Eq. 2.33). In this section, the P_{ow} values of the UG13, UG14 and UG15 datasets are analysed and compared to the existing prediction formulae. A new prediction formulae is derived from the Ghent University datasets.

6.3.1 Results

Figure 6.17 shows P_{ow} as a function of R_c/H_{m0} for the datasets UG13, UG14 and UG15, with the data divided per slope angle according to Table 1.1. For increasing values of R_c/H_{m0} , P_{ow} decreases.

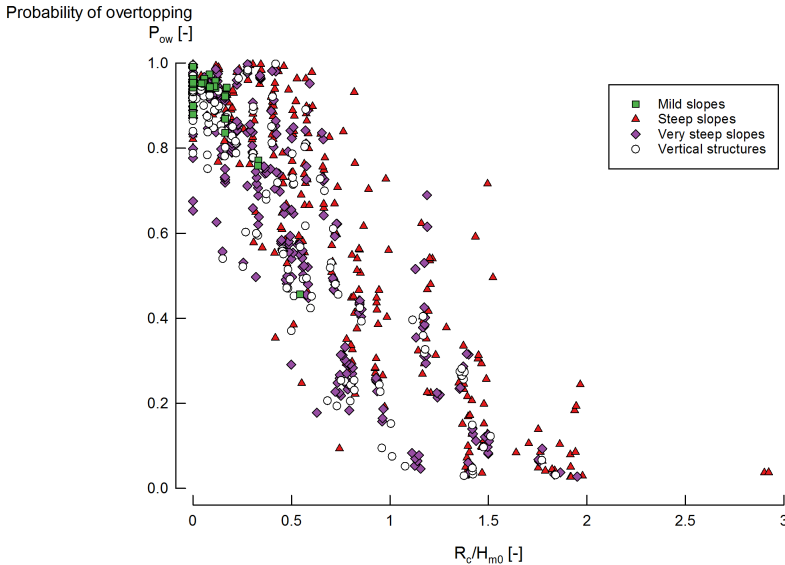


Figure 6.17: Probability of overtopping (P_{ow}) as a function of the relative crest freeboard R_c/H_{m0} for mild, steep, very steep slopes and vertical structures of the datasets UG13, UG14 and UG15.

As explained in Section 2.4.3, the maximum value of P_{ow} is 1 (all the incident waves are overtopping), and the minimum value is 0 (none of the incident waves is overtopping). For tests with very large overtopping rates, a probability of overtopping $P_{ow} > 1$ is possible to obtain as the result of a wrong analysis of the incident wave conditions or the wrong determination of the number of overtopping waves (see Section 4.3.2). In this case, a reanalysis of the incident wave conditions is performed, or the overtopping data is

processed again. If the probability of overtopping is still $P_{ow} > 1$, the value is excluded from the analysis.

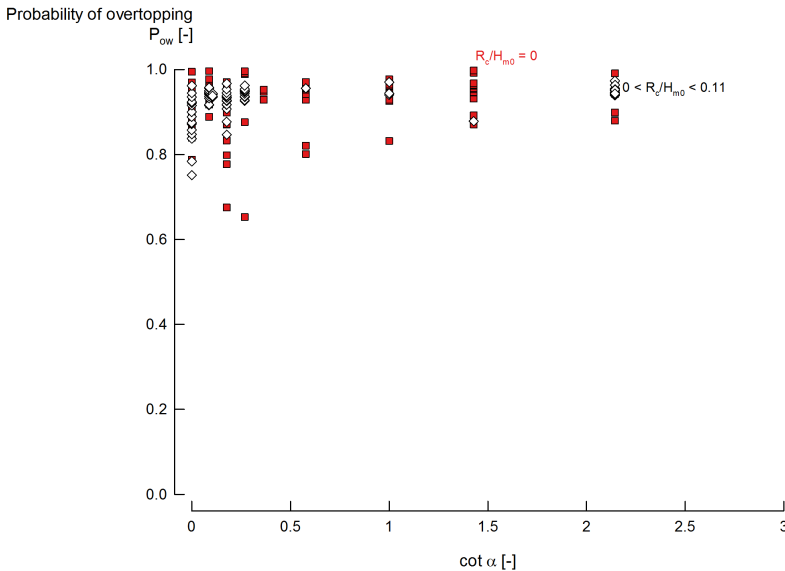


Figure 6.18: Probability of overtopping P_{ow} as a function of the slope angle $\cot \alpha$ for the datasets UG10, UG13, UG14 and UG15 for zero ($R_c = 0$) and very small ($0 < R_c/H_{m0} < 0.11$) relative freeboards.

Figure 6.18 shows the probability of overtopping for zero freeboard ($R_c = 0$) and very small relative freeboards ($0 < R_c/H_{m0} < 0.11$), and no effect of the slope angle $\cot \alpha$ is seen, as the values remain constant between 0.8 and 1. However, when analysing a larger relative crest freeboard such as $0.7 < R_c/H_{m0} < 0.8$ in Figure 6.19, the probability of overtopping P_{ow} decrease for smaller $\cot \alpha$ (steeper slopes).

An analysis of the P_{ow} data for the complete tested range of relative crest freeboard determines that P_{ow} is dependent on the slope angle α for the range $0.3 < R_c/H_{m0} < 1.1$. For $0 \leq R_c/H_{m0} < 0.3$, the freeboard available is very small and most of the waves are overtopping, with a probability of overtopping $0.8 < P_{ow} < 1$. In such a small freeboard the incident waves are not transformed by the slope angle of the structure, not playing any role in determining the number of waves overtopping. For $R_c/H_{m0} > 1.1$, the freeboard available is too large and most of the waves are not overtopping the structure, with values of the probability of overtopping $0 < P_{ow} < 0.4$. Due to this large freeboard, the number of waves overtopping is always small and it is not influenced by the slope angle of the structure. It is for the intermediate range of relative freeboards $0.3 < R_c/H_{m0} < 1.1$, with probabilities of overtopping $0.8 > P_{ow} > 0.4$, for which the slope angle α of the structure has

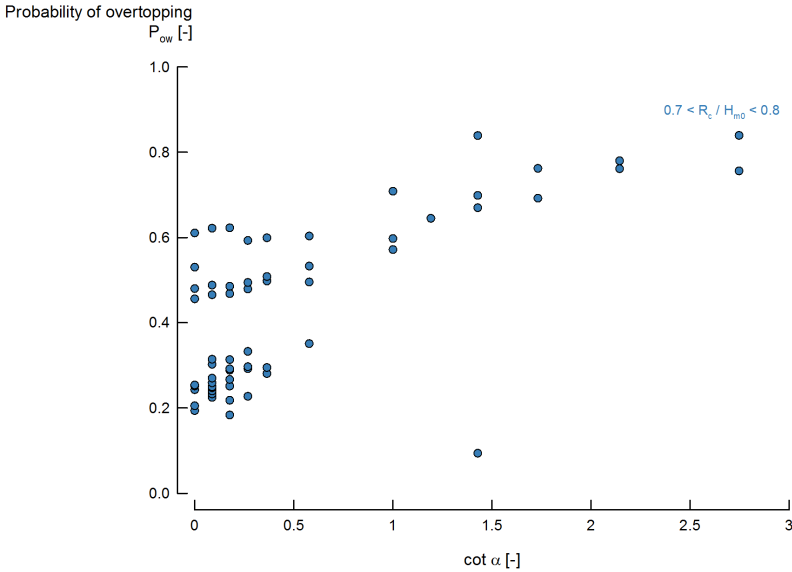


Figure 6.19: Probability of overtopping P_{ow} as a function of the slope angle $\cot \alpha$ for the datasets UG10, UG13, UG14 and UG15 for relative crest freeboards $0.7 < R_c/H_{m0} < 0.8$.

an effect on the number of overtopping waves, as the slope angle transform the incident waves.

This result is in contrast with all the literature available about the probability of overtopping. Victor et al. (2012) determined that the slope angle α had an effect on the the P_{ow} of the UG10 dataset, however, this effect was found for the whole tested range of relative crest freeboards (which did not include very small and zero freeboards). Van der Meer and Janssen (1994) and Franco et al. (1994) did not find an effect of the slope angle on the probability of overtopping.

Figure 6.18 also shows that the probability of overtopping P_{ow} values for zero freeboards ($R_c = 0$) have a scatter between $0.8 < P_{ow} < 1$, which contradicts the theoretical concept of all the incident waves overtopping the structure for the zero freeboard case ($R_c = 0$). This is explained by the incident and reflected waves from the structure interacting with each other, increasing the energy dissipation and decreasing the number of waves running up the slope and overtopping. This behaviour that can be seen in physical modelling is, however, not described in the P_{ow} studies and the various predictions available in literature.

An analysis of the probability of overtopping P_{ow} data based on the relative wave height H_{m0}/h for similar values of relative crest freeboard reveals that the relatively shallow water conditions do not affect the P_{ow} values.

Influence of the Surf Similarity Parameter $\xi_{m-1,0}$

The probability of overtopping P_{ow} is theoretically related to the relative 2% run-up height $R_{u2\%}/H_{m0}$ when the run-up heights are Rayleigh distributed. $R_{u2\%}/H_{m0}$ depends on the surf similarity parameter $\xi_{m-1,0}$ for mild slopes as suggested by Van der Meer and Janssen (1994) in Eq. 2.36 and by the TAW (2002) manual in Eqs. 2.39 and 2.40. P_{ow} increases for increasing values of $\xi_{m-1,0}$. For vertical structures there is no relation between $R_{u2\%}/H_{m0}$ and $\xi_{m-1,0}$.

Victor et al. (2012) reported that in the UG10 dataset the probability of overtopping P_{ow} values depend on the surf similarity parameter $\xi_{m-1,0}$. The UG10 results confirm that the P_{ow} values range between the prediction values for mild slopes and the prediction values for vertical structures, which is not a behaviour described by the prediction formulae for mild slopes (see Section 2.4.3). Victor et al. (2012) only indicated this effect, but the authors were not able to determine the range of relative crest freeboards R_c/H_{m0} for which this effect was taking place, although they hinted that for large overtopping rates, i.e., very small relative freeboards, the behaviour might be different as P_{ow} and $R_{u2\%}/H_{m0}$ are not related.

With the UG13, UG14 and UG15 datasets it is possible to determine the range of R_c/H_{m0} for which P_{ow} is related to $\xi_{m-1,0}$, and the behaviour of this relationship. Figure 6.20 shows P_{ow} as a function of $\xi_{m-1,0}$ for the zero freeboard case ($R_c = 0$) with an incident spectral wave height at the toe of the structure $H_{m0} = 0.11$ m. There is no influence of $\xi_{m-1,0}$ on P_{ow} for this case, as the probability of overtopping is constant in a range between 0.9 and 1. The increase in $\xi_{m-1,0}$ is explained by the increase in $\cot \alpha$ of the data, from mild slopes (small values of $\xi_{m-1,0}$) to very steep slopes (very large values of $\xi_{m-1,0}$) However, when analysing a larger relative crest freeboard, this behaviour changes.

Figure 6.21 shows P_{ow} as a function of $\xi_{m-1,0}$ for relative crest freeboards $0.4 < R_c/H_{m0} < 0.5$ with $H_{m0} = 0.1$ m, compared to the P_{ow} prediction formula by TAW (2002) with its 90% prediction band, the Franco et al. (1994) prediction for vertical structures, and the theoretical P_{ow} constant value for vertical structures. In this range of relative freeboards, the P_{ow} values depend on $\xi_{m-1,0}$. The small values of $\xi_{m-1,0}$ correspond to tests with mild slopes,

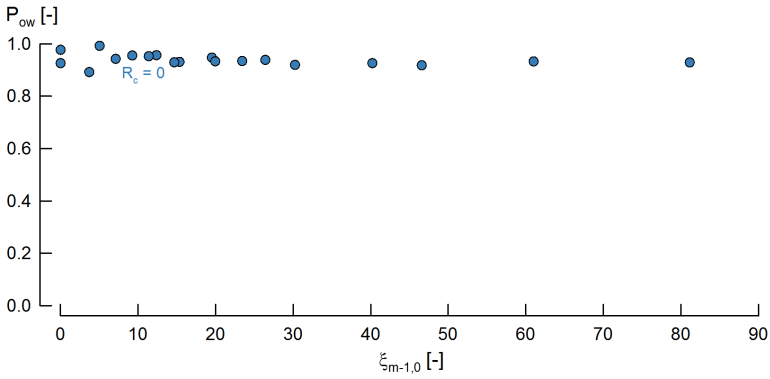


Figure 6.20: Probability of overtopping P_{ow} as a function of the surf similarity parameter $\xi_{m-1,0}$ for the datasets UG10, UG13, UG14 and UG15 for zero freeboard tests ($R_c = 0$) with $H_{m0} = 0.11$ m.

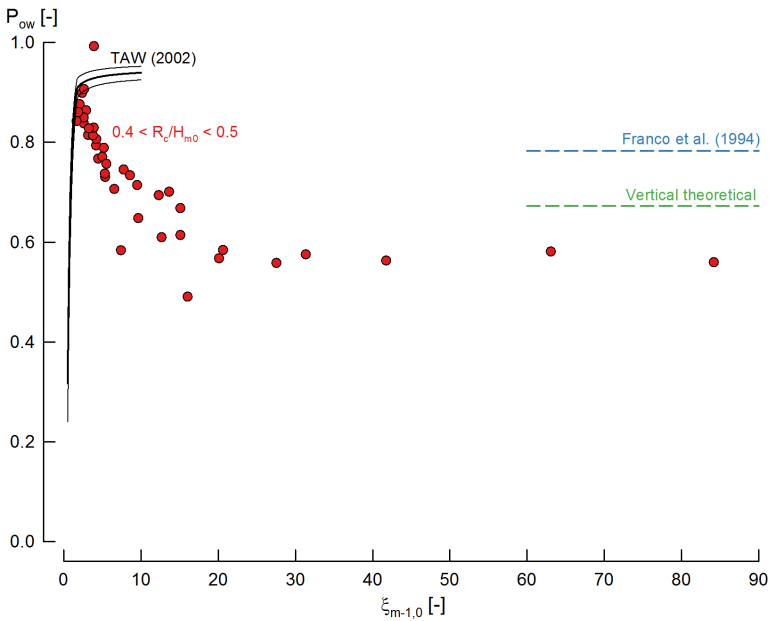


Figure 6.21: Probability of overtopping P_{ow} as a function of the surf similarity parameter $\xi_{m-1,0}$ for the datasets UG10, UG13, UG14 and UG15 for relative freeboards $0.4 < R_c/H_{m0} < 0.5$ with $H_{m0} = 0.1$ m, compared to the TAW (2002) prediction (Eq. 2.39 with a maximum on Eq. 2.40), the Franco et al. (1994) prediction (Eq. 2.43) and the theoretical value for vertical structures (Eq. 2.42).

which are correctly predicted by the TAW (2002) prediction. However, when increasing $\xi_{m-1,0}$ (i.e., steeper slopes), the TAW (2002) prediction is no longer predicting correctly the P_{ow} values, although it claims to be still valid for $\xi_{m-1,0} < 10$. The data decrease until reaching values for very large $\xi_{m-1,0}$ (very steep slopes) close to the vertical theoretical P_{ow} value. This is the same behaviour described by Victor et al. (2012) for the UG10 dataset.

After analysing the probability of overtopping P_{ow} data of the UG10, UG13, UG14 and UG15 datasets, it is seen that the values of relative crest freeboard for which the surf similarity parameter $\xi_{m-1,0}$ has a strong effect on P_{ow} is $R_c/H_{m0} > 0.4$. In between $0.1 > R_c/H_{m0} > 0.4$, there is a weak effect of $\xi_{m-1,0}$ on P_{ow} . Below $R_c/H_{m0} < 0.1$ the effect is negligible. This range of relative crest freeboards is very similar as the range aforementioned for which the slope angle α has an effect on P_{ow} , as $\xi_{m-1,0}$ is directly related to the slope angle α .

6.3.2 Comparison with Prediction Formulae

The P_{ow} results of the UG13, UG14 and UG15 datasets are compared to the existing prediction formulae by Victor et al. (2012), Van der Meer and Janssen (1994) and Franco et al. (1994). Victor et al. (2012) is the only P_{ow} prediction formula valid for the entire range of slope angles α and relative crest freeboards R_c/H_{m0} . Therefore, this prediction formula by Victor et al. (2012) (Eq. 2.44) is taken as the reference case.

Table 6.2 shows the RMSE and bias values of these two predictions for the mentioned datasets. The data is divided in the slope angle ranges shown in Table 1.1 and the relative crest freeboard ranges shown in Table 1.2.

For zero freeboards ($R_c = 0$), the RMSE value is approximately six times higher than for the rest of the relative freeboards. Theoretically, P_{ow} should be equal to 1 for zero freeboards, however, as explained in Section 6.3.1, the measured values result in values $0.8 < P_{ow} < 1$ due to the interaction between incident and reflected waves. Therefore, the results are overpredicted (positive value of the bias).

For (very) large relative freeboards $P_{ow} = 0$, meaning that no waves overtop the structure. This behaviour is included in all the prediction formulae of P_{ow} . The data confirm that for large relative freeboards the probability of overtopping is $P_{ow} = 0$, although the value of R_c/H_{m0} that reduces P_{ow} to 0 is dependent on the slope angle α of the structure.

For vertical structures the RMSE value is also six times higher than for the rest of slope angles, as Victor et al. (2012) takes the theoretical P_{ow} for vertical

Table 6.2: RMSE values (Eq. 3.1) and bias (Eq. 3.2) of the UG13, UG14 and UG15 datasets dataset for the probability of overtopping P_{ow} , in different ranges of relative crest freeboard R_c/H_{m0} and slope angle α .

Equation	Eq. 2.44	
Item	RMSE (-)	Bias (-)
All tests	0.34	0.09
Zero freeboard ($R_c = 0$)	0.67	0.48
$0 < R_c/H_{m0} < 0.05$	0.06	0.05
$0.05 < R_c/H_{m0} < 0.08$	0.17	0.10
$0.08 < R_c/H_{m0} < 0.11$	0.07	0.06
$0.11 < R_c/H_{m0} < 0.8$	0.15	0.01
$R_c/H_{m0} > 0.8$	0.17	-0.11
Mild slopes	0.10	0.07
Steep slopes	0.15	-0.04
Very steep slopes	0.14	0.005
Vertical structures	0.62	0.37

structures in the prediction and this theoretical value is overpredicting the results (positive value of the bias).

Figure 6.22 shows the probability of overtopping P_{ow} of the mild slopes and steep slopes of the UG13, UG14 and UG15 datasets, compared to the Van der Meer and Janssen (1994) prediction (valid for mild slopes) and the Victor et al. (2012) prediction for $\cot \alpha = 1$. The Van der Meer and Janssen (1994) prediction equals Victor et al. (2012) for $\cot \alpha = 2.5$. The data show a large scatter of the values. For mild slopes, Van der Meer and Janssen (1994) underpredicts the P_{ow} values, although the data are only for zero and very small relative freeboards. This prediction should be the upper limit of the data, as it is predicting the probability of overtopping for mild slopes. However, some data points for steep slopes are higher than the prediction. Victor et al. (2012) prediction yields values of P_{ow} in the middle of the data points cloud for steep slopes, although it is only plotted for the slope angle $\cot \alpha = 1$.

For very steep slopes, Figure 6.23 shows also a large scatter of the P_{ow} data, even reaching the prediction by Van der Meer and Janssen (1994) for mild slopes. Victor et al. (2012) is also predicting correctly the data points with the prediction for $\cot \alpha = 0.18$. For zero and very small relative freeboards, Victor et al. (2012) is overpredicting the data, as the prediction for the zero freeboard case is 1.

For vertical structures, Figure 6.24 shows that the vertical theoretical prediction (see Section 2.4.3) is overpredicting the P_{ow} values for zero and

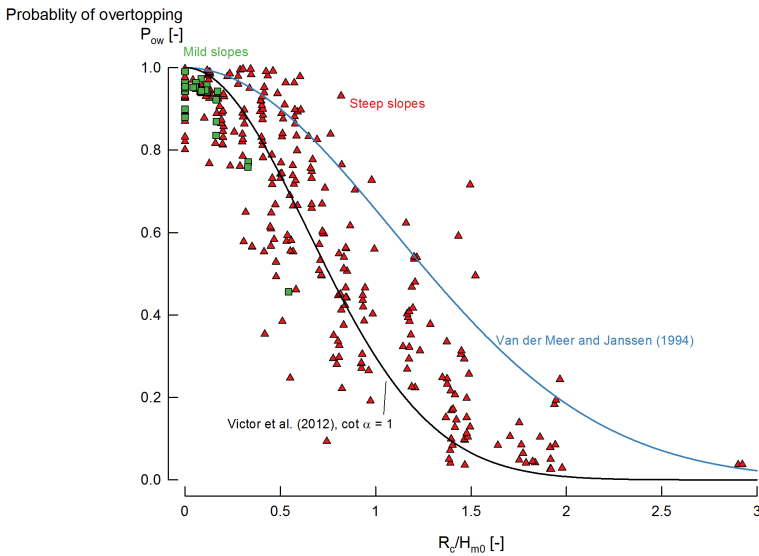


Figure 6.22: Probability of overtopping (P_{ow}) as a function of the relative crest freeboard R_c/H_{m0} for mild and steep slopes of the datasets UG13, UG14 and UG15, compared to Van der Meer and Janssen (1994) (Eq. 2.38) and Victor et al. (2012) (Eq. 2.44) for $\cot \alpha = 1$.

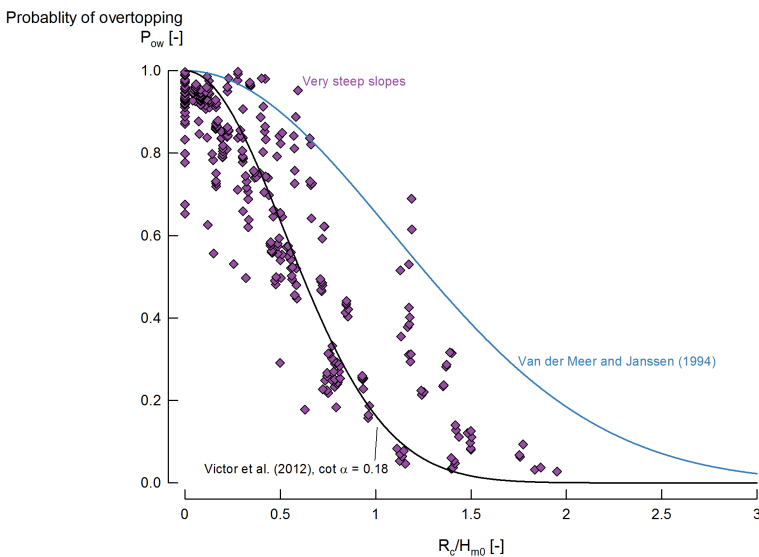


Figure 6.23: Probability of overtopping (P_{ow}) as a function of the relative crest freeboard R_c/H_{m0} for very steep slopes of the datasets UG13, UG14 and UG15, compared to Van der Meer and Janssen (1994) (Eq. 2.38) and Victor et al. (2012) (Eq. 2.44 for $\cot \alpha = 0.18$).

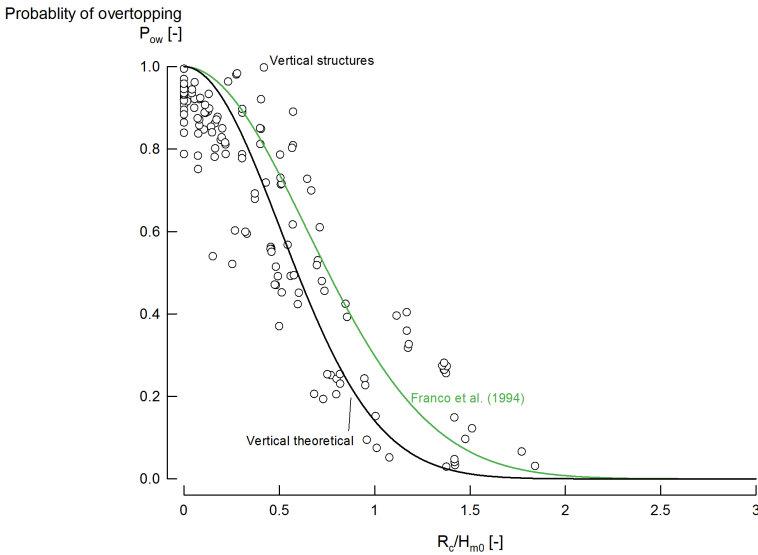


Figure 6.24: Probability of overtopping (P_{ow}) as a function of the relative crest freeboard R_c/H_{m0} for vertical structures of the datasets UG13, UG14 and UG15, compared to the theoretical prediction for vertical structures (Eq. 2.42) and Franco et al. (1994) (Eq. 2.43).

very small relative freeboards, as the P_{ow} values for this range of relative freeboards are lower than 1. For larger relative freeboards, the vertical theoretical prediction is underpredicting the P_{ow} values. The vertical theoretical prediction is the limit case of the Victor et al. (2012) prediction for vertical structures ($\cot \alpha = 0$). Franco et al. (1994) also proposed a probability of overtopping prediction for vertical structures. This prediction gives larger values than the theoretical one, and it is adapting better to the shape of the P_{ow} values of the three Ghent University datasets analysed, especially for $R_c/H_{m0} > 0.5$.

6.3.3 New Prediction Formula

A new prediction formula for the probability of overtopping P_{ow} is proposed in this section, to solve the inaccuracies of the existing predictions (see Section 6.3.2).

An improvement on the P_{ow} prediction accuracy is possible for mild slopes, as the prediction by Van der Meer and Janssen (1994) (which is also the limit case for mild slopes of Victor et al. (2012) prediction) is overpredicting the results. For vertical structures, both the theoretical value and the prediction by Franco et al. (1994) are underpredicting the results. For zero

freeboards, the predictions are theoretically $P_{ow} = 1$, while for very small relative freeboards is close to that value. However, the P_{ow} results of the UG13, UG14 and UG15 datasets are lower.

It is possible fit a new P_{ow} prediction formula by adding the UG13, UG14 and UG15 datasets to the UG10 dataset. This new prediction formula will improve the accuracy of Victor et al. (2012) for the slope angle and relative crest freeboards ranges with prediction inaccuracies.

Shape of the Prediction

The new probability of overtopping P_{ow} prediction formula has the expression shown in Eq. 6.10:

$$P_{ow} = \exp \left[- \left(p \frac{R_c}{H_{m0}} \right)^2 \right] \quad (6.10)$$

The formula describes the probability of overtopping P_{ow} as a function of the relative crest freeboard R_c/H_{m0} with an exponential function, following the theoretical approximation to the prediction described in Eq. 2.34. The only coefficient included in the formula is the coefficient p , which describes the shape of the exponential function.

Although the data show that the P_{ow} values for the zero freeboard case ($R_c = 0$) are lower than the theoretical $P_{ow} = 1$, it is decided that the new formula keeps the probability of overtopping at 1 so that the new prediction is mathematically and physically sound. However, this means that the overprediction of P_{ow} for zero freeboards is not solved by the new prediction.

Selection of the Overtopping Data

The set of tests to fit the new probability of overtopping P_{ow} prediction formula is formed by the tests of the UG10, UG13, UG14 and UG15 datasets, covering from mild slopes to vertical structures with relative crest freeboards from large to zero. The range from relatively deep to relatively shallow water conditions is also covered by the datasets (see Chapter 4 for a description of the datasets).

The tests included in the set to fit the new P_{ow} prediction have a number of overtopping waves $N_{ow} > 30$ so that the two-parameter Weibull distribution of the individual overtopping volumes is statistically significant (see Section 6.2). Also, tests with $P_{ow} > 1$ are excluded from the set as theoretically this situation is not possible (see Section 6.3.1). No selection

of tests based on the relative wave height H_{m0}/h is made, as P_{ow} is not dependent on this parameter. The total number of tests through which the new P_{ow} prediction formula is fitted is 1163, which compares to the 364 tests of the UG10 dataset used by Victor et al. (2012) (a factor three increase).

Fit of the Coefficients

Using a non-linear regression analysis, the best fit of the p coefficient of Eq. 6.10 per slope angle is found. The resulting expression is Eq. 6.11

$$p = 0.8 + 0.24(2 - \cot \alpha) \text{ with } p = 0.8 \text{ for } \cot \alpha \geq 2 \quad (6.11)$$

Combining the previous equation with Eq. 6.10, the suggested new probability P_{ow} prediction formula is Eq. 6.12:

$$P_{ow} = \exp \left[- \left([0.8 + 0.24(2 - \cot \alpha)] \frac{R_c}{H_{m0}} \right)^2 \right] \quad (6.12)$$

with $P_{ow} = \exp \left[- \left(0.8 \frac{R_c}{H_{m0}} \right)^2 \right]$ for $\cot \alpha \geq 2$

Eq. 6.12 can be rewritten as a function of the surf similarity parameter $\xi_{m-1,0}$ to be plotted in a similar graph as Figure 6.21. Considering the definition of the surf similarity parameter $\xi_{m-1,0} = \tan \alpha / \sqrt{s_{m-1,0}}$, then Eq. 6.13 is the prediction of the probability of overtopping P_{ow} as a function of $\xi_{m-1,0}$, valid for $\cot \alpha < 2$:

$$P_{ow} = \exp \left[- \left(\left[0.8 + 0.24 \left(2 - \frac{1}{\xi_{m-1,0} \sqrt{s_{m-1,0}}} \right) \right] \frac{R_c}{H_{m0}} \right)^2 \right] \quad (6.13)$$

Figure 6.25 shows the best fit of the p coefficient per slope angle of the tests selected to fit the new prediction. The value of p decreases linearly for increasing $\cot \alpha$ (milder slopes) until reaching an approximately constant value for $\cot \alpha \geq 2$. The best fit of p (Eq. 6.11) takes into account this constant value for $\cot \alpha \geq 2$ by including a limit for the linear expression.

The RMSE (Eq. 3.1) of Eq. 6.12 is 0.126, and the bias (Eq. 3.2) is 0.019. The reliability of the prediction can be expressed with this value of RMSE. The 90% prediction interval is determined by $P_{ow} \pm 1.64 \cdot \text{RMSE}$. The RMSE value is dominated by the overprediction of the P_{ow} for the zero freeboard case.

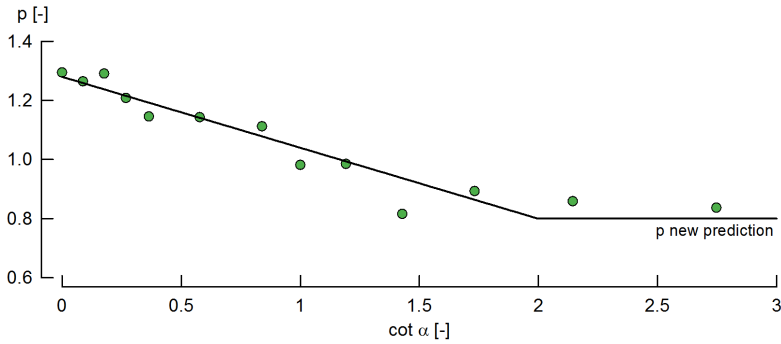


Figure 6.25: Best fit of the coefficient p per slope angle and expression of p for the new prediction (Eq. 6.11).

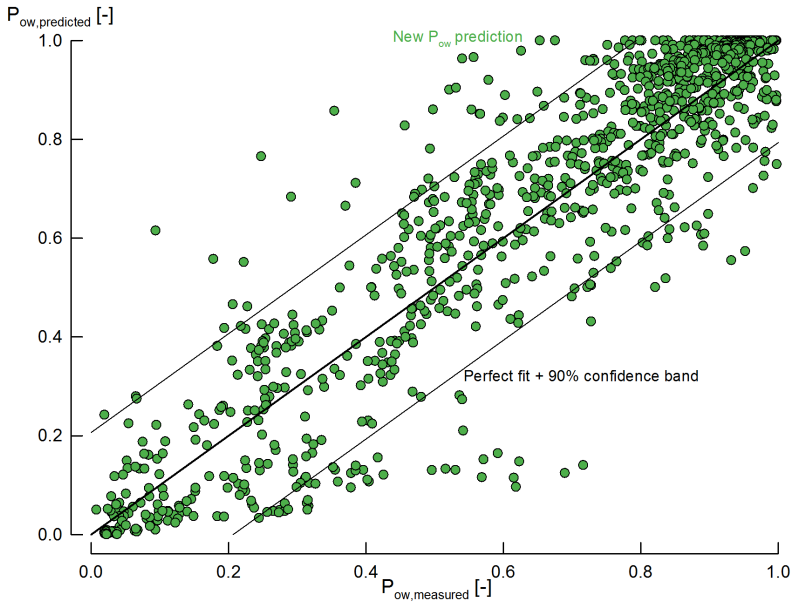


Figure 6.26: Measured probability of overtopping $P_{ow,measured}$ compared to the predicted $P_{ow,predicted}$ by Eq. 6.12, with the perfect fit line and the 90% confidence band.

Figure 6.26 shows $P_{ow,measured}$, the probability of overtopping measured values of the fitting set, compared to $P_{ow,predicted}$, the probability of overtopping predicted values by the new prediction (Eq. 6.12), with the perfect fit line and the 90% confidence band based on the aforementioned RMSE value. As expected, the tests with $0.8 < P_{ow,measured} < 1$ are being over-

predicted, as they correspond to the zero freeboard case ($R_c = 0$) which has a $P_{ow, predicted} = 1$.

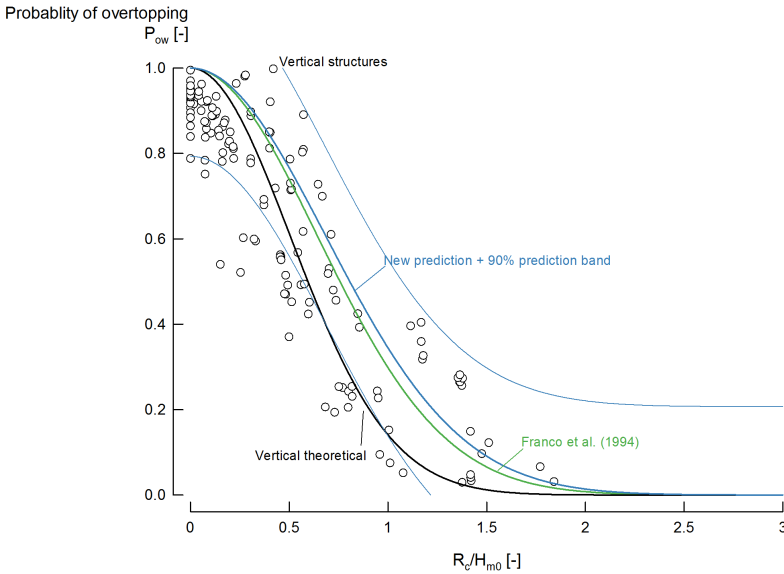


Figure 6.27: Probability of overtopping (P_{ow}) as a function of the relative crest freeboard R_c/H_{m0} for vertical structures of the datasets UG13, UG14 and UG15, compared to the theoretical prediction for vertical structures (Eq. 2.42), Franco et al. (1994) (Eq. 2.43 and the new prediction (Eq. 6.12) with its 90% prediction band.

Figure 6.27 adds the new P_{ow} prediction to the vertical structures data (c.f. Figure 6.24). The new prediction is closer to the Franco et al. (1994) prediction than to the theoretical prediction. The new prediction adapts better to the shape of the data, and predicts the P_{ow} values with more accuracy, except for the case of zero and very small relative freeboards where the P_{ow} prediction is 1.

6.4 Scale Factor A

The scale factor A of the two-parameter Weibull distribution of the individual overtopping volumes is proportional to the average overtopping discharge per wave. A is described by the expression Eq. 2.27 with A' being Eq. 2.28. These expressions are derived from equating the theoretical (\bar{V}_{theor}) and measured (\bar{V}_{meas}) mean individual overtopping volume, and assuming that \bar{V}_{theor} is described by a two-parameter Weibull distribution (Eq. 2.26).

To calculate the theoretical value of A for each test, it is necessary to know both the shape factor B and the probability of overtopping P_{ow} .

It is possible to calculate the best fit of the scale factor A (A_{calc}) for each test—as was done for the shape factor B —and compare it to the theoretical value of A (A_{theor}). The possible differences are due to the individual volumes in one test not following perfectly a two-parameter Weibull distribution. This leads to a different estimation of the Weibull distribution which directly affects the magnitude of the individual volumes.

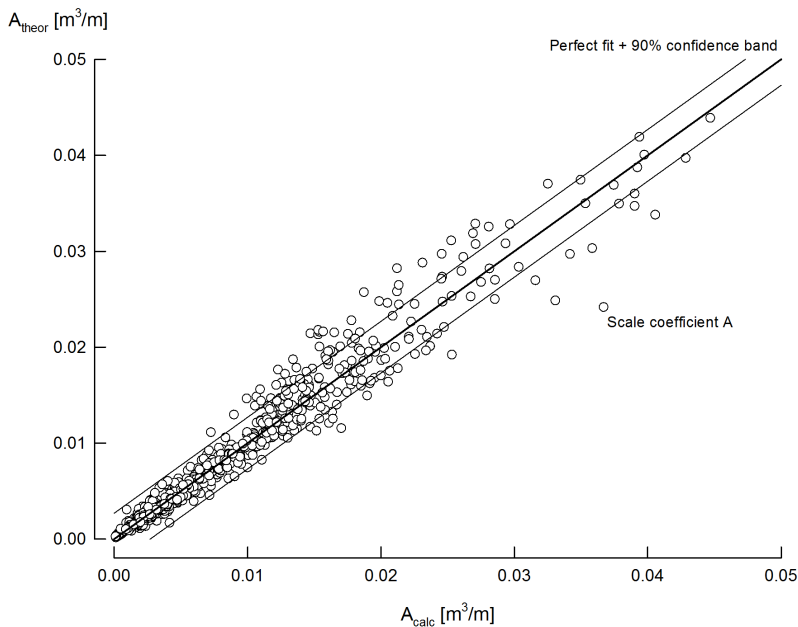


Figure 6.28: Theoretical scale factor (A_{theor}) versus the calculated scale factor (A_{calc}) for the datasets UG13, UG14 and UG15, compared to the perfect fit line with its 90% confidence band.

Figure 6.28 shows the comparison between the theoretical scale factor (A_{theor}) and the calculated scale factor (A_{calc}) for the datasets UG13, UG14 and UG15. The data follows the perfect fit line, although with a scatter. The root mean square error value of the calculated versus the theoretical A is $\text{RMSE} = 0.0016$, which is used to calculate the 90% confidence band.

The results seen in Figure 6.28 is a further prove that the individual volumes follow a two-parameter Weibull distribution. However, the chaotic behaviour of the overtopping process needs to be represented also in the estimation of the scale factor A by taking a representative uncertainty. No author has suggested previously an uncertainty value for A . From the re-

search presented in this dissertation, a standard deviation equal to the RMSE of $\sigma = 0.0016$ is suggested to be applied for the theoretical estimations of the scale factor A .

6.5 Individual Overtopping for Tests with Roughness Elements

The UG16 contains individual overtopping data for roughness elements in the structure slope. The results and the analysis with respect to the various wave and structural parameters are presented in this section.

6.5.1 Blocks and Ribs

Blocks and ribs were tested in the UG16 to reduce the overtopping rates (see Section 4.2) for the slope angles $\cot \alpha = 1$ ($\alpha = 45^\circ$) and $\cot \alpha = 0.58$ ($\alpha = 60^\circ$). The results for average overtopping rates and the reduction that these elements produced are presented and analysed in Section 5.5.1.

In the tests for the slope angle $\cot \alpha = 1$ ($\alpha = 45^\circ$) the overtopping detection wave gauge (WG7; see Section 4.3.2) was not correctly calibrated and the signal cannot be used to detect the individual overtopping events. As this part of the process is essential to determine the individual overtopping volumes, no individual overtopping results were obtained for the tests with blocks and ribs as roughness elements for the $\cot \alpha = 1$ ($\alpha = 45^\circ$) slope. Only tests with ribs for the slope angle $\cot \alpha = 0.58$ ($\alpha = 60^\circ$) are presented and analysed in this section.

The reference case to compare the results of the tests with roughness elements is the smooth slope case for the same slope angles from the UG10, UG13, UG14 and UG15 datasets. The coefficients w_{smooth} , x_{smooth} and y_{smooth} from the shape factor B prediction (Eq. 6.5), and the coefficient p_{smooth} from the probability of overtopping prediction (Eq. 6.10) are calculated for the slope angles $\cot \alpha = 1$ ($\alpha = 45^\circ$) and $\cot \alpha = 0.58$ ($\alpha = 60^\circ$). The results are shown in Table 6.3 with the RMSE value (Eq. 3.1) for each equation.

Figure 6.29 shows the shape factor B values as a function of the relative crest freeboard R_c/H_{m0} for tests of $\cot \alpha = 0.58$ ($\alpha = 60^\circ$) with ribs. The values do not show any influence of the roughness elements as they are aligned with the smooth reference case. The scatter of the values is also matching the scatter of the reference case as the values are within the 90% prediction band.

Figure 6.30 shows the probability of overtopping P_{ow} values as a function of the relative crest freeboard R_c/H_{m0} for tests of $\cot \alpha = 0.58$ ($\alpha = 60^\circ$)

Table 6.3: Best fit of the coefficients w_{smooth} , x_{smooth} , y_{smooth} of the shape factor B (Eq. 6.5) and p_{smooth} of the probability of overtopping P_{ow} (Eq. 6.10) for smooth slopes with $\cot \alpha = 1$ and $\cot \alpha = 0.58$, with the RMSE value (Eq. 3.1) for each equation.

$\cot \alpha$ (-)	B (Eq. 6.5)				P_{ow} (Eq. 6.10)	
	w_{smooth} (-)	x_{smooth} (-)	y_{smooth} (-)	RMSE (-)	p_{smooth} (-)	RMSE (-)
1	0.67	2.23	0.91	0.21	0.98	0.21
0.58	0.56	2.56	0.89	0.23	1.43	0.11

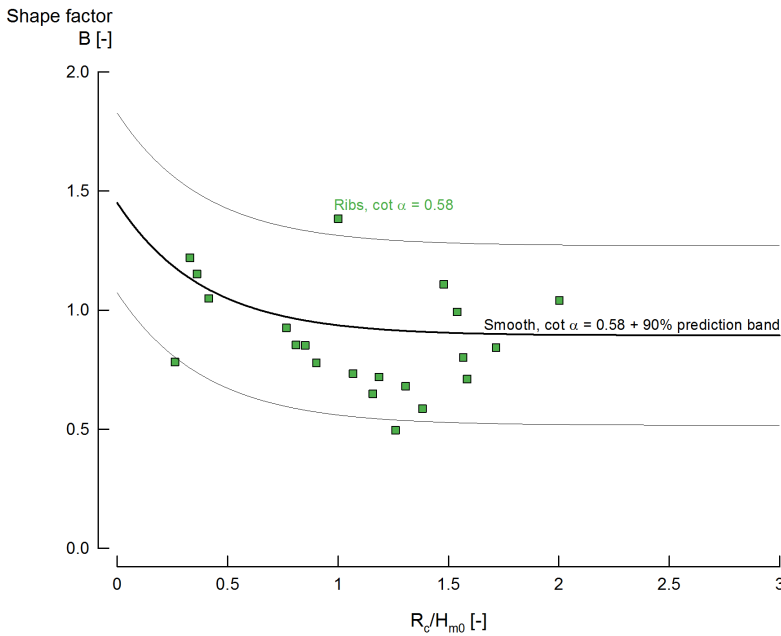


Figure 6.29: Shape factor B versus relative crest freeboard R_c/H_{m0} for tests of $\cot \alpha = 0.58$ ($\alpha = 60^\circ$) with ribs compared to the smooth reference case (Table 6.3) with its 90% prediction band.

with ribs. The P_{ow} values align almost perfectly with the smooth reference case, indicating that the roughness elements are not influencing the probability of overtopping for this slope angle.

The results of the slope angle $\cot \alpha = 0.58$ ($\alpha = 60^\circ$) indicate no influence of the roughness elements on the slope neither on the shape factor B nor on the probability of overtopping P_{ow} . For average overtopping, the influence was also rather limited (see Section 5.5.1), and therefore, it is logical that the influence on the individual overtopping is also very small or negligible. As this slope angle is the only one tested that could be analysed, it

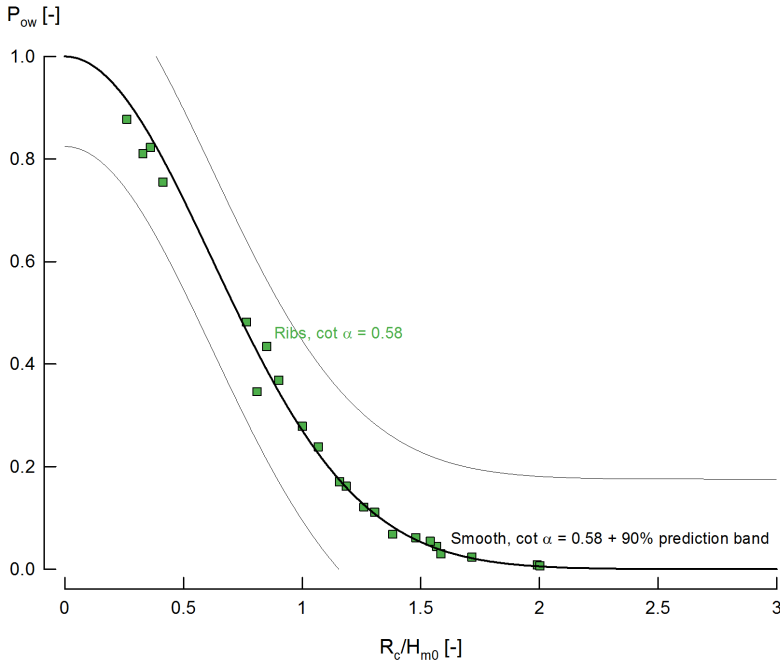


Figure 6.30: Probability of overtopping P_{ow} versus relative crest freeboard R_c/H_{m0} for tests of $\cot \alpha = 0.58$ ($\alpha = 60^\circ$) with ribs compared to the smooth reference case (Table 6.3) with its 90% prediction band.

is not possible to draw any conclusions about a different influence of the roughness elements on the individual overtopping for milder slopes. The influence of the roughness elements on the average overtopping for the slope angle $\cot \alpha = 1$ ($\alpha = 45^\circ$) is larger than for the slope $\cot \alpha = 0.58$ ($\alpha = 60^\circ$). It would be expected that this behaviour is similar for individual overtopping, although it is not possible to prove it with data.

6.5.2 Stepped Revetments

The individual overtopping data for stepped revetments of the UG16 dataset are analysed in this section. Following the average overtopping analysis of stepped revetments (see Section 5.5.2), the shape factor B and the probability of overtopping P_{ow} are analysed with respect to the relative step height H_{m0}/S_h and the surf similarity parameter $\xi_{m-1,0}$.

Figure 6.31 shows the shape factor B data versus the relative crest freeboard R_c/H_{m0} of stepped revetments for slope angles $\cot \alpha = 1$ ($\alpha = 45^\circ$) and $\cot \alpha = 0.58$ ($\alpha = 60^\circ$) for various ranges of the relative step height

H_{m0}/S_h , compared to the smooth reference cases of both slopes (Table 6.3) and their 90% confidence bands. Although the data are within the prediction band of the reference cases, most of the values are overpredicted by the reference case, meaning that there is a reduction of the shape factor B for stepped revetments.

This means that for stepped revetments the average overtopping rate is formed by larger maximum volumes than for a smooth slope of the same slope angle. This behaviour is similar for both slope angles. However, given that the scatter of the data is large (although similar to the scatter for the smooth reference cases), this conclusion needs to be further investigated.

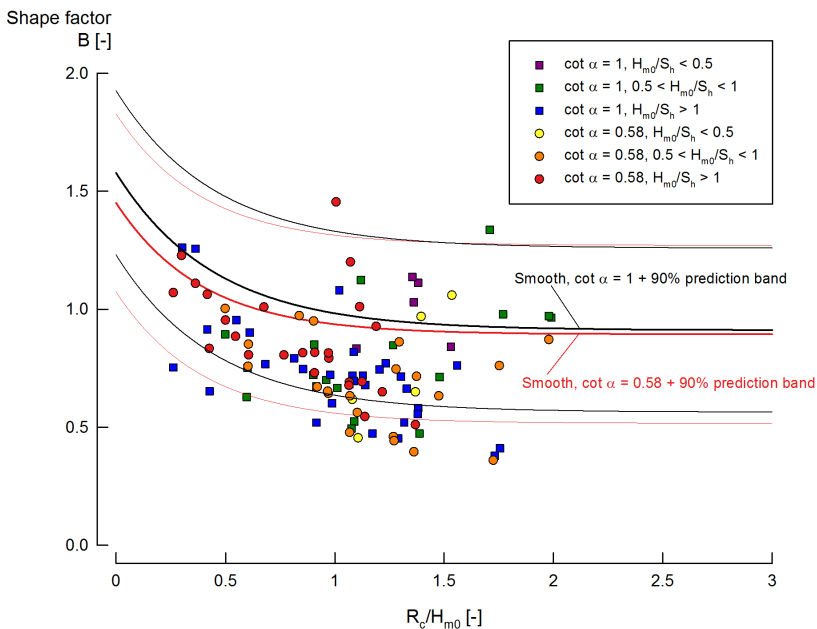


Figure 6.31: Shape factor B versus relative crest freeboard R_c/H_{m0} for stepped revetment tests with $\cot \alpha = 1$ ($\alpha = 45^\circ$) and $\cot \alpha = 0.58$ ($\alpha = 60^\circ$) compared to the smooth reference cases (Table 6.3) with their 90% prediction band.

Figure 6.32 shows the probability of overtopping P_{ow} versus to the relative crest freeboard R_c/H_{m0} of stepped revetments for slope angles $\cot \alpha = 1$ ($\alpha = 45^\circ$) and $\cot \alpha = 0.58$ ($\alpha = 60^\circ$) for various ranges of H_{m0}/S_h , compared to the smooth reference cases of both slopes (Table 6.3) and their 90% confidence bands. The stepped revetments results align almost perfectly with the smooth reference cases for both slope angles. There is no evidence in the data that the probability of overtopping P_{ow} (and therefore, the number of overtopping waves N_{ow}) is increasing or decreasing due to the presence of

a stepped revetment compared to a smooth slope with the same slope angle.

The analysis of the shape factor B and the probability of overtopping P_{ow} as a function of the surf similarity parameter $\xi_{m-1,0}$ does not result in a significant difference from the smooth reference case. The reduced number of slope angles tested allows to only analyse a reduced range of the surf similarity parameter, with $4 < \xi_{m-1,0} < 10$. However, it is not expected that the behaviour of B and P_{ow} is any different for very steep slopes (with very high surf similarity parameters up to $\xi_{m-1,0} = 90$) than it is for mild or steep slopes.

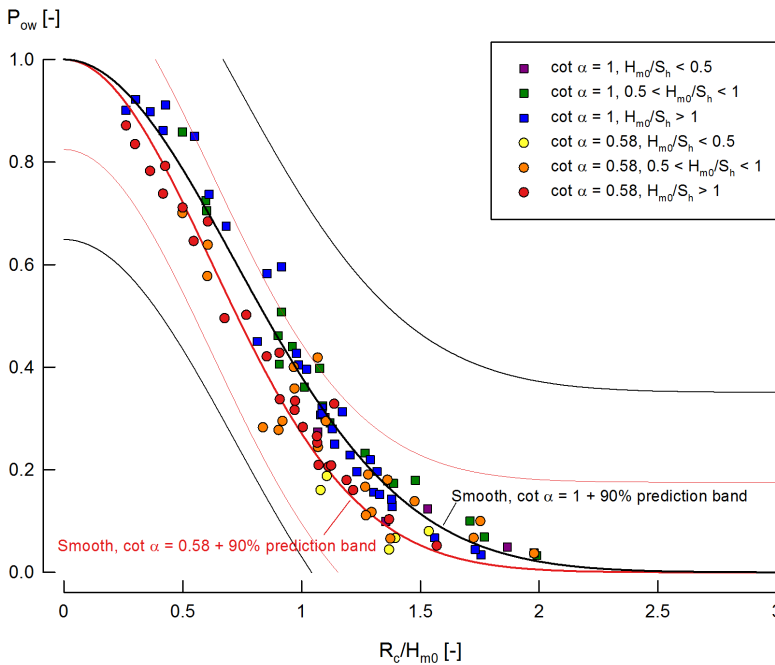


Figure 6.32: Probability of overtopping P_{ow} versus relative crest freeboard R_c/H_{m0} for stepped revetment tests with $\cot \alpha = 1$ ($\alpha = 45^\circ$) and $\cot \alpha = 0.58$ ($\alpha = 60^\circ$) compared to the smooth reference cases (Table 6.3) with their 90% prediction band.

6.6 Summary

The scale factor A , shape factor B and probability of overtopping P_{ow} are analysed and compared to the existing prediction formulae for the datasets UG13, UG14, UG15 and UG16.

The accuracy of the prediction formulae is validated, finding an under-prediction of the B values for very steep slopes and vertical structures, and large relative freeboards. A new prediction for B is obtained based on the new overtopping data acquired for this research. The values of B for the new prediction depend on the slope angle α for the zero freeboard case, while for large relative freeboards the values are constant and not depending on α .

The probability of overtopping P_{ow} of the zero freeboard case is theoretically $P_{ow} = 1$, although the data show that the values range from 0.8 to 1 due energy dissipation from the interaction between the incident and the reflected waves. A new prediction formula for P_{ow} is obtained using the new overtopping data available. The P_{ow} values of this new prediction range from 0 for large relative freeboards to 1 for the zero freeboard case, although it is advised to take into account the reduction of P_{ow} for zero freeboards shown by the data.

The artificial roughness elements on the structure slope, including stepped revetments, do not modify the behaviour of B and P_{ow} with respect to the smooth slope reference case.

Chapter 7

Conclusions

In this chapter, the main conclusions that can be extracted from the research are presented. First, an overview of the objectives and the methodology of the research is presented, together with a description of the overtopping datasets acquired at Ghent University during the research. Then, conclusions are extracted from the results of average overtopping and individual overtopping. Finally, recommendations about the next steps of the research are presented.

7.1 Overview of the Research

The sea level rise caused by climate change is threatening the coasts all over the world. As a consequence, the crest freeboard of the existing coastal structures is reduced, although its primary goal of protecting the coasts against wave attack should be maintained. The knowledge of wave overtopping for low-crested structures is rather limited, as this condition has not been thoroughly investigated in the scientific literature.

Besides coastal safety, another field in which low-crested structures are of application is the wave energy field. The working principle of the overtopping wave energy converters (OWECs) is the storage of waves running-up a slope and overtopping into a reservoir, which is emptied into the ocean through a set of low-head turbines, generating electricity. A low-crested structure increases the overtopping and maximizes the electricity production of the OWEC. The slope angle of the OWEC also determines the overtopping rate. A steep or very steep slope maximizes the overtopping, as opposed to a mild slope. However, also the knowledge of the overtopping behaviour for (very) steep structures is small, as these structures have a limited application for the defence of the coast against wave attack.

Research by Victor (2012) at Ghent University investigated overtopping for steep low-crested structures, performing physical model tests which resulted in the UG10 dataset. However, not the full range of slope angles and relative crest freeboards was investigated, as the very steep slopes and vertical structures were left out, as well as zero and very small relative freeboards. Victor and Troch (2012b) and Van der Meer and Bruce (2014) suggested average overtopping prediction formulae for steep low-crested structures based on the UG10 data, although the predictions have small inaccuracies due to the mentioned gaps in UG10. Victor et al. (2012) analysed the individual overtopping volumes of UG10, proposing various formulae to predict the distribution of the individual volumes.

A knowledge gap in the scientific literature for wave overtopping on steep low-crested structures is identified. The main objective of the research is to fill this knowledge gap. The methodology is based on performing 2D hydraulic model tests in the wave flume of the Department of Civil Engineering at Ghent University, and to analyse the average overtopping and the individual overtopping volumes. The model tests are structured in various datasets, each of them designed to address a wave or structural parameter in order to analyse the influence of this parameter on the wave overtopping. The wave parameters are measured for each test, as well as the overtopping rates.

The overtopping datasets obtained in this research are UG13, UG14, UG15 and UG16. The slope angle α , the relative crest freeboard R_c/H_{m0} , the relative wave height H_{m0}/h and the roughness of the slope are varied to fully cover the steep low-crested structures knowledge gap, including the gap left by the previous UG10 dataset. In total, 1211 physical model tests are part of the four mentioned datasets.

The UG13 dataset is obtained for smooth impermeable slopes with angles from mild to vertical structures ($2.14 \geq \cot \alpha \geq 0$) and relative crest freeboards from large to zero ($2.43 \geq R_c/H_{m0} \geq 0$). The tests of the UG13 are obtained for relatively deep water conditions ($H_{m0}/h \leq 0.2$), with some overlapping with the transitional zone ($0.2 < H_{m0}/h < 0.5$).

The UG14 dataset is obtained for smooth impermeable slopes angles from steep to vertical structures ($1.73 \geq \cot \alpha \geq 0$) and relative crest freeboards from large to zero ($2.92 \geq R_c/H_{m0} \geq 0$). The main difference with the UG13 dataset is that UG14 is obtained for relatively shallow water conditions ($H_{m0}/h \geq 0.5$) and the transitional zone ($0.2 < H_{m0}/h < 0.5$). The UG15 dataset is a continuation of the UG14 dataset focusing exclusively on relatively shallow water conditions.

With the datasets UG13, UG14 and UG15 the complete range (and their

limit cases) of slope angles, relative crest freeboards and relatively water depth conditions of the steep low-crested structures is investigated.

The effect on the overtopping of roughness on the slope is investigated by the UG16 dataset. Two types of roughness elements are selected to be tested: blocks and ribs (due to a lack of reduction of the overtopping rates the blocks are later transformed into ribs) and stepped revetments (with different step heights, therefore including a fifth parameter to investigate). Only two slope angles are selected for the UG16 dataset ($\cot \alpha = 1, \cot \alpha = 0.58$), and the range of freeboards tested is limited to small and large relative freeboards ($3.25 \geq R_c/H_{m0} \geq 0.11$) as it is expected that the overtopping is not influenced by the roughness in structures with very small relative freeboards.

The conclusions of the research for average overtopping are presented in Section 7.2, while the conclusions of the research for individual overtopping are presented in Section 7.3. Table 7.1 shows an overview of the new prediction formulae obtained in this research and the main accuracy improvements with respect to prediction formulae in the literature for ranges of slope angle $\cot \alpha$ and relative crest freeboard R_c/H_{m0} .

Table 7.1: New prediction formulae obtained in this research.

Predicted parameter	Eq.	Parameter ranges with main accuracy improvements
Average overtopping rate q	5.1–5.4	Zero and very small relative freeboards Very steep slopes
Shape factor B	6.9	Zero and very small relative freeboards Large relative freeboards
Probability of overtopping P_{ow}	6.12	General improvement of the accuracy

7.2 Conclusions on Average Overtopping

The average overtopping rates of each test obtained within this research are processed and analysed. The UG13, UG14 and UG15 dataset add new average overtopping data to the scientific literature for ranges of slope angles (very steep) and relative freeboards (very small and zero) that previously were not investigated in detail. This range of data defines the new zones Z1* ($0.27 \geq \cot \alpha > 0, 0.8 \geq R_c/H_{m0} \geq 0$), Z2* ($0.27 \geq \cot \alpha > 0, 2 \geq R_c/H_{m0} \geq 0.8$) and Z3* ($1.5 \leq \cot \alpha \leq 2.75, R_c/H_{m0} < 0.11$), which are extension zones with respect to the UG10 dataset. With the new zones the complete range of slope angles α and the relative crest freeboards R_c/H_{m0} is covered.

The Van der Meer and Bruce (2014) predictions suggests that the shape of the data in a log-linear plot is curved. However, Van der Meer and Bruce (2014) is underpredicting the overtopping rates for zero freeboard. A thorough analysis of the new data obtained in this research reveals that although the shape is curved, it is closer to a straight line than suggested by Van der Meer and Bruce (2014).

To solve these inaccuracies of the existing prediction, an update of the average overtopping prediction formula is obtained, which improves the prediction of the overtopping for steep low-crested structures. For this update, a smaller exponent for the prediction than Van der Meer and Bruce (2014) has been selected, improving the accuracy of the prediction for very small and zero freeboards while maintaining the accuracy of the prediction for mild slopes and large relative freeboards.

The overtopping data of the UG14 and UG15 datasets on relatively shallow water conditions is compared to the overtopping data of the UG10 and UG13 on relatively deep water conditions, allowing a study of the influence of the water depth conditions for non-breaking conditions on the average overtopping rates. An increase of the average overtopping for large relative freeboards on relatively shallow water conditions is found. This increase is within the uncertainty range of the overtopping data, which is larger for large relative freeboards than for small relative freeboards. As a consequence, it was decided not to consider the effect of relatively shallow water conditions separately from the main prediction in the update of the overtopping prediction. For vertical structures the average overtopping prediction decision tree of the EurOtop (2016) manual can be simplified by not considering the influencing foreshores separately from non-influencing foreshores.

UG16 featured overtopping tests with roughness elements on the slope of the structure. For these conditions the average overtopping rates are reduced. In the case of blocks and ribs as roughness elements, the reduction of the average overtopping rates is larger for milder slopes, depending also on the partial coverage of the slope by the roughness elements. The reduction is larger for ribs than for blocks as ribs cover more of the slope surface, increasing the energy dissipation of the incident waves and reducing the overtopping rate.

In the case of stepped revetments, the average overtopping is also reduced. The reduction is larger for milder slopes, with decreasing reduction of the average overtopping for increasing values of the surf similarity parameter $\xi_{m-1,0}$. For steeper slopes the overtopping reduction caused by stepped revetments is smaller and there is no influence of $\xi_{m-1,0}$. However, this conclusion is only supported by two different slope angles tested in the UG16 dataset and there is no information about the behaviour of this influence between

the two tested slope angles. Literature shows that for milder slopes than the ones tested in UG16 there is no influence of the slope angle.

The relative step height H_{m0}/S_h and the relative position of the SWL compared to the step position are also important when determining the overtopping rates. For $H_{m0}/S_h < 0.5$, impulsive conditions take place if the SWL is on the step closest to the crest of the structure. The impulsive conditions increase the average overtopping up to similar values as for the equivalent smooth slope, cancelling out the reduction effect of the stepped revetments. The edge step also influences the overtopping, with a further reduction of the average overtopping when the SWL is very close to the crest of the structure, due to the interaction between the incident wave and reflected wave from the highest step that increases energy dissipation.

7.3 Conclusions on Individual Overtopping

The probability distribution of the individual overtopping volumes follows a two-parameter Weibull distribution, defined by the scale factor A and the shape factor B . The probability of overtopping P_{ow} determines the percentage of waves overtopping the structure. The correct prediction of these parameters is important to assess the safety of existing coastal structures and to update the design guidelines.

The shape factor B is increasing for smaller relative crest freeboards, reaching values up to $B = 2.5$ for the zero freeboard case, which is a new result obtained from the analysis of datasets UG13, UG14 and UG15. This means that the average overtopping is formed by more equal volumes in the case of structures with very small and zero relative freeboards, than in the case of structures with larger freeboards for which the average overtopping is formed by a few very large volumes. The slope angle α is influencing the value of the shape factor B . For larger $\cot \alpha$ (milder slopes), B increases, especially for very small and zero relative freeboards. The relatively water depth conditions of the tests do not influence the value of B .

A new shape factor B prediction formula is suggested, based on the datasets obtained in this research and the UG10 dataset. Compared to the B predictions by Victor et al. (2012) and Hughes et al. (2012), the prediction adds a new coefficient that defines the value of B for the zero freeboard case, which according to the data depends on $\cot \alpha$ (smaller values for steeper slopes). The shape of the prediction on a linear plot is exponential and does not depend on the slope angle. The value of B for (very) large freeboards is set to be constant for all the slope angles, and is similar to the value of B suggested

by the EurOtop (2007) for all sea defence structures. This new prediction improves the accuracy of Victor et al. (2012) Hughes et al. (2012) predictions.

The probability of overtopping P_{ow} data show that for the zero freeboard case the values range from 0.8 to 1, which is in contradiction to the theoretical definition of P_{ow} (and all the prediction formulae) which state that all the waves overtop a structure with a zero freeboard ($P_{ow} = 1$). The physical meaning is that the incident waves are interacting with the reflected waves from the structure, increasing the energy dissipation and reducing the number of overtopping waves.

The probability of overtopping P_{ow} show a dependence on the slope angle α for values of the relative crest freeboard $0.3 < R_c/H_{m0} < 1.1$. For lower values of the relative freeboard, the available crest freeboard is very small and the incident waves are not affected by the slope angle of the structure. For larger values of the relative freeboard, the number of overtopping waves is always very small and a change of slope angle is not sufficient to increase (or further reduce) the number of overtopping waves.

The probability of overtopping P_{ow} is influenced by the surf similarity parameter $\xi_{m-1,0}$, although with a different behaviour from the one traditionally reported in literature. The increase in $\xi_{m-1,0}$ due to heavy breaking on (very) shallow foreshores results in an increase of P_{ow} . However, the (very large) increase in $\xi_{m-1,0}$ due to (very) steep slopes results in an increase in wave reflection and therefore, a decrease of P_{ow} . This duality in the behaviour of P_{ow} by the influence of $\xi_{m-1,0}$ was reported by Victor et al. (2012) and it is corroborated now by the UG13, UG14 and UG15 datasets, with an extension to the data for very steep slopes and the limit case with the vertical structure.

A new prediction formula for P_{ow} is suggested, based on the datasets obtained within this research and the UG10 dataset. It is decided to maintain the theoretical probability of overtopping for the zero freeboard case on $P_{ow} = 1$, although it is advised to consider that the real P_{ow} values are lower.

The scale factor A depends on B and P_{ow} assuming that the individual overtopping volumes follow a two-parameter Weibull distribution. However, the data shows a certain divergence from the theoretical Weibull distribution that results in a scatter of the measured A values with respect to the theoretical ones. This scatter is suggested to be introduced in the uncertainty of the scale factor A as a standard deviation.

The individual overtopping volumes of the UG16 are analysed to study the influence of the roughness elements on the slope on the shape factor B and the probability of overtopping P_{ow} . The blocks do not have any effect on B and P_{ow} . For stepped revetments there is a small reduction in the shape factor B with respect to the smooth reference case, while the P_{ow} values are

the same as the smooth reference case. There is no influence of the step height S_h or the surf similarity parameter $\xi_{m-1,0}$ on B and P_{ow} .

7.4 Publications

The results of this research have been partially presented in various scientific publications. As an international journal publication, Gallach-Sánchez et al. (2018a) presents an analysis and validation of the accuracy of the existing average prediction formulae for steep low-crested structures based on the UG13 dataset. As international conference publications, Troch et al. (2015) analyses the average overtopping rates of the UG13 dataset, while Gallach-Sánchez et al. (2015a) analyses the individual overtopping volume distribution of the same dataset. Gallach-Sánchez et al. (2014) analyses the average overtopping rates of the UG14 dataset, and Gallach-Sánchez et al. (2015b) compares the average overtopping of the UG13 and UG14 datasets. Gallach-Sánchez et al. (2016a) analyses the average overtopping rates of the UG15 dataset and compares them with the results of the UG14 dataset. Finally, Gallach-Sánchez et al. (2018b) presents an overview of the whole research including the updated average prediction formula, and the shape factor B and probability of overtopping P_{ow} prediction formulae. Other publications are Gallach-Sánchez et al. (2016b) and Gallach-Sánchez et al. (2017).

7.5 Recommendations for Further Research

Based on the conclusions for average overtopping and individual overtopping presented in Section 7.2 and Section 7.3 respectively, various recommendations for the continuation of this research are suggested.

More overtopping data with a relative wave height $H_{m0}/h > 0.5$ (i.e., completely in relatively shallow water conditions) is necessary to fully characterize the increase of the average overtopping rate for large relative freeboards with relatively shallow water conditions. These wave conditions are then tending to shallow foreshores where breaking is induced by the foreshore profile.

The transition of the average overtopping prediction formulae between breaking and non-breaking conditions has not been fully investigated, as this research focused on non-breaking wave conditions. This transition is based on the value of the surf similarity parameter $\xi_{m-1,0}$ or on giving a maximum prediction (which corresponds to non-breaking wave conditions). A new approach with a complete integration of the prediction formulae both for

breaking and non-breaking conditions would be desirable to have an integrated physical understanding of the overtopping process and a simplified set of prediction formulae.

The effect of oblique wave attack on wave overtopping has been investigated in literature only for mild slopes and not for steep low-crested structures. In the research presented in this dissertation, only 2D hydraulic model tests were obtained as a wave flume was available, while to investigate oblique wave attack a wave basin (i.e., a 3D facility) is necessary. Therefore, 3D hydraulic model tests for steep low-crested structures are suggested as a next step in the research to investigate the reduction of overtopping due to oblique wave attack.

Stepped structures proved to be efficient in reducing the overtopping, although the scientific research available on this type of structures is scarce, particularly for steep slopes. Only two slope angles were tested in the UG16 dataset, and to obtain full valid conclusions it would be necessary to investigate more slope angles. Testing steeper slopes than $\cot \alpha = 0.58$ ($\alpha = 60^\circ$) may prove unnecessary as the overtopping reduction is already small for this angle. However, it would be useful to know the effect of the slope angle for the transition between mild slopes (which are available in the literature) and steep slopes (available in the UG16 dataset) for the future design guidelines of such structures.

The relation between the 2% run-up and the probability of overtopping P_{ow} is not established in this research as the run-up was not measured during the experiments. As literature states that this relation may be not valid for very large overtopping rates (as it is the case for steep low-crested structures), it would be necessary to obtain data from physical model tests that corroborate or deny this relation.

The research on a physical process like wave overtopping may not ever be completed as new fields of application are developed, more accurate physical model methods are created and more challenging coastal structures are designed. However, this should not be a deterrent from the research going forward, seeking new goals to expand knowledge.

References

- Ahrens, J. (1977). Prediction of irregular wave overtopping. Technical report, U.S. Army, Corps of Engineers.
- Allsop, N. W. H., Besley, P., and Madurini, L. (1995). Overtopping performance of vertical and composite breakwaters, seawalls and low reflection alternatives. Technical report, Final report of Monolithic Coastal Structures Project, University of Hannover, Hannover, Germany.
- Altomare, C., Suzuki, T., Chen, X., Verwaest, T., and Kortenhaus, A. (2016). Wave overtopping of sea dikes with very shallow foreshores. *Coastal Engineering*, 116:236–257.
- Battjes, J. (1974). Computation of set-up, longshore currents, run-up and overtopping due to wind-generated waves. page 251.
- Battjes, J. A. and Groenendijk, H. W. (2000). Wave height distributions on shallow foreshores. *Coastal Engineering*, 40(3):161–182.
- Besley, P. (1999). Wave overtopping of seawalls. Design and assessment manual. R&D Technical Report W178. Technical report.
- Besley, P., Stewart, T., and Allsop, N. W. H. (1998). Overtopping of vertical structures: new prediction methods to account for shallow water conditions. In ICE, editor, *Proceedings of the International Conference on Coastlines, Structures and Breakwaters*, pages 46–57, London, UK. Thomas Telford.
- Bouma, J. J., François, D., Schram, A., and Verbeke, T. (2009). Assessing socio-economic impacts of wave overtopping: An institutional perspective. *Coastal Engineering*, 56(2):203–209.
- Bruce, T., Van der Meer, J. W., Franco, L., and Pearson, J. M. (2009). Overtopping performance of different armour units for rubble mound breakwaters. *Coastal Engineering*, 56(2):166–179.

- Chuenchai, W., Namphol, P., Phetchawang, S., and Rasmeemasmuang, T. (2014). Wave run-up on stepped slopes (in Thai). *KMUTT Research & Development Journal*, 36(3):329–340.
- CIRIA, CUR, and CETMEF (2007). *The Rock Manual. The use of rock in hydraulic engineering (2nd edition)*. C683, CIRIA, London.
- de Gerloni, M., Franco, L., and Passoni, G. (1991). The safety of breakwaters against wave overtopping. In *Proceedings of the Coastal Structures and Breakwaters conference*, pages 335–342, London, UK.
- De Rouck, J., Verhaeghe, H., and Geeraerts, J. (2009). Crest level assessment of coastal structures - General overview. *Coastal Engineering*, 56(2):99–107.
- De Waal, J. P. and Van der Meer, J. W. (1992). Wave runoff and overtopping on coastal structures. In *Proceedings of the 23rd International Conference on Coastal Engineering*, pages 1758–1771, Venice, Italy.
- Dept. of Civil Engineering Aalborg University (2013). WaveLab 3.
- Dept. of Civil Engineering Ghent University (2010). Wave Flume Manual. Technical report, Dept. of Civil Engineering, Ghent University, Ghent, Belgium.
- Di Lauro, E., Maza, M., L. Lara, J., Contestabile, P., Losada, I. J., and Vicinanza, D. (2017). Numerical Analysis of a Non- Conventional Breakwater for Wave. In *Proceedings of the International Short Course and Conference on Applied Coastal Research 2017*, Santander, Spain.
- Douglass, S. L. (1984). Irregular wave overtopping rates. In *Proceedings of the 19th International Conference on Coastal Engineering*, pages 316–327, Houston, Texas, USA.
- Douglass, S. L. (1986). Review and comparison of methods for estimating irregular overtopping rates. Technical report, U.S. Army, Corps of Engineers.
- EAK (2002). *Empfehlungen für die Ausführung von Küstenschutzwerken (in German)*, volume 65. Empfehlungen für die Ausführung von Küstenschutzwerken.
- EurOtop (2007). *Wave overtopping of sea defences and related structures: assessment manual*. Pullen, T., Allsop, W., Bruce, T., Kortenhaus, A., Schüttrumpf, H., Van der Meer, J. W. Kuratorium für Forschung im Küsteningenieurwesen, Hamburg, Germany.

- EurOtop (2016). *Manual on wave overtopping of sea defences and related structures*. Van der Meer, J. W., Allsop, W., Bruce, T., De Rouck, J., Kortenhaus, A., Pullen, T., Schüttrumpf, H., Troch, P., Zanuttigh, B.,.
- Falcão, A. F. O. (2010). Wave energy utilization: A review of the technologies. *Renewable and Sustainable Energy Reviews*, 14(3):899–918.
- Fernandez, H., Iglesias, G., Carballo, R., Castro, A., Fraguera, J. A., Taveira-Pinto, F., and Sanchez, M. (2012). The new wave energy converter WaveCat: Concept and laboratory tests. *Marine Structures*, 29(1):58–70.
- Franco, C. and Franco, L. (1999). Overtopping formulas for caisson breakwater with nonbreaking 3D waves. *Journal of Waterway, Port, Coastal, and Ocean Engineering*, 125(APRIL):98–108.
- Franco, L., de Gerloni, M., and Van der Meer, J. W. (1994). Wave overtopping on vertical and composite breakwaters. In ASCE, editor, *Proceedings of the 24th International Conference on Coastal Engineering*, pages 1030–1045, New York, USA.
- Franco, L., Geeraerts, J., Briganti, R., Willems, M., Bellotti, G., and De Rouck, J. (2009). Prototype measurements and small-scale model tests of wave overtopping at shallow rubble-mound breakwaters: the Ostia-Rome yacht harbour case. *Coastal Engineering*, 56(2):154–165.
- Frigaard, P. and Brorsen, M. (1995). A time-domain method for separating incident and reflected irregular waves. *Coastal Engineering*, 24:205–215.
- Frigaard, P. and Christensen, M. (1994). An absorbing wave-maker based on digital filters. In *Proceedings of the 24th International Conference on Coastal Engineering (ICCE 1980)*, pages 168–180, Kobe, Japan.
- Gallach-Sánchez, D., Illegems, M., Willems, Y., Troch, P., and Kortenhaus, A. (2016a). Experimental study of average overtopping performance on steep low-crested structures for shallow water conditions. In *Proceedings of the 6th International Conference on the Application of Physical Modelling in Coastal and Port Engineering and Science (Coastlab16)*, Ottawa, Canada.
- Gallach-Sánchez, D., Platteeuw, J., Troch, P., and Kortenhaus, A. (2015a). Individual overtopping volumes for steep low-crested structures. In Walendorf, L. and Cox, D. T., editors, *Proceedings of the Coastal Structures & Solutions to Coastal Disasters Joint Conference 2015*, pages 699–709, Boston, USA. ASCE.

- Gallach-Sánchez, D., Troch, P., and Kortenhaus, A. (2015b). Experimental study of overtopping behaviour of steep low-crested coastal structures. In *Proceedings of the 7th International Short Course and Conference on Applied Coastal Research (SCACR2015)*, pages 1–12, Florence, Italy.
- Gallach-Sánchez, D., Troch, P., and Kortenhaus, A. (2016b). Experimental study of overtopping behaviour of steep low-crested coastal structures. *PIANC Yearbook 2015*, pages 181–188.
- Gallach-Sánchez, D., Troch, P., and Kortenhaus, A. (2017). Wave overtopping on steep low-crested structures : another climate change challenge. In *VLIZ Marine Scientist Day*, pages 35–36, Brugge, Belgium.
- Gallach-Sánchez, D., Troch, P., and Kortenhaus, A. (2018a). A Critical Analysis and Validation of the Accuracy of Wave Overtopping Prediction Formulae for OWECs. *Energies*, 11(1):number 133.
- Gallach-Sánchez, D., Troch, P., and Kortenhaus, A. (2018b). Average and wave-by-wave overtopping performance of steep low-crested structures. In *Proceedings of the 36th International Conference on Coastal Engineering (ICCE2018) - In preparation*, Baltimore, USA.
- Gallach-Sánchez, D., Troch, P., Vroman, T., Pintelon, L., and Kortenhaus, A. (2014). Experimental study of overtopping performance of steep smooth slopes for shallow water wave conditions. In *Proceedings of the 5th Conference on the Application of Physical Modelling to Port and Coastal Protection (Coastlab14)*, number 1, pages 334–343, Varna, Bulgaria.
- Geeraerts, J., Kortenhaus, A., González-Escrivá, J. A., De Rouck, J., and Troch, P. (2009). Effects of new variables on the overtopping discharge at steep rubble mound breakwaters - The Zeebrugge case. *Coastal Engineering*, 56(2):141–153.
- Goda, Y. (1971). Expected rate of irregular wave overtopping of seawalls. *Coastal Engineering in Japan*, 14:45–51.
- Goda, Y. (2009). Derivation of unified wave overtopping formulas for seawalls with smooth, impermeable surfaces based on selected CLASH datasets. *Coastal Engineering*, 56(4):385–399.
- Goda, Y. and Kishira, Y. (1975). Laboratory investigation on the overtopping rates of seawalls by irregular waves. *Ports and Harbour Research (in Japanese)*, 14(4):4–39.

- Goda, Y. and Suzuki, Y. (1976). Estimation of incident and reflected waves in random wave experiments. In *Proceedings of the 15th International Conference on Coastal Engineering (ICCE 1976)*, pages 828–845, Honolulu, Hawaii, USA.
- Hofland, B., Chen, X., Altomare, C., and Oosterlo, P. (2017). Prediction formula for the spectral wave period $T_m-1,0$ on mildly sloping shallow foreshores. *Coastal Engineering*, 123(February):21–28.
- Hughes, S. A. (2015). Hydraulic Parameters of Individual Overtopping Wave Volumes. Technical report, Colorado State University (USA).
- Hughes, S. a. and Nadal, N. C. (2009). Laboratory study of combined wave overtopping and storm surge overflow of a levee. *Coastal Engineering*, 56(3):244–259.
- Hughes, S. A. and Thornton, C. I. (2016). Estimation of time-varying discharge and cumulative volume in individual overtopping waves. *Coastal Engineering*, 117:191–204.
- Hughes, S. A., Thornton, C. I., Van der Meer, J. W., and Scholl, B. (2012). Improvements in Describing Wave Overtopping Processes. In *Proceedings of the 33rd International Conference on Coastal Engineering*, pages 1–15, Santander, Spain.
- IBM (2016). IBM SPSS Statistics 24.
- Ingram, D. M., Gao, F., Causon, D. M., Mingham, C. G., and Troch, P. (2009). Numerical investigations of wave overtopping at coastal structures. *Coastal Engineering*, 56(2):190–202.
- Kerpen, N. and Schlurmann, T. (2016). Stepped Revetments- Revisited. *Physical Modelling in Coastal and Port Engineering and Science*, (May):1–10.
- Kerpen, N. B. (2017). *Wave-induced Responses of Stepped Revetments*. PhD thesis, Leibniz Universität Hannover.
- Kerpen, N. B., Goseberg, N., and Schlurmann, T. (2014). Experimental investigations on wave overtopping on stepped embankments. In *Proceedings of the 5th Conference on the Application of Physical Modelling to Port and Coastal Protection (Coastlab14)*, number 1, Varna, Bulgaria.
- Klopman, G. and Van der Meer, J. W. (1999). Random wave measurements in front of reflective structures. *Journal of Waterway, Port, Coastal, and Ocean Engineering*, 125(1):39–45.

- Kofoed, J. P. (2002). *Wave Overtopping of Marine Structures: utilization of wave energy*. PhD thesis, Aalborg University.
- Kofoed, J. P., Frigaard, P., Friis-Madsen, E., and Sørensen, H. C. (2006). Prototype testing of the wave energy converter wave dragon. *Renewable Energy*, 31(2):181–189.
- Kortenhaus, A., Oumeraci, H., Geeraerts, J., Rouck, J., Medina, J. R., and González-Escrivá, J. A. (2004). Laboratory effects and further uncertainties associated with wave overtopping measurements. In *Proceedings of the 29th International Conference on Coastal Engineering*, number Vol. 4, pages 4456–4468, Lisbon, Portugal.
- Kramer, M., Zanuttigh, B., Van der Meer, J. W., Vidal, C., and Gironella, F. X. (2005). Laboratory experiments on low-crested breakwaters. *Coastal Engineering*, 52(10-11):867–885.
- Liu, Z., Hyun, B.-S., and Jin, J. (2008). Numerical Prediction for Overtopping. In *Proceedings of the Oceans 2008 - MTS/IEEE Kobe Techno-Ocean*, Kobe, Japan.
- Lykke Andersen, T. and Burcharth, H. F. (2009). Three-dimensional investigations of wave overtopping on rubble mound structures. *Coastal Engineering*, 56(2):180–189.
- Lykke Andersen, T. and Frigaard, P. (2008). *Lecture notes for the course in Water Wave Mechanics*. Dept. of Civil Engineering, Aalborg University, Aalborg, Denmark.
- Mansard, E. P. D. and Funke, E. R. (1980). The Measurement of Incident and Reflected Spectra Using a least Squares Method. In *Proceedings of the 17th International Conference on Coastal Engineering (ICCE 1980)*, pages 154–172, Sidney, Australia.
- Margheritini, L., Vicinanza, D., and Frigaard, P. (2009). SSG wave energy converter: Design, reliability and hydraulic performance of an innovative overtopping device. *Renewable Energy*, 34(5):1371–1380.
- Mathworks (2015). MATLAB 2015b.
- McBride, M. W., Allsop, N. W. H., Besley, P., Colombo, D., and Madurini, L. (1995). Vertical walls and low reflection alternatives. Results of wave flume tests. Technical report, HR Wallingford.
- Mehlum, E. (1986). Tapchan. In Evans, D. V. and Falcão, A. F. O., editors, *Hydrodynamics of Ocean Wave Energy Utilization*, pages 51–55. Springer, Berlin.

- National Instruments (2003). LabVIEW User Manual.
- Nørgaard, J. Q. H., Lykke Andersen, T., and Burcharth, H. F. (2014). Distribution of individual wave overtopping volumes in shallow water wave conditions. *Coastal Engineering*, 83:15–23.
- Owen, M. W. (1980). Design of seawalls allowing for wave overtopping. Technical report, HR Wallingford.
- Owen, M. W. (1982). Overtopping of sea defences. In *Proceedings of the International Conference on the Hydraulic Modelling of Civil Engineering Structures*, Coventry, UK.
- Pan, Y., Kuang, C. P., Li, L., and Amini, F. (2015). Full-scale laboratory study on distribution of individual wave overtopping volumes over a levee under negative freeboard. *Coastal Engineering*, 97:11–20.
- Pan, Y., Li, L., Amini, F., and Kuang, C. (2013). Full-Scale HPTRM-Strengthened Levee Testing under Combined Wave and Surge Overtopping Conditions : Overtopping Hydraulics , Shear Stress , and Erosion Analysis. *Journal of Coastal Research*, 29(1):182–200.
- Pearson, J., Bruce, T., and Allsop, W. (2002). Prediction of Wave Overtopping at Steep Seawalls – Variabilities and Uncertainties. In *Proceedings of the 4th International Symposium on Ocean Wave Measurement and Analysis*.
- Pullen, T., Allsop, W., Bruce, T., and Pearson, J. (2009). Field and laboratory measurements of mean overtopping discharges and spatial distributions at vertical seawalls. *Coastal Engineering*, 56(2):121–140.
- Reeve, D., Soliman, A., and Lin, P. (2008). Numerical study of combined overflow and wave overtopping over a smooth impermeable seawall. *Coastal Engineering*, 55(2):155–166.
- Romano, A., Bellotti, G., Briganti, R., and Franco, L. (2015). Uncertainties in the physical modelling of the wave overtopping over a rubble mound breakwater: The role of the seeding number and of the test duration. *Coastal Engineering*, 103:15–21.
- Saville, J. T. (1955). Laboratory data on wave runup and overtopping on shore structures. Technical report, Beach Erosion Board. US Army Corps of Engineers.
- Saville, J. T. and Caldwell, J. M. (1953). Experimental study of wave overtopping on shore structures. In *Proceedings of the Minnesota International Hydraulics Convention*, Minneapolis, Minnesota, USA.

- Schüttrumpf, H. (2001). *Wellenüberlaufströmung bei Seedeichen. Experimentelle und theoretische Untersuchungen*. PhD thesis, Technischen Universität Carolo-Wilhelmina zu Braunschweig.
- Smid, R. (2001). Untersuchungen zur Ermittlung der mittleren Wellenüberlaufhöhe an einer senkrechten Wand und einer 1: 1, 5 geneigten Böschung für Versuche mit und ohne Freibord. Technical report, Study report at Leichtweiss-Institute for Hydraulics. Braunschweig (in German).
- Steendam, G. J., van der Meer, J. W., Verhaeghe, H., Besley, P., Franco, L., and Van Gent, M. R. A. (2004). The International Database on Wave Overtopping. In *Proceedings of the 29th International Conference on Coastal Engineering*, volume 1-4, pages 4301–4313, Singapore. World Scientific Publishing Co. Pte. Ltd.
- Szmytkiewitz, M., Kolodko, J., and Zeidler, R. B. (1994). Irregular wave run-up on various slopes and optimization guidelines. Technical report, Polish Academy of Sciences, Institute of Hydro-engineering, Poland.
- TAW (1989). *Leidraad voor het ontwerpen van rivierdijken. Deel 2 - Benedenrivierengebied (in Dutch)*. Delft, The Netherlands.
- TAW (2002). *Technical report wave run-up and wave overtopping at dikes*. Delft, The Netherlands.
- Tedd, J. and Kofoed, J. P. (2009). Measurements of overtopping flow time series on the Wave Dragon, wave energy converter. *Renewable Energy*, 34(3):711–717.
- Thornton, C. I., Van der Meer, J. W., and Hughes, S. A. (2011). Testing Levee Slope Resiliency At the New Colorado State University Wave Overtopping Test Facility. In *Proceedings of the 6th International Conference of Coastal Structures*, pages 155–166, Yokohama, Japan.
- Troch, P., Mollaert, J., Peelman, S., Victor, L., Van der Meer, J. W., Gallach-Sánchez, D., and Kortenhaus, A. (2015). Experimental study of overtopping performance for the cases of very steep slopes and vertical walls with very small freeboards. In *Proceedings of the 34th International Conference on Coastal Engineering (ICCE 2014)*, volume 138, pages 1–8, Seoul, South Korea.
- Tsuruta, S. and Goda, Y. (1968). Expected discharge of irregular wave overtopping. In *Proceedings of the 11th International Conference on Coastal Engineering*, pages 833–852, London, UK.

- Tuah, H. and Hudspeth, R. T. (1982). Comparison of Numerical Random Sea Simulations. *Journal of the Waterways, Port, Coastal and Ocean Division*, 108(4):569–584.
- US Army Corps of Engineers (1973). *Shore Protection Manual*. US Army Corps of Engineers. Coastal Engineering Research Center, 1st edition.
- US Army Corps of Engineers (2002). *Coastal engineering manual*. US Army Corps of Engineers, 1st edition.
- Van der Meer, J. and Bruce, T. (2014). New Physical Insights and Design Formulas on Wave Overtopping at Sloping and Vertical Structures. *Journal of Waterway, Port, Coastal, and Ocean Engineering*, 140(6):04014025.
- Van der Meer, J., Hardeman, B., Steendam, G. J., Schüttrumpf, H., and Verheij, H. (2010). Flow Depths and Velocities At Crest and Landward Slope of a Dike, in Theory and With the Wave Overtopping Simulator. *Coastal Engineering Proceedings*, 1(32):15.
- Van der Meer, J., Thornton, C. I., and Hughes, S. A. (2011). Design And Operation Of The U.S. Wave Overtopping Simulator. In *Proceedings of the 6th International Conference of Coastal Structures*, pages 167–178, Yokohama, Japan.
- Van der Meer, J. W. (1998). Wave run-up and overtopping. In Pilarczyk, K. W., editor, *Seawalls, dikes and revetments*, chapter 8.
- Van der Meer, J. W., Briganti, R., Zanuttigh, B., and Wang, B. (2005a). Wave transmission and reflection at low-crested structures: Design formulae, oblique wave attack and spectral change. *Coastal Engineering*, 52(10-11):915–929.
- Van der Meer, J. W., Bruce, T., Allsop, W., Franco, L., Kortenhaus, A., Pullen, T., and Schüttrumpf, H. (2013). EurOtop revisited. Part 1 : sloping structures. In *Proceedings of the ICE, Coasts, Marine Structures and Breakwaters*, volume 1, Edinburgh, United Kingdom.
- Van der Meer, J. W. and Janssen, J. (1994). Wave run-up and wave overtopping at dikes and revetments. Technical report, Delft Hydraulics, Delft, The Netherlands.
- Van der Meer, J. W. and Janssen, W. (1995). Wave run-up and wave overtopping at dikes. In Kabayashi and Demirbilek, editors, *Wave Forces on inclined and vertical wall structures*. ASCE.

- Van der Meer, J. W., Verhaeghe, H., and Steendam, G. J. (2005b). Database on wave overtopping at coastal structures. CLASH WP2 report. Technical report, Infram, Marknesse, The Netherlands.
- van der Meer, J. W., Verhaeghe, H., and Steendam, G. J. (2009). The new wave overtopping database for coastal structures. *Coastal Engineering*, 56(2):108–120.
- Van Gent, M. R. (1999). Physical model investigations on coastal structures with shallow foreshores. 2D model tests with single and double-peaked wave energy spectra. Technical report, WL - Delft Hydraulics.
- Van Gent, M. R. A., Van den Boogaard, H. F. P., Pozueta, B., and Medina, J. R. (2007). Neural network modelling of wave overtopping at coastal structures. *Coastal Engineering*, 54(8):586–593.
- Van Steeg, P., Wolters, G., and Van Gent, M. R. (2012). Invloedsfactor voor ruwheid van een getrapt talud bij golfoverslag bij dijken: Verslag fysieke modeltesten en analyse (in Dutch). Technical report, Deltares, Delft, The Netherlands.
- Verhaeghe, H. (2005). *Neural network prediction of wave overtopping at coastal structures*. PhD thesis, Ghent University (Belgium).
- Verhaeghe, H., De Rouck, J., and Van der Meer, J. W. (2008). Combined classifier-quantifier model: A 2-phases neural model for prediction of wave overtopping at coastal structures. *Coastal Engineering*, 55(5):357–374.
- Vicinanza, D., Contestabile, P., and Di Lauro, E. (2017). Overtopping Breakwater for Wave Energy Conversion : Status and Perspective. In *Proceedings of the 12th European Wave and Tidal Energy Conference*, pages 1194–1 – 1194–9, Cork, Ireland.
- Vicinanza, D., Contestabile, P., Quvang Harck Nørgaard, J., and Lykke Andersen, T. (2014). Innovative rubble mound breakwaters for overtopping wave energy conversion. *Coastal Engineering*, 88:154–170.
- Vicinanza, D., Margheritini, L., Kofoed, J. P., and Buccino, M. (2012). The SSG wave energy converter: Performance, status and recent developments. *Energies*, 5(2):193–226.
- Victor, L. (2012). *Optimization of the Hydrodynamic Performance of Overtopping Wave Energy Converters: Experimental Study of Optimal Geometry and Probability Distribution of Overtopping Volumes*. PhD thesis, Ghent University.

- Victor, L. and Troch, P. (2010). Development of a test set-up to measure large wave-by-wave overtopping masses. In *Proceedings of the 3rd International Conference on the Applications of Physical Modelling to Port and Coastal Protection (Coastlab10)*, number 1, pages 1–9, Barcelona, Spain.
- Victor, L. and Troch, P. (2012a). Experimental study on the overtopping behaviour of steep slopes - Transition between mild slopes and vertical walls. In *Proceedings of the 33rd International Conference on Coastal Engineering (ICCE 2012)*, pages 1–23, Santander, Spain.
- Victor, L. and Troch, P. (2012b). Wave Overtopping at Smooth Impermeable Steep Slopes with Low Crest Freeboards. *Journal of Waterway, Port, Coastal, and Ocean Engineering*, 138(5):372–385.
- Victor, L., Van der Meer, J. W., and Troch, P. (2012). Probability distribution of individual wave overtopping volumes for smooth impermeable steep slopes with low crest freeboards. *Coastal Engineering*, 64:87–101.
- Weggel, J. R. (1976). Wave overtopping equation. In *Proceedings of the 15th International Conference on Coastal Engineering*, pages 2022–2035, Honolulu, Hawaii, USA.
- Zanuttigh, B., Formentin, S. M., and Van der Meer, J. W. (2016). Prediction of extreme and tolerable wave overtopping discharges through an advanced neural network. *Ocean Engineering*, 127(September):7–22.
- Zanuttigh, B., Margheritini, L., Gambles, L., and Martinelli, L. (2009). Analysis of wave reflection from wave energy converters installed as breakwaters in harbour. In *8th European Wave and Tidal Energy Conference (EWTEC)*, Uppsala, Sweden.
- Zanuttigh, B., Van der Meer, J. W., Bruce, T., and Hughes, S. A. (2013). Statistical Characterisation of Extreme Overtopping Wave Volumes. In *Proceedings of the ICE, Coasts, Marine Structures and Breakwaters 2013*, number 2004, pages 1–10, Edinburgh, United Kingdom.
- Zelt, J. A. and Skjelbreia, J. (1992). Estimating Incident and Reflected Wave Fields Using an Arbitrary Number of Wave Gauges. In *Proceedings of the 23rd International Conference on Coastal Engineering (ICCE 1992)*, volume 1, pages 777–789.